Soft Tissue Constitutive Forms and Their Implications for Whole Knee Computational Models

by

Benjamin C. Marchi

A dissertation submitted in partial fulfillment
of the requirements for the degree of
Doctor of Philosophy
(Mechanical Engineering)
in the University of Michigan
2018

Doctoral Committee:

Professor Ellen M. Arruda, Chair
Assistant Professor Rhima M. Coleman
Professor Krishnakumar R. Garikipati
Professor Gregory M. Hulbert

Benjamin C. Marchi

bmarchi@umich.edu

ORCID iD: 0000-0002-8780-660X

To those who came before; for those still in the pursuit.

ACKNOWLEDGMENTS

I am indebted to my advisor, Dr. Ellen Arruda, for her insatiable pursuit of knowledge, keen research acumen, and unwavering support and guidance throughout my graduate studies at Michigan. Through the roughest of rough drafts and most unprepared of practice talks, you have always provided me a frank and honest assessment of where the work was and where it needed to be. I am grateful for the space through which you have allowed me to grow and develop into the independent and curious researcher that I am today. I came to your office one of my first days at a new school, in an entirely foreign environment, without any real knowledge of biomechanics or notion of what academic research was all about, but somehow managed to leave with a desk and the beginnings of a whole new perspective on the world. During my time with you, we have been around the globe talking about science—well, whenever we were not eating some of the best foods and exploring some of the most interesting places. You took a risk and provided me a truly extraordinary opportunity, and, for that, I will be forever grateful.

I would also like to thank the members of my doctoral committee, Drs. Rhima Coleman, Krishna Garikipati, and Greg Hulbert, for their generosity in reviewing my dissertation. Your insights and advice have made this work stronger and are much appreciated. In particular, I would like to thank Rhima for opening her doors and collaborating on part of the work in this dissertation. You are decidedly approachable and relentlessly affable. You have been unafraid to demand my best from me, and I believe, while at times I may have questioned it, that I am a better researcher for it.

I would be remiss if I did not thank those who have made the day-to-day research at Michigan immensely enjoyable. I am much appreciative to Drs. Jessica Deneweth and Lixang Yang for building the foundation of this work and getting me up to speed on all the relevant scientific aspects. The members of my research group have been indispensable; Tanaz, Kaitlyn, Zhouzhou, Callan, Marie, Ryan, Jon, and Uli: you have all made significant contributions to this work, even if you do not realize it. During my time at Michigan, we have always shared office and lab space. This has brought new methods, ideas, and material systems into my orbit, but, more than that, it has brought people. I know all about some seriously cool deformation mechanisms in metals thanks to Adam, Jarid, Micheal, Jason, Joyce, Will, and Marissa, and all about adhesives and fracture from Hai, Fanbo, and James.

I have known colleagues, acquaintances, and friends, but you are none of these. We share a bond that is largely beyond comprehension. Whether each of you like it or not, we are all part of some sort of weird family. Thank you for all of your support and encouragement, even at the times I just wanted to keep my headphones on and work.

It takes a certain kind of crazy to see a doctorate in your future. I am truly blessed to have been able to share this time with great friends, each of whom is touched by some of the same crazy. Jeffrey, Yev, Sarah, and Matt, your presence has been valuable beyond words. You have encouraged, berated, and dragged me along the path to completing this dissertation and my doctorate. The depth of kindness you have shown cannot be overstated.

Finally, I would like to thank my family. You have known me and you have nurtured me. I do not have the words to fully describe how utterly and completely essential you all are to me. Thank you to my parents, Lou and Lori, for your unending love and support. I can only imagine that having kids who only seem to talk about math is enough to drive anyone up a wall, but your ability to empathize and to know when I need a bit of encouragement is, to me at least, incomprehensible. Thank you to Scott, who, though across the country and in a field far, far way, has been in this endeavor with me from the start. I guess it only makes sense that two kids brought up in the school of Martinek and Kostal would end up here. Thank you to Jillian, a true and vital partner. I think the only thing more stressful than writing a dissertation is to watch someone write one. You are kind and challenging and every bit as critical to me as checking your code one last time to make sure you got all the signs correct.

PREFACE

Chapters 3-6 have been written as separate manuscripts. For this reason, there may be some repetition of material, particularly in the motivating material, between Chapters 3 and 4, as well as between Chapters 5 and 6.

TABLE OF CONTENTS

LIST OF FIGURES

LIST OF TABLES

LIST OF APPENDICES

LIST OF ABBREVIATIONS

FE finite element

MRI magnetic resonance imaging

CT computerized tomography

ACL anterior cruciate ligament

LCL lateral collateral ligament

MCL medial collateral ligament

PCL posterior cruciate ligament

OA Osteoarthritis

AMB anteromedial bundle

PLB posterolateral bundle

ATT anterior tibial translation

ITR internal tibial rotation

A-P anterior-posterior

M-L medial-lateral

RVE representative volume element

ABSTRACT

This work sought to determine the extent to which approximations in the constitutive theories and geometric representations of individual soft tissues affected the predictive power of computational knee models. Two tissue systems were evaluated: articular cartilage and structural ligaments, particularly focusing on the anterior cruciate ligament (ACL). These tissues were selected due to the rates and debilitating effects of their associated injuries and diseases, as well as their ubiquitous inclusion in computational knee models.

The mechanical consequences of various levels of articular cartilage constitutive complexity were investigated during physiologically representative loading. Additional complexity, compared to the common assumption of linear elasticity, was introduced through the systematic incorporation of nonlinear, directional, and spatially heterogeneous mechanical properties. Failure to include experimentally motivated cartilage material models resulted in overpredictions of joint motion and local tissue deformation. There were some diminishing returns with increasing complexity. In particular, there was a relatively small effect corresponding to the specific interpolation method used in the construction of each spatially heterogeneous mechanical property field. After determining the sensitivity of the representative computational knee model to cartilage constitutive behavior, the impacts of articular cartilage focal defect size and location were analyzed. Cartilage focal defects were shown to have a large effect on deformation in the neighborhood around their perimeters, though no consistent trends of altered deformation were observed in adjacent and opposing tissues. A defect of increased size was also shown to alter joint kinematics, while small defects, independent from their location, were found to have a minimal effect.

There has been a tremendous body of work directed at describing the deformation of ligaments. This work is largely built on the assumption that ligaments behave as transversely isotropic solids; however, there are limited and conflicting mechanical characterization data available for ligaments. Various constitutive theories were assessed on their ability to represent the stress-strain responses of structural ligaments in multiple loading configurations. Traditionally and commonly accepted transversely isotropic, hyperelastic constitutive theories proved incapable of describing the mechanical response of ligaments, predominantly failing in the transverse direction. Therefore, a new constitutive theory was

developed and shown to have superior accuracy in describing the breadth of experimental stress-strain responses from multiple loading directions. With this new understanding related to the deformation of ligaments, the internal loading and detailed anatomy of the ACL were evaluated. Specifically, the double bundled, prestrained structure of the ACL was quantified computationally for the first time, and its effect on joint motion and local tissue deformation during normal clinical assessments was examined. The incorporation of prestrain was shown to be an important mechanical feature of knee stability, bringing predicted joint motions within the acceptable ranges of healthy knees.

CHAPTER 1

Introduction and specific aims

1.1 Introduction

The knee is an intricate, biarticulating joint whose health is acutely linked to the stability and mobility of an individual. The use of the knee is prolific in everyday life; walking, running, jumping, standing, crouching, and even dancing can all require the flexibility provided by the knee. The joint is composed of a variety of physiological structures, ranging from stiff to compliant and from macroscopic to microscopic (Goldblatt and Richmond, 2003). These structures work in coordinated and complimentary ways to facilitate normal knee motion. With so many constituents, from hard bones and soft cartilage to large muscle groups and small extracellular molecules, it is easy to imagine that any one deficiency might be sufficient to diminish functionality, or even have the power to halt joint function altogether (Lawrence et al., 2008; Spindler and Wright, 2008). In conjunction with the initial mechanical implications, the pain typically associated with knee injury can also be incapacitating (Peat et al., 2001). Furthermore, due to the coupled nature of the structures in the knee, the failure of one structure may directly contribute to and be the proximate cause of another (Kessler et al., 2008; Lohmander et al., 2004; Petersson and Jacobsson, 2002; Thorlund et al., 2016).

Osteoarthritis (OA) is one example of a debilitating soft tissue disease that frequently develops in the knee. It is characterized by a progressive weakening, degeneration, and eventual failure of articular cartilage. OA is often accompanied by pain and reduced joint function, drastically affecting the quality of life of the individual (Felson et al., 2000). Approximately 13% of the adult population in the United States is suffering from diagnosed OA (Lawrence et al., 2008), and upwards of 25% of adults over 55 experience significant knee pain each year likely resulting from underlying OA (Peat et al., 2001). The United States is not singularly affected, with similar percentages of adults touched by OA globally (Jordan et al., 2013). Confounding the striking rates of OA is that its incidence rate is increasing. Despite OA already being ranked the sixth leading cause of disability, it is expected to rise to the fourth by 2020 (Woolf and Pfleger, 2003). In addition to the tremen-

dous physical effects of OA, its economic costs are staggeringly high. It has been estimated that the annual costs of OA in the United States exceed $90 billion (Leigh et al., 2001), and this only makes up a fraction of the over $300 billion spent domestically on arthritic conditions generally (Yelin et al., 2007). The physical and economic challenges associated with OA are especially stark given that there is no consensus approach for prevention and treatment, except for total knee replacement. Therefore, understanding the mechanisms of OA initiation and progression are essential for suppressing the growth and limiting the effect of this disease. This understanding may also provide insights for new treatments and strategies to better maintain a lifetime of quality joint function.

Complications related to articular cartilage are not only limited to diseases like OA, but also manifest as localized tissue degeneration. One such group of these concentrated abnormalities is called focal defects. Focal defects may solely affect articular cartilage (chondral) or have some bone involvement (osteochondral) (Brittberg and Winalski, 2003). As with OA, focal defects can present with significant joint pain and instability (Hangody and Füles, 2003). The clinical diagnosis of focal defects is still difficult with traditional, radiographical methods (Oberlander et al., 1993), though the proliferation of magnetic resonance imaging (MRI) has significantly increased the potential for early detection (Recht et al., 1993). However, the clinical advantage of non-invasiveness of MRI is often outweighed by its cost, meaning that most focal defects are still diagnosed during arthroscopy (Hjelle et al., 2002). Focal defects are observed across articular surfaces in the knee (Wong and Sah, 2010), and, given the constraints of non-invasive clinical diagnosis, they are first detected in a large distribution of sizes (Widuchowski et al., 2007). Defects have been found to occur most often in weight bearing regions of the knee, and they may be linked to the initiation and hasten the progression of diseases like OA (Årøen et al., 2004; Curl et al., 1997; Hjelle et al., 2002; Widuchowski et al., 2007). Furthermore, cartilage opposing and neighboring to focal defects has also shown signs of degeneration typical of early OA (Convery et al., 1972; Lefkoe et al., 1993) and, left untreated, focal defects increase in size (Wang et al., 2006). That being said, there does appears to be some size threshold under which a focal defect may remain untreated without any meaningful clinical consequences (Choi et al., 2009; Magnussen et al., 2008), though the exact relationship between physiological factors, like defect size, location, bone geometry, etc., still remains unclear (Behery et al., 2014). This means that a more comprehensive knowledge of how focal defects interact with their local environment is critical for devising optimized, patient-specific models for clinical decision making.

Soft tissue diseases and injuries in the knee are of course not limited to articular cartilage. Ligament rupture is a soft tissue injury whose incidence rate is, like OA, also on the

rise (Kim et al., 2011b). There are four major supporting ligament structures in the knee: the anterior cruciate ligament (ACL), the posterior cruciate ligament (PCL), the lateral collateral ligament (LCL), and the medial collateral ligament (MCL). Ligaments primarily act to provide stability during normal activities, while resisting potentially harmful motions (Goldblatt and Richmond, 2003). The ACL is particularly susceptible to failure (Spindler and Wright, 2008), though the MCL also fails in substantial numbers (Bollen, 2000). For many, ligament failure is associated with traumatic sports injury, like when a skier tumbles or a basketball player lands awkwardly (Krosshaug et al., 2007a; Majewski et al., 2006; Olsen et al., 2004), but ligaments can fail gradually as well as acutely (Beaulieu et al., 2015; Lipps et al., 2013). There are more than a quarter of a million ACL injuries every year in the United States (Griffin et al., 2006). These injuries typically result in decreased knee stability and abnormal joint kinematics (Butler et al., 2009; Chaudhari et al., 2008; Deneweth et al., 2010; Salmon et al., 2006; Selmi et al., 2006; Tashman et al., 2004). With time, these fundamental changes in the knee can lead to early onset, and often severe, OA (Butler et al., 2009; Chaudhari et al., 2008; Griffin et al., 2006; Lohmander et al., 2004, 2007; McLean et al., 2015; Spindler and Wright, 2008). Notwithstanding these long-term consequences of ACL, the acute cost of ACL treatment is upwards of $2 billion annually in the United States (Spindler and Wright, 2008). Women are also disproportionally affected by ACL rupture, with upwards of a five-fold increased likelihood of injury compared to men (Agel et al., 2005; Hewett et al., 2005; Waldén et al., 2011). As with OA and focal defects, understanding the mechanical contributions of ligaments, like the ACL, during normal activities in healthy knees has the potential to create a new paradigm for clinicians.

Despite the breadth of soft tissue injuries and diseases, they are all linked through fundamental changes in joint mechanics precipitated by their presence. With the onset of injury or the progression of disease, tissues are being damaged, altered, and/or remodeled, and these local transformations can have detrimental and nonlinear effects across locations and structures in the knee. One proposed mechanism of OA development is related to shifting knee mechanics associated with the onset of the disease (Andriacchi et al., 2009; Astephen et al., 2008; Matsuki et al., 2017; Setton et al., 1999; Tashman et al., 2004; Weidow et al., 2007) or with collateral injury, like ACL rupture (Bakker et al., 2016; Chouliaras et al., 2009; Deneweth et al., 2010; Gao and Zheng, 2010; Georgoulis et al., 2010; Haughom et al., 2012; Papannagari et al., 2006; Salem et al., 2003; Stergiou et al., 2007). This theory is based on the notion that the presence of the disease leads to alternations in the spatial distribution of deformation supported by articular cartilage (Andriacchi and Mündermann, 2006; Andriacchi et al., 2009; Carter et al., 2004; Chang et al., 2015; Hinman et al., 2012). As contact shifts within the joint, new tissues are being loaded, and these tissues may be ill

equipped to withstand their new mechanical environment (Griffin and Guilak, 2005; Sun, 2010). During dynamic activities, individuals at a high risk for OA tend to display altered knee kinematics (Chouliaras et al., 2009; Deneweth et al., 2010; Georgoulis et al., 2010; Stergiou et al., 2007; Tashman et al., 2007), and with increasing OA severity there is an associated increase in differences in knee motion compared to healthy individuals (Astephen et al., 2008; Sharma et al., 2001). One fundamental component of this theory is that there exists regional variation in articular cartilage mechanical properties and/or morphology. There is strong evidence to support this tenant (Appleyard et al., 2003; Athanasiou et al., 1991; Briant et al., 2015; Elliott et al., 2002; Froimson et al., 1997; Jurvelin et al., 2000; Swann and Seedhom, 1993; Thambyah et al., 2006; Young et al., 2007), particularly in response to dynamic and physiologically relevant loading (Deneweth et al., 2013b, 2015).

Similarly, focal defects may be associated with OA through deviations in intra-joint loading and contact brought on by the presence of physical changes in cartilage topology (Brown et al., 1991; Gratz et al., 2009; Wong and Sah, 2010). Defects have been shown to increase deformation around their perimeter (Braman et al., 2005; Gratz et al., 2008; Guettler et al., 2004), and these local increases might be sufficient to lead to cascading cell degeneration and death (Buckwalter and Brown, 2004; Chen and Torzilli, 2015; Kühn et al., 2004; Kurz et al., 2001; Quinn et al., 2001; Torzilli et al., 1999; van Haaften et al., 2017; Verteramo and Seedhom, 2007; Wilson et al., 2006). Despite compelling observational evidence, the exact relationship between defect size and location on local tissue deformation, particularly the effect of defects on surrounding tissues, is still not clear. By understanding how defects alter joint loading, the next generation of therapies and tissue replacements may be better positioned to restore native knee function.

In all these cases, the roadblock standing between current clinical methods and improving patient outcomes is specific knowledge of how individual knee structures respond to general loading. This is why modeling and simulation have important roles in our understanding of injury and disease. The complexity of life makes purely experimental efforts capable of describing the range of anatomies and physiologies found in nature unrealistic. This is especially true when the area of interest shifts from description to synthesizing predictions. The knee has been an early target for computation. A large portion of this work has focused on building models that are representative of healthy joints (Abdel-Rahman and Hefzy, 1998; Adouni et al., 2012; Beillas et al., 2004; Bendjaballah et al., 1997; Blankevoort and Huiskes, 1996; Donahue et al., 2002; Gardiner and Weiss, 2003; Hirokawa and Tsuruno, 2000; Kang et al., 2015; Kiapour et al., 2014a; Klets et al., 2016; Li et al., 1999a; Limbert et al., 2004; Mononen et al., 2015; Mootanah et al., 2014; Peña et al., 2006a; Penrose et al., 2002; Quatman et al., 2011; Shelburne et al., 2006; Song et al., 2004;

Venäläinen et al., 2016a; Xie et al., 2009; Zhang et al., 2008); however, informed models not only offer a platform for evaluating baseline joint performance, but also for determining the conditions under which the knee starts to break down, as well as methods for restoring its function (Atmaca et al., 2013; Bae et al., 2015; Baldwin et al., 2012; D D'Lima et al., 2009; Godest et al., 2002; Halloran et al., 2005; Hosseini et al., 2014; Huang et al., 2012; Kim et al., 2011a; Li et al., 2002; Liukkonen et al., 2017; Manda et al., 2011; Marouane et al., 2014; Mesfar and Shirazi-Adl, 2005; Mononen et al., 2016; Mootanah et al., 2014; Papaioannou et al., 2010; Peña et al., 2005a,b, 2006b, 2007; Ramaniraka et al., 2007; Shin et al., 2007; Shirazi and Shirazi-Adl, 2009a,b; Venäläinen et al., 2016b; Wang et al., 2014; Weiss et al., 1998; Woiczinski et al., 2016). The hope is, that by comparing predictions from injury and disease models to their healthy counterparts, it will be possible to identify the fundamental mechanical mechanisms of disease and injury initiation and progression. Yet, this is only possible when the basic, physical descriptions of each tissue structure are sufficiently representative.

1.2 Structure of dissertation

A large portion of this dissertation (**Chapters 3-6**) is composed from four separate investigations, which have all been published or submitted for publication in peer-reviewed journals. As such, there may be some redundant information presented in these chapters; chapters may also appear self-contained. Minor changes from previously published forms may exist, with most changes reflecting an attempt to maintain consistency throughout this dissertation. For brevity and clarity, all references have been placed at the end of this dissertation.

In **Chapter 2**, background on the knee, its tissues, and their injuries and diseases is presented. This includes detailed information on the anatomies, physiologies, and functions of soft tissues in the knee, particularly articular cartilage and structural ligaments. A detailed overview of articular cartilage and ligament mechanics and constitutive model considerations is also included.

Chapter 3 explores the role of articular cartilage constitutive form on soft tissue deformation and joint motion in the context of a whole knee computational model. Nonlinearity, directionality, and spatial heterogeneity is shown to be influential mechanical characteristics of articular cartilage. Using the insights from Chapter 3, **Chapter 4** examines how a common articular cartilage injury state, focal cartilage defects, affects joint performance. Focal defects substantially increase deformation in close proximity to their perimeter. They also alter the distribution and magnitude of deformation in healthy, opposing cartilages.

The spatial mechanical heterogeneity of articular cartilage is shown to have significant implications for the local loading of cartilage, with potential chondrocyte viability implications.

In **Chapter 5**, a general framework for determining and evaluating directional constitutive theories is presented and applied to the MCL. Given the form of MCL mechanical characterization data, commonly adapted material models fail to accurately capture the highly nonlinear and anisotropic response of the tissue. Therefore, a novel constitutive theory is developed and shown to have superior representative performance relative to comparable theories. **Chapter 6** uses the framework presented in Chapter 5 and applies it to the ACL. With a representative continuum model for the ACL, three commonly simplified mechanical features of the ligament are explored in the context of clinical assessments of ACL integrity. The double bundled structure, individual mechanical properties of these bundles, and their general internal loading for arbitrary knee configurations of the ACL are evaluated during anterior tibial translation (ATT) and internal tibial rotation (ITR). **Chapter 7** summarizes the major outcomes presented in Chapters 3-6, discusses some general limitations of the work, and provides possible directions for future study in the field.

CHAPTER 2

Background

2.1 An overview of knee anatomy and function

The knee is a joint located in the lower portion of the body. Its health is vital for maintaining unassisted mobility, and its injury often corresponds to a diminished overall well-being of the affected individual. A variety of tissue structures are found in the knee. Figure 2.1 illustrates the various biologic structural features located in the knee. Three major bones—the tibia, femur, and patella—compose the knee, though, due to its proximity, the fibula is also often considered a member of the overall joint system. There are two joints in the knee, between the patella and femur and between the tibia and femur (Goldblatt and Richmond, 2003). Bone is a relatively stiff structure and one of the primary mechanical load transfer mechanisms in the body (Gomez and Nahum, 2002). Bone itself has an incredibly nuanced structure (Keaveny et al., 2001), which has spawned an entire field of work dedicated to investigating its anatomy, physiology, and biomechanics (Frost, 2001; Goldstein, 1987; Huiskes et al., 2000; Radasch, 1999; Roesler, 1987; Turner et al., 1999).

On the other end of the stiffness spectrum, soft tissues make up the balance of solid structural components of the knee (Fig. 2.1). Soft tissues provide support and promote stability in the joint, while enabling joint motion (Bhosale and Richardson, 2008; Fox et al., 2015; Hungerford and Barry, 1979; LaPrade et al., 2007; McLean et al., 2015). They tend to undergo relatively large deformations, often well into the finite strain regime (Holmes and Mow, 1990; Pioletti et al., 1998). Highly aligned collagen structures connect bones to bones (ligaments) and bones to muscles (tendons) (McLean et al., 2015; Screen, 2009). Ligaments aid in joint coordination, preventing potentially dangerous deformations (Brantigan and Voshell, 1941). Located on the contacting surfaces of bones, articular cartilage provides critical cushioning during load transmission between bones (Mow et al., 1984). The menisci are semicircle tissues that are situated on the perimeter of the tibial articular cartilage and are attached to the tibial plateau. Each of these tissues has unique and multifaceted anatomies, physiologies, and mechanical properties (Brindle et al., 2001). Despite their diversity, ligaments, tendons, articular cartilage, and menisci do not form a

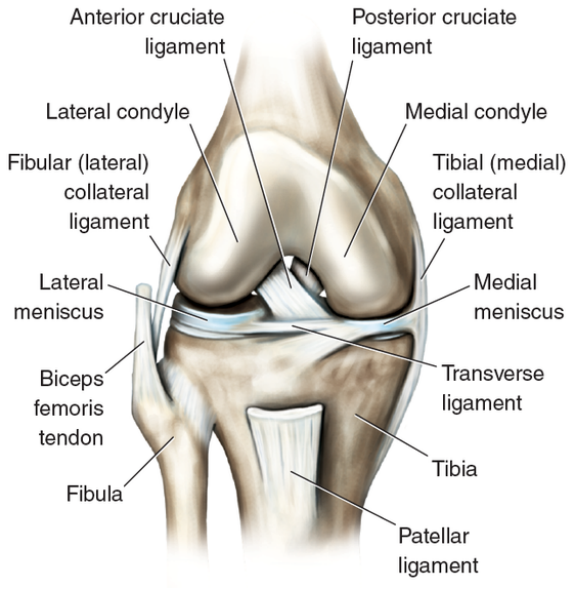

Figure 2.1: Anatomy of the knee. Figure from Human Kinetics (2017).

comprehensive list of all the soft tissues in the knee (Blackburn and Craig, 1980), but they do form a significant fraction of the mechanical foundation of joints and are the main focus of this work.

2.2 Articular cartilage in the knee

Soft tissues in the knee are particularly vexing. Articular cartilage is a relatively compliant tissue that is often found between contacting bodies in joints. In the knee, articular cartilage is predominately located on the tibial plateau and distal femoral head, as well as between the femur and the posterior aspect of the patella (Buckwalter, 1990). Articular cartilage functions to mitigate intrajoint loads through a nearly frictionless cartilage-to-cartilage contact surface (Mow et al., 1993). It cushions and distributes loads between stiff, load-bearing structures, like bones, reducing peak contact deformation localizations by increasing the effective contact area (Mow and Rosenwasser, 1988; Mow et al., 1995). Altered loading has been shown to affect cartilage physiology and mechanics (Herzog and Federico, 2006; Herzog et al., 1998), and these alterations may result in local tissue degradation (Buckwalter, 1990; Mankin, 1974; Sun, 2010). This cartilage deterioration is a major morphological characteristic of OA (Buckwalter and Mankin, 1997; Felson et al., 2000), though the precise link between mechanics and OA is still unresolved. A more detailed understanding of cartilage may prove valuable in elucidating the mechanisms of OA.

2.2.1 Articular cartilage physiology

Articular cartilage is primarily composed of extracellular matrix constituents, with a sparse population of cartilage cells called chondrocytes (Buckwalter and Mankin, 1997). Cartilage is composed from two primary phases: solid and liquid. The solid phase, approximately 10-25% of the total tissue mass, contains mostly collagen (largely Type II) and proteoglycans (Huber et al., 2000; Muir, 1980). Proteoglycans are negatively charged macromolecules, and they attract and maintain water within the cartilage bulk (Bhosale and Richardson, 2008; Mow et al., 1980). The fluid phase, which is a solution of permeable ions in water, makes up most of the remaining mass of articular cartilage, approximately 65-80% of the total tissue mass (Mow and Guo, 2002; Mow et al., 1984). A schematic representation of articular cartilage is shown in Fig. 2.2.

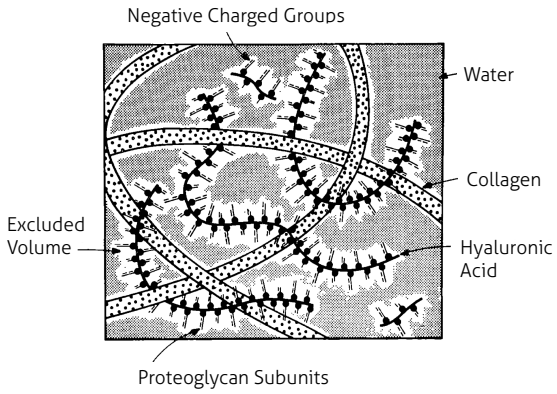

Figure 2.2: Schematic of the macromolecular components and phases of articular cartilage (Lai and Mow, 1980).

The microstructural composition of articular cartilage has been shown to be highly heterogeneous both depth-wise through its thickness and regionally across its surface. Through its thickness, articular cartilage is typically characterized by four structurally different layers (Buckwalter et al., 1994). From the articular surface to the bone, the layers are: the superficial tangential zone, the middle zone, the deep (radial) zone, and the calcified cartilage at the interface of the underlying bone (Bhosale and Richardson, 2008). The layers of articular cartilage and the orientations of their microstructural constituents can be seen in Fig. 2.3. In the superficial tangential zone, there is a small, randomly oriented population of chondrocytes supported by a dense network of collagen fibers (Weiss et al., 1968). These fibers are predominately oriented in the plane parallel to the articular surface (Lane and Weiss, 1975). In the middle zone, the directions of collagen fibers are more randomly distributed (Buckwalter et al., 1994; Mow et al., 1984) and the chondrocytes sightly

larger compared to those in the superficial tangential zone (Eyre et al., 2006). Transitioning to the deep zone, collagen fibers and chondrocytes are aligned radially in directions normal to the terminating bone geometry (Minns and Steven, 1977; Poole, 1997).

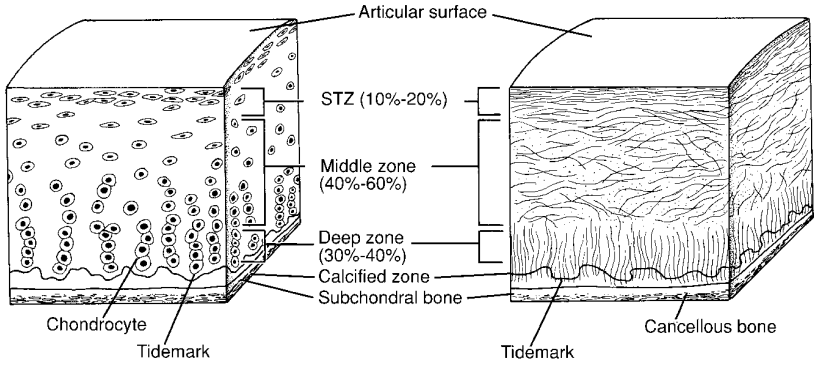

Figure 2.3: Schematic diagram of chondrocyte and collagen fiber depth-wise configurations through the four clinical zones of articular cartilage (Buckwalter et al., 1994).

Proteoglycans make up a larger percentage of the total weight of femoral cartilage compared to tibial cartilage (Treppo et al., 2000). Differences between and within the T2 times of tibial and femoral cartilages have also been observed (Smith et al., 2001)—T2 relaxation times (acquired with MRI) represent the decay time of proton precession in the plane transverse to the magnetization direction and are directly related to the macromolecular motion of water (Mosher and Dardzinski, 2004). Within the femoral cartilage, specific proteoglycan levels have been linked to certain regions throughout the trochlea, with greater concentrations in regions in contact with patellar cartilage compared to regions in contact with tibial cartilage (Froimson et al., 1997). The density and morphology of chondrocytes are also regionally dependent, with load bearing regions tending to have lower count densities and higher cell volumes compared to less load bearing regions (Eggli et al., 1988). There is tremendous spatial variation in the thickness of articular cartilage, with weight bearing regions tending to have larger thickness compared to peripheral tissue (Ateshian et al., 1991; Buckland-Wright et al., 1995; Cohen et al., 1999). Furthermore, split-line mappings (see representative images in Fig. 2.4) have shown that surface collagen orientations are highly heterogeneous (Below et al., 2002; Meachim et al., 1974).

2.2.2 Articular cartilage mechanics

Like many soft tissues in biology, the physics of deformation in articular cartilage are multifaceted. The deformation mechanics of articular cartilage have been shown to include elements of time, strain rate, directional, depth, and regional dependencies, as well as non-

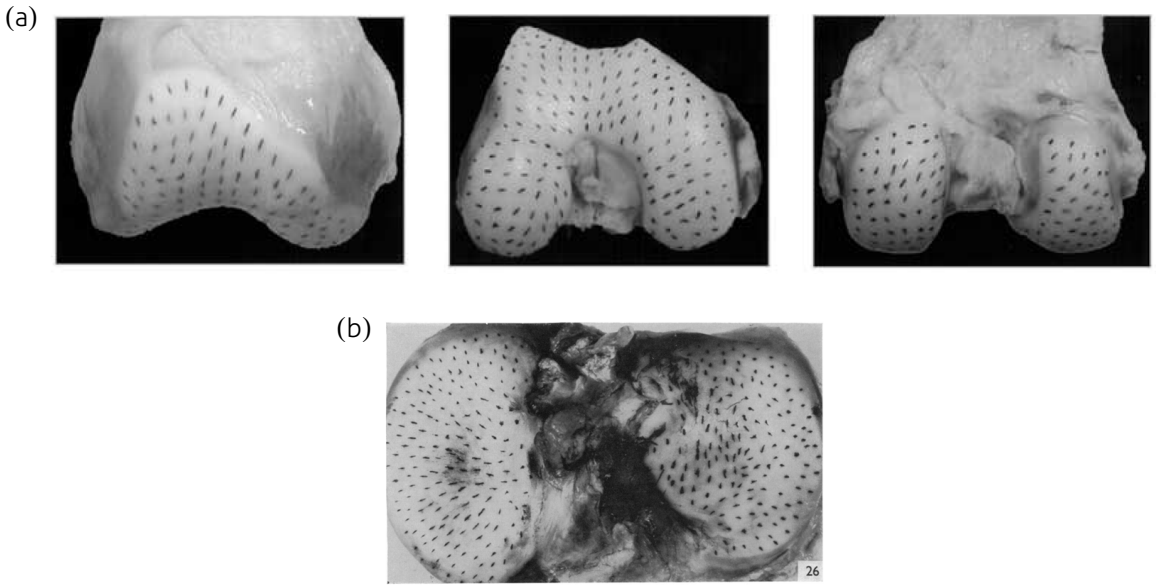

Figure 2.4: Split-line patterns of the (a) femoral (Below et al., 2002) and (b) tibial (Meachim et al., 1974) cartilage articular surface.

linearities in its elasticity and viscoelasticity. There has been significant interest in the behavior of articular cartilage in the time domain, where classical mechanics techniques, like creep and stress relaxation, have been used to explore various deformation mechanisms within the tissue (Ateshian et al., 1997; Hayes and Mockros, 1971; Mow et al., 1980). Time dependency in articular cartilage manifests from both the frictional drag produced by fluid flowing through the porous solid cartilage matrix and intrinsic viscoelasticity of the macromolecular network of the solid matrix (Hayes and Bodine, 1978; Huang et al., 2001; Lu and Mow, 2008; Mak, 1986a; Mow et al., 1984; Park and Ateshian, 2006).

Stress-strain behavior of articular cartilage is also sensitive to loading rate. The stress-strain behavior of articular cartilage appears stiffer with increasing strain-rates (DiSilvestro et al., 2001a; Lai et al., 1981; Langelier and Buschmann, 2003; Li et al., 2003; Verteramo and Seedhom, 2004), though the effect becomes saturated at higher strain rates (Oloyede et al., 1992). For the range of strain-rates seen by articular cartilage during normal, physiological activities, the rate dependency of the tissue is minimal (Mann and Hagy, 1980; Oloyede et al., 1992). At these loading rates, the response is largely driven by the solid phase of articular cartilage due to insufficient time for fluid transport (Bader and Kempson, 1994; Mizrahi et al., 1986; Rieppo et al., 2003). Consequently, articular cartilage, during physiologically interesting events, is typically assumed to be incompressible and strain-rate insensitive (Armstrong et al., 1984; Bachrach et al., 1998; Eberhardt et al., 1990). In addition to its strain rate dependency, the stress-strain behavior of articular cartilage has been

shown to be nonlinear, where larger increments of stress are observed for increasing strains (Brown et al., 2009; Charlebois et al., 2004; Deneweth et al., 2013b, 2015; Korhonen et al., 2002a).

The structure and orientations of the macromolecular constituents of articular cartilage directly contribute to directionalities in its mechanical response. This directional behavior manifests as tissue-level anisotropy (Jurvelin et al., 2003), depth-dependency (Schinagl et al., 1997), and spatial heterogeneity (Appleyard et al., 2003). Much of the directionality is related to the relative density and orientation of collagen fibers in the solid matrix (Brama et al., 2000a,b; Hunziker et al., 2007; Jurvelin et al., 2003; Mow and Guo, 2002). There is a significant asymmetry in the tensile and compressive mechanical responses of collagen fibers, which typically dictates the preferred material direction(s) (Buehler, 2006; Huang et al., 2003; Soltz and Ateshian, 2000; Woo et al., 1979). The structure of the solid matrix also affects fluid flow, and, consequently, the flow-dependent components of the mechanical behavior of articular cartilage (Federico and Herzog, 2008).

As the composition of the solid phase of articular cartilage varies through its depth, so too do its mechanical properties (Julkunen et al., 2008; Saarakkala et al., 2010). The compressive modulus of articular cartilage increases significantly from its articular surface to bony interface (Klein et al., 2007; Schinagl et al., 1997). There also exists a complex relationship between cartilage depth and its response to shear loading (Buckley et al., 2008; Motavalli et al., 2014; Silverberg et al., 2013) and hydraulic permeability (Chen et al., 2001; Federico and Herzog, 2008; Gannon et al., 2012). Similar structural variations result in the mechanical response of articular cartilage exhibiting a spatial dependency. The mean stiffness of femoral cartilage has been shown to be greater than the tibial cartilage (Arokoski et al., 1999; Deneweth et al., 2013b, 2015). Within the femoral cartilage, cartilage found on the condyles tends to be stiffer than that located on the trochlea (Jurvelin et al., 2000; Swann and Seedhom, 1993). Furthermore, cartilage predominately covered by the menisci on the perimeter of the tibial plateau has been shown to be stiffer than cartilage more centrally located on the plateau (Barker and Seedhom, 2001; Deneweth et al., 2013b; Thambyah et al., 2006). Within these zonal generalizations, the exact spatial distribution of articular cartilage mechanical properties is highly heterogeneous (Deneweth et al., 2013b, 2015; Jurvelin et al., 2000; Young et al., 2007). All this tissue-level directionality tends to lead to inhomogeneous distributions of deformation within the cartilage bulk, even for nearly uniform loading (Chan et al., 2009; Lai and Levenston, 2010; Neu et al., 2005).

2.2.3 Articular cartilage constitutive modeling

Continuum models of articular cartilage have run the gamut of complexities, from basic linear elastic to nonlinear, multiphysics models. Linear elasticity has proven largely successful at describing the small strain instantaneous and equilibrium responses of articular cartilage (Hayes et al., 1972; Jin and Lewis, 2004; Moshtagh et al., 2016; Sakamoto et al., 1996; Töyräs et al., 2001), and is still commonly employed in geometrically detailed whole knee computational models (Donahue et al., 2002; Kiapour et al., 2014a,b; Mootanah et al., 2014; Peña et al., 2005a, 2006a). Nonlinear elastic theories have also been used to describe articular cartilage (Brown et al., 2009; Deneweth et al., 2013a, 2015; Robinson et al., 2016; Schwartz et al., 1994; Świeszkowski et al., 2006). Assuming articular cartilage behaves as a single phase, a viscoelastic continuum has also been a useful framework for representing the creep and stress relaxation responses of cartilage (Han et al., 2012; Peters et al., 2017; Richard et al., 2013; Woo et al., 1980). Single phase theories have been particularly conducive to problems where an analytical solution, like indentation, is desired (Hori and Mockros, 1976; Jurvelin et al., 1997; Kiviranta et al., 2008; Lin et al., 2009).

To address the underlying composite phase composition of articular cartilage, multiphasic constitutive models have been developed to describe the time dependent behavior of articular cartilage. These models first assumed cartilage could be represented as an incompressible, linear elastic solid matrix permeated with an inviscid, incompressible fluid (Mow and Mansour, 1977; Mow et al., 1980; Torzilli and Mow, 1976a,b). Within this theory, stresses evolve as a function of both elastic strain and frictional resistance of fluid flowing through the solid matrix (Mow et al., 1984). Linear biphasic theory has been incredibly popular in representing the response of articular cartilage during confined compression (Armstrong and Mow, 1982; Schinagl et al., 1997; Soltz and Ateshian, 1998; Woo and Kwan, 1991), unconfined compression (Armstrong et al., 1984; Brown and Singerman, 1986; Spilker and Suh, 1990), and indentation (Mak et al., 1987; Miller and Morgan, 2010; Mow et al., 1989; Spilker et al., 1992). However, as traditionally posed, linear biphasic theory is limited by its implicit small strain assumption (Ateshian et al., 1997; Holmes and Mow, 1990) and inability to describe relatively low and high strain-rate deformations (Li et al., 2003).

Linear biphasic theory has been extended to more accurately capture certain aspects of real articular cartilage deformation. The solid phase is now more commonly assumed to be hyperelastic (Holmes and Mow, 1990), and this modification has proven beneficial in a variety of cartilage loading configurations (Ateshian et al., 1997; Kwan et al., 1990; Suh and Spilker, 1994). Nonlinearity within the biphasic framework has also been introduced through strain dependent permeability (Boschetti et al., 2004; Lai et al., 1981; Suh et al.,

1991). Various other deformation physics have been incorporated into biphasic cartilage theory, including poroviscoelasticity (DiSilvestro and Suh, 2001, 2002; DiSilvestro et al., 2001b,c; Ehlers and Markert, 2001; Mak, 1986a,b; Suh and Bai, 1998), fibril-reinforcement (Fortin et al., 2000; Li et al., 1999b; Soulhat et al., 1999), and tension-compression asymmetry (Huang et al., 2001; Soltz and Ateshian, 2000), as well as coupled cartilage swelling and ion transport (Gu et al., 1998; Lai et al., 1991; Lu and Mow, 2008; Wilson et al., 2005a,b).

Many of these articular cartilage constitutive models have been further generalized to allow for material directionality. Transversely isotropic, linear biphasic theory has been used to model the response of articular cartilage during compression (DiSilvestro et al., 2001c), indentation (Korhonen et al., 2002b), and impact loading (Garcia et al., 1998). Orthotropy has also been investigated in the context of linear biphasic theory (Bachrach et al., 1998). There have been a few efforts to consider the depth-wise heterogeneity of articular cartilage (Chegini and Ferguson, 2010; Li et al., 2000; Shirazi et al., 2008; Wang et al., 2001; Wilson et al., 2005b; Wu and Herzog, 2002). More recently, constitutive models that consider the spatial dependency of articular cartilage have also been developed (Deneweth et al., 2013a, 2015; Marchi and Arruda, 2017a; Mononen et al., 2012; Tanska et al., 2015).

2.3 Knee ligaments

Another important class of soft tissues in the knee are ligaments. There are four principal stabilizing ligaments in the knee: the ACL, PCL, MCL, and LCL. These ligaments connect one bone to another and help to maintain normal knee range of motion (Fu et al., 1993). Most ligamentous injuries in the knee, over 90% by some estimates (Miyasaka et al., 1991), involve the ACL and/or MCL (Gianotti et al., 2009). Recent studies have shown that women are disproportionately affected by ACL injury (Arendt et al., 1999; Hewett et al., 2005; Waldén et al., 2011). Due to their limited vascularization and innervation, ligaments tend to lack the ability to self-heal (Arnoczky, 1982; Duthon et al., 2006; Kennedy et al., 1974; Odensten and Gillquist, 1985; Petersen and Tillmann, 1999); notably, the MCL has shown some propensity for spontaneous repair following rupture (Frank et al., 1983; Kannus, 1988), however, the healed ligament structure and biochemistry are altered (Niyibizi et al., 2000; Weiss et al., 1991). In practice, this means that the effects of ligament injuries can be staggering and widespread. The absence of major ligament structures, in particular the ACL, is associated with significant secondary soft tissue damage and disease (Aglietti et al., 1997; Bach et al., 1998; Shelbourne et al., 1995; Yagi et al., 2002). Consequently,

surgical intervention is commonly required, but reconstruction poses similar adverse long-term implications for joint health (Andersson et al., 1989; Salmon et al., 2006; Selmi et al., 2006; Shelbourne et al., 2009). Therefore, the hope is that, with a more comprehensive understanding of ligament biomechanics, healing, and remodeling, new and innovative solutions for ligament injury prevention and reconstruction can be unlocked.

2.3.1 Knee ligament physiology

Fibroblasts are the predominate cell type found in ligaments (Birk and Trelstad, 1984). They are situated sporadically throughout and function to maintain a dense network of highly aligned collagen fiber bundles (Dodds and Arnoczky, 1994). The collagen structure of ligaments is remarkably hierarchical (Danylchuk et al., 1978; Provenzano and Vanderby, 2006). Individual tropocollagen triple helices group into fibrils, which in turn assemble into fascicles, and then into macroscopic ligament structures (Kastelic et al., 1978). Various volume fractions of extracellular tissue are found between and within each hierarchical level (Amis and Dawkins, 1991; Petersen and Tillmann, 2002). A schematic representation of the various levels of ligament structural organization can be seen in Fig. 2.5.

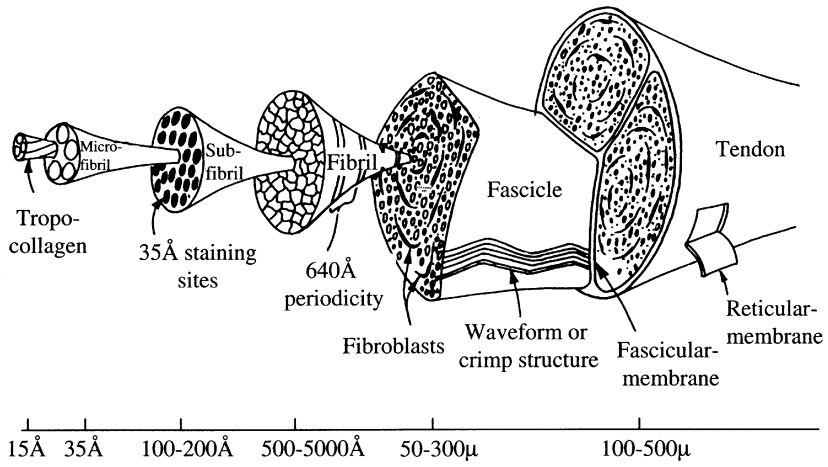

Figure 2.5: Hierarchical collagen structure in tendons and ligaments (Weiss and Gardiner, 2001).

Like articular cartilage, a large percentage of ligament total mass is trapped water (Daniel et al., 1990). Type I collagen makes up approximately 70-80% of the dry mass of ligaments (Amiel et al., 1983; Weiss and Gardiner, 2001), but other collagen types (II, III, V, X, XI, and XII) are also found within ligaments (Birk and Mayne, 1997; Fukuta

et al., 1998; Linsenmayer et al., 1993; Liu et al., 1995; Niyibizi et al., 1996; Visconti et al., 1996). Throughout a majority of ligaments, collagen has a wavy morphology (Danylchuk et al., 1978; Ottani et al., 2001). This feature can readily be observed optically or via second harmonic generation (Cox et al., 2003; Franchi et al., 2007; Williams et al., 2005; Yahia and Drouin, 1989); a representative image is shown in Fig. 2.6.

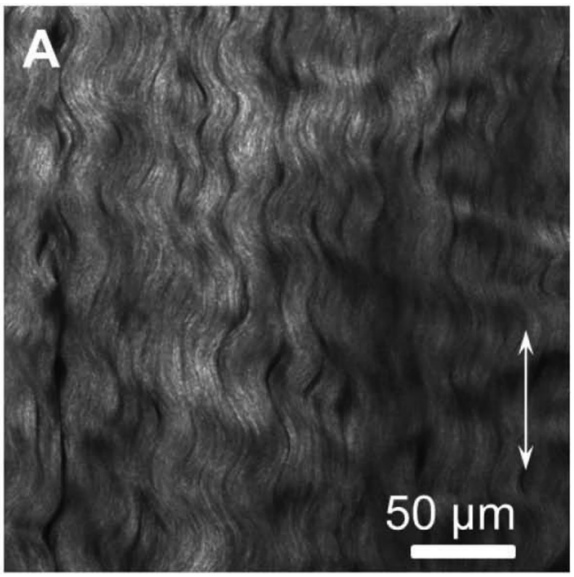

Figure 2.6: MCL collagen microstrctural arrangement acquired with second harmonic generation (Henninger et al., 2015). Arrow indicates the mean collagen fiber direction.

The structural complexities of ligaments are not limited to their bulk. The attachments, or entheses, of ligaments to bones are characterized by their own unique microstructures. At its enthesis, a relatively compliant ligament transitions to much stiffer bone (Liu et al., 2014). Interfaces with a high mechanical mismatch typically lead to the development of stress concentrations (Williams, 1952), but it has been shown that ligament entheses are constructed to minimize this effect (Genin and Thomopoulos, 2017; Genin et al., 2009; Thomopoulos et al., 2006). Within the attachment zone, there exists a distribution of tissues (Arnoczky, 1982; Cooper et al., 1970), with distributions of mineralizations and macromolecular orientations (Benjamin et al., 2002; Moffat et al., 2008; Petersen and Tillmann, 1999; Schwartz et al., 2012; Wopenka et al., 2008). Other attenuating mechanisms exist at the transition between ligaments and bone, including interdigitation of the bone with the ligament bulk, smooth geometric transitions from bone to ligament, and optimizing ligament insertion angles (Liu et al., 2011). Ligament entheses can be direct, like that shown in Fig. 2.7, or indirect (Zhao et al., 2017). Direct attachments are generally well-defined, with collagen oriented normal to the bone surface (Benjamin and Ralphs, 1998; Iwahashi et al., 2010). In indirect attachments, there is a more gradual transition from ligament to

bone, and collagen fibers tend to terminate into the transitional fibrocartilage at more acute angles (Benjamin et al., 1986; Moulton et al., 2017).

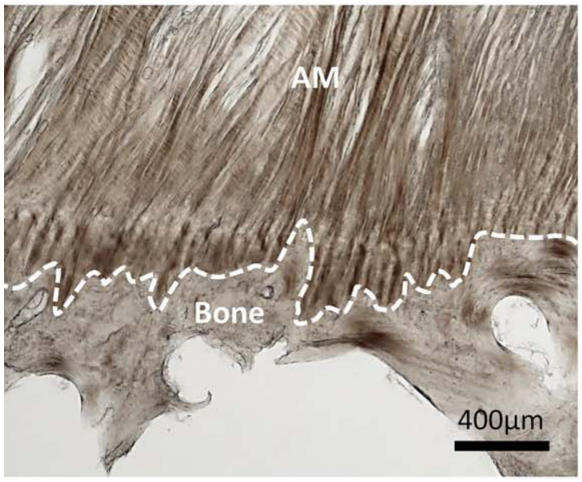

Figure 2.7: Enthesial topology and collagen fiber organization of the ACL, an example of a direct enthesis (Zhao et al., 2017).

The macroscopic anatomies of the four main stabilizing ligaments have various levels of spatial configurational intricacies. The MCL is a long, ribbon like structure, which runs distally from the medial femoral epicondyle to the posteromedial aspect of the metaphysis of the tibia (Liu et al., 2010b). Geometrically similar, the LCL spans distally from the lateral femoral epicondyle to the top of the fibular head (Meister et al., 2000). The two cruciate ligaments cross each other and are located within the center of the joint (Girgis et al., 1975). The PCL extends from the posterior tibial intercondylar region to the anterolateral portion of the femoral intercondylar fossa (Van Dommelen and Fowler, 1989). With a nearly opposite spatial configuration, the ACL originates from the anterior tibial intercondylar region and ends in the posterolateral region of the femoral intercondylar fossa (Arnoczky, 1982; Kennedy et al., 1974). Furthermore, the ACL is not a single ligament structure, but instead composed from two macroscopically identifiable, but coordinated, fiber bundles (Amis et al., 2005; Dienst et al., 2002; Petersen and Zantop, 2007). The spatial configurations of the bundles of the ACL, the anteromedial bundle (AMB) and posterolateral bundle (PLB), can be seen physically separated in Fig. 2.8. Within the gross attachment areas of the ACL, the AMB emanates from and terminates at the anteroproximal and anteromedial regions of the femur and tibia, respectively (Edwards et al., 2007; Takahashi et al., 2006). The attachment area of the PLB makes up the balance of the total ACL bony footprint, originating at the posterodistal region of the femoral attachment and inserting at the posterolateral region of the tibial attachment (Edwards et al., 2008; Harner et al., 1999). The individual bundles of the ACL are thought to provide significant con-

tributions to knee function, with the AMB and PLB playing an important role in limiting anterior-posterior (A-P) translations and internal tibial rotations, respectively (Yagi et al., 2002).

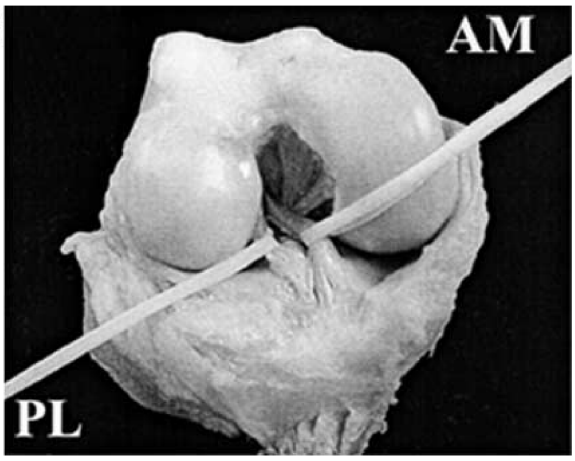

Figure 2.8: Representative image of the spatial configurations of the AMB and PLB (Loh et al., 2003).

2.3.2 Knee ligament mechanics

Like with articular cartilage, the macromolecular structure of ligaments significantly contributes to and dictates their mechanical properties. Differences in the relative densities and distributions of their constituents can be directly correlated with ligament mechanical properties, driven by the breadth of their functional requirements (Woo et al., 2006). Factors like collagen fiber diameter (Hart et al., 1992), fibroblast morphology (Lyon et al., 1991), and collagen type volume fractions (Amiel et al., 1983) vary with ligament type and directly affect mechanics. There have been countless studies that aim to characterize the mechanical response of structural ligaments. The primary function of ligaments is to transmit loads between bones; therefore, most efforts have focused on the apparent uniaxial behavior of ligaments along their mean collagen fiber direction (Butler et al., 1990; Chandrashekar et al., 2006; Jones et al., 1995; Ma and Arruda, 2013; Mallett and Arruda, 2017; Noyes and Grood, 1976; Paschos et al., 2010; Quapp and Weiss, 1998; Race and Amis, 1994; Setton et al., 1994; Smith et al., 1996; Warden et al., 2006; Woo et al., 1983, 1991). The resulting stress-strain relationships of ligaments tend to follow the prototypical curve shown in Fig. 2.9, where, in the elastic region, an initial nonlinear region is followed by a more linear response. These experiments are useful tools for quantifying material properties like terminal stiffness, ultimate stress, and strain at failure. Using these classic

mechanical characterization techniques, the tangent stiffness of the MCL has been shown to be approximately twice that of the ACL (Woo et al., 1992). Similarly, the ultimate tensile strength and stiffness of the AMB is greater than the PLB (Butler et al., 1992; McLean et al., 2015; Skelley et al., 2015, 2016; Wright et al., 2016). However, these methods tend to be sensitive to geometric (Girgis et al., 1975), environmental (Noyes et al., 1974), and configurational (Beynnon et al., 1992) factors.

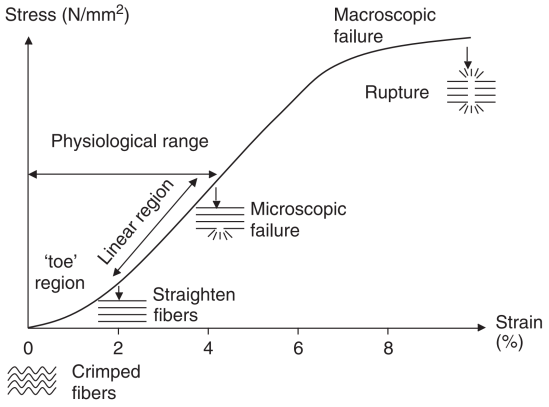

Figure 2.9: Typical observed macroscopic stress-strain behavior of ligaments and tendons (Wang, 2006).

Given the microstructural arrangement of collagen within ligaments, a certain degree of anisotropy in their mechanical response is to be expected. Indeed, there has been some evidence that the response of ligaments is substantially more compliant normal to its mean collagen fiber direction (Gardiner and Weiss, 2003; Quapp and Weiss, 1998); however, the relative magnitude of ligament anisotropy is still unclear. There are new data in the transverse direction that imply an even more compliant response (Henninger et al., 2013, 2015), but, given the limited and conflicting nature of these data, any definitive conclusions concerning ligament anisotropy are currently premature.

The interactions between ligament macromolecules and between solid and liquid constituents tend to result in time and history dependent deformation physics. Creep and stress relaxation experiments have been used to help describe the response of ligaments in the time domain (Abramowitch and Woo, 2004; Grood and Noyes, 1976; Kwan et al., 1993; Woo et al., 1981). Looking at multiple strain levels during stress relaxation experiments, it has been shown that there exists a nonlinear relationship between strain and relaxation in ligaments (Hingorani et al., 2004; Provenzano et al., 2001; Thornton et al., 1997). The stress-strain behavior of ligaments also depends on the applied rate of loading (Bonner et al., 2015; Pioletti et al., 1999; Woo et al., 1990), displays hysteresis upon unloading

(Gillis et al., 1995; Woo et al., 1986b), and is history dependent (Bonifasi-Lista et al., 2005; Markolf et al., 2002; Quinn and Winkelstein, 2011; Yahia and Drouin, 1990).

2.3.3 Knee ligament constitutive modeling

Ligaments found in the body are real, three-dimensional structures. Yet, it is still common to find ligaments represented computationally as uniaxial springs (Abdel-Rahman and Hefzy, 1998; Adouni et al., 2012; Beillas et al., 2004; Bendjaballah et al., 1997; Blankevoort and Huiskes, 1996; Li et al., 1999a, 2002; Marouane et al., 2014; Mesfar and Shirazi-Adl, 2005; Shin et al., 2007; Shirazi and Shirazi-Adl, 2009a,b) or two-dimensional shells (Ellis et al., 2007; Newman et al., 2003). Furthermore, despite all the aspects of their strain, history, and time dependent biomechanics, a large portion of computational models that include continuum ligament realizations are constructed assuming transversely isotropic, hyperelastic material behaviors. There is now a large and ever growing pool of transversely isotropic, hyperelastic constitutive theories used to describe ligaments, largely built using the separable strain energy framework developed by Weiss et al. (1996). This class of material models has enjoyed some success in representing the stress-strain behavior of the MCL along and transverse to its mean collagen fiber direction (Quapp and Weiss, 1998). These theories are extensively detailed and summarized in **Chapter 5**.

Viscoelasticity has been incorporated into a variety of ligament constitutive models. Structural elastic theories, like that developed by Lanir (1979), have been extended to include viscoelastic effects (Decraemer et al., 1980; Lanir, 1983). Viscoelasticity has also been added to ligament material descriptions using mechanical analogs adopted from rheology (Bischoff et al., 2004; Ma and Arruda, 2013; Machiraju et al., 2006; Pande et al., 1977; Sanjeevi, 1982; Zhang et al., 2007), as well as using ideas from the polymer mechanics community (Bingham and DeHoff, 1979; Dehoff, 1978). Nonlinear viscoelastic models have also been developed for and applied to ligaments. In particular, the single integral finite strain model incorporates fading memory and fiber recruitment (Johnson et al., 1996; Lakes and Vanderby, 1999). It can be linearized to yield classic linear viscoelasticity and finite strain elasticity can be recovered for very short and long times (Woo et al., 2006).

2.4 Summary

Soft tissue injuries and diseases are simultaneously prolific, complicated, and debilitating. Clinicians still do not have general solutions to problems like OA and ligament failure. Sufficient prevention strategies are lacking, and reconstructive procedures plagued by col-

lateral effects. Acute and degenerative soft tissue injuries and diseases are on the rise, relentlessly affecting younger and younger individuals. There are strong indications that abnormality begets the development and progression of these conditions. When certain soft tissues are compromised, loading shifts within the joint. These alterations may be the key to understanding the mechanical bases for injury and disease, and minimizing these deviations from nominal knee motion and intrajoint contact may provide the opportunity to devise optimal preventative and reconstructive techniques. Computation has opened the door to previously unobtainable distributions of individuals, with near infinite permutations available to investigate the mechanical effects of factors across length and time scales. However, fundamental to their success is the inclusion of physiologically and mechanically representative constitutive models.

CHAPTER 3

A study on the role of articular cartilage soft tissue constitutive form in models of whole knee biomechanics

This chapter has been previously published and may be referenced as:

> B. C. Marchi and E. M. Arruda. A study on the role of articular cartilage soft tissue constitutive form in models of whole knee biomechanics. *Biomechanics and Modeling in Mechanobiology*, 16(1):117–138, 2017a

3.1 Introduction

Computational models of whole joint biomechanics have the potential to be extremely powerful clinical tools. They provide researchers and clinicians with the opportunity to investigate the importance of individual tissue structures in the contexts of native and abnormal joint motions. Joints are incredibly complex mechanical systems characterized by their nontrivial geometry and intrinsically coupled behavior, and numerical tools can offer insights into both local tissue deformation and global joint kinematics with normal physiology by illustrating the role of each constituent tissue structure in maintaining functionality. Physiological effects corresponding to age, sex, usage, injury, and disease affect realized joint motion, and this variation may substantially contribute to a cascade of tissue degeneration, leading to a progression of diminished joint performance. Therefore, understanding the normal operating conditions of joints is paramount in building computational frameworks capable of making meaningful predictions related to factors that precipitate traumatic injury, like ligament rupture, and degenerative diseases, like OA.

The human knee is a biarticulating lower limb joint whose stability and performance are maintained by a variety of integral hard and soft biological structures including bones, ligaments, tendons, muscles, cartilage, and menisci. Soft tissues are particularly vulnerable to injury, both acute and progressive. The ACL is an important translation and rotation stabilizing tissue, attaching proximally to the distal lateral femoral condyle and terminating distally on the anterior tibial plateau. The ACL is the most commonly injured and surgically reconstructed ligament, with an estimated 175,000 reconstructions performed in the

United States alone with an associated cost of over 2 billion dollars (Spindler and Wright, 2008). Not only is there an exceedingly high incidence of ACL traumatic injury, but the frequency of rupture is drastically increasing (Kim et al., 2011b) and the mean age is dropping with profound and lasting effects (Ingram et al., 2008; Kessler et al., 2008). Young women are particularly susceptible ACL injury, with a 4 to 6 times elevated risk compared to young men, and the preponderance of ACL injuries in young people are noncontact, without external trauma (Hewett et al., 2005).

While the acute success rate of current surgical interventions for ACL injury are as high as 87% (Wright et al., 2008), there are potentially significant long-term secondary effects associated with reconstruction. OA is a degenerative tissue disease that presents with pain, loss of mobility, and degradation of articular cartilage integrity. Despite the high incidence of OA, which affects approximately 15% of the adult population in the United States (Lawrence et al., 2008), the underlying mechanisms of the disease initiation and progression remain unclear. ACL reconstruction is potentially linked to OA through associated biomechanical alterations of the knee relative to joints with native physiology (Kessler et al., 2008; Lohmander et al., 2004; Petersson and Jacobsson, 2002), manifesting in differences between macroscopic kinematics and soft tissue contact within the joint capsule (Deneweth et al., 2010). Therefore, as the mean age of ACL rupture and other soft tissue traumas, like meniscal tears, decreases, so to does the onset of degenerative diseases, seriously threatening the sustained quality of life of an ever increasing patient population.

While it is often difficult for experimental studies to accurately capture a comprehensive description of joint behavior, they have been instrumental in furthering the understanding of native and deficient joint biomechanics. Various experimental and clinical efforts have examined the role of physiological and morphological risk factors for ligament injury (Alentorn-Geli et al., 2009; Beaulieu et al., 2014, 2015; Bedi et al., 2014; Hashemi et al., 2010a; Krosshaug et al., 2007a; Lipps et al., 2012; Meyer and Haut, 2008; Wall et al., 2012; Withrow et al., 2006). These works begin to provide possible explanations for soft tissue injury initiation and disease progression mechanisms, and offer a convenient starting point for clinical evaluations and diagnostics. However, they are fundamentally limited in their inability to capture the complex, simultaneous global and local biomechanics starting from a stress free reference configuration (Amis and Dawkins, 1991; Hirokawa and Tsuruno, 2000; McLean et al., 2015; Yamamoto et al., 1998), information critical for systematic constitutive evaluation. Additionally, experimental studies are limited by resources. Researchers often find it challenging to obtain cadaveric specimens, and near impossible to characterize statistically significant sample sizes of tissues that have never been frozen—especially whole joint specimens. The viability of tissue is critical because the mechanical

properties of tissues can be significantly altered by freezing and thawing (Gottsauner-Wolf et al., 1995; Maiden and Byard, 2016; Stemper et al., 2007), though there is still uncertainty related to the magnitude of this effect (Pelker et al., 1983; Woo et al., 1986a). It is also demanding to collect a clinically representative population of test specimens that accurately captures the breadth of physiologies and anatomies to isolate factors that contribute to injury and disease.

This is where computational models of whole joint biomechanics enter. Whole knee models have been used to examine individual soft tissue contributions during physiologically relevant loading conditions where traditional experimental methods prove impractical or impossible. Numerical models are uniquely situated to describe individual tissue deformation while quantifying joint motion (Abdel-Rahman and Hefzy, 1998; Adouni et al., 2012; Beillas et al., 2004; Bendjaballah et al., 1997; Blankevoort and Huiskes, 1996; Donahue et al., 2002; Gardiner and Weiss, 2003; Hirokawa and Tsuruno, 2000; Kang et al., 2015; Kiapour et al., 2014a; Li et al., 1999a; Limbert et al., 2004; Mootanah et al., 2014; Peña et al., 2006a; Penrose et al., 2002; Quatman et al., 2011; Shelburne et al., 2006; Song et al., 2004; Xie et al., 2009; Zhang et al., 2008), to perform parametric studies to analyze individual tissue constitutive and structural effects (Atmaca et al., 2013; Baldwin et al., 2012; Donahue et al., 2003; Kiapour et al., 2014b; Li et al., 2002; Marouane et al., 2014; Mesfar and Shirazi-Adl, 2005; Peña et al., 2005a; Shin et al., 2007; Shirazi and Shirazi-Adl, 2009a,b; Wang et al., 2014), and to provide a platform for the evaluation of surgical intervention techniques (Bae et al., 2015; Godest et al., 2002; Halloran et al., 2005; Huang et al., 2012; Kim et al., 2011a; Ramaniraka et al., 2007). These contributions represent a substantial effort in the pursuit of elucidating joint biomechanics; however, not fully appreciating the inherent simplifications and approximations within a particular model or study can lead to potentially spurious conclusions, often with meaningful clinical consequences.

Computational models can be differentiated by their level of anatomic representation, numeric implementation, physical motivation for constraints and boundary conditions, and constitutive complexity. Anatomic simplifications usually manifest as the absence of structures from the model, either hard or soft tissues. It is common practice to remove the patellofemoral joint entirely (Abdel-Rahman and Hefzy, 1998; Atmaca et al., 2013; Bae et al., 2015; Bendjaballah et al., 1997; Blankevoort and Huiskes, 1996; Donahue et al., 2002, 2003; Hirokawa and Tsuruno, 2000; Huang et al., 2012; Limbert et al., 2004; Shirazi and Shirazi-Adl, 2009a,b; Song et al., 2004; Xie et al., 2009; Zhang et al., 2008), or to assume uniaxial representations of critical tissue structures (Abdel-Rahman and Hefzy, 1998; Adouni et al., 2012; Beillas et al., 2004; Bendjaballah et al., 1997; Blankevoort and Huiskes, 1996; Li et al., 1999a, 2002; Marouane et al., 2014; Mesfar and Shirazi-Adl, 2005;

Shin et al., 2007; Shirazi and Shirazi-Adl, 2009a,b). Important supporting tissue structures like the articular cartilage (Abdel-Rahman and Hefzy, 1998; Bae et al., 2015; Baldwin et al., 2012; Limbert et al., 2004; Song et al., 2004; Xie et al., 2009; Zhang et al., 2008), menisci (Abdel-Rahman and Hefzy, 1998; Bae et al., 2015; Baldwin et al., 2012; Blankevoort and Huiskes, 1996; Gardiner and Weiss, 2003; Song et al., 2004; Xie et al., 2009; Zhang et al., 2008), and ligaments (Atmaca et al., 2013; Bae et al., 2015; Beillas et al., 2004; Donahue et al., 2002, 2003; Limbert et al., 2004; Song et al., 2004; Xie et al., 2009; Zhang et al., 2008) are also frequently ignored and removed from the joint model.

Individual tissue material descriptions are also diverse, though representations typically fall on the simple end of the continuum of constitutive complexity, especially in comprehensive computational joint models. In whole knee models, tissue material properties are usually determined from limited experimental data—see Weiss et al. (2005) for a discussion of challenges associated with constitutive model construction specifically for ligaments in the context of finite element (FE) models—explicitly tuned to match expected joint motion (Mootanah et al., 2014), or adjusted to minimize deviations from experimentally determined tissue deformation (Donahue et al., 2003).

While there are costs associated with increasing constitutive complexity, they are usually offset by the gains in model accuracy and the corresponding clinical relevance. However, these gains tend to have a diminishing marginal rate of return with respect to complexity. This compromise has led to a significant and concerted shift from simple, isotropic material models for ligaments toward physiologically and experimentally motivated transversely isotropic, hyperelastic descriptions—Kiapour et al. (2014b) offers a brief investigation into the biomechanical influence of incorporating a transversely isotopic, hyperelastic ACL constitutive response in a whole knee model. Curiously, the same trend towards complexity in assumptions of articular cartilage constitutive behavior has not been observed (Atmaca et al., 2013; Beillas et al., 2004; Donahue et al., 2002, 2003; Huang et al., 2012; Kang et al., 2015; Kiapour et al., 2014a,b; Li et al., 2002; Mootanah et al., 2014; Oh et al., 2012; Peña et al., 2005a, 2006a; Quatman et al., 2011; Ramaniraka et al., 2007; Shelburne et al., 2006; Wang et al., 2014; Withrow et al., 2006).

In this study we show the tremendous impact of articular cartilage constitutive assumptions, derived from rigorous experimental observations, on predicted localized tissue deformation and macroscopic joint kinematics. By illustrating the relationship between complexity and accuracy for articular cartilage it is feasible to construct biomechanical models that are as accurate as possible in critical regions, while simultaneously using previously accepted results in the literature to motivate simplifications elsewhere in the model where the effects are less pronounced. This combination of assumptions yields models that have

high clinical fidelity and low computational cost.

We explored the role of articular cartilage constitutive assumptions by examining the relative differences between increasing levels of complexity. Tibial and femoral articular cartilages have been shown to be mechanically nonlinear and transversely isotropic, and also, cartilage material properties have a substantial location dependence (Appleyard et al., 2003, 2001; Athanasiou et al., 1991; Briant et al., 2015; Deneweth et al., 2013a,b, 2015; Jurvelin et al., 2000; Swann and Seedhom, 1993; Thambyah et al., 2006; Young et al., 2007). The sensitivity of traditional linear elastic, isotropic cartilage models is examined and compared to nonlinear, transversely isotropic articular cartilage definitions; the sensitivity of this homogeneously applied nonlinear and transversely isotropic constitutive model is also explored. We also show the importance of the incorporation of cartilage heterogeneity, highlighting the required level of mathematical complexity necessary to capture the tissue deformation and joint motion simultaneously.

3.2 Methods

A three dimensional, subject specific FE model was constructed to evaluate the role of articular cartilage constitutive complexity on local tissue deformation and joint kinematics. The kinematics were monitored throughout the foot flat portion of the stance phase of gait, while the maximum tissue deformations were compared at the time within the loading cycle of maximum ground reaction force. The foot flat portion of the stance phase of gait was modeled in an explicit FE framework to accurately capture all time dependent and inertial effects. The model included major tissue and bone structures contained in healthy knee joints; soft tissues in the joint—ligaments, muscles, tendons, articular cartilage, and menisci—were modeled based on experimental evidence of constitutive responses.

3.2.1 Geometry and Mesh Generation

The tissue geometries contained within the FE model were obtained from the right knee of a healthy adult female with no history of lower limb injuries or pathologies using a combination of computerized tomography (CT) and MRI modalities. The images, in the axial, sagittal, and coronal planes, were acquired with slice thickness and inplane resolution equal to 0.35 mm and (527×527), respectively, with the individual oriented in the supine position. The image slices were imported into Mimics V17.0 (Materialise, Leuven, Belgium), allowing for the segmentation of individual tissue structures. The three dimensional surfaces created in Mimics were smoothed and defeatured to minimize geometric

artifacts generated during the segmentation process—Wittek et al. (2015) provides a thorough review of the current state of the art in geometry extraction specifically for models of computational biomechanics.

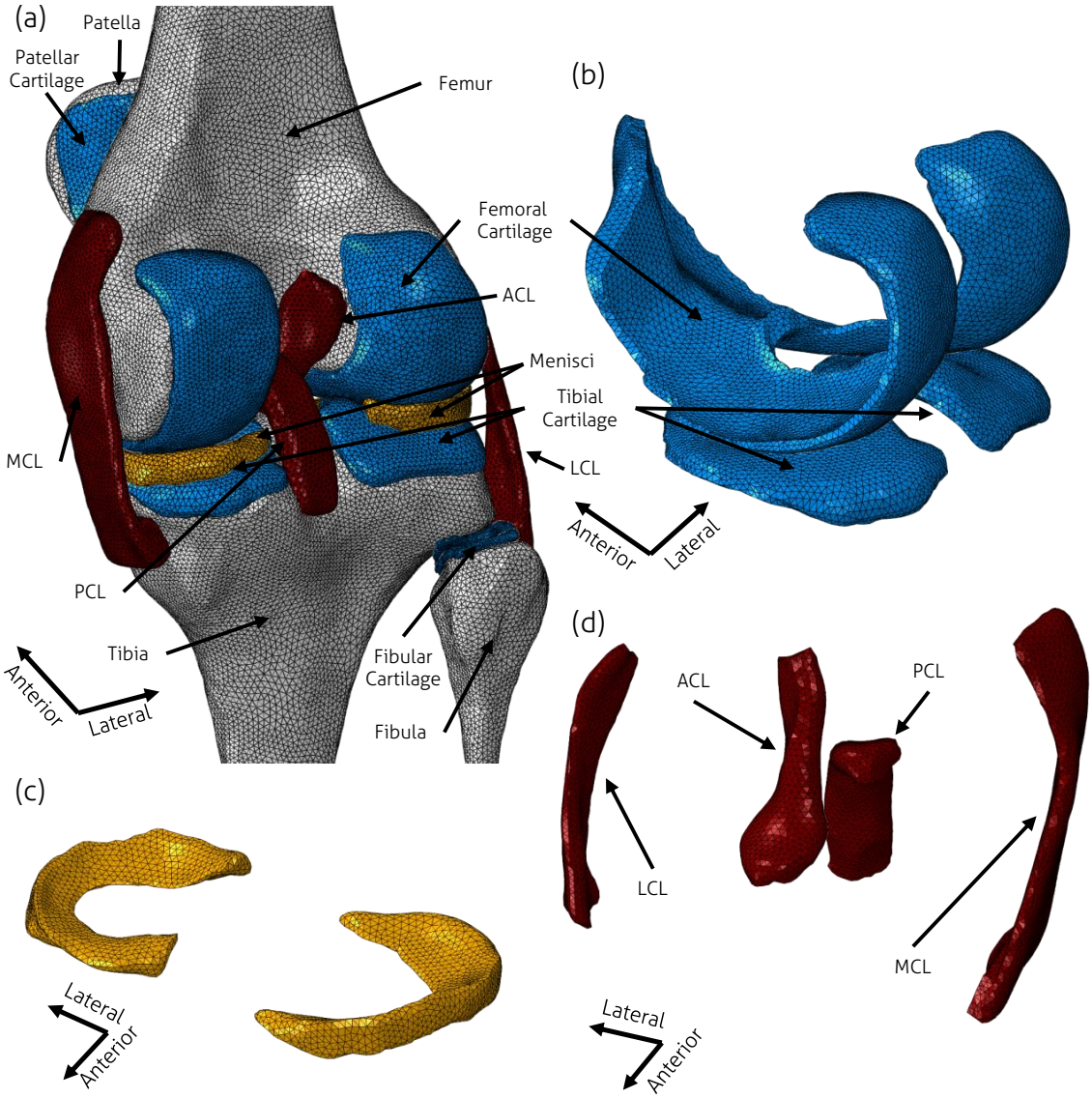

Figure 3.1: (a) Computational FE model of the right knee of a healthy adult female and its soft tissue constituents. The geometric accuracies of the articular cartilage (b), menisci (c), and supporting ligaments (d) are highlighted. In each figure cartilage is displayed in blue, menisci in orange, ligaments in red, and bones in white.

Smoothed surface representations of tissues were converted into FE meshes using Hypermesh 12.0 (Altair HyperWorks, Troy, Michigan, United States). All tissue structures, hard and soft tissues, were meshed using 4 node tetrahedral elements with linear shape functions. Soft tissue meshes for ligaments and cartilages were modified to account for

any gaps or overlaps resulting from segmentation, smoothing, and defeaturing by projecting the nodal boundary nearest to the bone surface onto the external perimeter of the bone, yielding a model with exactly matching mesh boundaries between structures following the procedure described in Mootanah et al. (2014). Element sizes for bones were selected to minimize element count, while preserving geometric features. The characteristic element size for the ligaments, cartilages, and menisci were determined in a similar manner; however, element sizes were verified by performing a convergence analysis to ensure that calculated strains and joint kinematics were mesh density independent. Mesh density independence was determined using the criteria outlined in Donahue et al. (2002). The model was assumed to converge when the next level of mesh refinement—characterized by a reduction in the average characteristic element length by approximately 25%—did not yield deviation in deformation and kinematic quantities outside the Donahue et al. (2002) criteria. Figure 3.1 shows the three dimensional tissue representations incorporated in the knee joint model.

Absent from Figure 3.1 are the remainder of the knee ligament and muscle structures. The meniscal ligaments, trans-knee muscles, muscle tendons, and auxiliary ligaments were modeled using uniaxial elements. Uniaxial elements for these tissue types represent a good trade-off between the computational burden of the model and maintaining the accuracy of results in the predominately load carrying tissues (Kiapour et al., 2014a). All meshed geometries and uniaxial tissues structures were incorporated in a general purpose FE code, ABAQUS v6.13 (SIMULA, Providence, Rhode Island, United States), and assembled into the final knee joint FE model.

3.2.2 Constitutive Modeling

Individual tissues were modeled using a combination of experimental data and accepted numerical models available in the literature. Bones—femur, tibia, patella, and fibula—were defined as rigid bodies, as their deformation has been shown to have minimal impact on soft tissue deformation of whole joint biomechanics models (Donahue et al., 2002). The density of bones was assumed to be constant regardless of bone type (cortical or trabecular) at 2 g/cm^3. This approximation to the true distribution of densities within bones does not appear to substantially affect tissue deformations within the context of this study, with the maximum ratio of kinetic to strain energy during the simulations on the order of 0.05.

The menisci were modeled using a transversely isotropic, linear elastic material description; the local material directions were defined cylindrically, with the preferred direction oriented circumferentially around the menisci. The material parameters for the menisci

were as follows: Young's moduli: $E_1 = 20$ MPa, $E_2 = 120$ MPa, and $E_3 = 20$ MPa; Poisson's ratios: $\nu_{12} = 0.3$, $\nu_{13} = 0.45$, and $\nu_{23} = 0.3$; density: 1.5 g/cm^3, where direction 1 is radial, direction 2 is circumferential, and direction 3 is oriented axially along the bone (Skaggs et al., 1994; Tissakht and Ahmed, 1995). The menisci were attached to the tibial plateau using multiple uniaxial representations of the meniscal horn attachment ligaments; the stiffness of the meniscal ligaments was determined by calculating the total number of uniaxial elements, total effective area of attachment, and average ligament length to compute force displacement relationships corresponding to an effective Young's modulus equal to 111 MPa (Donahue et al., 2002; Villegas et al., 2007).

The four major supporting ligaments in the knee—the ACL, the PCL, the MCL, and the LCL—provide stability to the joint during normal activity. Knee supporting ligaments are hierarchical structures composed of highly organized and aligned collagen fibrils embedded in a compliant extracellular matrix, and this structure directly contributes to the nonlinear, anisotropic response of the tissues (McLean et al., 2015; Weiss et al., 2005). The supporting ligaments were modeled using a transversely isotropic extension of an isotropic eight-chain model for rubber elasticity originally proposed by Arruda and Boyce (1993) (Bischoff et al., 2002a). The geometric representations of the ACL, LCL, MCL, and PCL can been seen in Fig. 3.1d. The strain energy density function for the supporting ligaments can be expressed as

$$\begin{aligned} U(\mathbf{x}) =& U_0 + \frac{C_r}{4}\left(N\sum_{i=1}^{4}\left[\frac{\rho^{(i)}}{N}\beta_\rho^{(i)} + \ln\frac{\beta_\rho^{(i)}}{\sinh\beta_\rho^{(i)}}\right]\right. \\ &\left. - \frac{\beta_P}{\sqrt{N}}\ln\left[\lambda_{\mathbf{a}}^{a^2}\lambda_{\mathbf{b}}^{b^2}\lambda_{\mathbf{c}}^{c^2}\right]\right) + \frac{B}{\alpha^2}\left\{\cosh\left[\alpha\left(J-1\right)\right]-1\right\}, \end{aligned} \tag{3.1}$$

where the chains are representative of the protein structures present in soft tissues (e.g., collagen and elastin networks), U_0 is a constant, C_r is the rubbery modulus, $\sqrt{N}$ is the root mean square chain length in the reference configuration, $\rho^{(i)}$ is the deformed chain length in the current configuration of the i^{th} chain, $\lambda_{\mathbf{a}}$, $\lambda_{\mathbf{b}}$, $\lambda_{\mathbf{c}}$ are the stretches along the principal material axes **a**, **b**, **c**, respectively (depicted in Fig. 3.2), a, b, c are the normalized dimensions of the representative volume element (RVE) (see Fig. 3.2), B is the bulk modulus, α describes curvature of the relationship between hydrostatic pressure and volume at large volume changes, and J is the determinant of the deformation gradient. From non-Gaussian probability density functions of freely jointed chains,

$$\beta_\rho^{(i)} = \mathcal{L}^{-1}\left(\rho^{(i)}/N\right) \tag{3.2}$$

and

$$\beta_P = \mathcal{L}^{-1}\left(P/N\right), \tag{3.3}$$

where P is the undeformed chain length, $P = \sqrt{N} = \frac{1}{2}\sqrt{a^2 + b^2 + c^2}$, and $\mathcal{L}^{-1}\left(x\right)$ is the inverse Langevin function. To reduce the orthotropic constitutive equation presented in Eq. 3.1 to describe transversely isotropic continua, two of the nondimensional lengths are set to be equal ($a = b$, $b = c$, or $a = c$).

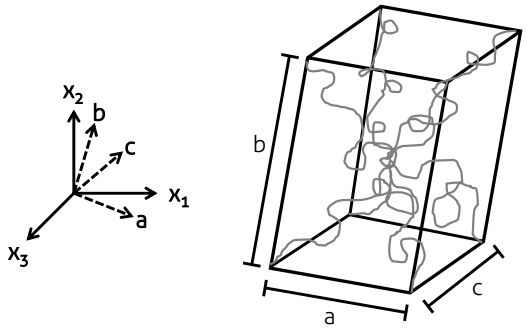

Figure 3.2: RVE of orthotropic eigth-chain network model, with material axes **a**, **b**, **c** and nondimensional lengths a, b, c. Figure adapted from Bischoff et al. (2002a).

The constitutive descriptions for each supporting ligament were determined by fitting Eq. 3.1 to uniaxial experimental data. The fitting of Eq. 3.1 to experimental data is nontrivial and involves finding the optimal material parameters within a system of nonlinear, coupled equations at each stretch since no closed form relationship between uniaxial stretch and stress exists. Constitutive parameters were determined using differential evolution (Storn and Price, 1997) to maximize the coefficient of determination, R^2, for the experimental data corresponding to each ligament using an approximate form of the inverse Langevin function (Marchi and Arruda, 2015) by minimizing the error of the fitted model to the experimental data. The MCL and LCL were modeled identically (Peña et al., 2006a) using experimental data from Quapp and Weiss (1998). Data for the uniaxial response of the PCL was obtained from Butler et al. (1990). The ACL is a structurally complex ligament composed of two independent fiber bundles (AMB and PLB), each with discrete material properties (Ma and Arruda, 2013; McLean et al., 2015). In this work the ACL was modeled as structurally homogeneous, assuming a continuous tissue bulk, with its constitutive response determined by fitting the average response of the two fiber bundles. Figure 3.3 illustrates the individual ACL fiber bundle constitutive responses (McLean et al., 2015), the numerically implemented bulk, averaged response, and the ability of Eq. 3.1 to capture the nonlinearity of this tissue in uniaxial extension. Due to the near incompressibility of the supporting ligaments α was assumed to be equal to unity. The material parameters of

Eq. 3.1 for each supporting ligament are presented in Table 3.1. Note the density of each ligament was assumed to be constant regardless of ligament type (Dhaher et al., 2010), and the preferred fiber direction, **a**, was oriented axially along the length of each ligament.

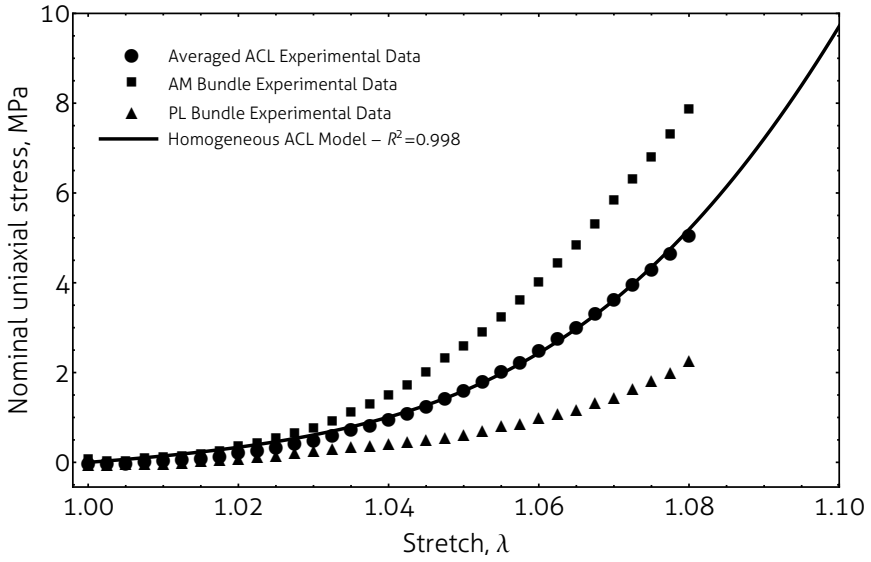

Figure 3.3: Uniaxial loading curves for AMB and PLB of the ACL, and the corresponding averaged response assuming equal contributions from each fiber bundle.

Table 3.1: Supporting ligament material properties

	$\rho\,(\mathrm{g/cm^3})$	$C_r\,(\mathrm{MPa})$	a	$b=c$	$B\,(\mathrm{MPa})$	α
ACL	1	0.13765	1.5532	1.0049	100	1
PCL	1	0.93447	1.5996	0.96781	100	1
MCL/LCL	1	0.44865	1.6172	0.95308	100	1

Given the expected loading rates during normal and injury causing activities, constitutive behavior of the patellar cartilage was assumed to be isotropic and hyperelastic (Oloyede et al., 1992), with material parameters adopted from Kiapour et al. (2014a) by matching the small strain behavior from linear elasticity. The force versus displacement relationships of the trans-knee muscles, muscle tendons, and auxiliary ligaments were obtained from relevant studies in the literature (Abdel-Rahman and Hefzy, 1998; Atkinson et al., 2000; Baldwin et al., 2012; Oh et al., 2012; Shin et al., 2007). Each tissue was characterized by a linear or bilinear response, which did not necessarily have zero force at zero displacement (McLean et al., 2011) and may contain regions of tension with no load carrying capacity (Oh et al., 2012). The uniaxial elements were constructed such that their lines of action corresponded to the appropriate real anatomy of the tissues (Abdel-Rahman and Hefzy, 1998; Kiapour et al., 2014a).

A large proportion of computational models that investigate whole knee biomechanics assumes isotropic, linear elastic material descriptions of tibial and femoral articular cartilages (Atmaca et al., 2013; Beillas et al., 2004; Donahue et al., 2002, 2003; Huang et al., 2012; Kang et al., 2015; Kiapour et al., 2014a,b; Li et al., 2002; Mootanah et al., 2014; Oh et al., 2012; Peña et al., 2005a, 2006a; Quatman et al., 2011; Ramaniraka et al., 2007; Shelburne et al., 2006; Wang et al., 2014; Withrow et al., 2006). However, there is ample experimental evidence to indicate that articular cartilage is not only nonlinear, but anisotropic, viscoelastic, multiphasic, and spatially heterogeneous (Appleyard et al., 2003, 2001; Athanasiou et al., 1991; Briant et al., 2015; Deneweth et al., 2013a,b, 2015; Jurvelin et al., 2000; Mow and Guo, 2002; Mow et al., 1984; Oloyede et al., 1992; Swann and Seedhom, 1993; Thambyah et al., 2006; Young et al., 2007). In this work the sensitivity of articular cartilage—shown in Fig. 3.1b—to its stiffness was examined by varying the Young's modulus in the generally accepted range $E = 5 - 20$ MPa, while holding the Poisson's ratio fixed at $\nu = 0.45$. In Deneweth et al. (2013a) and Deneweth et al. (2015), the ability of an incompressible form of Eq. 3.1 was shown to accurately capture the uniaxial compression response of articular cartilage across patient populations with only one spatially varying parameter, the initial stiffness (C_r), while holding the degree of transverse isotropy, $a : b$, constant throughout the tibial and femoral surfaces at $1 : 1.33$ and $1 : 1.348$, respectively, where **a** is oriented normal to the bone surface. Recasting the experimental moduli distributions from Deneweth et al. (2013b) and Deneweth et al. (2015) into constitutive descriptions consistent with Eq. 3.1 (the bulk modulus was assumed to be homogeneously distributed with $B = 1$ GPa), the average initial stiffness $\pm$ one standard deviation of the tibial and femoral articular cartilage surfaces were determined to be 88.6 ± 51.7 kPa and 413 ± 157 kPa, respectively. The range of cartilage responses can be seen in Fig. 3.4.

The role of spatial heterogeneity in articular cartilage surfaces was also examined. The heterogeneity was incorporated numerically into the material descriptions of the tibial and femoral cartilages through spatial initial stiffness distributions such that

$$C_{r,\text{tibia}} = C_{r,\text{tibia}}\left(x, y\right) \tag{3.4}$$

and

$$C_{r,\text{femur}} = C_{r,\text{femur}}\left(z, \theta\right), \tag{3.5}$$

where (x, y) and (z, θ) correspond to the coordinates of integration points in the planes parallel to the tibial and femoral bone surfaces—note it is convenient to describe the femoral cartilage in a pseudo-cylindrical coordinate frame where the radial direction is oriented

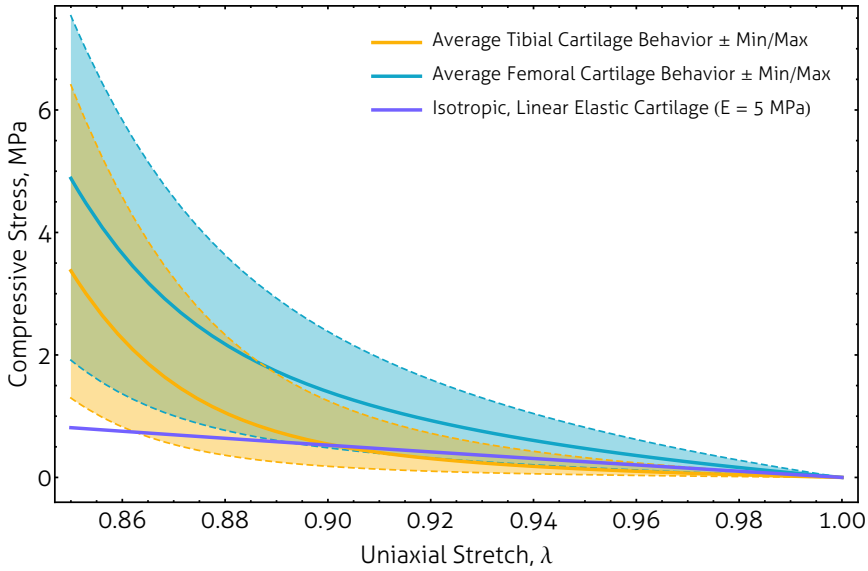

Figure 3.4: Comparison of uniaxial, through-thickness compression responses of tibial and femoral cartilage determined by converting the tangent moduli distributions presented in Deneweth et al. (2013a) and Deneweth et al. (2015) into the form of Eq. 3.1 and isotropic, linear elastic cartilage constitutive behavior with $E = 5$ MPa.

normal to the bone surface and to project through the thickness of the cartilage onto the $z - \theta$ plane to obtain homogeneous through-thickness moduli descriptions consistent with the curvature of the bony geometry.

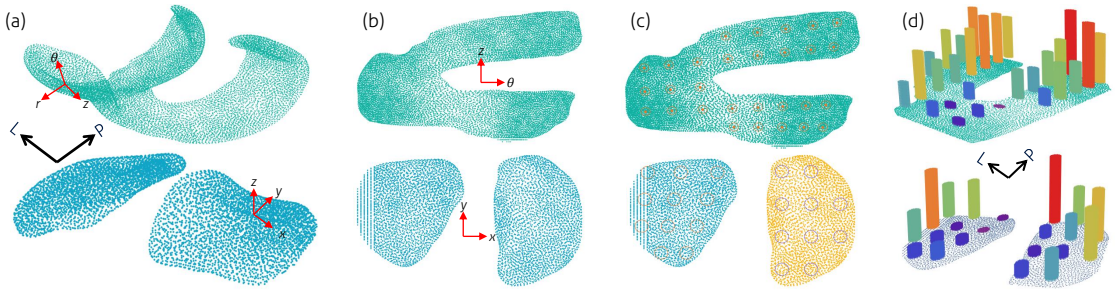

Figure 3.5: Workflow for the construction of sparse heterogeneous moduli fields: (a) from three dimensional geometry, represented as nodal points, to (b) two dimensional projections in the planes normal to the respective bone surfaces, to (c) the partitioning of experimental regions, to (d) the reconstitution of experimental zones of homogeneous moduli.

Applying Eqs. 3.4 and 3.5 to physical cartilage geometries, Fig. 3.5a, yields distributions of cartilage moduli that are heterogeneous in the planes parallel to the bone surfaces, Fig. 3.5b, but homogeneous through the thickness of the cartilage. Figure 3.5 depicts a schematic for the numerical implementation of the sparse heterogeneous experimental moduli fields for the tibial and femoral articular cartilages described in Deneweth et al.

(2013a) and Deneweth et al. (2015), respectively, recast in the form of Eq. 3.1. The substantial variation in the numeric application of the experimental moduli is illustrated by Fig. 3.5d; it was assumed that experimental regions contained cartilage with homogeneous initial stiffness throughout each corresponding zone.

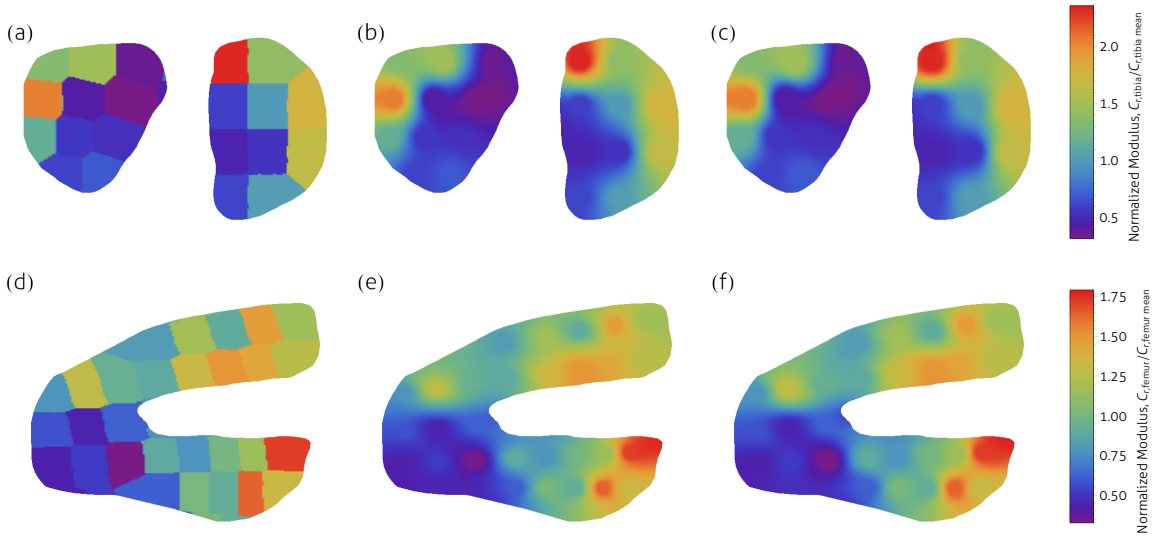

Figure 3.6: Tibial normalized moduli distributions ($C_{r,\text{tibia}}/C_{r,\text{tibia mean}}$): (a) discontinuous, (b) continuous, (c) smooth and continuous; and femoral normalized moduli distributions ($C_{r,\text{femur}}/C_{r,\text{femur mean}}$): (d) discontinuous, (e) continuous, (f) smooth and continuous

Various interpolation schemes were evaluated to determine the effect of increasing levels of mathematical complexity and neatness on the construction of full field forms of Eqs. 3.4 and 3.5. Physical articular cartilage stiffness distributions were determined by multiplying the relative moduli fields, shown in Fig. 6, by the mean initial stiffness, $C_{r,\text{mean}}$—88.6 kPa and 413 kPa for the tibial and femoral cartilage, respectively. The moduli fields were filled through interpolation with either nearest neighbor, linear, or thin-plate spline radial basis functions resulting in discontinuous, continuous, and smooth and continuous complete moduli fields, respectively. The interpolations were computed numerically using Mathematica Version 10.0 (Wolfram Research, Inc., Champaign, Illinois, United States). The spatially heterogeneous and complete moduli fields corresponding to discontinuous, continuous, and smooth and continuous interpolations for the tibial and femoral articular cartilage surfaces are shown in Figs. 3.6a-c and 3.6d-f, respectively. While exact geometric representations of tissues are always preferred, the material property application technique described herein is sufficiently robust to tissue edge profile deviations, whether due to unusual individual tissue anatomy or errors during image segmentation.

3.2.3 Boundary Conditions and Constraints

Contact was modeled generally between all bodies and tissues in the joint. Contact in the direction normal to the surface was prescribed using a penalty contact enforcement method, allowing for separation of contact surfaces after initial contact. Friction was described between contact surfaces with an exponential relationship between coefficient of friction and relative shear slip rate with finite sliding. The relationship was derived from experimental data representative of the tribological properties of cartilage to cartilage contact (Qian et al., 2006; Unsworth et al., 1975).

To simulate the foot flat phase of walking gait, a linear time varying load, $F_{\text{max}} = 800$ N, was applied to the tibia at the ankle. This force corresponds to the force of approximately one body weight acting on the joint. The loading time, $t_{\text{max}} = 0.4$ sec, was selected to approximate the total time of the stance phase assuming typical walking speeds (Besier et al., 2009; Shelburne et al., 2005). Due to the explicit nature of the computation, a short, $t_{\text{Step 1}} = 1 \times 10^{-7}$ sec, simulation step was calculated prior to the simulated gait loading to allow for the application of muscle and tendon pretension; a second pregait simulation step was also computed, $t_{\text{Step 2}} = 1 \times 10^{-2}$ sec, to allow for the joint motion manifesting from the muscle and tendon pretension to quiesce—during this simulation step all tissues with uniaxial representations were assumed to have constant force regardless of displacement.

During all simulation steps all femoral degrees of freedom were kinematically coupled to a reference point located at the hip, and the displacement of the hip was fixed; all rotational degrees of freedom at the hip were free. Similarly, all the tibial degrees of freedom were kinematically coupled to a reference point at the ankle; however, only the translations of the ankle in the A-P/medial-lateral (M-L) plane were constrained to zero, allowing for axial displacement of the tibia during the gait cycle. The rotations of the ankle were likewise unconstrained. Soft tissues in the model were attached to the rigid bones by coupling the translational and rotational degrees of freedom on their respective shared mesh interfaces.

3.3 Results

3.3.1 Linear Elasticity Stiffness Sensitivity of Articular Cartilage

In the context of isotropic, linear elasticity, the stiffnesses of femoral and tibial articular cartilages affects both local tissue deformation and joint motion significantly. Figures 3.7a and 3.7b illustrate the contribution of linear elastic cartilage stiffnesses on joint motion, while Figs. 3.7c and 3.7d show how individual tissue strain states are linked to cartilage

stiffnesses. From Figs. 3.7a and 3.7b it can be seen that with increasing cartilage stiffness there is a general decrease in relative ATT (the displacement of the tibia relative to the femur), relative ITR, and knee flexion angle.

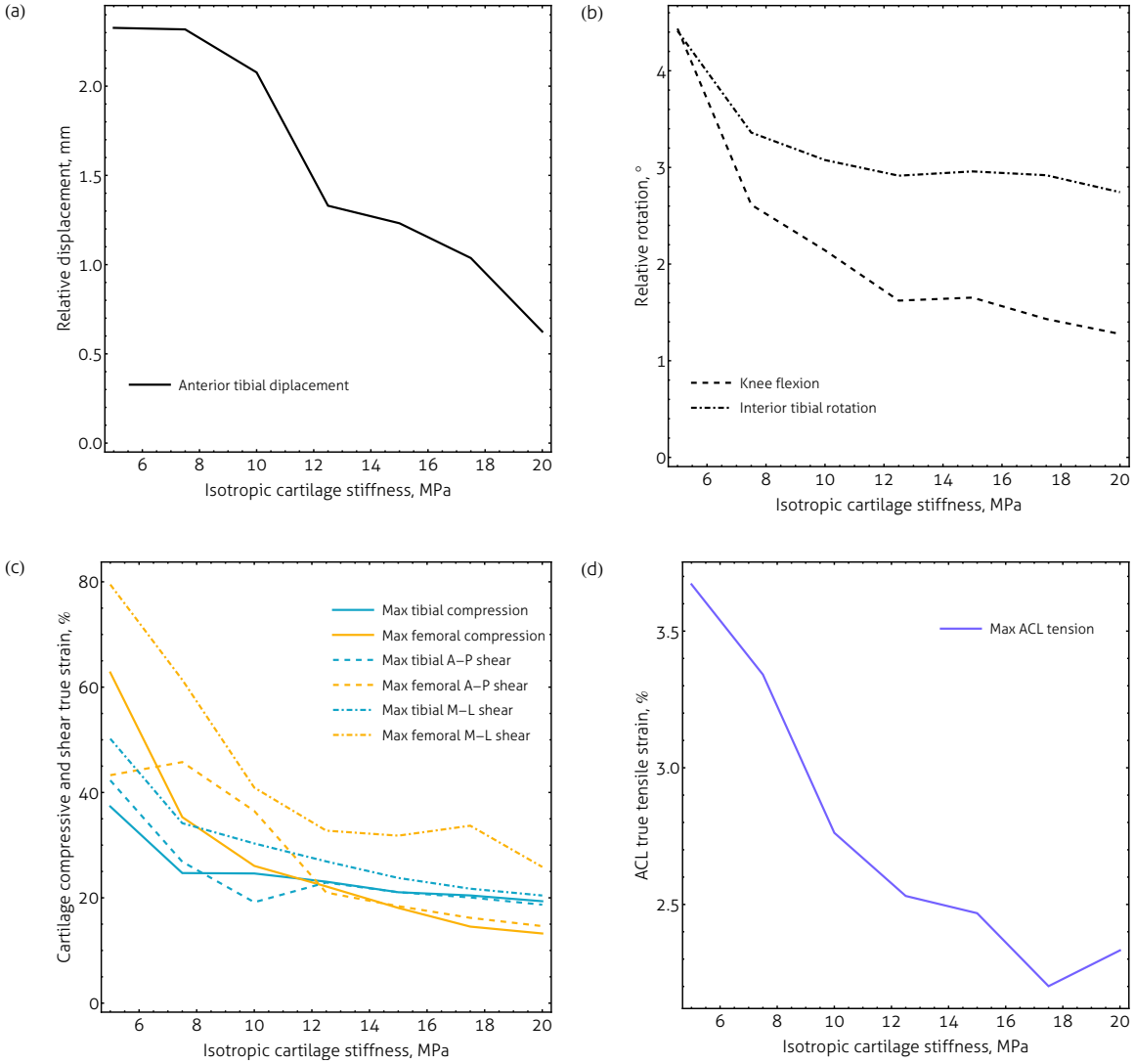

Figure 3.7: Effect of stiffness on (a) translational and (b) rotational joint motions and (c) local femoral, tibial and (d) ACL tissue strains with isotropic, linear elastic descriptions of articular cartilage.

Similarly, with increasing cartilage stiffness there is a general decrease in the observed soft tissue strains. Figures 3.7c and 3.7d depict the decrease of tibial and femoral cartilage compressive strains from 37.3% to 19.4% and 62.8% to 13.2%, respectively, and a decrease in ACL tensile strain from 3.67% to 2.20%, representing a 40.0% reduction in predicted ACL tensile strain. Not only is there substantial nominal variation in predicted strain with cartilage stiffness, but also in the location of strain maxima and minima. Figures 3.8a and

3.8b show the absolute variation in tensile and A-P shear strain, respectively, resulting from changes in cartilage stiffness—in Figs. 3.8a and 3.8b strain variations were calculated by subtracting a reference strain distribution, i.e., the strain corresponding to cartilage with $E = 10$ MPa, from each strain field. Absolute variations are plotted to describe full-field differences between two distributions and should not be confused with relative percent differences; in relative error calculations subtle differences between distributions can be difficult to appreciate, particularly when accounting for directionality in shear strains. The tensile and A-P shear strain distributions assuming articular cartilage with $E = 10$ MPa are also shown in Figs. 3.8a and 3.8b to provide context for the relative distributions. There was a slight lateral shift in the point of maximum compressive strain, Fig. 3.8a, and a large variation in the location of maximum and minimum A-P shear strains, Fig. 3.8b, with increasing stiffness as the maxima and minima move from locations covered to uncovered by menisci—the menisci are crescent shaped, Fig. 3.1c, and located on the perimeter of the joint capsule between the femoral and tibial articular surfaces, Fig. 3.1a. Note the paths traced by the red and blue arrows in Fig. 3.8b as the maximum and minimum shear strains, respectively, move medially then posteriorly from the lateral aspect of the medial tibial cartilage to the uncovered central region of the medial tibial cartilage—note that arrows show deviations from the reference distribution, $E = 10$ MPa, extrema, meaning all matching arrow tails are coincident.

3.3.2 Effect of Homogeneous Nonlinearity and Transverse Isotropy

The incorporation of transversely isotropic, nonlinear descriptions of articular cartilage contributes to differences in local cartilage deformation. The initial stiffnesses of the tibial and femoral articular cartilages were applied homogeneously using their mean values—88.6 kPa or 412 kPa for the tibial or femoral cartilage, respectively. Figures 3.9 and 3.10 show the tensile and A-P shear strain fields for the tibial and femoral articular cartilage surfaces assuming homogeneous applications of isotropic, linear elastic, $E = 5$ MPa and $E = 20$ MPa (Figs. 3.9a, 3.9g, 3.10a, and 3.10g and Figs. 3.9d, 3.9j, 3.10d, and 3.10j, respectively), and transversely isotropic, nonlinear (Figs. 3.9b, 3.9e, 3.9h, 3.9k, 3.9b, 3.10e, 3.10h, and 3.10k) material behavior, respectively.

In the tibial cartilage there was a reduction of maximum predicted compressive strain from 37.3% and 16.8% to 12.4% (Figs. 3.9a-f), and, in the femoral cartilage there was a reduction in compressive strain from 62.8% and 59.0% to 9.63% (Figs. 3.9g-l) as the cartilage constitutive model transitioned from isotropic, linear, $E = 5$ MPa and $E = 20$ MPa, respectively, to transversely isotropic, nonlinear elastic descriptions. The location of maxi-

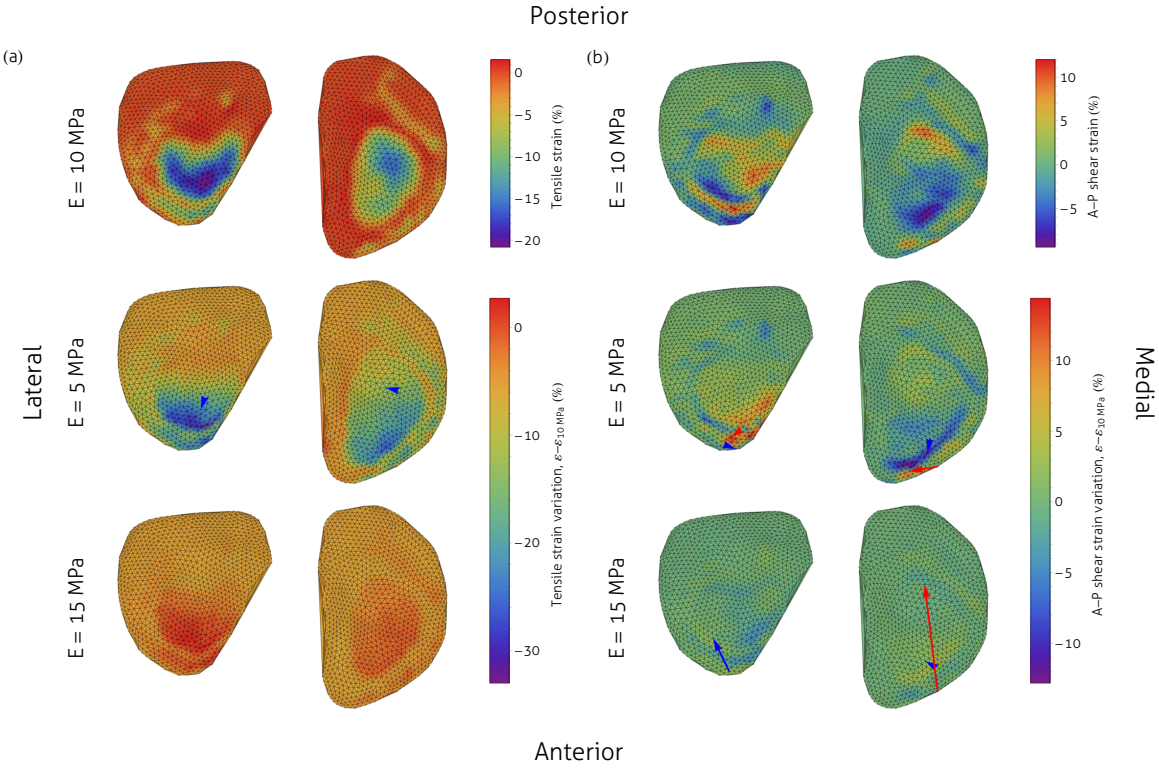

Figure 3.8: Effect of stiffness on relative tibial cartilage (a) tensile strain and (b) A-P shear strain with isotropic, linear elastic descriptions of cartilages on the articular surface. Red and blue arrows correspond to shifts in locations of maximum and minimum strains as cartilage stiffnesses are perturbed from $E = 10$ MPa, respectively; the absence of a particular arrow indicates no change in the location of the corresponding maximum or minimum strain.

mum compression on the femoral cartilage—constructed using a homogeneous application of Eq. 3.1—shifted medially with respect to the cartilage assumed to be linear elastic, moving from the parameter of the lateral condyle to center of the medial condyle (Figs. 3.9i and 3.9l). There was also a small variation in ACL tensile strain from 3.67% and 2.33% to 2.53% with the substitution of nonlinear for linear elastic cartilage with moduli $E = 5$ MPa and $E = 20$ MPa, respectively.

As with increasing isotropic, linear elastic stiffness, homogeneous applications of nonlinear Eq. 3.1 to the tibial and femoral articular cartilage altered the location of strain maxima and minima, shown for A-P shear strain in Figs. 3.10c, 3.10f, 3.10i, and 3.10l. On the tibial cartilage, strain maxima and minima shifted from regions covered to uncovered by menisci in a manner strikingly analogous to that observed with increasing isotropic stiffness, illustrated by Fig. 3.8, even when compared to the stiffest application of linear elasticity (Fig. 3.10f). This similarity can be attributed to the form of Eq. 3.1, which exhibits increasing effective stiffness with stretch. The motion of the joint was also affected

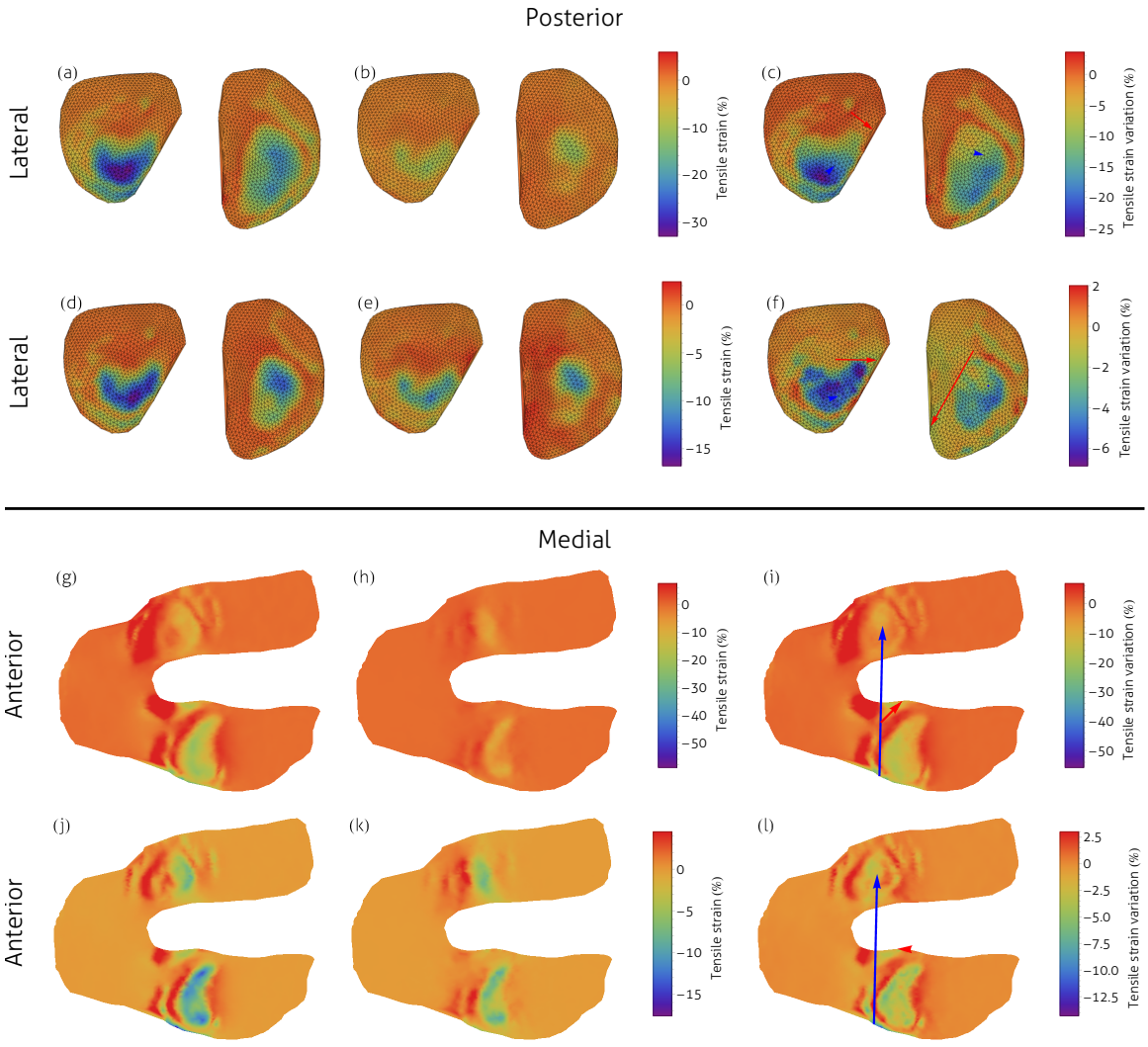

Figure 3.9: Tensile strain on the articular surface of tibial and femoral cartilage with isotropic, linear elastic, (a, g) $E = 5$ MPa and (d, j) $E = 20$ MPa, and (b, e, h, k) transversely isotropic, nonlinear (Eq. 3.1) constitutive behavior, respectively. Note that (b)–(e) and (h)–(k) are the same strain distributions, but scaled differently according to the relevant comparison. (c, f, j, l) Tensile strain variation between (a)–(b), (d)–(e), (g)–(h), and (j)–(k), respectively—red and blue arrows correspond to shifts in location of maximum and minimum strains between strain fields in comparison, respectively; the absence of a particular arrow indicates no change in the location of the corresponding maximum or minimum strain.

by the experimentally motivated cartilage constitutive descriptions. There was variation in the observed relative ATT, from 2.33 mm and 0.625 mm to 0.598 mm, relative ITR, from 4.41° and 2.74° to 3.19°, and knee flexion, from 4.44° and 1.28° to 1.42°, corresponding to the implementation of transverse isotropy and nonlinearity in articular cartilage compared to linear elastic cartilage descriptions with $E = 5$ MPa and $E = 20$ MPa, respectively.

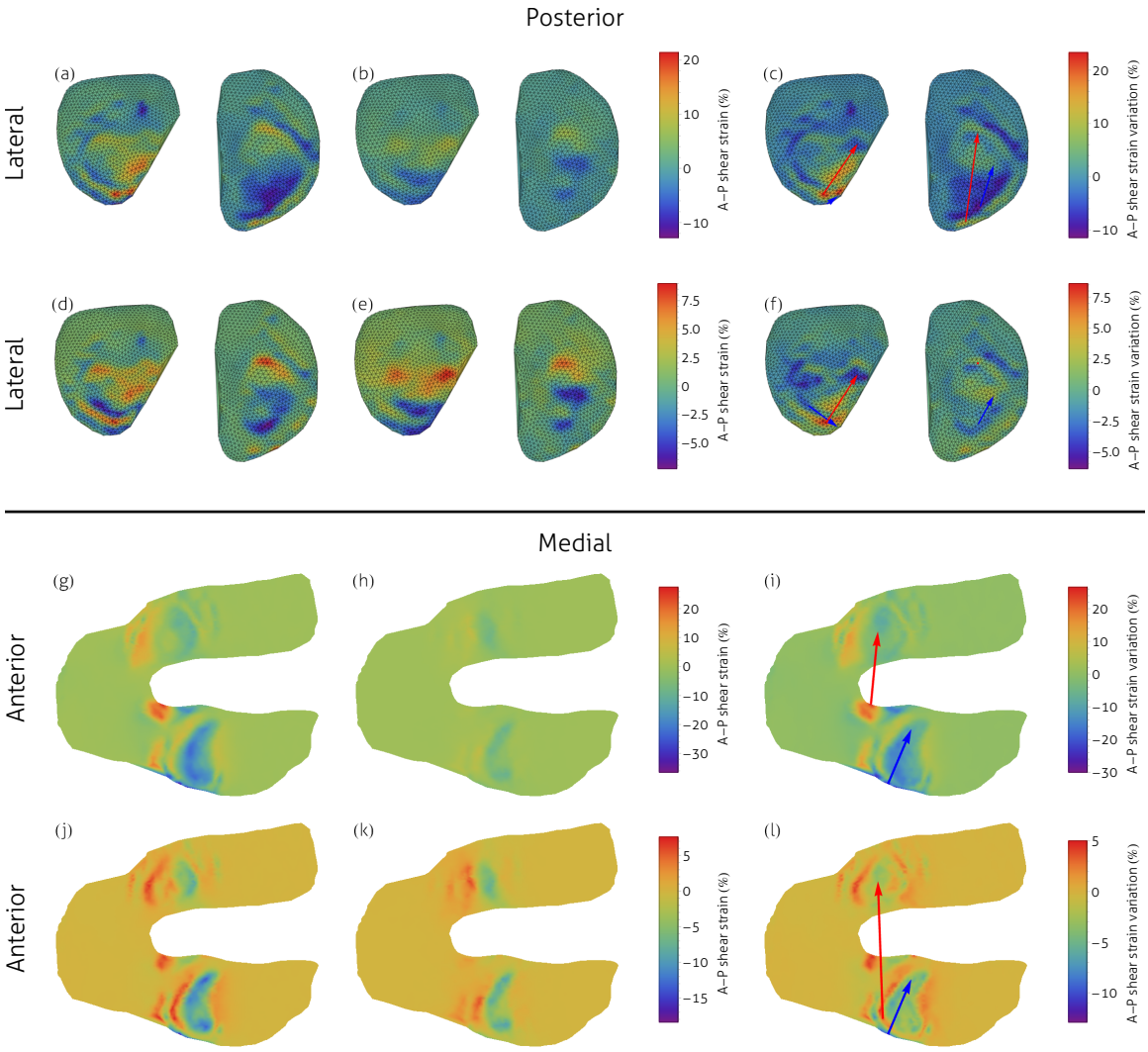

Figure 3.10: A-P shear strain on the articular surface of tibial and femoral cartilage with isotropic, linear elastic, (a, g) $E = 5$ MPa and (d, j) $E = 20$ MPa, and (b, e, h, k) transversely isotropic, nonlinear (Eq. 3.1) constitutive behavior, respectively. Note that (b)–(e) and (h)–(k) are the same strain distributions, but scaled differently according to the relevant comparison. (c, f, j, l) A-P shear strain variation between (a)–(b), (d)–(e), (g)–(h), and (j)–(k), respectively—red and blue arrows correspond to shifts in location of maximum and minimum strains between strain fields in comparison, respectively; the absence of a particular arrow indicates no change in the location of the corresponding maximum or minimum strain.

3.3.3 Sensitivity of Homogeneous Nonlinearity and Transverse Isotropy in Articular Cartilage

The sensitivity of homogeneous applications of Eq. 3.1 was evaluated by examining local and global deformation corresponding to articular cartilage with average tibial and femoral

initial stiffness ± one standard deviation determined from experimental moduli presented in Deneweth et al. (2013a) and Deneweth et al. (2015), respectively. Figure 3.11b illustrates the rotational insensitivity of the knee model to variations in cartilage stiffnessl—explicitly in terms of knee flexion and relative ITR. Interestingly, a local minima in relative ATT was found when mean experimental cartilage stiffnesses were applied (Fig. 3.11a). A detailed examination of the sensitivity of cartilage stiffness on local tissue deformations is presented in Figs. 3.11c and 3.11d.

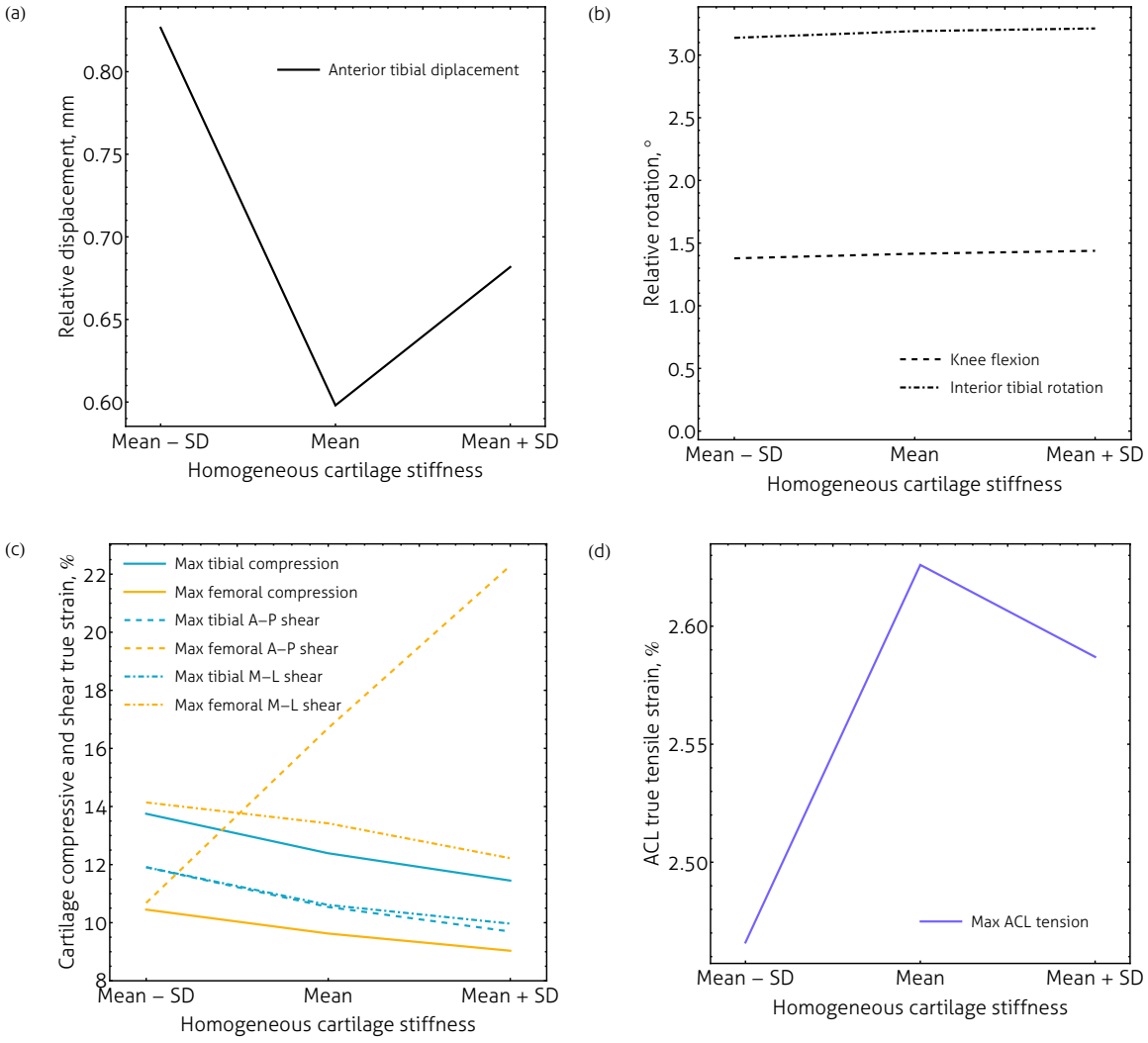

Figure 3.11: Effect of homogeneous initial stiffness on (a) translational and (b) rotational joint motions—relative ATT, knee flexion, and ITR—and local (c) femoral and tibial cartilage compressive, A-P shear, and M-L shear strains and (d) ACL tensile strains with transversely isotropic, nonlinear elastic descriptions of articular cartilage.

As stiffness increased, the compressive strain in both the tibial and femoral articular cartilage decreased. Similar tends were observed in both A-P and M-L shear strains, save

for femoral A-P shear strain, which increased with increasing stiffness. A local maxima in ACL tensile strain was found to correspond to the mean cartilage stiffness material description, coupled to the observed minima in the relative ATT, though differences between homogeneous cartilage stiffnesses with respect to ACL tensile strains and ATT—driven by small deviations in varus/valgus rotations—are likely not significant within the context of clinical diagnostics and evaluation.

3.3.4 Effect of the Incorporation of Cartilage Mechanical Heterogeneity

The addition of experimentally motivated and validated constitutive descriptions of articular cartilage further refined predictions of local tissue deformation and macroscopic joint kinematics. The three heterogeneous mappings—depicted in Figs. 3.6a-c and 3.6d-e for discontinuous, continuous, and smooth and continuous moduli mappings of tibial and femoral cartilage, respectively—predicted higher local compressive strains, with the maximum compressive strains located in the lateral compartment of the tibial cartilage, as compared to homogeneous cartilages with constitutive behavior described by Eq. 3.1 where homogeneous initial stiffnesses were based on mean experimental moduli data.

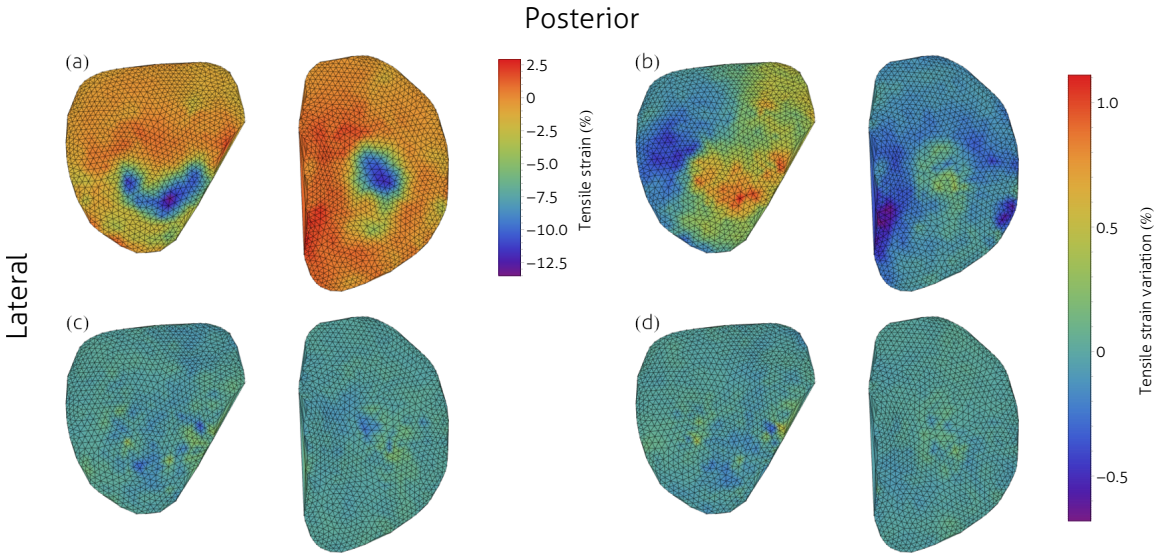

Figure 3.12: (a) Tibial cartilage articular surface tensile strain assuming a smooth and continuous heterogeneous moduli field. Tensile strain field variations between the smooth and continuous moduli mapping of (a) and (b) homogeneous, (c) discontinuous, (d) continuous moduli distributions.

The effect of heterogeneity on compressive strains is illustrated by Fig. 3.12. Figure 3.12b highlights the widespread variation between homogeneous and heterogeneous mod-

uli mappings with respect to compressive strain on the tibial cartilage articular surface. This trend, heterogeneity corresponding to higher predicted strains, is consistent in other states of deformation within the tibial cartilage, described in detail by Table 3.2, except for an overprediction of maximum M-L shear strain. For minimum and maximum strain relative percent error calculations negative values correspond to lower relative strain levels. Heterogeneity yields the largest A-P and M-L shear strain field variations in the lateral and medial compartments of the tibial cartilage, respectively.

Table 3.2: Comparison of maximum and minimum relative percent errors, $\left(\frac{\text{strain}_{\text{max,min}}}{\text{strain}_{\text{smooth}}} - 1\right) \times 100$, of various deformation states between homogeneous and heterogeneous moduli distributions with respect to smooth and continuous mapping on the femoral and tibial cartilages. For the tibial cartilage, the location of the maximum or minimum percent error, either the lateral or medial compartment, is indicated by (L) or (M), respectively.

		Homogeneous		Discontinuous		Continuous	
		Femoral	Tibial	Femoral	Tibial	Femoral	Tibial
Compressive strain	Maximum Strain	-0.395	-8.21 (M)	0.793	-2.53 (M)	-1.11	-1.71 (M)
A-P shear strain	Minimum Strain	-7.34	-7.07 (L)	17.7	1.39 (M)	-45.8	1.03 (M)
	Maximum Strain	-4.57	10.3 (L)	0.355	-1.46 (L)	0.895	0.505 (M)
M-L shear strain	Minimum Strain	-2.02	-8.11 (M)	6.13	1.76 (L)	19.5	0.706 (M)
	Maximum Strain	1.94	-11.3 (M)	0.294	2.05 (M)	-0.322	0.953 (M)

Heterogeneity also affects local deformation in the femoral cartilage. Figure 3.13a shows the M-L shear strain distribution on the articular surface of the femoral cartilage at the end of the stance phase. The variations in M-L shear strain fields for homogeneous, discontinuous, and continuous moduli mappings are presented in Figs. 3.13b-d. Heterogeneous cartilage descriptions have a much smaller, relative to the tibial cartilage, impact on compressive strain predictions, see Table 3.2, though the method of heterogeneity application does have an effect on inplane shear strain predictions. There was an underestimation in the minimum A-P and M-L shear strains corresponding to the continuous moduli field compared to articular cartilage with smooth and continuous constitutive behavior. Similarly, there was an underestimation in the maximum A-P shear strain assuming discontinuous mappings. Large deviations of minimum A-P and M-L shear strains were observed between heterogeneous moduli distributions (Table 3.2).

Table 3.3 describes the role of cartilage constitutive assumptions on macroscopic joint motion. Nonlinearity and transverse isotropy, implemented homogeneously or heteroge-

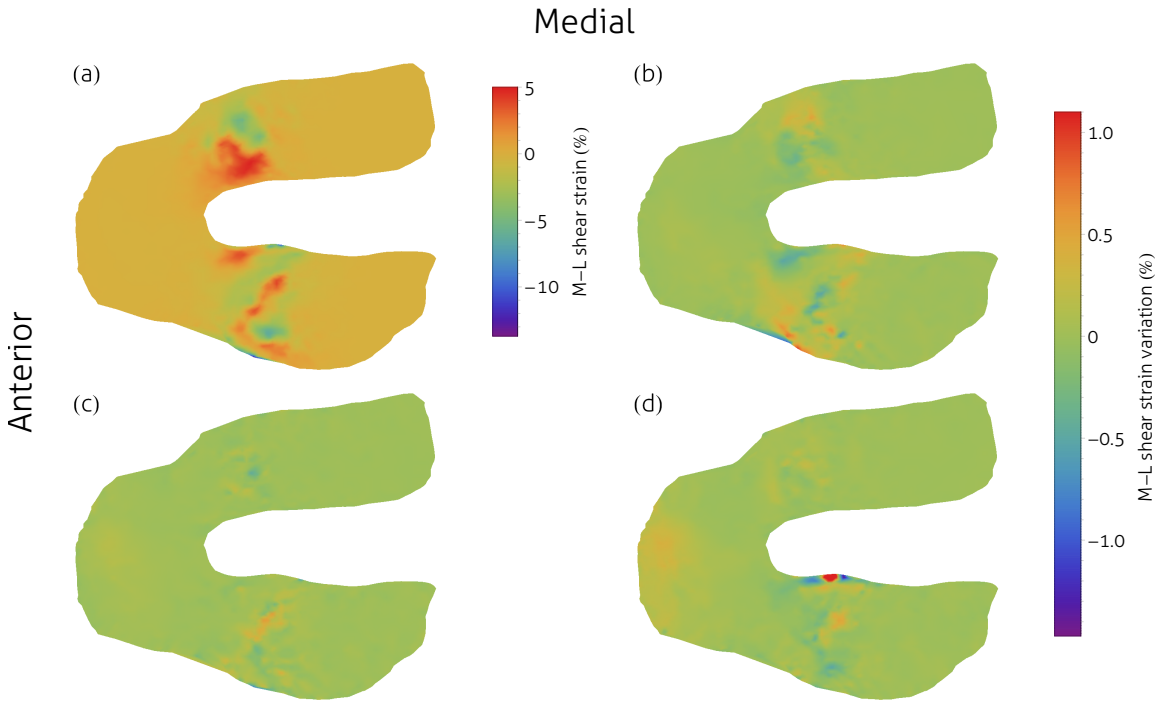

Figure 3.13: (a) Femoral cartilage articular surface M-L shear strain assuming a smooth and continuous heterogeneous moduli field. M-L shear strain field variations between (b) homogeneous, (c) discontinuous, (d) continuous moduli distributions and smooth and continuous moduli mapping.

neously, significantly alters predicted relative ATT, relative ITR, and knee flexion compared to isotropic, linear elastic cartilage descriptions. The incorporation of heterogeneity, compared to a homogeneous modulus field, appears to have an effect on relative ATT, while having a minimal effect on joint rotations (internal rotation and flexion); this result is consistent with the low rotational sensitivity of homogeneous nonlinear, transversely isotropic cartilage with respect to initial stiffness—this characteristic of homogeneous modulus fields is illustrated by Fig. 3.11b.

Table 3.3: Effect of constitutive complexity on joint motion

	Relative ATT (mm)	Relative ITR (°)	Knee flexion (°)
$E = 5$ MPa	2.34	4.41	4.44
$E = 20$ MPa	0.625	2.74	1.28
Homogeneous	0.598	3.19	1.42
Discontinuous	0.736	3.21	1.43
Continuous	0.733	3.27	1.42
Smooth and Continuous	0.742	3.26	1.42

The role of mathematical complexity in heterogeneous mappings is more nuanced than that of general mechanical heterogeneity. Figures 3.14a-d depict the shear strain field variations among the heterogeneous mappings. Local shear strain artifacts, manifesting from the physical requirement of continuity in displacement fields, are present on the articular surface of the tibial cartilage with discontinuous heterogeneity (Figs. 3.14a and 3.14c) that are not present in the continuous mapping (Figs. 3.14b and 3.14d) in M-L and A-P shear, respectively. These shear strain artifacts are situated at the boundary between homogeneous moduli zones in the discontinuous distribution—homogeneous moduli regions in the discontinuous mapping of tibial cartilage can be seen in Fig. 3.6a. Multiple A-P shear strain artifacts are present in the lateral compartment (Fig. 3.14c), and M-L shear strain artifacts can be observed in the medial compartment (Fig. 3.14a).

This effect is not limited to the tibial cartilage. There is large variation between strains corresponding to heterogeneous mappings in the femoral cartilage. In Fig. 3.13d, looking at the lateral aspect of the medial femoral condyle, there is a significant effect of adding smoothness to the moduli field; variation is also present on the medial and lateral aspects of the medial condyle of the discontinuous moduli distribution, Fig. 3.13c, though this effect is more disperse.

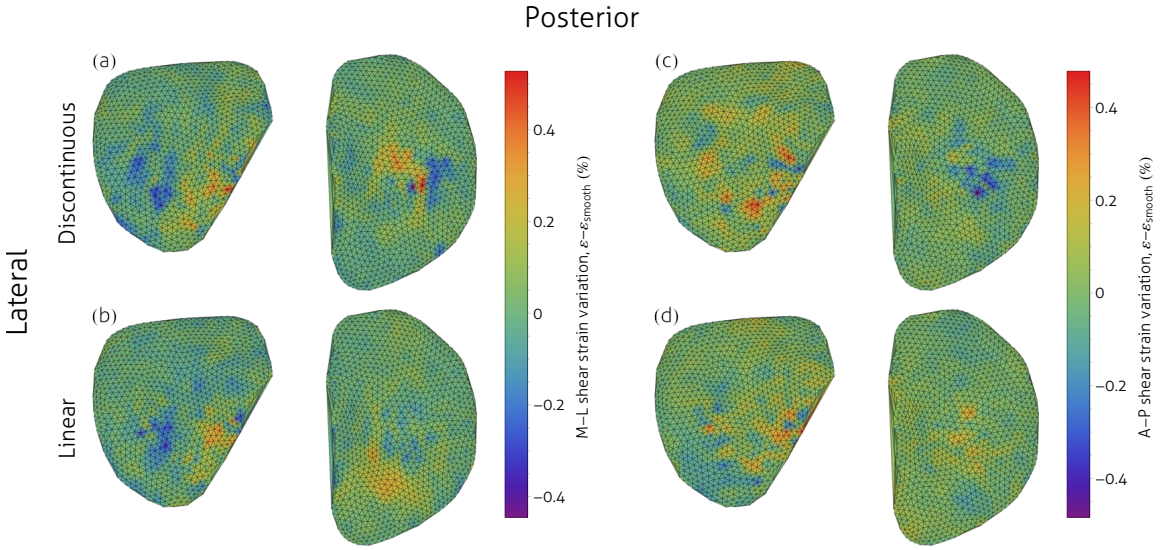

Figure 3.14: M-L and A-P shear strain variations of (a, c) discontinuous and (b, d) continuous moduli mappings compared to a smooth and continuous distribution, respectively.

3.4 Discussion

Computational models of whole knee biomechanics provide a compelling means to investigate soft tissue injury and disease. They have the potential to be instrumental in advancing the understanding of the coupling between individual tissue structures during normal activities, providing insights into how deviations from this normal deformation can contribute to injury initiation and disease progression. Computational models are also capable of extending the knowledge of the complex mechanical response of joints, both at the tissue and joint levels, beyond the limits of experimental investigation. FE models excel in traditionally challenging experimental areas, providing the ability to perform comprehensive parametric studies to investigate geometric, physiologic, and external contributions within and among patient populations. Specifically in the context of computational models of whole knee biomechanics, fully three dimensional descriptions of tissues yield the real inhomogeneous deformation of constituent structures, information concerning contact pressures and distributions, and the link between physically motivated boundary conditions and macroscopic joint motion.

While FE models possess impressive potential, cautious skepticism is required when evaluating their predictive power. The accuracy of FE models is entirely predicated on the validity of their construction; the applied boundary conditions and constraints, geometric representations of tissues, and constitutive behavior all affect FE biomechanics models. There have been significant contributions with respect to the application of geometrically accurate tissue structures and systematic implementation of physical boundary conditions in knee FE models (Atmaca et al., 2013; Baldwin et al., 2012; Beillas et al., 2004; Donahue et al., 2002, 2003; Gardiner and Weiss, 2003; Kang et al., 2015; Kiapour et al., 2014a; Limbert et al., 2004; Mesfar and Shirazi-Adl, 2005; Mootanah et al., 2014; Peña et al., 2005a, 2006a; Penrose et al., 2002; Quatman et al., 2011; Shelburne et al., 2006; Song et al., 2004; Wang et al., 2014; Zhang et al., 2008), but the extent of the effect of individual tissue material model selection, and the sensitivity of that selection, has not been as fully explored.

Biological structures generally exhibit complex mechanical behavior—a cursory examination of tissue microstructure and composition motivates this complexity—but there have been relatively few numerical studies that investigate the role of constitutive behavior in the prediction of local deformation and joint motion. There has been a shift from relatively simple descriptions of ligaments toward material models that are transversely isotropic and nonlinear; recently Kiapour et al. (2014b) highlighted the corresponding effect on local ACL strains, as well as joint motion, under various loading conditions. However, the

contribution of physically accurate and experimentally validated constitutive behavior of articular cartilage has not been analyzed rigorously, with most FE models of whole knee biomechanics incorporating simple, linear elastic material descriptions—there have been some exceptions to this trend (Adouni et al., 2012; Marouane et al., 2014; Shirazi and Shirazi-Adl, 2009a,b).

This work fundamentally attempts to understand why articular cartilage has evolved with the particular mechanical characteristics observed experimentally. Using relatively simple loading conditions, corresponding to the foot flat phase of gait, the level of constitutive complexity was systematically increased and evaluated in an effort to elucidate the motivation for the nonlinear, anisotropic, and spatially heterogeneous mechanical properties of articular cartilage (Appleyard et al., 2003, 2001; Athanasiou et al., 1991; Briant et al., 2015; Deneweth et al., 2013a,b, 2015; Jurvelin et al., 2000; Swann and Seedhom, 1993; Thambyah et al., 2006; Young et al., 2007)—the response of cartilage was assumed to be rate independent at loading rates investigated in this work, and more generally during normal and injury causing activities, due to the low rate dependency at strain rates greater than 5 $\%$/sec (Oloyede et al., 1992).

With most whole knee computational models assuming isotropic, linear elastic descriptions of articular cartilage, the sensitivity of predicted local tissue deformation and joint motion were examined. Generally, with increasing stiffness there was a decrease in the calculated relative ATT, ITR, and knee flexion, as well as decrease in nearly all measures of local tissue deformation, both in the articular cartilage and the ACL. As cartilage was assumed stiffer the contact area decreased and the contact pressure increased within the joint capsule, increasing by 56.6% and 24.0% on the tibial and femoral cartilage surfaces, respectively. These trends are largely in line with those described by Wang et al. (2014), in which, over the linear elastic Young's modulus range $E \in [8, 12]$ MPa, the contact area decreased by approximately 13% and the contact pressure increased by approximately 17% for a fully extended knee subjected to a 1000 N axial load. Qualitatively, there is also good agreement between the distribution of contact pressure presented in Wang et al. (2014) and the distribution of compressive strains on the linear elastic tibial articular surfaces in the present work.

Peña et al. (2005a) found a maximum contact pressure on the articular cartilage of 3.18 MPa, as compared to 5.38 MPa in the current work, using simple cartilage ($E = 5$ MPa) and ligament (neo-Hookean) material properties during joint compression ($F_{axial} = 1000$ N). Similarly, in Donahue et al. (2002), the maximum contact pressure during unconfined joint compression with $F_{axial} = 800$ N was determined to be 2.50 MPa; the deviation can be explained in part by the incorporation of trans-knee muscles, muscle tendons, and auxiliary

ligaments, as well as a more complete description of supporting ligaments and the inclusion of patellofemoral joint in the current work, which included structures with nonzero force at the onset of loading. To put this variation in context, contact pressures between $2.4 - 34$ MPa have been reported corresponding to various loading conditions and tissue constitutive representations (Mootanah et al., 2014; Wang et al., 2014).

The nominal effect of cartilage stiffness was not only apparent locally—the predicted maximum shear strains of the tibial and femoral cartilage ranged between $18.7 - 50.2\%$ and $14.6 - 79.5\%$, respectively—but also with respect to the location and dispersion of strain experienced during loading. As with increasing isotropic linear stiffness, there was a shift in the location of maximum shear strains on the tibial cartilage from regions covered to uncovered by menisci. It is clear that whole knee models are indeed incredibly sensitive to cartilage material behavior, and that an analyst may fall victim to unsubstantiated conclusions related to tissue injury or disease without a careful examination of cartilage constitutive descriptions, especially if the relevant failure criteria are strain dependent.

Increasing the constitutive complexity of articular cartilage to numerically describe the experimentally and microstructurally motivated nonlinearity and bulk transverse isotropy fundamentally changes soft tissue deformation and joint kinematics. There was a substantial reduction in the amount of relative ATT (2.33 mm to 0.598 mm), ITR (4.41° to 3.19°), and knee flexion (4.44° to 1.42°) corresponding to the shift from isotropic, linear elasticity. There was also a decrease in the sensitivity of local strains, notwithstanding maximum femoral A-P shear strains, and knee motion to variation in cartilage stiffness. Increasing isotropic cartilage stiffness does seem to close gap between joint models built using linear elasticity with respect to transversely isotropic, nonlinear elastic constitutive behavior or, more generally, heterogeneously applied transversely isotropic, nonlinear elastic constitutive behavior (Table 3.3), but it is important to note that significantly different local tissue deformations persist. This means that while computational joint models may appear to be validated, all predictions, particularly at the tissue level, may not be representative if only kinematic data is used in the model validation protocol.

The incorporation of nonlinear and transversely isotropic mechanical descriptions of articular cartilages is instrumental in driving kinematic predictions of joint motion into the range seen experimentally. In particular, during the predominate weight bearing phases of gait, the predicted ATT of heterogeneous cartilage is well within the range reported by Kozanek et al. (2009), while the predicted ATT corresponding to linear elastic cartilage is not contained within the relevant experimental range. Predicted knee internal rotations are also supported by experimental observations (Kozanek et al., 2009). Transitioning to homogeneous, nonlinear cartilage descriptions also shifts the location of maximum A-P

shear onto the medial condyle (Fig. 3.10), the region consistent with approximately 33% of focal defects observed clinically (Wong and Sah, 2010). While the kinematics of the joint are shifted in the experimental range corresponding to normal gait with the inclusion of transversely isotropic, nonlinear mechanical descriptions, it is important to note that calculated ACL strains, approximately on the order of 2.5% (Fig. 3.11d), are within the normal operating range for the tissue and below those seen during potential injury causing events (McLean et al., 2015; Withrow et al., 2006). It is quite apparent that the form of constitutive descriptions, particularly the nonlinearity of articular cartilage, though often neglected in whole knee models, is critical to understanding the expected response of the joint.

There is a mechanically meaningful contribution corresponding to the incorporation of spatial heterogeneity, with the method of initial stiffness mapping also of practical consequence. Differences were observed between homogeneous and heterogeneous moduli fields in articular cartilage with respect to knee motion. The most substantial variation was in the predicted relative ATT. ATT is an important clinical diagnostic tool for determining ACL integrity and joint stability. During the corresponding joint motion the ACL supports up to 87% of the load, making ATT a potentially catastrophic deformation state (Fukubayashi et al., 1982; Markolf et al., 1976; Noyes and Grood, 1976; Piziali et al., 1980b; Spindler and Wright, 2008).

Local tissue deformation variations were also found between homogeneous and heterogeneous cartilage descriptions, as well as between heterogeneous moduli mappings. Interestingly, the mathematical neatness of the moduli field had almost no impact on the joint kinematics. Yet the combination of low and high variation between heterogeneous mappings with respect to joint kinematic and local deformation predictions, respectively, imply the importance of some application of heterogeneity in describing the macroscopic motion of the knee, while continuity, and to some extent smoothness, in the moduli distribution is necessary to accurately predict the distribution of strain without the presence of strain localization artifacts in articular cartilage.

Halonen et al. (2014) reported mean tibial strains, determined using conical beam CT, in the lateral and medial compartments during similar loading of 9% and 5%, respectively. A slightly larger maximum compressive strain (13.5%) was similarly observed in the lateral compartment of the smooth and continuous tibial cartilage as compared to the medial compartment (11.8%)—see Fig. 3.12. The distribution of instantaneous compressive strains shown in Halonen et al. (2014) is strikingly similar to those shown in Fig. 3.12a, particularly the crescent shape of the high compressive strains in the lateral compartment. Lateral and medial maximum tibial cartilage compressive strains were also within the ranges ob-

served by Liu et al. (2010a) during the first phases of gait which most closely correspond to the loading conditions examined in the present study.

3.5 Conclusions

This work underscores the criticality of individual tissue constitutive modeling, even in the context of whole joint biomechanical models. A three dimensional FE model was developed from real, patient specific geometry, resulting in a whole knee model with representations of the major mechanical structures in the joint, including the patellofemoral and tibiofemoral joints and their corresponding soft tissues. The foot flat portion of the stance phase of gait was used to illustrate how cartilage constitutive behavior manifests locally, in terms of realized soft tissue deformation, and globally, with respect to relative joint motion; the model was validated through the comparison of relevant joint kinematic and tissue level predictions to appropriate experimental joint metrics. Assuming linear elastic material descriptions of articular cartilage, a popular practice in the construction of whole knee FE models, yields biomechanical predictions that are incredibly sensitive to articular cartilage stiffness, potentially providing misleading information related to the evaluation of native and diseased joints. Incorporating physically representative cartilage constitutive behavior acts to minimize predicted local deformation and relative joint motion compared to linear elastic tissue, with further refinement of local deformation derived from spatial mechanical heterogeneity, built using representative population distributions of relative cartilage stiffnesses.

The strength of FE models is not only in their potential to inform the understanding of joints in normal and injury causing activities, but also to describe how clinical interventions affect, both locally and globally, the response of joints and to elucidate the initiation and progression of degenerative diseases, like OA. Biomechanical joint models may be used to design individual specific surgical procedures and medical devices that minimize post-surgical complications and maximum positive short and long term patient outcomes. It is now possible to construct computational frameworks to investigate these questions, but care must be used in their development and their conclusions must be evaluated judiciously.

CHAPTER 4

The effect of articular cartilage focal defect size and location in whole knee biomechanics models

This chapter has been submitted for publication and may be referenced as:

> B. C. Marchi, E. M. Arruda, and R. M. Coleman. The effect of articular cartilage focal defect size and location in whole knee biomechanics models. *In Review*, 2017a

4.1 Introduction

The knee is a complex biomechanical structure consisting of a variety of hard and soft tissues. Articular cartilage provides support within the joint by cushioning the contact between bony geometries, dispersing high impact loads through nearly frictionless surfaces. Problems arise when cartilages are disrupted by tissue defects and during abnormal loading. Articular cartilage focal defects have been linked to the initiation and progression of degenerative tissue diseases, like OA, with the preponderance of cartilage arthritic lesions initially developing in weight bearing and high wear zones (Årøen et al., 2004; Curl et al., 1997; Hjelle et al., 2002; Widuchowski et al., 2007). Given the limited ability of articular cartilage to heal and remodel, it has been shown that untreated focal defects tend to grow (Wang et al., 2006) and collateral healthy cartilage tissues adjacent to or in contact with the affected cartilage tend to exhibit symptoms of cartilage degeneration, potentially leading to OA (Lefkoe et al., 1993). These mechanical alterations are coupled to the presence of abnormal biochemical environments, such as increased expression of proinflammatory cytokines, potentially leading to a cascade of additional extracellular matrix degradation (Goldring and Goldring, 2004).

Based on extensive arthroscopic studies, approximately 60% of focal defects are located in femoral cartilage; patellar cartilage defects also appear in substantial numbers (Årøen et al., 2004; Curl et al., 1997; Hjelle et al., 2002; Widuchowski et al., 2007). More than half of all femoral cartilage focal defects occur on the medial femoral condyle. Focal defects have been reported to have a mean affected area equal to 2.1 cm^2 and a corresponding range

of 0.5 – 4 cm^2 (Årøen et al., 2004; Curl et al., 1997; Hjelle et al., 2002; Widuchowski et al., 2007).

There have been numerous experimental (Brown et al., 1991; Gratz et al., 2009; Guettler et al., 2004; Wong and Sah, 2010) and computational (D D'Lima et al., 2009; Dabiri and Li, 2015; Dong et al., 2011; Heuijerjans et al., 2017; Manda et al., 2011; Papaioannou et al., 2010; Peña et al., 2007; Shirazi and Shirazi-Adl, 2009b; Venäläinen et al., 2016b; Weiss et al., 1998) studies that examine various aspects of how cartilage deformation changes in the presence of defects, as well as to evaluate potential intervention strategies. These investigations begin to provide possible explanations for the presence of post-traumatic OA in the area around the primary defect by showing elevations in cartilage stresses at the perimeter and in the neighborhood around the defect. These local mechanical metrics are important in predicting acute and sustained chondrocyte viability. It is possible to maximize cartilage integrity by limiting regions of cartilage tissue experiencing deformation above critical thresholds (Chen and Torzilli, 2015; Torzilli et al., 1999; Verteramo and Seedhom, 2007; Wilson et al., 2006). However, the exact mechanical mechanisms of progressive cartilage damage, specifically the role of altered tissue deformation associated with focal defects, has not been comprehensively established and validated. That being said, there have been some recent phenomenological efforts to computationally represent progressive cartilage damage in healthy cartilage (Hosseini et al., 2014; Liukkonen et al., 2017; Mononen et al., 2016).

Computational models, like FE models, are potentially powerful tools for studying the mechanics of cartilage focal defects. However, the mechanical behavior of articular cartilage is challenging to describe and implement computationally due to its nonlinearity, viscoelasticity, anisotropy, and spatial mechanical heterogeneity (Appleyard et al., 2003, 2001; Deneweth et al., 2013a,b, 2015; Fick et al., 2015; Mow et al., 1984; Oloyede et al., 1992; Ronkainen et al., 2016; Tomkoria et al., 2004). This often results in approximating the mechanics of cartilage, either as linear elastic (D D'Lima et al., 2009; Papaioannou et al., 2010; Peña et al., 2007) or a spatially homogeneous, fiber reinforced composite containing discrete depth-dependency (Shirazi and Shirazi-Adl, 2009b), based on the particular research focus. We have recently shown the sensitivities of both local tissue deformation and joint motion to femoral and tibial articular cartilage stiffnesses, with additional spatial and nominal deformation variability observed when accounting for cartilage mechanical heterogeneity (Marchi and Arruda, 2017a).

With knee injury and disease, joint loading and tissue geometries may evolve with time (Chaudhari et al., 2008; Deneweth et al., 2010). As internal loading patterns change, the local stiffness of the cartilage being loading is likely different compared to a healthy joint

(Appleyard et al., 2003, 2001; Deneweth et al., 2013b, 2015; Tomkoria et al., 2004), and this may have implications for local cartilage deformation and, consequently, chondrocyte viability (Butler et al., 2009; Fick et al., 2015; Ronkainen et al., 2016; Thoma et al., 2017). Kinetic analyses are well-suited to evaluating problems where kinematic differences between models are expected; however, they require representative collateral tissues, like ligaments, to faithfully represent joint motion (Kiapour et al., 2014b).

This work attempts to quantify differences in cartilage deformation and joint kinematics due to various femoral cartilage focal defects. Defects in both femoral condyles were examined using a previously validated FE model, which has been used to show the importance of incorporating experimentally validated spatial mechanical heterogeneity within whole knee models with healthy physiology (Marchi and Arruda, 2017a). We show how defect size and location substantially increases maximum femoral cartilage deformation when subjected to loads typical of the stance phase of gait near full extension. Significantly, and previously unexplored, we also show how changes in predicted deformation of tissues adjacent to and opposing the primary defect are altered, offering insights into how the biomechanical contributions of defects may lead to post-traumatic OA development. Local changes in deformation are especially meaningful in the context of the mechanically nonlinear and spatially heterogeneous articular cartilage because small or nonexistent nominal differences in strain may manifest as large differences in predicted stress.

4.2 Methods

4.2.1 General finite element model construction and considerations

A previously validated, three-dimensional FE model of the knee was used as the basis for both the intact and focal defect models developed in this work (Marchi and Arruda, 2017a). Bone and soft tissue geometries were constructed using a combination of CT and magnetic resonance images from a healthy adult female right knee with no history of lower limb injury or disease. Native tissue FE model construction, grid insensitivity, and element formulation appropriateness were described in previous work (Marchi and Arruda, 2017a). Figure 4.1 depicts the three dimensional tissue structures in the knee joint model, with Fig. 4.1b illustrating the joint capsule tissues. Meniscal ligaments, muscle tendons, and trans-knee muscles were modeled and included using uniaxial elements (not shown in Fig. 4.1). Tissue mesh geometries and uniaxial structures were assembled into a complete computational domain of the joint in ABAQUS v6.14 (SIMULA, Providence, Rhode Island, United States).

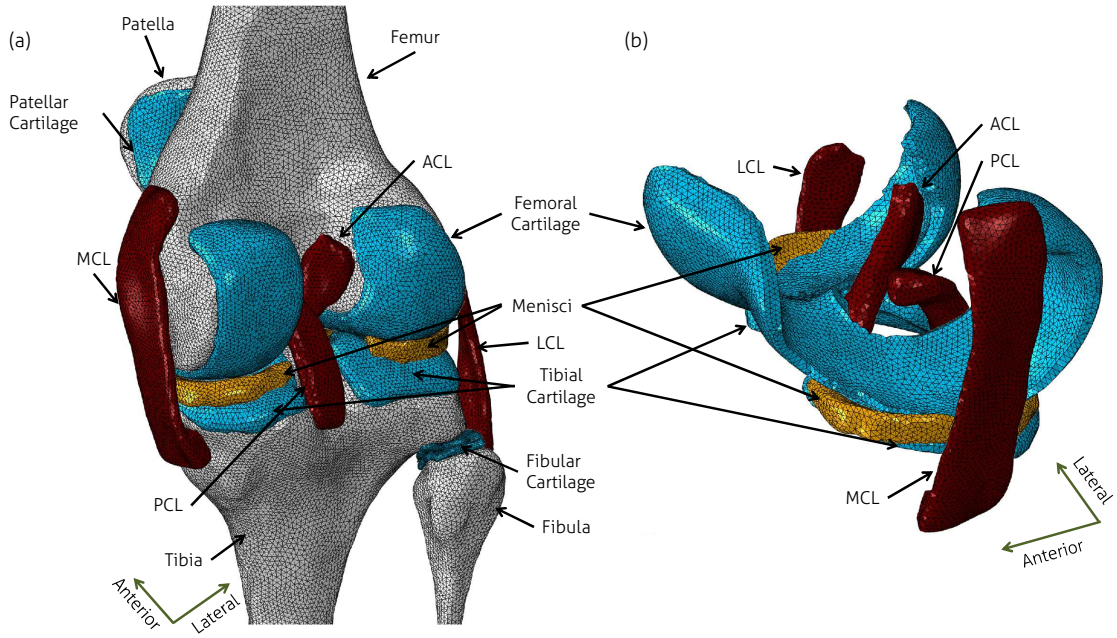

Figure 4.1: (a) Computational FE model of the right knee of a healthy adult female including its bones and soft tissue constituents. (b) The geometric accuracies of the articular cartilage and supporting ligaments are represented. In each figure cartilage is displayed in blue, menisci in orange, ligaments in red, and bones in white. Knee model images adapted from Marchi and Arruda (2017a). Some collateral tissues have be removed for visual clarity.

4.2.2 Focal defect models

Two full-thickness focal defect sizes were considered, small and average, that corresponded to the lower bound (0.5 cm^2) and mean (2.1 cm^2) areas of focal defects observed experimentally (Årøen et al., 2004; Curl et al., 1997; Hjelle et al., 2002; Widuchowski et al., 2007). Figure 4.2 shows the femoral cartilage without (Fig. 4.2a) and with (Figs. 4.2b-d) focal defects. Small focal defects were constructed on both the lateral (Fig. 4.2b) and medial (Fig. 4.2c) femoral condyles, while an average sized defect was constructed on the medial condyle (Fig. 4.2d).

The defects were created by projecting a circular profile normal to the underlying bone surface through the entire thickness of the cartilage. Following the procedure outlined in D D'Lima et al. (2009), the center of each defect was positioned such that the center of the circular profile was coincident with the approximate midpoint of the local condyle cartilage width in the M-L plane and in the A-P plane to maximize the percentage of the defect within high weight bearing regions. The accuracy of local deformation around and adjacent to the perimeter of focal defects, as well as any contribution to the global kinematics of the

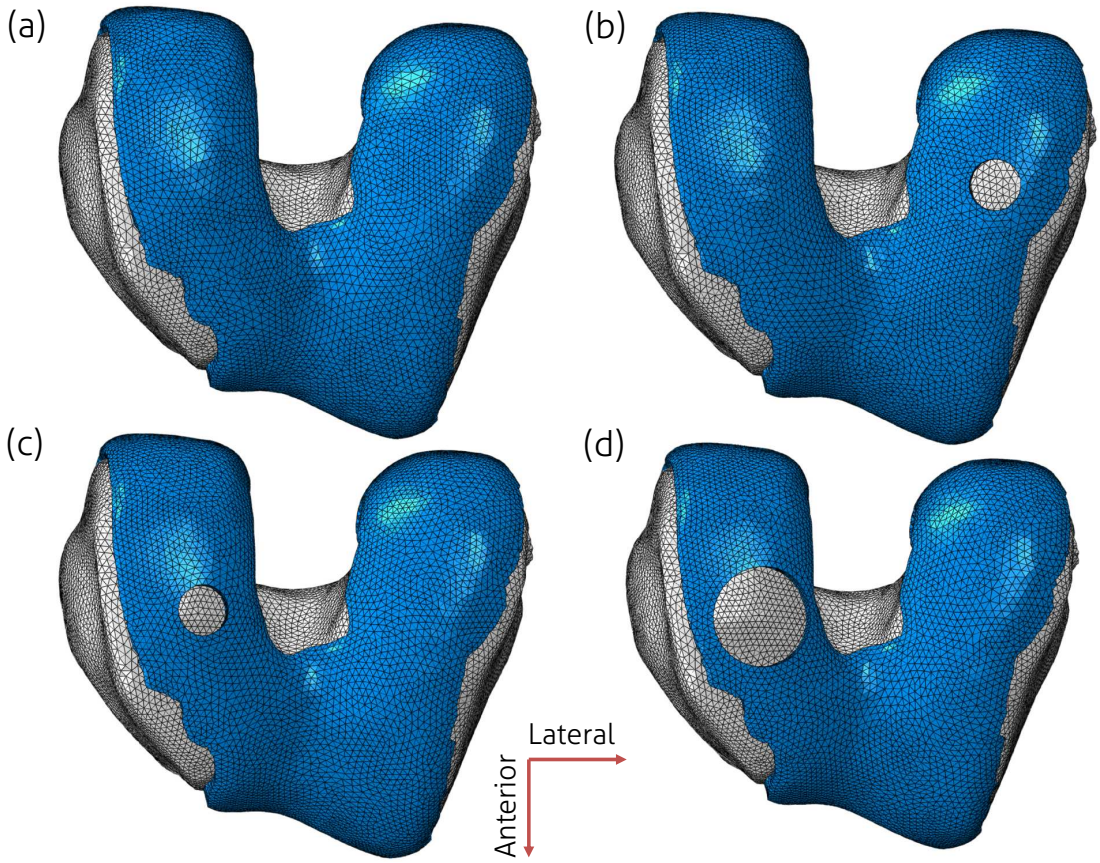

Figure 4.2: Femur and femoral cartilage of an adult female right knee with (a) healthy cartilage, a small (b) lateral or (c) medial focal defect, and (d) an average medial focal defect.

joint, was verified for each defect model by doubling the mesh density around the defect. Computed strains and joint motions were determined to be within the generally accepted mesh independence criterion (outlined by Donahue et al. (2002) as less than 5% variation associated with mesh refinement).

4.2.3 Constitutive modeling

Bone geometries were modeled as rigid structures with constant density equal to 2000 kg/m^3 due to the minimal influence of bone deformation in models of whole knee biomechanics (Beillas et al., 2004; Donahue et al., 2002; Kiapour et al., 2014a). Menisci were assumed to be transversely isotropic, linear elastic, where the preferred material direction was oriented circumferentially around each meniscal horn (Skaggs et al., 1994; Tissakht and Ahmed, 1995). The menisci were attached to the tibial plateau with linear uniaxial elements representing the meniscal ligaments (Donahue et al., 2002; Marchi and Arruda,

2017a; Villegas et al., 2007). Total equivalent stiffness of the meniscal ligaments was chosen as E_{equiv} = 2000 N/mm (Guess et al., 2010; Zielinska and Donahue, 2006).

The major supporting ligaments—the ACL, PCL, MCL, and LCL—were assumed to have responses represented by a slightly compressible, nonlinear, and transversely isotopic extension of a freely jointed eight-chain model of rubber elasticity (Arruda and Boyce, 1993; Bischoff et al., 2002a). Details on the constitutive form of supporting ligaments can be found in Appendix A and ligament material parameters can be found in Table A.1.

Articular cartilage was modeled assuming the same constitutive form as the ligaments (Deneweth et al., 2013a, 2015), without time dependency due to the low rate sensitivity of cartilage during active events (Oloyede et al., 1992). In addition to the constitutive behavior described in Appendix A, articular cartilage was modeled with spatial mechanically heterogeneity in accordance with experimental observations (Deneweth et al., 2013a,b, 2015). The mechanical heterogeneity in cartilage, defined in the plane parallel to the tibial plateau and in the pseudo-cylindrical surface parallel to the distal end of the femur, was incorporated through initial moduli distributions calculated using smooth and continuous interpolations of sparse experimental moduli data (Marchi and Arruda, 2017a). Due to the numeric interpolation framework used in describing the cartilage moduli fields, no modifications to the fields were necessary to accommodate focal defects—*i.e.*, the moduli of tissue located on the rim of a particular focal defect had the exact same initial modulus as similarly located tissue in the intact cartilage.

4.2.4 Boundary conditions and constraints

Following the boundary conditions outlined in Marchi and Arruda (2017a), an axial, compressive load was applied to the distal tibia at the ankle. Using an explicit FE framework, the final configuration of the foot flat portion of the stance phase of gait was approximated by applying a linear time varying load, with $F_{\text{max}} = 800$ N and $T_{\text{loading}} = 0.4$ sec, corresponding to roughly one body weight being entirely supported by the joint. All simulations were conducted without local mass scaling to minimize inertial errors. The A-P and M-L translations of the ankle (distal tibia) were constrained, while the hip (proximal femur) was translationally fixed. All rotational degrees of freedom at the ankle and hip were unconstrained. These conditions were selected to approximate the far field boundary conditions typical of this type of motion, while simultaneously allowing for local joint deformation to be dictated solely by the tissue structures contained within the knee.

Contact was allowed between all solid structures in the joint. Normal behavior was modeled using a general penalty enforcement method, and finite strain tangential behavior

was modeled assuming an exponential relationship between the local relative facet-to-facet sliding rate and the coefficient of friction; the relationship was constructed from experimental observations of cartilage-to-cartilage sliding (Marchi and Arruda, 2017a; Qian et al., 2006; Unsworth et al., 1975). Muscle and tendon pretension was applied prior to the load step, allowing for any associated knee motion and tissue deformation to equilibrate (Marchi and Arruda, 2017a; McLean et al., 2011; Oh et al., 2011; Pflum et al., 2004; Withrow et al., 2006, 2008). All joint kinematics were calculated with respect to a dynamic, nonorthogonal knee coordinate system (Grood and Suntay, 1983).

4.3 Results

4.3.1 Joint kinematics

Relative translations and rotations between the tibia and femur were found to be tied to the presence of defects (Table 4.1). In all defect models, the amount of tibial rotation decreased compared to intact cartilage. A lateral defect increased predicted flexion, while medial defects (small and average sized) had the opposite effect. All defect models predicted increased anterior tibial translation relative to healthy cartilage, with the largest difference corresponding to the average sized medial defect.

Table 4.1: Joint kinematics of native and focal defect models

	Anterior tibial translation (mm)	External tibial rotation (°)	Knee flexion (°)
Healthy	-1.2	3.3	-1.4
Lateral – Small	-1.1	2.6	-2.1
Medial – Small	-0.76	2.5	-1.1
Medial – Average	-0.22	2.2	-0.46

4.3.2 Femoral cartilage mechanics

Variation in joint kinematics associated with cartilage defects corresponded to differences between tissue-level strain distributions in the femoral cartilages (Fig. 4.3). Compressive strains increased from 9.7 to 12% with the presence of a lateral defect (Fig. 4.3b). Additionally, the location of maximum compression shifted from the medial condyle to the medial aspect of the lateral focal defect. This shift in the spatial location of maximum

compressive strain resulted in mechanically different cartilage (9% more compliant compared to the initial modulus of the spatial point of maximum compression in the healthy cartilage model) supporting the elevated loading environment. In medial defect models, the maximum compressive strains were similarly observed on the rim of the defect. Maximum compressive strains increased to 15% (Fig. 4.3c) and 21% (Fig. 4.3d) in knee models with small and average sized defects, respectively. Similar to the lateral defect model, the spatial points of maximum compression in medial defect containing models were different than healthy cartilage. This resulted in 2% reductions in local cartilage initial stiffnesses compared to the spatial point of maximum compression in the healthy cartilage model. Medial defects had little effect on deformation on the lateral condyle compared to healthy cartilage (Figs. 4.3a, 4.3c, and 4.3d).

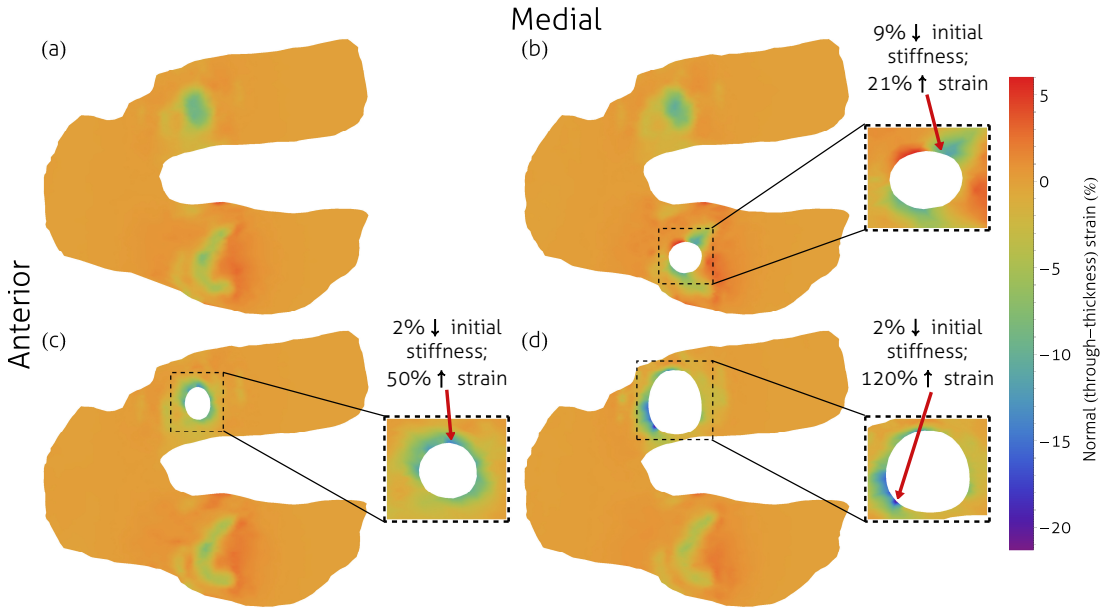

Figure 4.3: Tensile and compressive through-thickness strains on the articular surface of femoral cartilage assuming (a) healthy cartilage, femoral cartilage with a small (b) lateral or (c) medial focal defect, or (d) an average medial focal defect. A magnified view of the strain field around the perimeter of the defect is shown adjacent to each model containing a defect (b-d).

Strains evolving from axial rotations and M-L translations of the femur relative to the tibia (M-L shear strains) were strongly tied to the position of focal defects in the femur (Fig. 4.4). Medial defects eliminated the shear strain localization present on the medial condyle in healthy cartilage due to the physical absence of cartilage tissue. Larger medial defects also altered the distribution and location of the M-L shear strains on the lateral condyle articular surface (Fig. 4.4d). The presence of a small medial defect had no significant

effect on the maximum absolute M-L shear strain, while increasing the size of the defect on the medial condyle decreased the maximum absolute M-L shear strain from 14% to 11%. Cartilage containing a lateral defect experienced an increase in maximum absolute M-L shear strains from 14% to 16% with respect to healthy cartilage.

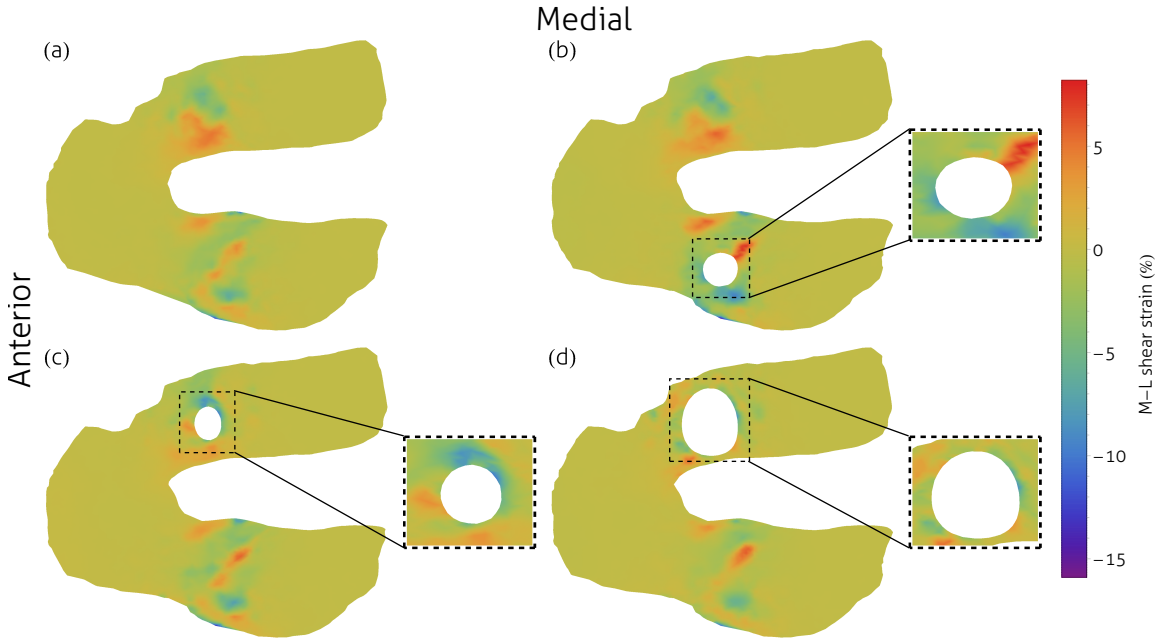

Figure 4.4: M-L shear strains on the articular surface of femoral cartilage assuming (a) healthy cartilage, femoral cartilage with a small (b) lateral or (c) medial focal defect, or (d) an average medial focal defect. A magnified view of the strain field around the perimeter of the defect is shown adjacent to each model containing a defect (b-d).

4.3.3 Tibial cartilage mechanics

Femoral cartilage focal defects also influenced compressive strains in the tibial cartilage (Fig. 4.5). A small defect on the lateral femoral condyle resulted in an increase in the maximum compressive strain on the lateral tibial plateau from 14% in healthy cartilage to 17% and resulted in a shift in the spatial point of maximum compression medially and posteriorly on the lateral plateau (Fig. 4.5b). This locational shift was associated with a 6% reduction in initial cartilage modulus at the spatial point of maximum compressive strain compared to healthy cartilage. There were reductions in maximum compressive strains from 14% in native cartilage to 13% and 11% with small (Fig. 4.5c) and average (Fig. 4.5d) sized medial defects, respectively. Additionally, the large medial defect shifted the maximum compressive strain laterally.

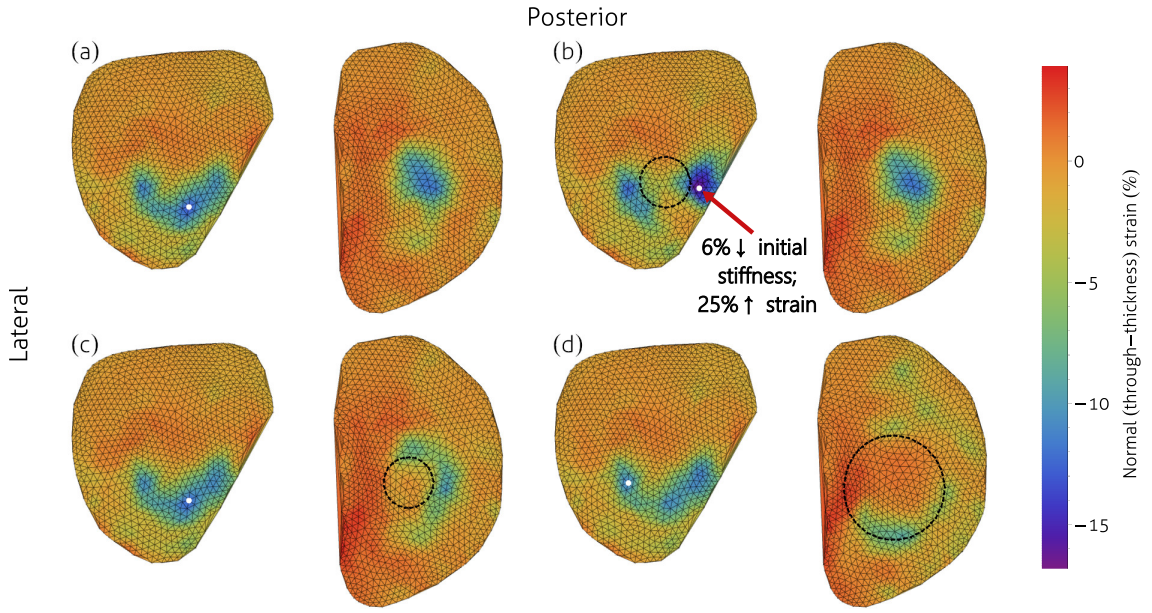

Figure 4.5: Normal strains on the articular surface of tibial cartilage with (a) healthy femoral cartilage, a small (b) lateral or (c) medial focal defect, and (d) average medial focal defect. For each figure the perimeter of the corresponding femoral cartilage defect is outlined in black and the point of maximum compression is located at the center of the white dot.

Variations in the distributions of A-P (Fig. 4.6) and M-L (Fig. 4.7) shear strains were observed on the tibial cartilage; however, there was relatively small nominal deviations (<1%) in the maximum absolute shear strains. Small and average medial defects reduced the distance between regions of positive and negative A-P shear strains on the medial tibial plateau (Figs. 4.6c-d). The presence of medial defects also altered the location of maximum A-P shear strains anteriorly with respect to healthy cartilage. As the size of the defect increased on the medial condyle, the A-P shear strain localization on the medial plateau diffused, and a large positive A-P shear strain emerged on the medial plateau corresponding to the shifting knee flexion and axial rotation (Fig. 4.6d; Table 4.1). A small medial defect disturbed the large region of M-L shear strains on the medial plateau compared to healthy cartilage (Fig. 4.7c), whereas an average medial femoral defect caused widespread alterations to the M-L shear strain field on the medial plateau (Fig. 4.7d).

The maximum, area-averaged contact stresses on the articular surface of the tibial and femoral cartilages increased from 16 MPa in healthy cartilage to 21 MPa, 18 MPa, and 18 MPa in small lateral, small medial, and average sized medial defect models, respectively. Area-averaged values were calculated by identifying the cartilage location supporting the maximum contact stresses over a region defined by a 1 mm diameter disk. In medial defect containing models, the location of maximum contact pressure moved from the midsub-

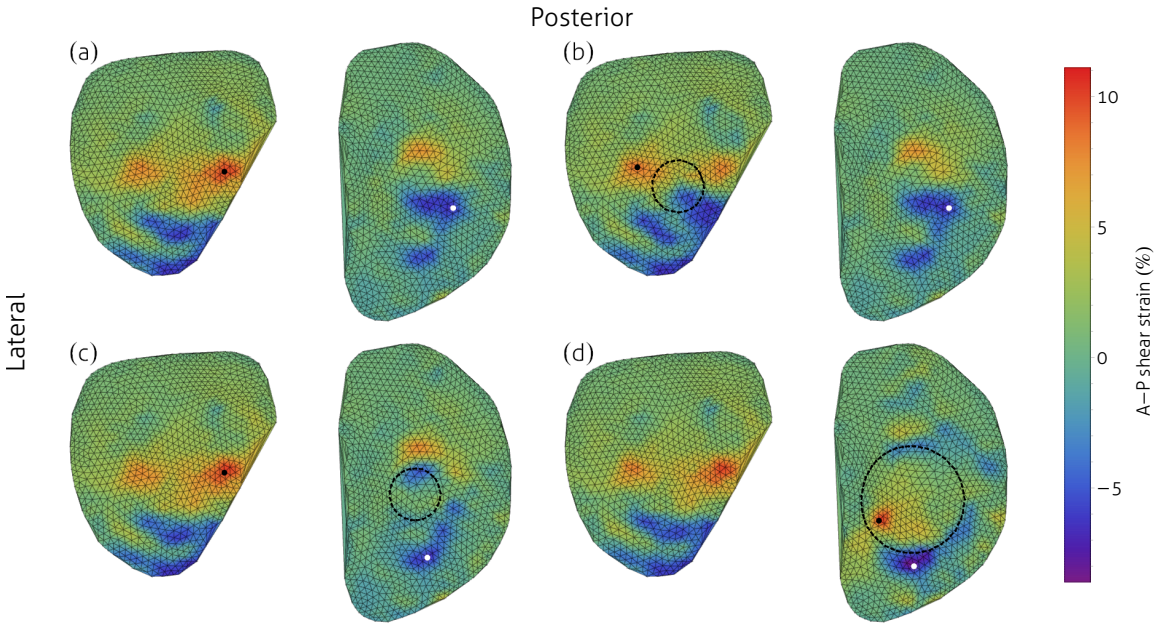

Figure 4.6: A-P shear strains on the articular surface of tibial cartilage with (a) healthy femoral cartilage, a small (b) lateral or (c) medial focal defect, and (d) an average medial focal defect. For each figure the perimeter of the corresponding femoral cartilage defect is outlined in black and the point of maximum and minimum A-P shear strain is located at the center of the black and white dots, respectively.

stance of the tibial cartilage to the perimeter of the femoral cartilage defect. As opposed to strain distributions, contact stresses were found to be highly localized due to the nonlinearity and heterogeneity of the cartilage constitutive models. A complete summary of various maximum observed strain and stress measures for healthy and defect containing models can be found in Table 4.2.

Table 4.2: Summary of maximum tissue strains and contact stresses among various cartilage models. In defect containing models ↑ and ↓ indicate local increases and decreases with respect to the healthy cartilage predictions, respectively.

	Healthy	Small defect		Average defect
		Lateral	Medial	Medial
Femoral compressive strain, % (Fig. 4.3)	9.7	12 (↑)	15 (↑)	21 (↑)
Femoral M-L shear strain, % (Fig. 4.4)	14	16 (↑)	14	11 (↓)
Tibial compressive strain, % (Fig. 4.5)	14	17 (↑)	13 (↓)	11 (↓)
Tibial A-P shear strain, % (Fig. 4.6)	10	9.1 (↓)	10	11 (↑)
Tibial M-L shear strain, % (Fig. 4.7)	11	9.5 (↓)	11	10 (↓)
Max contact stress, MPa	16	21 (↑)	18 (↑)	18 (↑)

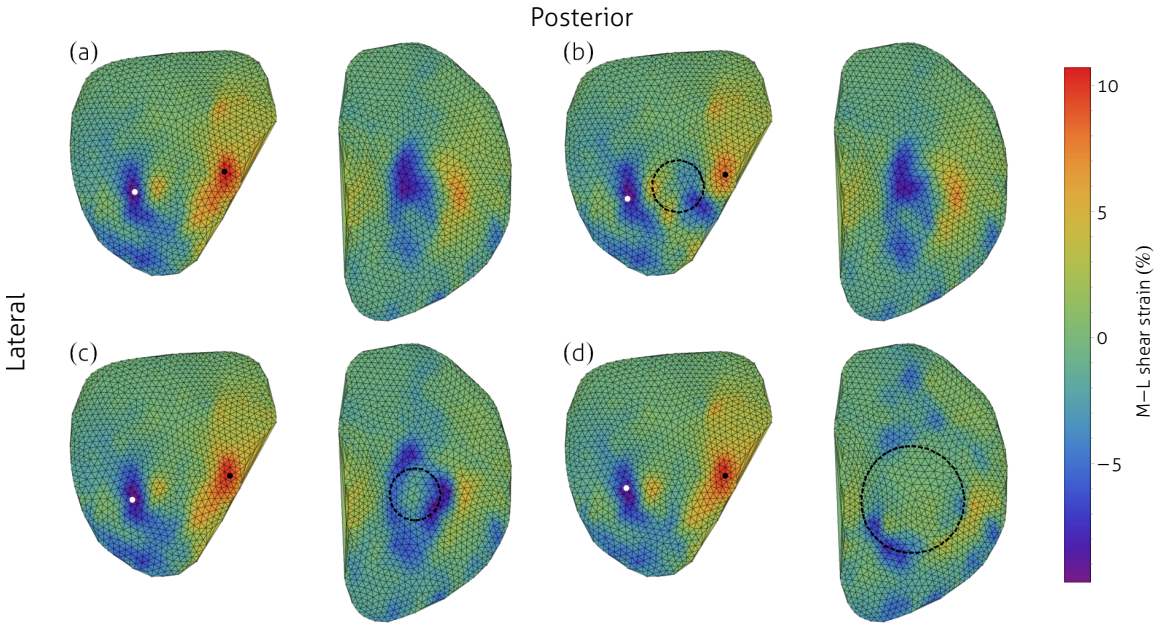

Figure 4.7: M-L shear strains on the articular surface of tibial cartilage with (a) healthy femoral cartilage, a small (b) lateral or (c) medial focal defect, and (d) an average medial focal defect. For each figure the perimeter of the corresponding femoral cartilage defect is outlined in black and the point of maximum and minimum M-L shear strain is located at the center of the black and white dots, respectively.

4.4 Discussion

Cartilage tissue degeneration has been linked to the size and geometry of focal defects potentially precipitated by local changes in the mechanical loading of the area surrounding defects. It has been shown that focal defects, if left untreated, are detrimental to tissue viability and integrity (Lefkoe et al., 1993; Wang et al., 2006). The increase in local mechanical stresses triggered by the presence of defects near their edges may be indicative of potentially dangerous mechanical overloading of the cells in the vicinity of injured tissues. Representative three dimensional joint models provide the ability to quantify the complete deformation state of tissues, as opposed to simply providing traditional contact parameters, a limitation of many experimental techniques. This was demonstrated in a model by Venäläinen et al. (2016b), which found that strains throughout the depth of the tissue adjacent to a tibial cartilage defect exceeded levels shown to induce chondrocyte apoptosis.

The objective of this study was to investigate how local tissue deformation in both femoral and tibial cartilages was altered as the size and location of femoral condylar defects in an anatomically correct whole knee model that integrates the spatial variability of cartilage mechanical properties across the bone surfaces (Marchi and Arruda, 2017a) were

varied. With this model, kinematic motion of the knee was assessed as a function of defect location and local stress calculated for regions of peak strain. Our model demonstrates that changes in the local deformation of cartilage due to the presence of defects can translate to new and mechanically different tissues to be loaded during normal activity. To our knowledge, this is the first model to demonstrate this phenomenon. Accounting for the regional variation in stiffness can more accurately define the local cell-level deformations and stresses to predict the risk of cell apoptosis due to traumatic cartilage injuries.

The results presented herein are in agreement with the outcomes of previous computational studies that have shown femoral cartilage near-field contact stresses and compressive strains were strongly correlated to defect size in weight bearing regions, particularly at the perimeter of the defect (D D'Lima et al., 2009; Papaioannou et al., 2010; Peña et al., 2007; Weiss et al., 1998). Peña et al. (2007) illustrated the contribution of focal defect size and location in high and low load-bearing regions on the medial femoral condyle. The strain values in that study were much higher than this work, possibly due to the difference in shape of the defect and the assumptions of linear elastic cartilage with a relatively low modulus ($E = 5$ MPa). As we have previously shown, the assumed linear elastic stiffness of cartilage significantly affects cartilage deformation, with increased compliance corresponding to increased strain (Marchi and Arruda, 2017a). The effect of this relationship can be seen in D D'Lima et al. (2009), which investigated the effect of chondral defects in a model that assumed linear elasticity with $E = 15$ MPa. Similar to their data, the peak strain in healthy cartilage in our study was 9.7% (compared to $\sim$8%) and 15% (compared to $\sim$13%) with an 8 mm defect (0.5 cm^2) on the medial condyle (an approximately 150% increase compared to healthy cartilage). A larger defect corresponded to an increase of the maximum rim strain to 21% (an approximately 200% increase compared to healthy cartilage), in good agreement to the increases found by Peña et al. (2007) of 185% and 200% for 1.76 cm^2 and 3.14 cm^2 defects, respectively, notwithstanding differences in absolute strain values. Healthy cartilage compressive strains predicted by Venäläinen et al. (2016b) were elevated compared to those presented in this study; however, the relative increase between defect containing and healthy cartilage models is approximately of the same order (roughly a 2-3 fold increase in maximum compressive strains of the defect containing tissue associated with the inclusion of a focal defect).

The effects of defects are not isolated to the damaged tissue, but have also been shown to alter joint kinematics and deformation in opposing tissues. Convery et al. (1972) illustrated that large focal defects located in weight bearing regions on the femoral cartilage caused cartilage wear and degeneration on the opposing tibial cartilage articular surface. The presence of focal cartilage defects has also been correlated with increased incidence

of OA throughout the joint (Lefkoe et al., 1993; Linden, 1977). Despite experimental evidence of the joint-wide disruption of defects, many computational studies investigating defects are limited to the cartilage surface that is affected (D D'Lima et al., 2009; Dabiri and Li, 2015; Dong et al., 2011; Peña et al., 2007; Venäläinen et al., 2016b). The distribution of loads on the tibial plateau assuming healthy cartilage is largely consistent with previous studies (Ahmed and Burke, 1983; Peña et al., 2006a). In a full knee model similar to the one presented here, Peña et al. (2006a) found a maximal compressive stress of 4.4 MPa compared to 16 MPa in the current work, with a similar relative distribution of deformation; nominal differences between stress values can be attributed to the assumed forms of the cartilage constitutive models. Additionally, Papaioannou et al. (2010) measured the effect of defects located on the medial and lateral femoral condyles under a 700 N load on contact stresses in tibial cartilage and found that stresses were elevated compared to baseline measures, similar to the increases in tibial cartilage strains and contact stresses observed herein (Table 4.2). These studies highlight that investigating the effects of focal defects on adjacent tissues may contribute to our understanding of the mechanical etiology of arthritic lesions in healthy cartilage tissue distant from focal defects.

The connection between the shift in location of maximum loading and cartilage mechanical properties has not been previously reported. We have previously shown that the mechanical properties of articular cartilage vary across the surface of the femur and tibia (Deneweth et al., 2013b, 2015) and integrated these data into a whole knee FE model (Marchi and Arruda, 2017a). Our model demonstrates that changes in the local deformation of cartilage due to the presence of defects translates to new and mechanically different tissues being loaded during normal activity. At the spatial point of maximum compression, the local initial cartilage moduli decreased by 9%, 2%, and 2% corresponding to small lateral, small medial, and average medial defects, respectively, compared to healthy femoral cartilage. Therefore, as the locations of high deformation vary with the inclusion of focal defects, the local mechanical behavior of the chondrocytes may be ill-equipped to support the new loading distributions. Surprisingly, the relocation of the point of maximum deformation medially and posteriorly with the inclusion of a lateral defect resulted in a 25% increase in compressive strain on the tibial cartilage. This shift corresponded to a decrease in local tibial cartilage initial modulus at the spatial point of maximum compression by over 6%. In the context of spatially varying mechanical properties, these predicted cartilage strain distributions may prove to have incredible clinical value, potentially being used to justify the use of one treatment plan over another in an effort to best preserve or restore local cartilage deformation distributions.

Relative motion between the tibia and femur drives the distributions of deformation in

knee soft tissues, and focal defects haven been closely tied to deviations from normal joint motion. Andriacchi et al. (2009) showed that cartilaginous injury may manifest as changes in gait, potentially linked to the progression of OA. Furthermore, determining changes in joint kinematics may be valuable for understanding the mechanical causes of OA in patients with ACL reconstruction, as chondral defects are often found in these patients (Årøen et al., 2004; Bobić, 1996; Curl et al., 1997; Engebretsen et al., 1993; Hjelle et al., 2002; Matsusue et al., 1993; Murrell et al., 2001; Widuchowski et al., 2007). Differences in joint kinematics will likely impact the stress distributions within ligaments and may be correlated with higher revision rates of ACL repair in patients with concomitant cartilage damage (Borchers et al., 2011; Cox et al., 2014). The femur rotates internally during stance phase of gait (Kozanek et al., 2009), similar to the rotations predicted herein (Table 4.1). Our model predicted 3.3° external tibial rotation in joints with intact cartilage, which is on the order of similar studies (Marouane et al., 2014; Mootanah et al., 2014; Peña et al., 2006a). Small defects on either condyle resulted in only minor kinematic changes relative to healthy cartilage, while the largest deviations in joint motion were found when considering an average medial defect (Table 4.1). Shifts in kinematics corresponding to an average medial defect increased the magnitude and altered the location of absolute maximum A-P shear strains on the tibial plateau (Fig. 4.6d), as well as the spatial position of maximum compressive strain (Fig. 4.5d). This model can be extended to evaluate the complex mechanics of joints with injury to multiple tissues, and the kinematic results presented herein suggest that clinical strategies that minimize medial cartilage damage may minimize the macroscopic effects of focal defects.

Chondrocyte viability is partially limited by mechanical factors, like strain. Our model showed that the presence of focal defects did not elevate compressive strains above relevant strain-based thresholds ($\sim$30%) (Wilson et al., 2006), while predicted stresses were near the upper end of stress-based thresholds ($\sim$20-25 MPa) (Chen and Torzilli, 2015; Torzilli et al., 1999; Verteramo and Seedhom, 2007). Native cartilage maximum, area-averaged contact stresses were observed approaching the critical, stress-based threshold at 16 MPa, while compressive strains were well below their corresponding strain-based threshold at 14%. Area-averaged contact stresses were calculated in the current work to allow for more direct comparisons to experimental measurements of contact stress that use pressure sensitive films (Beck et al., 2005). While stress values presented herein may be high relative to stress-based viability thresholds, it is also important to note that these ranges were determined under the assumption of high rate and uniform impact loading. Additionally, stress-based viability thresholds were also established without any consideration of fundamental mechanical heterogeneity of cartilage or how shifts from normal loading regions to

unloaded regions may be coupled to biochemical activity and adaptability within chondrocytes. Notwithstanding these considerations, the elevated mechanical loading environment found in defect models could potentially lead to a dangerous cascade of cell damage and tissue degeneration. This was observed experimentally by Jackson et al. (2001), which showed the degradation of cartilage at the defect perimeter with time and normal joint use.

This model has several limitations. First, deformation was only considered for the stance phase of gait (with the joint starting at approximately full extension). As loading significantly changes throughout the gait cycle, it would be important to study how different joint configurations affect cartilage deformation as a function of defect size and location. In the context of whole joint models, axial tibial loading has been a typical approximation to the global loading of the knee during the stance phase of gait (D D'Lima et al., 2009; Donahue et al., 2002; Marchi and Arruda, 2017a; Peña et al., 2007; Shirazi and Shirazi-Adl, 2009b; Weiss et al., 1998), though there have been some recent computational studies that have directly incorporated experimentally derived kinematics as simulation boundary conditions (Halonen et al., 2016; Hosseini et al., 2014; Klets et al., 2016; Mononen et al., 2015, 2016). Another limitation of this model is that the bone is assumed to be rigid, and the model does not consider the rapid changes in the subchondral bone that occur soon after cartilage injury (Gomoll et al., 2010; Radin and Rose, 1986), which is expected to affect cartilage stresses (Shirazi and Shirazi-Adl, 2009b; Venäläinen et al., 2016a). Computational joint models also universally struggle with intrinsic variation in the joint anatomy and soft tissue mechanical properties of individual patients. Finally, this work does not consider how alterations manifesting from physical changes to the cartilage geometry may affect expected joint loading.

Despite these limitations, this work provides insights into the mechanical contribution of femoral cartilage focal defects through their inclusion in whole knee FE models, which include major tissue structures built with accurate constitutive descriptions. The models used in this work show how focal defects contribute to deviations in joint kinematics, leading to altered tissue strains near the defect and on the opposing cartilage surfaces. Even during normal activity, focal defects disrupt knee motion and the distribution of soft tissue strains (Elias et al., 1999). During abnormal, injury causing events these perturbations are likely to be exaggerated, increasing the risk to future soft tissue injuries and diseases. The framework developed herein provides a step forward in the ability of clinicians to assess patient specific cartilage susceptibility to OA by accurately predicting full field, tissue level deformation in the knee. This work also provides a platform for investigating potential clinical inventions and repair devices aimed at restoring native joint mechanics.

CHAPTER 5

Evaluating continuum level descriptions of the medial collateral ligament

This chapter has been submitted for publication and may be referenced as:

> B. C. Marchi, C. M. Luetkemeyer, and E. M. Arruda. Evaluating continuum level descriptions of the medial collateral ligament. *In Review*, 2017b

5.1 Introduction

Ligaments are soft tissue structures that span the gaps between bones, connecting them together. Macroscopic joint motion and stability are coordinated and maintained by ligaments in combination with additional soft tissue structures like muscles, articular cartilage, menisci, and tendons. Ligaments support and direct normal joint motions, while acting to resist potentially harmful motions. While ligaments often play a critical role in mitigating the risk of a traumatic event—either contact or noncontact—from resulting in acute injury, ligaments do fail. This failure may be catastrophic, as in ligament rupture resulting in hyper-mobility of the joint. Alternatively, in progressive ligament injuries microscopic damage accumulates, leading to structural and mechanical changes within the tissue bulk. These subtle changes in ligament mechanical behavior and structural geometry can have a significant impact on total joint motion, as well as local deformation in the joint; deviations from expected local tissue deformations can potentially lead to collateral tissue degenerative diseases, like OA.

Ligament failure is both prolific and complex. The ACL is the most commonly injured supporting ligament in the knee, with over 175,000 surgical reconstructions performed annually in the United States (Spindler and Wright, 2008), and, problematically, the average age of those affected by soft tissue injury is dropping drastically (Ingram et al., 2008; Kim et al., 2011b). Yet, even with the nearly 90% short term success rate of ACL reconstruction (Wright et al., 2008), these injuries are linked to increased susceptibility for collateral soft tissue diseases, like OA (Kessler et al., 2008)—a disease that already affects over 15% of the adult United States population (Lawrence et al., 2008). The existence

and frequency of ligament injury, and its contribution to secondary soft tissue injuries and diseases, has motivated researchers and clinicians to examine their mechanical behavior in myriad contexts. Experimental studies have explored macroscopic joint motion in healthy and ligament-deficient knees (Berchuck et al., 1990; Georgoulis et al., 2003; Morrison, 1970; Noyes et al., 1992), ligament injury mechanisms (Boden et al., 2000; Hewett et al., 2005; Krosshaug et al., 2007b; Olsen et al., 2004), reconstructive techniques (Hughston and Eilers, 1973; Kurosaka et al., 1987; Yagi et al., 2002), and rehabilitation protocols (Beynnon et al., 1995; Shelbourne and Nitz, 1990).

Given the fundamental role of ligaments in maintaining joint functionality, a mechanistic understanding of ligaments is critically important. The mechanics of individual ligament structures can provide insights into the specific contributions of a particular ligament in preserving joint integrity, minimizing the risk of injury, and potential mechanical pathways of ligament injury. A mechanical appreciation of ligaments can also be instrumental in investigating, evaluating, and differentiating between clinical interventions. Experimental efforts at this low level have indeed furthered our characterization and understanding of ligaments; however, experimental studies, particularly related to experimental biomechanics, have a number of irreconcilable limitations, including structural and geometric specimen-to-specimen variability, low spatial and temporal resolution, prohibitive specimen acquisition and storage costs, and an inability to describe deformation states generally.

Where experiments are limited, computational tools and models have the potential to excel. Computational models, particularly FE models, can provide specific information on individual tissue contributions with respect to global joint function, as well as the coupling and coordination among tissues during macroscopic joint motions. Computational models offer precise, full-field, and complete descriptions of deformation manifesting from normal motions (Adouni et al., 2012; Beillas et al., 2004; Donahue et al., 2002; Gardiner and Weiss, 2003; Limbert et al., 2004; Marchi and Arruda, 2017a; Mootanah et al., 2014; Peña et al., 2006a; Shelburne et al., 2006; Song et al., 2004; Xie et al., 2009; Zhang et al., 2008), injury causing activities (Abdel-Rahman and Hefzy, 1998; Kiapour et al., 2014a; Penrose et al., 2002; Quatman et al., 2011), injured and diseased joints (Manda et al., 2011; Marchi et al., 2017a; McLean et al., 2011; Mootanah et al., 2014; Peña et al., 2007; Shirazi and Shirazi-Adl, 2009b; Weiss et al., 1998), and reconstructive procedures (Bae et al., 2015; Godest et al., 2002; Halloran et al., 2005; Huang et al., 2012; Kim et al., 2011a; Peña et al., 2005b, 2006b; Ramaniraka et al., 2007; Westermann et al., 2013, 2016). FE models also afford a convenient platform for the systematic evaluation of relevant geometric and mechanical properties through parametric studies (Atmaca et al., 2013; Baldwin et al., 2012; Donahue et al., 2003; Kiapour et al., 2014b; Li et al., 2002; Marouane et al., 2014; Mesfar and

Shirazi-Adl, 2005; Peña et al., 2005a; Shin et al., 2007; Shirazi and Shirazi-Adl, 2009a,b; Wan et al., 2013; Wang et al., 2014) and have the potential to conduct clinically meaningful, individualized joint analyses (Gardiner and Weiss, 2003; Jones et al., 2015).

The accessibility and power of FE models have pushed forward our understanding of tissue-level contributions to joint mechanics, but with so much available information researchers must be judicious in evaluating the significance of studies. Constitutive models of individual tissues dictate the basic physics of any structural biomechanics analysis; however, they are often relegated to minutia of methods sections and rarely examined in a systematic or forthright manner. Constitutive models need to be evaluated on their ability to describe observed deformation, while simultaneously predicting deformations not used in their construction. Often whole joint computational models rely on a single set of experimental data—which may or may not sufficiently describe all the relevant physics—and the weight of precedent to build soft tissue material behaviors. This approach is convenient, but not very elastic to new or conflicting experimental observations.

With an eye towards adaptability and implementation, this work seeks to test the hypothesis that the commonly employed family of invariant-based transversely isotropic, exponential models is capable of capturing the bulk mechanical response of knee supporting ligaments. Specifically, the appropriateness of various transversely isotropic, hyperelastic constitutive models containing a single material direction are examined, using the commonly adopted Holzapfel-Gasser-Ogden (HGO) model as a benchmark. Constitutive forms are assessed in the context of their ability to describe historic and current quasi-static experimental stress-strain behaviors of the MCL. The HGO model is evaluated on its ability to capture both longitudinal and transverse deformations and compared to alternative transversely isotropic, hyperelastic material models. This work shows that the traditional HGO model is largely able to capture the response of the MCL based on historic data. However, the model, as it is traditionally posed, is less flexible to data that are more anisotropic and nonlinear, like those found in recent efforts. Therefore, the HGO model, and those of its type, may be ill-suited to describe the complete physics of the ligament. Representative constitutive theories are critically important when building descriptive models that incorporate real deformations, which potentially include multi-axis loading and shear. This failure motivates the need to systematically assess the appropriateness of a larger pool of candidate constitutive theories, including novel theories, for describing ligaments. In addition to gauging their descriptive performance, candidate theories were incorporated into a simple, three-dimensional FE model to evaluate how constitutive form affects bulk deformation.

5.2 MCL experimental characterization

The addition of directionality in constitutive models requires knowledge of the material response in multiple loading configurations. This need has led to the application of traditional mechanical characterization techniques to capture the stress-strain behavior of tissues assumed to be transversely isotropic, like ligaments (Butler et al., 1990; Henninger et al., 2013, 2015; Lujan et al., 2007; Quapp and Weiss, 1998). In particular, tension experiments have been used to determine the bulk response of ligaments along (longitudinal) and normal (transverse) to the preferred material direction. In the case of ligaments, the material orientation is typically assumed to be aligned with the mean orientation of collagen fibers (Debski et al., 2003; Weiss et al., 2005).

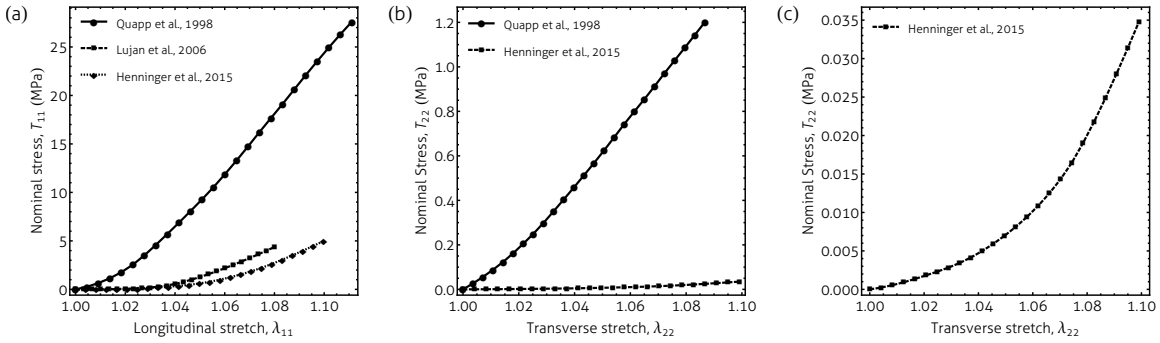

Figure 5.1: The quasi-static stress-strain response of human MCL (a) along and (b,c) normal to the preferred material direction. Experimental data extracted from Henninger et al. (2015), Lujan et al. (2007), and Quapp and Weiss (1998).

In this work, both historic (Quapp and Weiss, 1998) and recent (Henninger et al., 2013, 2015; Lujan et al., 2007) experimental efforts were used as the foundation of the assessment of each candidate constitutive theory. Figure 5.1 illustrates the unidirectional mechanical response of cadaveric human MCLs along (Fig. 5.1a) and normal to (Figs. 5.1b-c) the highly aligned collagen fibers of the ligament. Typically, the preferred stress-strain response of soft tissues is characterized by two physiologically relevant domains: the toe and linear regions. The toe region is associated with initial nonlinearity observed at relatively small stretches, while the linear region is said to occur beyond some transition stretch after which the stress-strain response is nearly linear. For example, a visual inspection of the longitudinal stress-strain behavior presented in Quapp and Weiss (1998) (Fig. 5.1a) might lead one to conclude a transition between the toe and linear regions at approximately $\lambda_{11} = 1.02$ in the longitudinal direction.

5.3 Methods

5.3.1 Constitutive modeling: Phenomenological theories

5.3.1.1 Constitutive theory preliminaries

There has been a recent trend over the last two decades in describing macroscopic ligament mechanical behavior using transversely isotropic, hyperelastic constitutive models constructed with exponential behavior along the preferred fiber direction (material descriptions containing a single fiber family) in combination with a neo-Hookean matrix phase (Bae et al., 2015; Dhaher et al., 2010; Gardiner and Weiss, 2003; Guo et al., 2009; Kiapour et al., 2014a,b; Kim et al., 2011a; Limbert et al., 2004; Orsi et al., 2015; Peña et al., 2005b, 2006a,b, 2007; Quapp and Weiss, 1998; Wan et al., 2013, 2014; Westermann et al., 2013, 2016; Zhang et al., 2008). This movement towards more accurate tissue-level constitutive models in ligaments has been shown to have a meaningful effect on both tissue deformation and joint motion (Kiapour et al., 2014b). Models of this form—transversely isotropic hyperelasticity—also have the benefit of generally being physiologically motivated by the macromolecular organization of ligaments, where aligned collagen fibrils are situated in a more compliant, isotropic extracellular matrix (McLean et al., 2015; Weiss et al., 2005).

In particular, strain energy density functions for ligaments have taken the compressible, decoupled form adopted from Weiss et al. (1996)

$$U\left(\tilde{\mathbf{C}}, \mathbf{a}_0\right) = \tilde{U_1}\left(\tilde{I}_1\right) + \tilde{U_2}\left(\tilde{I}_4\right) + \tilde{U_3}\left(J\right), \tag{5.1}$$

where J is the determinant of the deformation gradient ($\mathbf{F}$), $\tilde{\mathbf{C}}$ is the isochoric Cauchy-Green tensor ($\tilde{\mathbf{C}} = \tilde{\mathbf{F}}^T\tilde{\mathbf{F}} = J^{-2/3}\mathbf{C} = J^{-2/3}\mathbf{F}^T\mathbf{F}$), $\tilde{I}_1$ is the first deviatoric invariant of $\tilde{\mathbf{C}}$ ($\tilde{I}_1 = \text{tr}\left(\tilde{\mathbf{C}}\right)$), and $\tilde{I}_4$ is the fourth deviatoric invariant ($\tilde{I}_4 = \mathbf{a}_0\tilde{\mathbf{C}}\mathbf{a}_0$, where $\mathbf{a}_0$ is the preferred fiber direction in the reference configuration).

These isochoric invariant-based descriptions of ligament anisotropy have been largely successful in describing the bulk uniaxial behavior along the preferred material direction—see fitting data from either Kiapour et al. (2014a) or Gardiner and Weiss (2003). However, decoupled, transversely isotropic strain energy functions have recently been shown to be incapable of describing true compressible, anisotropic material behavior due to their non-physical response to volumetric deformation (Vergori et al., 2013).

5.3.1.2 Isotropic strain energy contributions

Due to the fundamental issues related to constitutive models with isochoric anisotropic invariants (Eq. 5.1), anisotropic strain energy functions evaluated in this work will take the general, coupled form,

$$U\left(\mathbf{C},\mathbf{a}_0\right)=U_1\left(I_1\right)+U_2\left(I_4\right)+U_3\left(J\right), \tag{5.2}$$

where I_1 and I_4 are the first invariant $\left(I_1=\text{tr}\left(\mathbf{C}\right)=\text{tr}\left(\mathbf{F}^T\mathbf{F}\right)\right)$ and fourth invariant $\left(I_4=\mathbf{a}_0\mathbf{C}\mathbf{a}_0\right)$, respectively. The stretch, λ, along the preferred material direction is related to I_4 by the following:

$$\lambda^2=I_4, \tag{5.3}$$

assuming $\mathbf{a}_0$ is a unit vector; in this work, $\mathbf{a}_0$ is assumed to be a unit vector.

In the context of ligaments, the isotropic contribution of Eq. 5.2 $\left(U_1\right)$ has been predominately assumed to have the form

$$U_1=C_1\left(J^{-2/3}I_1-3\right) \tag{5.4a}$$

or

$$U_1=C_1\left(I_1-3\right)-2C_1\ln\left(J\right), \tag{5.4b}$$

representing an isotropic neo-Hookean solid (Quapp and Weiss, 1998). Note that Eqs. 5.4a-b are not strictly dependent on I_1, but also J. This is a common notational quark from traditional decoupled, isotropic strain energy functions and the choice of form has no practical consequence.

The volumetric component of the general strain energy function, U_3 in Eq. 5.2, has taken a variety of forms in the description of ligaments, though their forms, particularly for physiologically relevant loading ranges, have relatively little impact on the overall constitutive performance (Nolan and McGarry, 2015). Based on the insensitivity shown in Nolan and McGarry (2015), volumetric strain energy contributions examined herein are predominately assumed to have the form

$$U_3=\frac{B}{2}(J-1)^2, \tag{5.5}$$

where B is the bulk modulus.

5.3.1.3 Anisotropic strain energy contributions

For ligaments, the directional component of strain energy functions has been assumed to take a number of forms. Preferred material behavior has been described in terms of its derivatives (Chatelin et al., 2013; Quapp and Weiss, 1998; Weiss et al., 1996), as polynomial functions (Feng et al., 2013), and exponentials (Gasser et al., 2006; Holzapfel et al., 2000, 2002; Kiapour et al., 2014a,b; Weiss et al., 1996). It naturally follows from Eq. 5.2 that total strain energy functions may be constructed by adding isotropic and volmetric strain energy contributions with any particular directional strain energy contribution (U_2).

Nolan et al. (2014) proposed a coupled, compressible form of the HGO (cHGO) model, with the anisotropic strain energy contribution described as

$$U_2 = \frac{k_1}{2k_2}\left\{\exp\left[k_2(I_4-1)^2\right]-1\right\}, \tag{5.6}$$

to address the volumetric deficiencies of isochoric, anisotropic strain energy functions, where k_1 and k_2 control the degree of anisotropy (the ratio of the magnitude of the stress-strain response in the preferred direction to the transverse direction) and magnitude of nonlinearity along the preferred material direction, respectively.

Similarly, other previously employed, decoupled anisotropic strain energy functions may be written in terms of total strain invariants. The derivative based description of anisotropy first presented by Weiss et al. (1996) can be recast as

$$\begin{aligned}
\lambda\frac{\partial U_2}{\partial\lambda} &= 0, && \lambda \leq 1;\\
\lambda\frac{\partial U_2}{\partial\lambda} &= C_3\left\{\exp\left[C_4\left(\lambda-1\right)\right]-1\right\}, && 1<\lambda\leq\lambda^*;\\
\lambda\frac{\partial U_2}{\partial\lambda} &= C_5\lambda + C_6, && \lambda^* \leq \lambda,
\end{aligned} \tag{5.7}$$

where C_i are fitting parameters, λ^* is the linear region transition stretch, and continuity constraints are typically placed on C_6:

$$C_6 = C_3\left\{\exp\left[C_4\left(\lambda-1\right)\right]-1\right\} - C_5\lambda. \tag{5.8}$$

Note, Eq. 5.7 contains an explicit definition for the toe region, $1<\lambda\leq\lambda^*$. Alternatively, a slightly reduced form of the model proposed in Feng et al. (2013) may be posed as

$$U_2 = C_1\zeta\left(I_4-1\right)^2, \tag{5.9}$$

where ζ represents the relative contribution of the fiber to the total material response. In the same vein as Eq. 5.6, both simplified,

$$U_2 = C_3 \left(\exp \left[I_4 - 1 \right] - I_4 \right), \tag{5.10}$$

and expanded,

$$U_2 = \frac{k_1}{2k_2} \left\{ \exp \left[k_2 \left(\kappa I_1 + (1 - 3\kappa) I_4 - 1 \right)^2 \right] - 1 \right\}, \tag{5.11}$$

exponential-based strain energy functions have been used to describe ligaments by Weiss et al. (1996) and Gasser et al. (2006), respectively. Equation 5.11 offers the flexibility for the existence of distributed fiber orientations around the preferred material direction, introduced into the anisotropic strain energy function through the scaling parameter κ.

5.3.1.4 Anisotropic, total invariant strain energy functions

Due to the fundamental issues related to constitutive models with anisotropic isochoric invariants, anisotropic strain energy functions evaluated in this work will take the general, coupled form shown in Eq. 5.2, where the isotropic, volumetric, and anisotropic strain energy functions are expressed with respect to total invariants. The resulting strain energy functions for the coupled Feng (Eq. 5.9), Weiss_{A} (Eq. 5.10), cHGO (Eq. 5.6) and distributed HGO (dcHGO; Eq. 5.11) models may be expressed as

$$U \left(\mathbf{C}, \mathbf{a}_0 \right) = C_1 \left(J^{-2/3} I_1 - 3 \right) + C_1 \zeta \left(I_4 - 1 \right)^2 + \frac{B}{2} (J - 1)^2, \tag{5.12}$$

$$U \left(\mathbf{C}, \mathbf{a}_0 \right) = C_1 \left(J^{-2/3} I_1 - 3 \right) + C_3 \left(\exp \left[I_4 - 1 \right] - I_4 \right) + \frac{B}{2} (J - 1)^2, \tag{5.13}$$

$$U \left(\mathbf{C}, \mathbf{a}_0 \right) = C_1 \left(J^{-2/3} I_1 - 3 \right) + \frac{k_1}{2k_2} \left\{ \exp \left[k_2 (I_4 - 1)^2 \right] - 1 \right\} + \frac{B}{2} (J - 1)^2, \tag{5.14}$$

and

$$\begin{aligned} U \left(\mathbf{C}, \mathbf{a}_0 \right) =& C_1 \left(J^{-2/3} I_1 - 3 \right) + \frac{B}{2} (J - 1)^2 \\ &+ \frac{k_1}{2k_2} \left\{ \exp \left[k_2 \left(\kappa I_1 + (1 - 3\kappa) I_4 - 1 \right)^2 \right] - 1 \right\}, \end{aligned} \tag{5.15}$$

respectively. The total strain energy function for the coupled Weiss_B model must be expressed piecewise, and follows naturally from Eq. 5.7.

5.3.2 Constitutive modeling: Mechanistic theories

5.3.2.1 Generalized, orthotropic eight-chain network models

Statistical mechanics models offer an attractive alternative to phenomenological constitutive theories. They can provide insights to the underlying mechanisms driving observed mechanical behavior (Ma et al., 2010), and can often describe and predict finite deformations using relatively few material parameters (Boyce and Arruda, 2000). Using a micromechanical, network based model, solid continua can be represented using a network of flexible molecular chains (Arruda and Boyce, 1993). The assembly of these macromolecular chains in a representative volume element (RVE) dictates the mechanical response of the material.

This network-based approach can be extended to a generalized orthotropic framework to describe continua with RVEs built using arbitrary chain descriptions (Bischoff et al., 2002b). For a general chain, the strain energy of an eight-chain orthotropic RVE is given by

$$\begin{aligned} U_{\text{stat}}\left(\mathbf{C},\mathbf{a},\mathbf{b},\mathbf{c}\right) = U_0 + \frac{n}{4}\left\{\left[\sum_{i=1}^{4} u_{\text{chain}}\left(\rho^{(i)}\right)\right] - \frac{1}{P}\left(\frac{du_{\text{chain}}\left(\rho\right)}{d\rho}\right)\Bigg|_{\rho=P} \ln\left(\lambda_{\mathbf{a}}^{a^2}\lambda_{\mathbf{b}}^{b^2}\lambda_{\mathbf{c}}^{c^2}\right)\right\} \\ + \frac{B}{\alpha^2}\left\{\cosh\left[\alpha\left(J-1\right)\right]-1\right\}, \end{aligned} \tag{5.16}$$

with n reflecting chain density, $\rho^{(i)}$ the deformed chain length in the deformed configuration of the i^{th} chain, $\lambda_{\mathbf{a\text{-}c}}$ the stretches along the principal material axes ($\mathbf{a}, \mathbf{b},$ and $\mathbf{c}$), a, b, c the normalized dimensions of the RVE, α the curvature of the relationship between hydrostatic pressure and volume at large volume changes (given the small expected volume changes during physiological deformations, α is assumed to be unity), $u_{\text{chain}}\left(\rho^{(i)}\right)$ the strain energy of the i^{th} chain, and $\left(\frac{du_{\text{chain}}(\rho)}{d\rho}\right)\Big|_{\rho=P}$ the derivative of the chain strain energy function evaluated at the reference chain length. The orthotropic constitutive equation presented in Eq. 5.16 can be simplified to describe transversely isotropic materials by prescribing two of the nondimensional lengths to be equal ($a = b$, $b = c$, or $a = c$); in this work, transverse isotropy was enforced by specifying $b = c$. The strain energy of a particular chain, equivalent to the chain work, can be determined by integrating its force-extension relationship,

$$u_{\text{chain}} = \int F_{\text{chain}} \mathrm{d}r. \tag{5.17}$$

5.3.2.2 Specific, orthotropic eight-chain network models

Specific forms of the orthotropic eight-chain model (Eq. 5.16) can be determined by incorporating different chain realizations. One such definition involves freely jointed chains (FJCs). This form has been shown to accurately describe the mechanical behavior of biological structures (Bischoff et al., 2002a; Deneweth et al., 2013a, 2015; Marchi and Arruda, 2017a). In particular, the strain energy density function for the orthotropic, freely jointed eight-chain (oFJC) model may be written as

$$\begin{aligned} U_{\text{oFJC}}\left(\mathbf{C},\mathbf{a},\mathbf{b},\mathbf{c}\right) = U_0 + \frac{C_r}{4}\left(N\sum_{i=1}^{4}\left[\frac{\rho^{(i)}}{N}\beta_\rho^{(i)} + \ln\frac{\beta_\rho^{(i)}}{\sinh\beta_\rho^{(i)}}\right]\right. \\ \left. -\frac{\beta_P}{\sqrt{N}}\ln\left[\lambda_{\mathbf{a}}^{a^2}\lambda_{\mathbf{b}}^{b^2}\lambda_{\mathbf{c}}^{c^2}\right]\right) + \frac{B}{\alpha^2}\left\{\cosh\left[\alpha\left(J-1\right)\right]-1\right\}, \end{aligned} \tag{5.18}$$

where U_0 is a constant, C_r is the rubbery modulus, and $\sqrt{N}$ is the root mean square chain length in the undeformed configuration. From non-Gaussian probability density functions of FJCs,

$$\beta_\rho^{(i)} = \mathcal{L}^{-1}\left(\rho^{(i)}/N\right) \tag{5.19}$$

and

$$\beta_P = \mathcal{L}^{-1}\left(P/N\right), \tag{5.20}$$

where P is the reference chain length $\left(P=\sqrt{N}=\frac{1}{2}\sqrt{a^2+b^2+c^2}\right)$ and $\mathcal{L}^{-1}\left(\cdot\right)$ is the inverse Langevin function $\left(\mathcal{L}\left(x\right)=\cosh\left(x\right)-\frac{1}{x}\right)$. Eq. 5.18 has been shown to be capable of capturing the bulk mechanical response of ligaments in tension along the preferred material direction and has been successfully implemented in whole knee computational models (Marchi and Arruda, 2017a).

One alternative to FJCs are wormlike chains (WLCs). WLCs are flexible rod structures with contour length L, persistence length A, and normalized contour length $\Lambda = L/A$. Bischoff et al. (2002b) incorporated WLCs into the general framework shown in Eq. 5.16

to yield

$$U_{\text{oWLC}}(\mathbf{C},\mathbf{a},\mathbf{b},\mathbf{c}) = U_0 + \frac{C_r}{16}\left\{\left[\sum_{i=1}^{4}\left(\frac{\Lambda^2}{\Lambda-\rho^{(i)}} + \frac{2{\rho^{(i)}}^2}{\Lambda} - \rho^{(i)}\right)\right] - \frac{\left(8+6\Lambda-9\sqrt{2\Lambda}\right)}{\Lambda\left(\sqrt{2}-\sqrt{\Lambda}\right)^2}\ln\left(\lambda_{\mathbf{a}}^{a^2}\lambda_{\mathbf{b}}^{b^2}\lambda_{\mathbf{c}}^{c^2}\right)\right\} + \frac{B}{\alpha^2}\left\{\cosh\left[\alpha\left(J-1\right)\right]-1\right\}, \tag{5.21}$$

representing the total orthotropic strain energy function using approximate realizations of WLCs.

Similar in formulation to the WLC model, the MacKintosh chain (MAC) model was proposed to address the intermediate space between soft and stiff structures. MacKintosh chains are semi-flexible macromolecular chains that are highly resistant to bending, with the persistence length on the order of the contour length (MacKintosh et al., 1995), and have been successful in describing the mechanics of biological macromolecules (Palmer and Boyce, 2008). The force-extension relationship of a MacKintosh chain can be determined explicitly, though its form strongly depends on the particular of inverse Langevin function approximation used in its construction. Palmer and Boyce (2008) used a Padé-type approximation from Cohen (1991) to approximate the inverse Langevin function, though other, more accurate approximations have recently been proposed (Darabi and Itskov, 2015; Jedynak, 2015; Marchi and Arruda, 2015). Using the Cohen (1991) approximation for the inverse Langevin, Palmer and Boyce (2008) expressed the chain force-extension relationship in terms of the end-to-end chain length, r, as

$$F_{\text{MAC}} = \frac{k\Theta L^2\left(L^2+6A\left(r-L\right)\right)}{4A(L-r)^2\left(L^2+2A\left(r-L\right)\right)}, \tag{5.22}$$

where k is Boltzmann's constant and Θ is the absolute temperature ($nk\Theta = C_r$). Again normalizing model parameters with respect to A, the normalized chain strain energy for a MAC chain follows from applying Eq. 5.17 to Eq. 5.22 yielding

$$u_{\text{MAC}} = \frac{k\Theta}{4}\left(\frac{\Lambda^2}{\Lambda-\rho} + \ln\left[\frac{(\Lambda-\rho)^4}{A^4(\Lambda^2+2\rho-2\Lambda)^4}\right]\right) + u_0. \tag{5.23}$$

Note that for the MAC model the persistence length is not completely eliminated from the chain strain energy function. Operating within the general orthotropic framework, Eq. 5.16

takes the form

$$U_{\text{oMAC}}(\mathbf{C},\mathbf{a},\mathbf{b},\mathbf{c}) = U_0 + \frac{C_r}{16}\left\{\left[\sum_{i=1}^{4}\left(\frac{\Lambda^2}{\Lambda-\rho^{(i)}} + \ln\left[\frac{\left(\Lambda-\rho^{(i)}\right)^4}{A^4(\Lambda^2+2\rho^{(i)}-2\Lambda)^4}\right]\right)\right] - \frac{\Lambda^2\left(\Lambda^2+6\left(P-\Lambda\right)\right)}{P(P-\Lambda)^2\left(\Lambda^2+2\left(P-\Lambda\right)\right)}\ln\left(\lambda_{\mathbf{a}}^{a^2}\lambda_{\mathbf{b}}^{b^2}\lambda_{\mathbf{c}}^{c^2}\right)\right\} + \frac{B}{\alpha^2}\left\{\cosh\left[\alpha\left(J-1\right)\right]-1\right\} \tag{5.24}$$

when using MacKintosh chains in the construction.

5.3.3 Constitutive modeling: A Novel hybrid approach

While there are advantages to both mechanistic and phenomenological material models, it is possible to construct hybrid models with elements derived from each constitutive framework where they fail individually. For example, Kuhl et al. (2005) proposed combining a transversely isotropic eight-chain realization of the model from Bischoff et al. (2002a) with an isotropic bulk material to describe the anisotropic behavior of skin. In the case of ligaments, the highly nonlinear and initially concave shape of the stress-strain response in their transverse direction is potentially inconsistent with neo-Hookean solids (Henninger et al., 2013, 2015), the material description traditionally assumed to dominate the material response in this deformation state. Instead, these mathematical features of the transverse stress-strain behavior closely resemble the physics illustrated by MacKintosh chain networks (Palmer and Boyce, 2008). Therefore, we propose a hybrid constitutive model constructed by adding a slightly compressible form of an isotropic, eight-chain model built using MacKintosh chains to any of the previously described phenomenological, anisotropic strain energy functions (Eqs. 5.6-5.11).

5.3.3.1 The isotropic contribution

Using the same eight-chain construction presented in Arruda and Boyce (1993), an isotropic, eight-chain network model composed from MacKintosh chains can be formulated; see Palmer and Boyce (2008). However, ligaments are rarely modeled as incompressible within the context of FE; this is done both to model the real physics of ligaments, as well as for numerical conditioning. Compressibility can be introduced into the isotropic, incompressible eight-chain strain energy function,

$$U_{\text{MAC,incomp}} = U_0 + \frac{C_r}{4}\left(\frac{L^2}{A\left(L-r\right)} + 4\ln\left[\frac{L-r}{L^2+2A\left(r-L\right)}\right]\right), \tag{5.25}$$

by adding a volumetric dependency and ensuring that there is zero stress in the unloaded configuration. In particular, an energy term of the form

$$U_{\text{MAC,comp}} = -\frac{C_r L^2 r_0 \left(L^2 + 6A\left(r_0 - L\right)\right)}{12A(L - r_0)^2 \left(L^2 + 2A\left(r_0 - L\right)\right)} \ln\left(J\right), \tag{5.26}$$

where r_0 is the chain end-to-end length in the reference configuration, can be added to Eqs. 5.5 and 5.25 to yield the total isotropic strain energy. For isotropic eight-chain models of the form presented in Arruda and Boyce (1993), r may be expressed in terms of I_1 as

$$r = r_0\sqrt{I_1/3}. \tag{5.27}$$

Therefore, the total isotropic, compressible eight-chain MacKintosh network model can be expressed as a function of I_1 and J,

$$U_{\text{MAC,iso}} = U\left(I_1, J\right), \tag{5.28}$$

with the explicit form

$$\begin{aligned} U_{\text{MAC,iso}}\left(\mathbf{C}\right) = C_r \Bigg(& \frac{3L^2}{12AL - 4Ar_0\sqrt{3I_1}} + \ln\left[\frac{L - r_0\sqrt{I_1/3}}{L^2 - 2AL + 2Ar_0\sqrt{I_1/3}}\right] \\ & - \frac{L^2 r_0 \left(L^2 + 6A\left(r_0 - L\right)\right)}{12A(L - r_0)^2 \left(L^2 + 2A\left(r_0 - L\right)\right)} \ln\left(J\right)\Bigg) + \frac{B}{2}(J-1)^2. \end{aligned} \tag{5.29}$$

5.3.3.2 The anisotropic function

It is now possible to construct a transversely isotropic, hybrid model of the form presented in Eq. 5.2 using Eq. 5.29 as the isotropic and volumetric contributions to the total strain energy function, in combination with any of the previously described anisotropic strain energy functions (Eqs. 5.6-5.11). In the current work, the anisotropic contribution to the total strain energy function was assumed to have the form of Eq. 5.6. The resulting anisotropic MacKintosh (aMAC) strain energy function may be written as

$$\begin{aligned} U_{\text{aMAC}}\left(\mathbf{C}, \mathbf{a}_0\right) = C_r \Bigg(& \frac{3L^2}{12AL - 4Ar_0\sqrt{3I_1}} + \ln\left[\frac{L - r_0\sqrt{I_1/3}}{L^2 - 2AL + 2Ar_0\sqrt{I_1/3}}\right] \\ & - \frac{L^2 r_0 \left(L^2 + 6A\left(r_0 - L\right)\right)}{12A(L - r_0)^2 \left(L^2 + 2A\left(r_0 - L\right)\right)} \ln\left(J\right)\Bigg) \\ & + \frac{k_1}{2k_2}\left\{\exp\left[k_2(I_4 - 1)^2\right] - 1\right\} + \frac{B}{2}(J-1)^2. \end{aligned} \tag{5.30}$$

5.3.4 Constitutive theory evaluation methods

5.3.4.1 The assessment optimization problem

The effectiveness of each transversely isotropic model (the coupled Feng (Eq. 5.12), coupled Weiss_A (Eq. 5.13), coupled Weiss_B, cHGO (Eq. 5.14), dcHGO (Eq. 5.15), oFJC (Eq. 5.18), oWLC (Eq. 5.21), oMAC (Eq. 5.24), and aMAC (Eq. 5.30)) was evaluated by its ability to describe the mechanical behavior of the MCL in multiple deformation states. In particular, tensile responses parallel and normal to the primary collagen axis were used to fit the models, assuming uniaxial loading. Experimental stress-strain curves for the MCL were obtained from the literature (Henninger et al., 2013, 2015; Quapp and Weiss, 1998). Discrete stress-strain observations, 25 points in each loading case, were obtained by resampling experimental curves. Optimal material parameters for each model were determined by solving the general constrained minimization problem

$$\underset{\mathbf{p}}{\text{minimize}} \left\{ \frac{\sum \left(\sigma_{\text{exp},T_{11_i}} - \sigma_{\text{model},T_{11_i}}\left(\mathbf{C}_{T_{11_i}}, \mathbf{a_0}, \mathbf{p}\right)\right)^2}{\sum \left(\sigma_{\text{exp},T_{11_i}} - \bar{\sigma}_{\text{exp},T_{11}}\right)^2} + \frac{\sum \left(\sigma_{\text{exp},T_{22_i}} - \sigma_{\text{model},T_{22_i}}\left(\mathbf{C}_{T_{22_i}}, \mathbf{a_0}, \mathbf{p}\right)\right)^2}{\sum \left(\sigma_{\text{exp},T_{22_i}} - \bar{\sigma}_{\text{exp},T_{22}}\right)^2} \right\}, \tag{5.31}$$

where $\mathbf{p}$ is an array containing all material parameters for a particular constitutive model, $\sigma_{\text{exp},T_{11_i}}$ and $\sigma_{\text{exp},T_{22_i}}$ are the i^{th} experimental (Cauchy) stresses along the longitudinal and transverse directions, respectively, $\bar{\sigma}_{\text{exp},T_{11}}$ and $\bar{\sigma}_{\text{exp},T_{22}}$ are the mean stress responses, and $\sigma_{\text{model},T_{11_i}}\left(\mathbf{C}_{T_{11_i}}, \mathbf{a_0}, \mathbf{p}\right)$ and $\sigma_{\text{model},T_{22_i}}\left(\mathbf{C}_{T_{22_i}}, \mathbf{a_0}, \mathbf{p}\right)$ are the i^{th} predicted stresses. The objective function shown in Eq. 5.31 may be written equivalently in terms of the coefficients of determination, r^2, in each of the loading directions as

$$\underset{\mathbf{p}}{\text{minimize}} \left\{2 - r^2_{T_{11}} - r^2_{T_{22}}\right\}. \tag{5.32}$$

5.3.4.2 Stress functions

Solving the optimization problem specified in Eq. 5.31, or Eq. 5.32, requires an explicit definition for the stress corresponding to each constitutive model. For a general hyperelastic material, the second Piola-Kirchhoff (PK) stress at finite strains may be obtained directly from the strain energy function through differentiation,

$$\mathbf{S} = 2\frac{\partial U\left(\mathbf{C}, \mathbf{a}_0\right)}{\partial \mathbf{C}}, \tag{5.33}$$

where $\mathbf{S}$ is the second PK stress tensor. For transversely isotropic hyperelastic materials with a single fiber family in the form of Eq. 5.2, $\mathbf{S}$ may be rewritten in terms of strain invariants as

$$\mathbf{S} = 2\left[\frac{\partial U}{\partial I_1}\mathbf{I} + I_3\frac{\partial U}{\partial I_3}\mathbf{C}^{-1} + \frac{\partial U}{\partial I_4}\mathbf{a}_0 \otimes \mathbf{a}_0\right], \tag{5.34}$$

where $\mathbf{I}$ is the identity matrix and I_3 is related to J via $I_3 = J^2$. $\mathbf{S}$ can be pushed forward into the current configuration to determine the Cauchy stress,

$$\boldsymbol{\sigma} = J^{-1}\mathbf{F}\mathbf{S}\mathbf{F}^{\mathbf{T}}, \tag{5.35}$$

which can similarly be expressed in terms of strain invariants as

$$\boldsymbol{\sigma} = 2J^{-1}\left[I_3\frac{\partial U}{\partial I_3}\mathbf{I} + \frac{\partial U}{\partial I_1}\mathbf{B} + \frac{\partial U}{\partial I_4}\mathbf{a} \otimes \mathbf{a}\right], \tag{5.36}$$

where $\mathbf{B}$ is the left Cauchy-Green strain tensor $\left(\mathbf{B} = \mathbf{F}\mathbf{F}^{\mathbf{T}}\right)$ and $\mathbf{a}$ is the fiber orientation in the current configuration $(\mathbf{a} = \mathbf{F}\mathbf{a}_0)$. The Cauchy stress is related to the nominal stress, $\mathbf{N}$, through

$$\mathbf{N} = J\mathbf{F}^{-1}\boldsymbol{\sigma}. \tag{5.37}$$

Specific forms of stress functions corresponding to phenomenological (Eqs. 5.12-5.15, as well as the Weiss_B model), mechanistic (Eqs. 5.18, 5.21, and 5.24), and hybrid (Eq. 5.30) models can be found in B.

For each material model and experimental stress-strain curve, the optimization problem described by Eq. 5.31 was solved using differential evolution (Storn and Price, 1997). For compressible materials, particularly the statistical mechanics models, no closed form expression exists between the applied stretch and resulting uniaxial stress; therefore, for each applied stretch, a second optimization (root-finding) problem must be solved to determine the magnitudes of the stretches normal to the applied stretch. Once optimal material parameters for each model type were determined, the corresponding r^2 for each loading direction was calculated. The resulting values were compared to determine the ability of a particular constitutive form to describe the bulk deformation of the MCL.

5.3.5 An example ligament deformation

The contribution of constitutive form assumptions on continuum deformation was examined within the context of a simplified, yet clinically applicable, loading situation. A geometrically simplified FE ligament model was stretched and twisted into a configuration similar to the native ACL macroscopic spatial orientation (McLean et al., 2015). In par-

ticular, one end of a cylindrical specimen (original diameter: 10 mm) was fixed, while displacing the opposing end to 10% end-to-end nominal strain. During the load increment, displacements in the radial direction were unconstrained at the ends of the specimen. Concurrent with the applied displacement, the displacement surface was rotated 90° about the centerline of the cylinder. This was accomplished by kinematically coupling the nodes on the displacement boundary condition surface to a reference point located at the center of the circular section. Tissue level strains and macroscopic configuration changes were quantified for each constitutive model form.

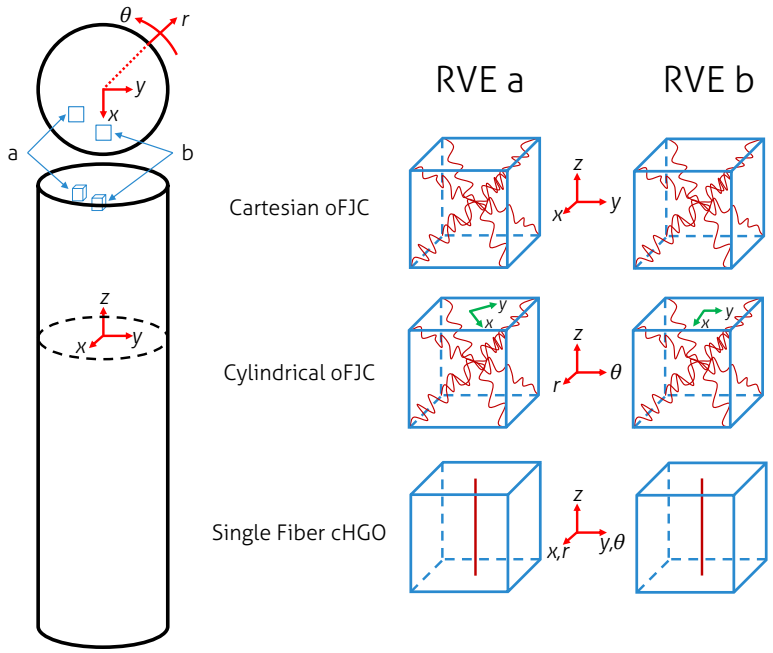

Figure 5.2: Directionality of structural elements corresponding to different locations and constitutive formulations. Example RVEs are shown in blue and material structural elements are shown in red.

The cHGO, dcHGO, oFJC, and aMAC models were numerically implemented using the algorithmic structure described in C. For each model type, transverse isotropy was defined both in a Cartesian and cylindrical sense. This was done to highlight fundamental structural differences between model formulations. Figure 5.2 shows RVEs extracted from two locations within the cylindrical specimen. The RVEs of the cHGO and dcHGO models, which contain a single fiber family, are insensitive to the description of transverse isotropy; however, the formulation of the oFJC model is not independent of coordinate frame. For the oFJC model, this dependence manifests as a local rotation of the RVE when comparing Cartesian and cylindrical bases with respect to the RVE structural elements. Notice in the cylindrical implementation the chains in the RVE are oriented at an angle with respect to

the Cartesian basis (Fig. 5.2)—the Cartesian basis has been superimposed for reference on the cylindrical oFJC RVE.

5.4 Results

5.4.1 Determining an optimal constitutive model

The appropriateness of particular constitutive forms was predominately driven by the shape of the stress-strain behavior normal to the preferred material orientation. Assuming data of the form presented by Quapp and Weiss (1998), the coefficient of determination, r^2, was found to be strictly greater than 0.97 for any loading direction (Table 5.1). However, data of the form presented in Henninger et al. (2013, 2015) were not well captured by all constitutive model forms (Table 5.1). In particular, models that contain preferred material descriptions compatible with high initial concavity (see Fig. 5.1c) provided more accurate representations of the experimental behavior. Complete material parameter sets can be found in Table 5.2.

Table 5.1: Constitutive model coefficients of determination

	Quapp and Weiss (1998) data		Henninger et al. (2013, 2015) data	
Constitutive model	$r^2_{T_{11}}$	$r^2_{T_{22}}$	$r^2_{T_{11}}$	$r^2_{T_{22}}$
Feng	0.97	0.97	0.76	0.78
Weiss_A	0.98	0.97	0.78	0.78
Weiss_B – No linear region	0.99	0.97	0.99	0.79
Weiss_B	1.0	0.97	1.0	0.79
cHGO	0.99	0.97	0.98	0.78
dcHGO	0.99	0.97	0.98	0.78
oFJC	0.99	0.97	0.95	0.78
oWLC	0.99	0.97	0.98	0.78
oMAC	0.99	0.97	0.98	0.77
aMAC	0.99	1.0	0.98	1.0

When transverse behavior is approximately linear, like those in Quapp and Weiss (1998), neo-Hookean type models, or models that behave nearly linearly at small stretch, can generally capture the experimental response in both loading directions. The optimal constitutive model fits, assuming stress-strain behavior consistent with Quapp and Weiss (1998), are shown in Fig. 5.3. Figures 5.3a-c show the relative insensitivity of model form in describing the stress-strain behavior along the preferred material direction, while Figs. 5.3d-f illustrate how nearly linear stress-strain behavior is well represented by nearly linear models.

Table 5.2: Best fit constitutive parameters of various transversely isotropic, hyperelastic material models

Feng	C_1 (MPa)	B (MPa)	ζ			
Quapp and Weiss (1998)	1.87	100	12.8			
Henninger et al. (2013, 2015)	0.0339	100	108			
Weiss$_{\mathrm{A}}$	C_1 (MPa)	B (MPa)	C_3 (MPa)			
Quapp and Weiss (1998)	1.87	100	43.5			
Henninger et al. (2013, 2015)	0.0339	100	6.74			
Weiss$_{\mathrm{B}}$ - No linear region	C_1 (MPa)	B (MPa)	C_3 (MPa)	C_4		
Quapp and Weiss (1998)	2.30	100	11.1	11.9		
Henninger et al. (2013, 2015)	0.0435	100	0.153	36.6		
Weiss$_{\mathrm{B}}$	C_1 (MPa)	B (MPa)	C_3 (MPa)	C_4	C_5 (MPa)	λ^*
Quapp and Weiss (1998)	2.30	100	2.91	27.5	335	1.05
Henninger et al. (2013, 2015)	0.0435	100	0.0589	49.7	120	1.07
cHGO	C_1 (MPa)	B (MPa)	k_1 (MPa)	k_2		
Quapp and Weiss (1998)	1.87	100	38.9	5.73		
Henninger et al. (2013, 2015)	0.0339	100	2.72	33.1		
dcHGO	C_1 (MPa)	B (MPa)	k_1 (MPa)	k_2	κ	
Quapp and Weiss (1998)	1.87	100	38.9	5.73	0.00	
Henninger et al. (2013, 2015)	0.0339	100	2.72	33.1	0.00	
oFJC	C_r (MPa)	B (MPa)	a	b, c		
Quapp and Weiss (1998)	4.99	100	2.11	0.734		
Henninger et al. (2013, 2015)	0.228	100	2.204	0.406		
oWLC	C_r (MPa)	B (MPa)	a	b, c		
Quapp and Weiss (1998)	1.79	100	4.33	1.67		
Henninger et al. (2013, 2015)	0.0180	100	4.13	1.23		
oMAC	C_r (MPa)	B (MPa)	a	b, c	Λ	
Quapp and Weiss (1998)	1.08	100	8.44	3.40	6.00	
Henninger et al. (2013, 2015)	0.0174	100	4.59	1.45	2.81	
aMAC	C_r (MPa)	B (MPa)	Λ	ρ_0/Λ	k_1 (MPa)	k_2
Quapp and Weiss (1998)	10.3	100	0.771	0.878	39.3	5.41
Henninger et al. (2013, 2015)	0.0289	100	0.260	0.958	2.74	32.9

In the case Henninger et al. (2013, 2015) type data, nearly all constitutive models have equivalent suboptimal performance in the transverse direction ($r^2_{T_{22}} \cong 0.78$ for all but the aMAC model). The nonlinearity in the stress-strain behavior in the preferred material direction of the MCL is again well-captured and largely independent of model type (Figs. 5.4a-c), except for the Feng (Eq. 5.12) and Weiss$_{\mathrm{A}}$ (Eq. 5.13) models. However, the high initial nonlinearity in the transverse direction forces nearly linear constitutive models to be equally non-descriptive (Figs. 5.4d-f). This failure provides an opportunity for constitutive models with alternative transverse behavior formulations to favorably model the multi-

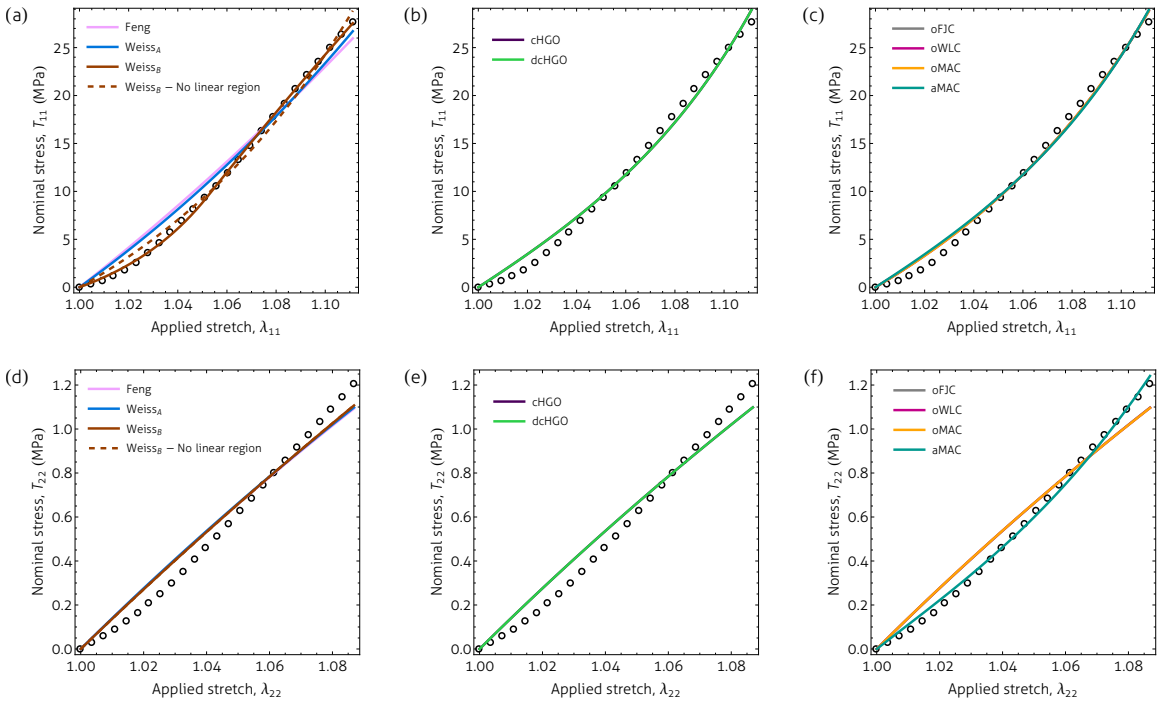

Figure 5.3: Best constitutive model fits along (a-c) and normal to (d-f) the preferred material direction assuming stress-strain data from Quapp and Weiss (1998).

directional stress-strain behavior. The aMAC model has excellent agreement with stress-strain data in both loading directions ($r^2_{T_{11}} = 0.98$, $r^2_{T_{22}} = 1.0$ (Table 5.1); Figs. 5.4c,f), with the nonlinearities well captured by the physics of the model.

Independent from the form of the stress-strain behavior, differences between the cHGO and dcHGO were not discernable (Table 5.1). Specifically, the fiber dispersion parameter, κ, was determined to be zero within numerical precision (Table 5.2). Both sets of experimental data—from Quapp and Weiss (1998) and Henninger et al. (2013, 2015)—appear to lack sufficient power to justify the full complexity of the constitutive model proposed by Weiss et al. (1996) (Weiss$_B$; Table 5.1). Finally, differences between the chain based models—oFJC, oWLC, and oMAC—were virtually negligible.

5.4.2 Physiological ligament loading

A representative deformation was applied to a model ligament to highlight the structural nuances of the various constitutive forms. Figures 5.5 and 5.6 show the final configurations of a cylindrical specimen subjected to an unconstrained axial displacement and rotation. Results in Figs. 5.5 and 5.6 are shown assuming Cartesian and cylindrical assignments of material bases (see Fig. 5.2 for visualizing the differences between these two implemen-

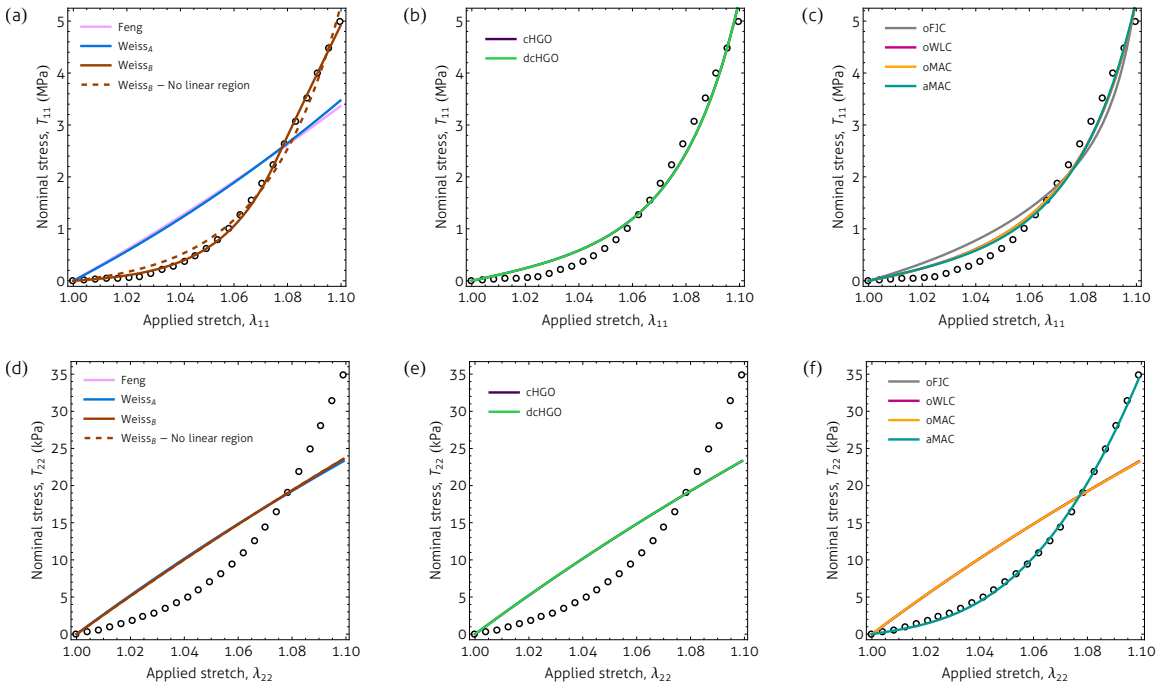

Figure 5.4: Best constitutive model fits along (a-c) and normal to (d-f) the preferred material direction assuming stress-strain data from Henninger et al. (2013) and Henninger et al. (2015).

tations). Figures 5.5a,b,e,f show the insensitivity of the cHGO and aMAC models to the material basis construction, with the Cartesian sense on the left and cylindrical on the right within each subfigure. Figures 5.5c,g and 5.6d,h assume a Cartesian material basis with the oFJC model, while Figs. 5.5d,h and 5.6c,g contain a cylindrical implementation. From Figs. 5.5c,g and Figs. 5.6d,h the importance of implicit material structure becomes apparent. By assuming Cartesian local material orientations there is a loss of complete radial symmetry in the predicted deformation field. Total radial symmetry can be preserved with the oFJC model by using a cylindrical mapping of material bases (Figs. 5.5d,h and 5.6c,g).

5.5 Discussion

The constitutive theory of ligaments is, paradoxically, both well-researched and incomplete. Material descriptions of ligaments are, and must be, constructed and tested with respect to experimental observations. Typically this takes the form of stress-strain behavior, but these experimental observations are often difficult to obtain repeatably and reliably. This is further complicated by data for soft tissues taking numerous and potentially conflicting forms, including quasi-static extension (unidirectional and bidirectional) and com-

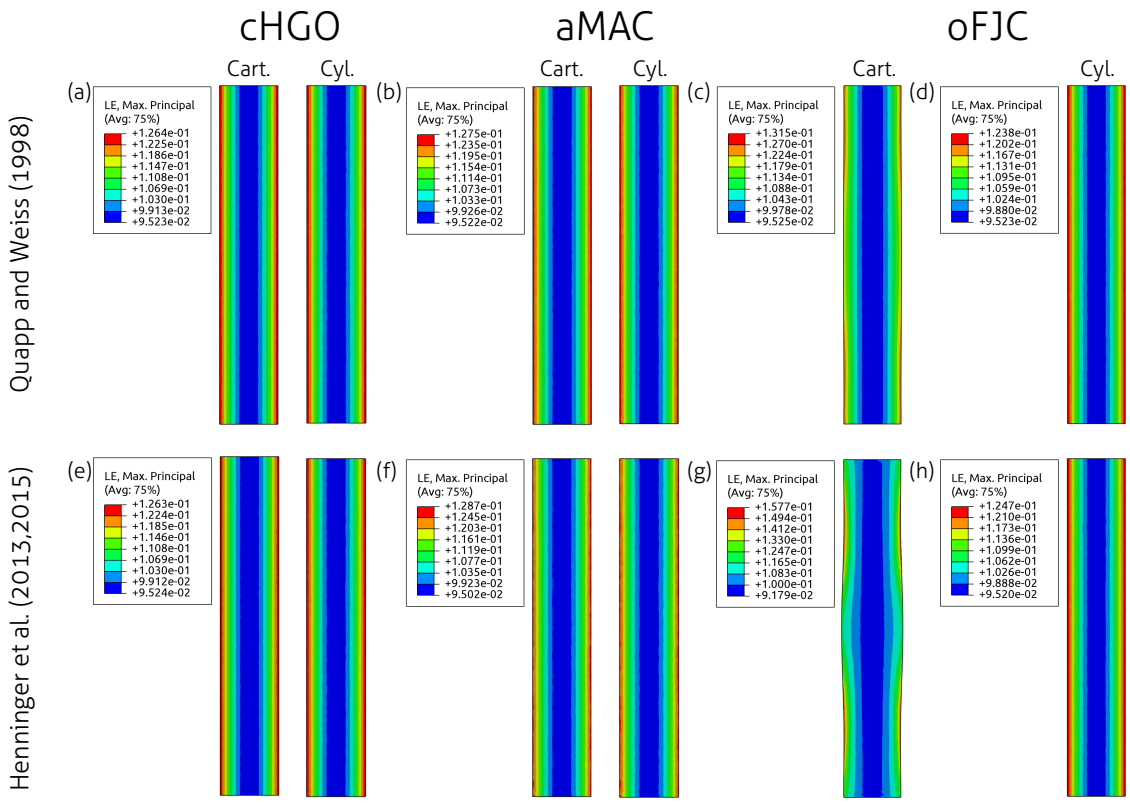

Figure 5.5: Central cross-sections of FE maximum principal strains assuming best fit (a,e) cHGO, (b,f) aMAC, (c-d,h-g) oFJC models assuming data from Quapp and Weiss (1998) and Henninger et al. (2013, 2015), respectively. Cart. and Cyl. refer to Cartesian and cylindrical local material bases, respectively.

pression, dynamic/impact loading, and indentation. Moreover, increasingly there are new data in the time domain in the form of creep, stress relaxation, and fatigue loading, and these experiments are performed across length scales—from the cellular scale up through joint level mechanics.

Constitutive theories are critically important in evaluating deformable biological structures and systems. They represent the link between deformation and internal loading, intrinsically driving the response of their system. General, physiologically representative, and accurate constitutive theories are crucial for describing biological systems because the loading states of tissues tend to be complex. Even during simple activities, individual tissues may undergo significant amounts of shear, bending, tension, and compression, which may be further complicated by the existence of the deformation manifesting heterogeneously. This means that sufficiently robust constitutive theories are necessary for predicting real loading and deformation within and among tissues. Once established, constitutive theories afford a practical means for validating and justifying FE models of tissues;

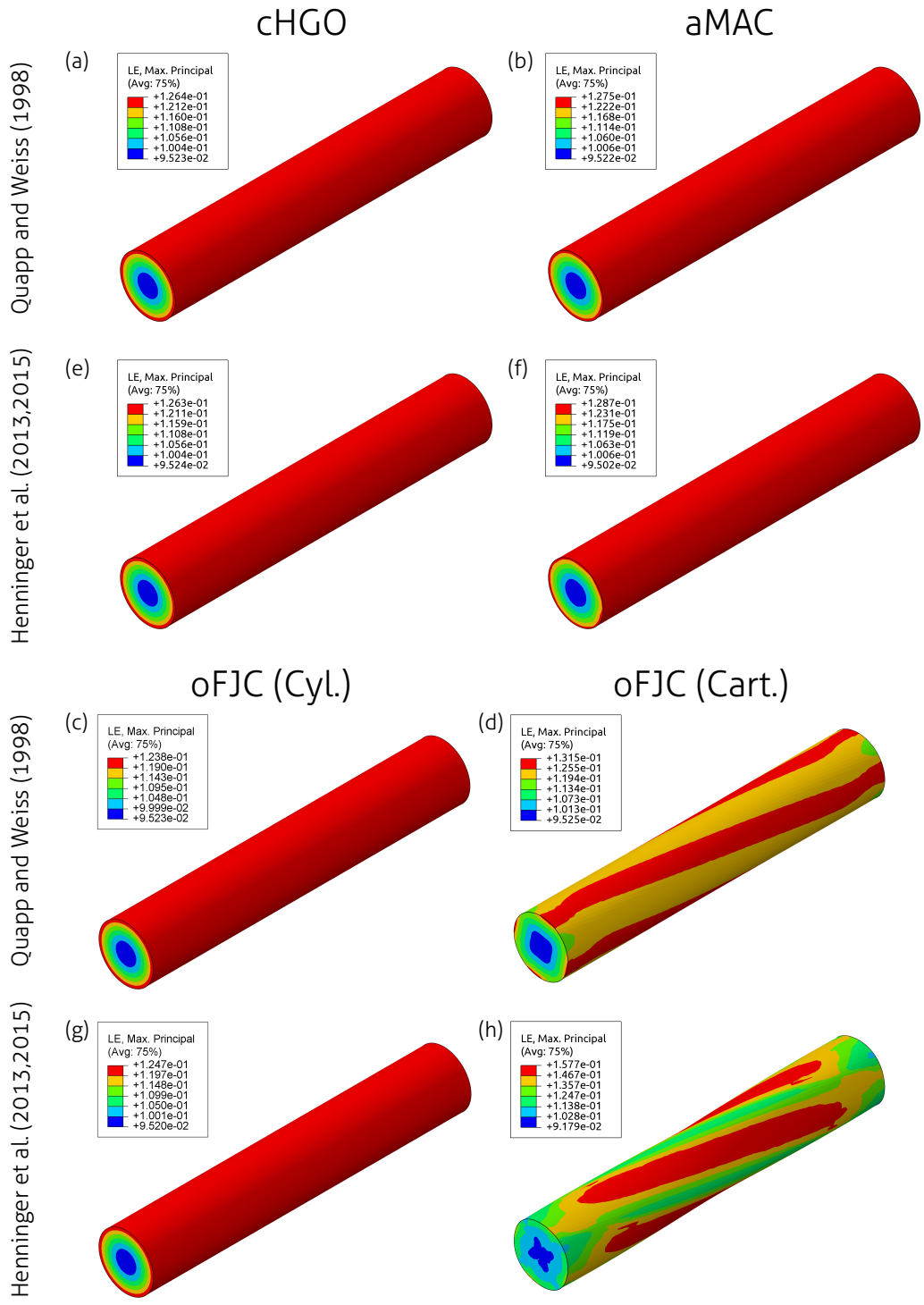

Figure 5.6: FE maximum principal strains assuming best fit (a,e) cHGO, (b,f) aMAC, (c-d,g-h) oFJC models assuming data from Quapp and Weiss (1998) and Henninger et al. (2013, 2015). For the oFJC model (c,g) cylindrical and (d,h) Cartesian bases are shown.

they also provide a platform for evaluating, in a parametric sense, factors that may predispose individuals to injury or disease.

In this work, we reexamined the mechanisms for evaluating constitutive models of ligaments. In the context of quasi-static stress-strain of the MCL along and normal to the preferred material (collagen) direction (Henninger et al., 2013, 2015; Quapp and Weiss, 1998), we investigated the ability of a variety of material models to capture those observations. Commonly employed transversely isotropic, exponential-type material models were recast in terms of total strain invariants and compared to generalized orthotropic statistical chain-based and hybrid theories. Both historic (Quapp and Weiss, 1998) and recent (Henninger et al., 2013, 2015) stress-strain behaviors were used in the determination of optimal material parameters for each candidate material model. Once determined, optimal material parameters were implemented in an FE framework to illustrate the ability of each constitutive theory to describe generalized deformation in soft tissues.

5.5.1 Assessing model performance: Quapp and Weiss (1998) data

An elementary criterion for differentiating between competing constitutive theories is the number of material parameters used in their construction. Minimizing the number of material parameters necessary to describe observed deformations increases the power of the model; a constitutive theory with a smaller number of material parameters reduces the chances of nonuniqueness in the fitting and generally improves confidence that the model is actually motivated by the physics of deformation, not a result of overfitting. Material descriptions evaluated in this study used between 3 and 6 parameters, with varying degrees of success. Each material model contained parameters that describe the small stretch (either C_1 or C_r) and volumetric (B) behaviors.

From the explicit I_4 models, the Feng and Weiss$_{\text{A}}$ modles each have an additional parameter, ζ and C_3, respectively, that describes the nonlinearity of material along the preferred direction. The Weiss$_{\text{B}}$, without a linear region, (a reduced form of Eq. 5.7) and cHGO models each add an additional parameter (4 total) to better control the nonlinearity along the preferred material direction. The dcHGO model adds one more parameter over the cHGO model, bringing the total up to 5, allowing for directionality to be distributed over a range of orientations. Finally, the general Weiss$_{\text{B}}$ model contains 6 material parameters, with the additional two unique parameters describing the transition point and slope of the linear region of the stress-strain response in the preferred material direction.

The chain-based models are formulated differently than the explicit invariant-based models, though their material parameters can be similarly described in terms of the ba-

sic physics they represent. The oFJC and oWLC models each contain 2 additional material parameters over the initial and volumetric stiffnesses (for a total of 4 parameters): one that describes the nonlinearity (a) and the other the relative transverse isotropy ($a : b$). The oMAC adds an additional parameter (5 total) to allow for arbitrary chain loading in the reference configuration. The proposed hybrid, aMAC, model has 6 material parameters, which offer more control over nonlinearity along and normal to the preferred material direction.

In addition to the number of required material parameters within a particular model, the ability of the model to describe the observed stress-strain behavior of the MCL is fundamental in determining its appropriateness. Quapp and Weiss (1998) presented stress-strain behavior of the MCL along and normal to the preferred material direction that is nearly linear in the transverse (typically assumed as the pure matrix response of the tissue) direction (Fig. 5.1b), which has been prolific in its adoption by the knee modeling community that uses anisotropic MCL representations (Doweidar et al., 2010; Ellis et al., 2006; Gardiner and Weiss, 2003; Halloran et al., 2005; Huang et al., 2012; Kiapour et al., 2014a,b; Marchi and Arruda, 2017a; Marchi et al., 2017a; Mootanah et al., 2014; Peña et al., 2005a,b, 2006a,b, 2007; Quatman et al., 2011; Wan et al., 2013; Weiss et al., 2005).

For data of this type, the material models presented herein all generally capture the experimental stress-strain data—the minimum r^2 in either loading direction was 0.97. Material models with 3 material parameters (Feng and Weiss$_{\text{A}}$) performed marginally worse than those containing 4 or more parameters (Table 5.1); differences were found in the diminished ability to describe the nonlinearity in the preferred material direction, with no noticeable differences in the description of the transverse behavior. Material models with 4 parameters predicted the variance in the experimental data identically (Table 5.1; $r^2_{T_{11}}$ and $r^2_{T_{22}}$ equal to 0.99 and 0.97, respectively). This performance and parameter equivalency complicates differentiating and selecting an appropriate material model for a particular analysis.

Five material parameters did not improve performance over their 4 material parameter equivalents; neither fiber distribution in the dcHGO nor arbitrary chain loading the oMAC models adds, for these data, descriptive power over the aligned cHGO or implicitly defined oFJC/oWLC models, respectively. Similarly, adding the linear region to the Weiss$_{\text{B}}$ model adds only a small marginal benefit—$r_{T_{11}} = 0.99 \rightarrow r_{T_{11}} = 1.0$ (Table 5.1)—in model/experiment agreement along the preferred material direction (Fig. 5.3a and Fig. 5.4a), albeit at the cost of two additional material parameters (C_5 and λ^*).

While the proposed hybrid model does allow for the most accurate representation of the Quapp and Weiss (1998) experimental data ($r^2_{T_{11}}$ = 0.99 and $r^2_{T_{22}}$ = 1.0; Table 5.1) and is a

slight improvement over the full Weiss_B model (comparable in number of material parameters), the real benefit comes from its ability to precisely describe the concavity, even in this nearly linear case, of the transverse stress-strain behavior (Fig. 5.3f). Notwithstanding the hybrid model, constitutive theories explored herein assume explicit or pseudo neo-Hookean small stretch behavior in the transverse direction. This fundamental difference, driven by the compressible, eight-chain MacKintosh chain network in the material matrix phase of the hybrid (aMAC) model, affords model flexibility and increased adaptability in describing a larger family of stress-strain responses.

5.5.2 Assessing model performance: Henninger et al. (2013, 2015) data

Stress-strain data of the form presented in Henninger et al. (2013, 2015) (Fig. 5.1b,c) illustrates this difference in the basic model physics more drastically. In the context of these data there are two new obstacles to tackle: another order of magnitude difference—compared to data in Quapp and Weiss (1998)—between the longitudinal and transverse responses and increased concavity in both loading configurations, particularly in the transverse direction at small stretch.

Increased longitudinal concavity and nonlinearity are handled well by nearly all the candidate constitutive theories ($r^2_{T_{11}} > 0.95$; Figs. 5.4a-c), save for the 3 material parameter Feng ($r^2_{T_{11}}$ = 0.76) and Weiss_A ($r^2_{T_{11}}$ = 0.78) models. This limitation can be explained by understanding that, for the assumption of uniaxial extension along the preferred material direction, the Feng model is linear in I_4 (quadratic in applied stretch), while for the range of applied stretches the Weiss_A model is approximately linear in I_4; for the range of applied stretches ($\lambda \in [1, 1.1]$), functions linear in I_4 are also approximately linear in stretch.

So while there is a clear distinction in the ability to describe the longitudinal stress-strain behavior, the same matrix phase limitation, namely assuming a neo-Hookean form, fails to differentiate between models in the transverse direction. However, this model equivalency now, as opposed to that observed with Quapp and Weiss (1998) experimental data, comes with comparably poor performance ($r^2_{T_{22}} \in [0.77, 0.79]$; Table 5.1; Figs. 5.4e-f). It is interesting to note that there is again only a similarly small gain in adding a linear region within the Weiss_B model assuming Henninger et al. (2013, 2015) data. The consistency of this particularly small marginal benefit of including a linear region is illustrative and brings up some reasonable reservations about its appropriateness in modeling the MCL.

This suboptimal performance parity opens the door for improvement. High nonlinearity and initial concavity in the transverse direction are well suited to the underlying physics

of the MacKintosh chain network in the matrix phase of the aMAC model. Data of this form highlights the adaptability of the proposed aMAC model, characterized by similarly descriptive behavior along the preferred material direction ($r^2_{T_{11}}$ = 0.98) and superior predictive ability in the transverse direction ($r^2_{T_{22}}$ = 1.0).

Despite the descriptive successes of the constitutive theories presented in current work, they must be tempered and placed in the appropriate context. There are some limitations that are implicit to the forms of the candidate material models, though some of the most vexing challenges manifest from the data themselves. For the MCL there are only limited quasi-static experimental data that describe the stress-strain behavior of the tissue in multiple orientations with respect to the preferred material direction, and these data are at best inconsistent and at worst contradictory (Henninger et al., 2013, 2015; Lujan et al., 2007; Quapp and Weiss, 1998).

Moreover, all constitutive theories examined in this work were fitted and their performance evaluated with respect to the available experimental data, and not tested against additional data not used in their formulation. If significant variation and limited quantities of basic characterization data are accepted as immutable, any predictions made using a fitted constitutive model are necessarily limited to the range of data used in its construction. Extrapolation outside the bounds defined by the underlying experimental data should only be done with caution—inherent nonlinearity and anisotropy further complicate this issue.

Additionally, none of the theories presented herein include elements of ligament plasticity or damage. These factors are likely to be important in analysis related to the prediction of ligament injury or rupture during excessive loading events. It should also be noted that theories involving chain-based mechanics proved computationally more costly to determine best fit constitutive parameters than explicit invariant models with an equivalent number of material parameters. It is unclear the extent to which this increase was due to the complexity of the stress-strain behavior or the shape of the solution space of the corresponding objective function.

5.5.3 Idealized ligament deformation

Once a sufficiently representative constitutive theory has been determined, the next step in the analysis workflow is typically its incorporation into a FE model. Various best fit material models were examined in the context of an example ligament deformation. The extension and twisting of a cylindrical specimen were selected to highlight differences between material models, particularly with respect to implicit structural elements. In material models with a single fiber family, like the cHGO and aMAC models, there exists total

rotational symmetry of the RVE with respect to the fiber preferred material direction.

These implicit symmetries manifest as consistency between FE models constructed with Cartesian and cylindrical local coordinate bases (Fig. 5.2 and 5.5a-b,e-f). While this may be the desired result, many systems are structured such that stiffening elements interact to varying degrees. If this is the case, single fiber models may fail to be representative; however, chain based network models that have been extended to an orthotropic setting, like the oFJC model, contain structure (Fig. 5.2). Now the orientation of local material bases in the cross-sectional plane of the specimen has real consequences for the expected deformation (Fig. 5.6). This implicit material structure is not necessarily a shortcoming of the model, but may be an asset in explaining ligament deformation through a readily accessible micromechanical analog, as long as there is a strong foundation for its appropriateness.

5.6 Conclusion

For soft tissues, and in solid mechanics generally, there is an ongoing balance between describing the observed deformations and simultaneously motivating the underlying physics of the deformation process. Continuum approaches in structural biomechanics with clinical applications have made previously inaccessible problems possible and have the power to be at the center of incredibly valuable descriptive and predictive tools. Theoretical descriptions of the basic physics of deformation are at the heart of continuum mechanics. Constitutive theories describe deformation, and they can be constructed in myriad ways. They are approximations designed to faithfully represent the actual mechanical response to loading. In this work we examine the ability of various transversely isotropic, hyperelastic constitutive theories to represent the breadth of stress-strain responses of the MCL. We provide a detailed discussion of the requisite form of slightly compressible constitutive theories, and outline a straightforward procedure for their implementation in commonly used FE solvers. In the case of the MCL, when constitutive theories fail to be representative it tends to be due to the nature of the stress-strain response transverse to the preferred material direction. To address this shortcoming, a novel hybrid model is proposed and shown to superiorly describe both nearly linear and highly nonlinear data in the transverse direction.

CHAPTER 6

Stability in computational knee models driven by physiologically and anatomically representative ligaments

This chapter has been submitted for publication and may be referenced as:

> B. C. Marchi and E. M. Arruda. Stability in computational knee models driven by physiologically and anatomically representative ligaments. *In Review*, 2017b

6.1 Introduction

The ACL is one of the four major stabilizing ligament structures in the knee, two that span collaterally and two internally. The ACL has a significant role in preventing excessive ATT and ITR. There is a large and ever growing consensus that under the application of an anterior tibial load the ACL is the primary restraint to ATT (Brantigan and Voshell, 1941; Butler et al., 1980; Draganich et al., 1990; Fukubayashi et al., 1982; Furman et al., 1976; Haimes et al., 1994; Kondo et al., 2014; Loh et al., 2003; Markolf et al., 1976; Piziali et al., 1980b; Sakane et al., 1997; Takai et al., 1993; Torg et al., 1976; Woo et al., 1999; Zantop et al., 2007a). The anatomy of the ACL motivates this stabilizing feature; its attachments, located proximally on the femoral condyle and distially on the tibial plateau, are oriented such that ATT causes them to separate, resulting in increased ACL tension and resistance to motion (McLean et al., 2015; Woo et al., 2006). It has been shown that the ACL can carry up to 90% of the applied anterior load during ATT, and that by completely sectioning the ACL ATT can increase by more than a factor of two (Draganich et al., 1990; Fukubayashi et al., 1982; Haimes et al., 1994; Kondo et al., 2014; Markolf et al., 1976; Piziali et al., 1980b; Zantop et al., 2007a). While the resistive role of the ACL to ATT is easily visualized and well-established, the exact mechanisms by which the ACL regulates ITR are still unclear. There seems to be an effect of ACL transection on internal/external rotational stability (Amis et al., 2005; Andersen and Dyhre-Poulsen, 1997; Gabriel et al., 2004; Kanamori et al., 2000; Kondo et al., 2014; Lipke et al., 1981; Noyes et al., 2017; Zantop et al., 2007b), though the extent of this effect is still disputed (Draganich et al., 1990; Lane et al., 1994; Reuben et al., 1989).

The integrity of soft tissues in the knee is critical for maintaining normal joint functionality and performance. Problematically, ACL injury is common, typically with associated pain and diminished mobility. It is estimated that there are over 200,000 ACL reconstructions performed annually in the United States, with an associated cost of more than two billion dollars (Gasser and Uppal, 2006; Griffin et al., 2006; Spindler and Wright, 2008). ACL injuries range from sprains to partial tears and full-thickness ruptures. Though the morphologies of ACL injuries are complex, it has been shown that significant numbers of ACL tears and ruptures initiate in the posterior aspect of the proximal third of its PLB (Beaulieu et al., 2014, 2015; Kennedy et al., 1974; Lipps et al., 2013; Meyer and Haut, 2008; Meyer et al., 2008; Wojtys et al., 2016). Physical examination, in particular the Lachman (Torg et al., 1976) and pivot shift tests, is still the predominate method for determining ACL injury (Griffin et al., 2006; McLean et al., 2015; Spindler and Wright, 2008; Woo et al., 1999). These macroscopic assessments use knee laxity as an indicator of ligament health. After a positive joint laxity examination, magnetic resonance imaging has become a popular confirmation diagnostic modality (Spindler and Wright, 2008). The effects of ACL injuries are not only acute, but are also associated with an elevated risk of secondary soft tissue diseases, like OA (Griffin et al., 2006; Lohmander et al., 2004; Spindler and Wright, 2008).

Given the importance of the ACL in joint stability and its frequency of injury, there has been a concerted effort to learn how it responds to knee loading. Understanding the native and injury causing biomechanics of the ACL is complicated, however, by the real, nontrival anatomy of the ligament. The ACL is a hierarchical structure composed primarily of aligned collagen, encapsulated in a complaint extracellular matrix (Petersen and Tillmann, 1999; Petersen and Zantop, 2007; Weiss and Gardiner, 2001). The ACL has a location dependent cross-section (Harner et al., 1999), with a large, discernible macroscopic lateral twist (McLean et al., 2015; Moghaddam and Torkaman, 2013; Petersen and Zantop, 2007). Its attachments have a unique structure that can be characterized by the flattening and fanning of collagen fibers at the bony entheses (McLean et al., 2015).

This bulk anatomical description of the ACL is, however, also incomplete. In addition to the gross ACL complexity, it has been well-established that the ACL contains two independent fiber bundles, the AMB and PLB (Arnoczky, 1982; Duthon et al., 2006; Girgis et al., 1975; Petersen and Zantop, 2007). The bundles twist around each other throughout the ligament bulk, contributing to the observed macroscopic ligament twist (McLean et al., 2015; Petersen and Zantop, 2007). The AMB has been shown to be significantly longer than the PLB, and there does not exist a physiological configuration in which both of the bundles are completely unloaded (ACL prestrain) (Beynnon et al., 1992, 1995; But-

ler, 1989; Fleming et al., 1994; Howe et al., 1990; McLean et al., 2015). All this anatomical complexity is further complicated by the mechanics of the ACL, which potentially includes elements of nonlinear elasticity, viscoelasticity, anisotropy, and spatial heterogeneity. It has been shown that these features can manifest at the bundle-level, with the AMB and PLB exhibiting independent constitutive behaviors (McLean et al., 2015).

Taken together, the intricacy of the ACL makes reconstruction seem like a daunting task. ACL reconstruction typically involves replacing the injured ligament with some graft material, which is secured in place within tunnels drilled into the femur and tibia approximately coincident with their native ACL attachment sites (Spindler and Wright, 2008). Currently there are two primary graft types used in ACL reconstruction (patellar tendon and hamstring tendon), and they are usually either allo- or autografts (Anderson et al., 2001; Freedman et al., 2003; Han et al., 2008; Jackson et al., 1993; Marder et al., 1991). Presently, ACL reconstruction techniques focus on restoring native ligament anatomy in an effort to reestablish joint stability. Modern ACL reconstruction has proven to be successful in reducing joint instability and decreasing the likelihood of secondary soft tissue trauma (Andersson et al., 1989; George et al., 2007).

Despite the successes of ACL reconstruction, there are still a number of challenges associated with surgical intervention. Most of these shortcomings, in particular accelerated secondary OA development (Griffin et al., 2006; Lohmander et al., 2004; McLean et al., 2015; Spindler and Wright, 2008) and increased risk of ligament reinjury (Shelbourne et al., 2009), manifest from the fundamental change in local tissue mechanics associated with replacing one tissue type with another. It has been shown that individuals who have undergone ACL reconstruction exhibit divergent joint kinematics and local tissue deformation compared to healthy joints (Deneweth et al., 2010; Tashman et al., 2004) and report increased knee laxity with time (Salmon et al., 2006; Selmi et al., 2006).

These challenges have motivated investigations into ACL structure/function relationships. Most notably, researchers have employed sequential sectioning procedures in an attempt to experimentally quantify the mechanical contributions of individual tissue structures (Brantigan and Voshell, 1941; Diermann et al., 2009; Draganich et al., 1990; Fukubayashi et al., 1982; Furman et al., 1976; Haimes et al., 1994; Kanamori et al., 2000; Kondo et al., 2014; Loh et al., 2003; Markolf et al., 1976; Nielsen et al., 1984; Noyes et al., 2017; Piziali et al., 1980a,b; Zantop et al., 2007a,b). These studies have the ability to show general kinematic effects and can be used to approximate average tissue-level mechanical contributions, but are limited in their capacity to describe detailed, full-field deformations and important structural features across length scales.

To address some of the weaknesses of experimental techniques, FE methods have

been employed to investigate both healthy (Kiapour et al., 2014a,b; Limbert et al., 2004; Mootanah et al., 2014; Song et al., 2004; Wan et al., 2013; Xie et al., 2009; Zhang et al., 2008) and reconstructed (Bae et al., 2015; Huang et al., 2012; Kim et al., 2011a; Peña et al., 2005b; Ramaniraka et al., 2007; Wan et al., 2017; Westermann et al., 2013, 2016) ACL physiologies. These studies provide some context for the role of the ACL in joint stability, but often overpredict knee translations and rotations with respect to clinical assessments of stable knees. They also tend to overestimate local tissue strains relative to comparable experimental studies. Furthermore, while there have been some attempts to understand the role of the double bundled structure of the ACL, these efforts have largely been focused on idealized reconstructive ligament geometries without any consideration of the differences between the mechanical properties of the AMB and PLB (Huang et al., 2012; Kim et al., 2011a; Ramaniraka et al., 2007). What has been missing from this body of work is an investigation into the specific contributions of native ACL double bundled structure in combination with intrinsic, native ACL prestrain and unique bundle constitutive behavior on healthy joint motions.

We hypothesize that ACL prestrain is an important stabilizing feature that will result in joint motions consistent with clinical observations of knees with healthy ACLs, and that without prestrain knee motions will not be within relevant clinical ranges. Starting from a healthy, representative model of an adult knee, we computationally reconstruct the individual bundle domains of the ACL. From this nonphysiological, stress-free configuration, in which each bundle is assumed to be truly unloaded, the AMB and PLB are deformed back into their physiological configurations through a series of macroscopic joint and tissue manipulations. This procedure establishes an estimate of the heterogeneous internal loading of the ACL. This double bundle model—both with and without predicted prestrain fields—is compared to a traditional, single bundle ACL representation using two clinical assessments of ACL integrity, the Lachman and pivot shift tests. Within the clinical assessment framework, we also explore the effects of incorporating experimentally observed, independent bundle mechanical properties. We show how the inclusion of ACL prestrain brings predicted joint kinematic and macroscopic strain measures into clinically observed ranges, and how failure to consider ACL prestrain drastically decreases predicted joint stability. ACL prestrain may also help to explain the small relative changes in local tissue strain observed during clinical assessments, and provides insights into individual bundle contributions during different loading conditions.

6.2 Methods

6.2.1 ACL constitutive theory

Given the composition of structural ligaments, it is typically assumed that they behave mechanically like transversely isotropic continua (Bae et al., 2015; Dhaher et al., 2010; Gardiner and Weiss, 2003; Guo et al., 2009; Huang et al., 2012; Kiapour et al., 2014a,b; Kim et al., 2011a; Limbert et al., 2004; Orsi et al., 2015; Peña et al., 2005b, 2006a,b, 2007; Quapp and Weiss, 1998; Wan et al., 2013, 2014, 2017; Westermann et al., 2013, 2016; Zhang et al., 2008). Within this mechanical framework, the preferred material direction is assumed to be oriented along the mean collagen direction. Useful descriptions of deformation rely on accurate and representative mechanical characterization experiments. Mechanical characterization data in the preferred direction for the AMB and PLB were acquired from the relevant tissues (McLean et al., 2015); however, given the limited mechanical data in the transverse direction, transverse stress-strain data of the AMB and PLB were assumed to be similar to that observed in the medial collateral ligament (Quapp and Weiss, 1998). In addition to considering unique bundle mechanics, an averaged ACL response was also approximated and examined. Experimental data in both loading directions are shown in Fig. 6.1.

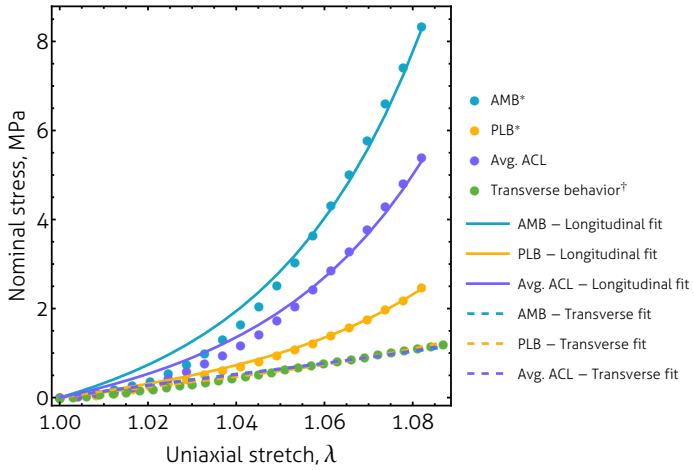

Figure 6.1: Experimental (*: McLean et al. (2015); †: Quapp and Weiss (1998)) and constitutive model fits of transversely isotropic average ACL and individual bundle mechanical responses.

A simplified form of a general, orthotropic hyperelastic constitutive theory was used to describe each realization of the ACL or its bundles. The constitutive theory used herein is an extension of an isotropic, freely jointed eight-chain model originally developed with applications in rubber elasticity (Arruda and Boyce, 1993; Bischoff et al., 2002a,b) and has

been shown to faithfully describe soft tissues assumed to be transversely isotropic (Bischoff et al., 2002c; Kang et al., 2008; Kuhl et al., 2005; Ma and Arruda, 2013; Ma et al., 2010; Marchi and Arruda, 2017a; Marchi et al., 2017a,b). The exact form of the strain energy function assuming transverse isotropy, as well as details regarding the determination of optimal constitutive model material parameters and its implementation in FE models, can be found in Marchi et al. (2017b). Best fits for each set of mechanical characterization data (AMB, PLB, and average ACL) are plotted in Fig. 6.1 and optimal material parameters are presented in Table 6.1.

Table 6.1: ACL and bundle material parameters

	C_r (kPa)	B (MPa)	a	b/a
AMB	83.9	100	1.278	0.887
PLB	70.2	100	1.218	0.959
Average ACL	80.6	100	1.255	0.914

6.2.2 Construction of FE geometries

Individual ACL bundles and their associated prestrain distributions were determined by computationally reconstructing their domains from a homogeneous segmentation of magnetic resonance images from a healthy adult ACL. The methodology for bundle separation and prestrain calculation is shown in Fig. 6.2. From the healthy, homogeneous segmentation (typically assumed to be representative of true ACL anatomy in FE studies), the ligament was manipulated at the joint-level to approximately unload the bulk of the structure. This unloading predominately involves untwisting and translating the bulk ACL about an axis of rotation approximately aligned with the expected volume of the PLB (McLean et al., 2015; Petersen and Zantop, 2007). Next, the bundles were separated in accordance with experimental observation (Kopf et al., 2009; Luites et al., 2007; McLean et al., 2015; Petersen and Zantop, 2007). To account for the longer mean length of the AMB compared to the PLB (Butler, 1989; McLean et al., 2015), the AMB was further extended, resulting in an additional 5% nominal end-to-end strain after the bundles were separated.

In this configuration, with individual AMB and PLB domains, the complete deformation histories associated with the model creation were cleared. This stress and strain free configuration served as the basis for all prestrain calculations; it represents an approximation of the true reference configurations of the AMB and PLB to which they would return if unloaded and unconstrained. ACL prestrain was calculated by applying equal and opposite boundary conditions relative to those used in the unloading procedure. That is, the AMB

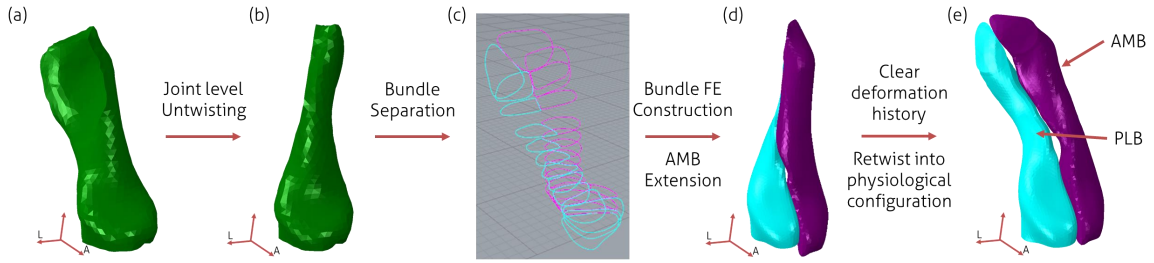

Figure 6.2: Workflow for constructing a double bundle, prestrained ACL FE model. (a) A physiologically twisted and strained ACL (constructed from magnetic resonance images) is unloaded into its (b) bulk untwisted configuration. (c) Individual bundles are isolated. (d) The AMB is extended and the deformation history is cleared. In this configuration, both bundles of the ACL are assumed to be completely unloaded and strain-free. (e) Final double bundle configuration and associated prestrain calculated by applying untwisting boundary conditions in reverse. This produces an estimate for the physiological configurations and associated strains of the AMB and PLB.

was first compressed from its unloaded configuration, then the joint manipulated such that the bundles of the ACL wound around each other and the bone positions are coincident with their original locations (Fig. 6.2e). Bundle prestrain distributions were determined assuming both homogeneous (average ACL) and individual bundle mechanical properties. To account for loose connective tissue usually found between and around the AMB and PLB, the volume between the bundles was filled with a compliant material (not shown in Fig. 6.2) (Petersen and Zantop, 2007). This tissue structure, assumed to behave like a neo-Hookean solid with initial modulus on the order of the ligament transverse stiffness, helped to coordinate bundle motion during macroscopic joint manipulation, while preventing the AMB and PLB from separating in a nonphysical manner during the prestraining procedure.

6.2.3 Computational approximations to clinical assessments

The role of ACL prestrain was examined in the context of two common clinical assessments of ACL integrity: the Lachman (ATT) and pivot shift (ITR) tests. In each assessment two geometric models were evaluated: single and double bundle ACL representations. For the single bundle ACL model, average ACL material properties were assumed, with the preferred material direction following the bulk centerline of the tissue. In the double bundle models, two cases were considered: with prestrain and without prestrain. In each of these models both homogeneous and individual bundle mechanics were assessed. As with the single bundle ACL model, preferred material directions for the AMB and PLB were assumed to follow their respective bulk centerlines. Therefore, a total of five models were analyzed in each of the clinical assessments: single bundle ACL with homogeneous (aver-

age) ACL properties (SBH), double bundle without prestrain and with homogeneous bundle properties (DBH), double bundle with prestrain and with homogeneous bundle properties (DBPH), double bundle without prestrain and with individual bundle properties (DBI), and double bundle with prestrain and with individual bundle properties (DBPI). During the clinical assessments, the proximal (femoral) attachments of the ACL bundles—in either single or double bundle representations—were tied to a rigid representation of the femur, while the distal ACL bundle (tibial) attachments were fully constrained. All computations were performed in Abaqus/Standard v6.14 (SIMULA, Providence, Rhode Island, United States). Contact between all bodies was modeled generally, without friction.

6.2.3.1 Lachman (ATT) test

The Lachamn test has been commonly modeled as an anterior tibial load of 134 N relative to a fixed femur (Gabriel et al., 2004; Loh et al., 2003; Torg et al., 1976; Yasuda et al., 2006; Zantop et al., 2007a). Computationally, this assessment was implemented by applying a posterior femoral load, while constraining all rotations and medial-lateral and superior-inferior translations. The distal attachments of the AMB and PLB—the tibial attachments—were fixed during the application of load.

6.2.3.2 Pivot shift (ITR) test

To determine the role of the ACL in internal tibial rotational stability, an incremental external rotational displacement was applied to the femur up to 30°. While the femur was rotated, all translations and all other rotations of the femur were constrained. As with the ATT test, during the assessment the distal ACL bundle attachments were fixed throughout the load step.

6.2.4 Tissue-level strain measures

Maximum tissue-level strain measures—like the maximum tensile and principal strain observed in a particular tissue—were calculated at the 99^{th} percentile of nodal strain distributions. Maximum strain measures were presented at the 99^{th} percentile to account for any spurious deformation that may have occurred artificially due to geometric, boundary, or discretization inaccuracies. Due to the prestrain of the ACL, it is typically only possible to calculate strains relative to some general, deformed configuration during a real clinical assessment. This limitation of experimental studies means that the strains presented are often not representative of the true strain state of the tissue, but are, in reality, only strain

differences from the physiological, deformed configuration. Therefore, in simulations involving ACL prestrain, maximum tissue-level measures were calculated through a two step procedure. First, the appropriate ACL prestrain strain field was subtracted from the final strain distribution of the corresponding clinical assessment. Then, the relevant maximum tissue-level strain measure was determined from the resulting difference strain field. This approach provides a more realistic mapping of computational strain predictions to experimental data due to the nonzero strain fields present in assumed reference configurations of the ACL.

6.2.5 Macroscopic deformation metrics

Joint-level kinematics were calculated as relative displacements and translations between the tibia and femur. ATT was computed by measuring the amount of anterior tibial displacement relative to the femur and was established directly from femoral displacements. Similarly, ITR was determined from femoral rotations due to the rigid body assumption of the bones. Macroscopic ACL strains were determined by quantifying changes in the end-to-end distance from the centroid of the tibial attachment to the centroid of the femoral attachment.

6.2.6 Statistical methods

Statistical methods were employed to parse the contribution of individual bundle mechanics on predicted deformation within the AMB and PLB. For each tissue structure (AMB or PLB) during an assessment (prestraining, ATT, or ITR), strain distributions assuming homogeneous and independent mechanical properties were compared to identify if significant differences existed. Three statistical tests were used to explore the role of individual bundle mechanics in either the AMB or PLB: a Kolmogorov-Smirnov (KS) goodness-of-fit test (Massey Jr, 1951), a Mann-Whitney (MW) test (Mann and Whitney, 1947), and a Signed Rank (SR) test (Wilcoxon, 1945) on matched nodal pairs.

The KS test was used to test the null hypothesis that the homogeneous and individual mechanical property strains belonged to the same population, with the alternative hypothesis that they belonged to different population distributions. The MW test was used to test the null hypothesis that there was no difference between the medians of the strain distributions, with the alternative hypothesis that the medians were not equal. The SR tests were performed on distributions of locationally matched nodal strain differences between homogeneous and individual bundle mechanical property ACL models. This distribution was calculated by subtracting the strains predicted in homogeneous models from the cor-

responding individual bundle mechanics models at each node. The SR test was then used to test the null hypothesis that the median of the resulting distribution was zero, with the alternative hypothesis that it was not. In each statistical test the threshold for significance was set at $\alpha = 0.05$.

Physically, the KS test was used to determine if significant differences existed between strains predicted using homogeneous and individual bundle properties. If the form of constitutive behavior resulted in different strain predictions, the MW test was used to determine if there was a corresponding median shift. Finally, the SR test on matched nodal strain data pairs was used to investigate if there were any spatial changes in the distributions of predicted strain—*i.e.*, to determine if there existed significant differences in the locations of predicted strains.

6.3 Results

6.3.1 ACL prestrain

Prestrain in both bundles of the ACL was calculated at full extension. The macroscopic ACL strain associated with the prestrain procedure, calculated with respect to the tibial and femoral attachment centroids, was approximately 1%. Tensile strain and maximum principal strain distributions are shown in Figs. 6.3a-b and 6.3c-d, respectively. Prestrain in the AMB and PLB were determined assuming homogeneous (Figs. 6.3a,c) and individual (Figs. 6.3b,d) bundle mechanical properties. 99$^{\text{th}}$ percentile tensile strains in the ACL (AMB/PLB) were 17.3%/18.4% and 16.5%/19.7% assuming homogeneous and individual bundle mechanics, respectively; 99$^{\text{th}}$ percentile maximum principal strains in the ACL (AMB/PLB) were 17.6%/19.9% and 17.1%/20.3% assuming homogeneous and individual bundle mechanics, respectively. Qualitatively, there is not a large difference between the distributions of strain—either tensile or maximum principal—assuming homogeneous or individual bundle mechanics (Fig. 6.3), though nominal increases in predicted strains were observed with individual bundle mechanics. In both bundle formulations, high strains were predicted on the posterior aspect of the proximal third of the PLB near the femoral attachment. High strain regions were also observed in the midsubstance, both on the posterior aspect of the PLB and anterio-medial aspect of the AMB.

While qualitatively large differences between bundle formulations were not apparent (Fig. 6.3), statistical methods were employed to attempt to quantify the role of individual bundle mechanical properties. p-values for the KS, MW, and SR tests for the AMB and PLB are shown in Table 6.2. The incorporation of individual mechanical properties re-

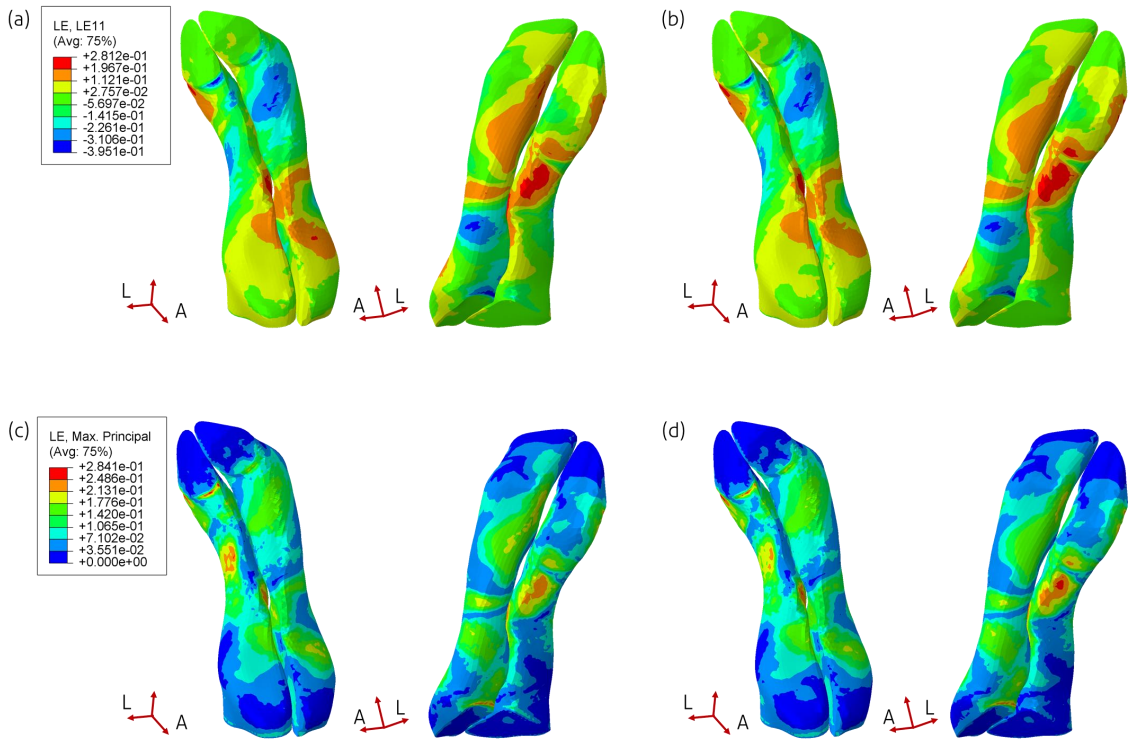

Figure 6.3: ACL tensile and maximum principal prestrain assuming (a,c) homogeneous and (b,d) individual bundle mechanical behaviors, respectively.

sulted in significantly different distributions, medians, and spatial variations of tensile and maximum principal strains in the PLB (Table 6.2). The distributions and medians of maximum principal strains corresponding to the AMB failed to provide sufficient evidence to reject the null hypotheses. Additionally, the medians of the tensile strain distributions in the AMB failed to provide sufficient evidence to reject the null hypothesis. The distributions of tensile strains, as well as the spatial variations of tensile and maximum principal strains, assuming homogeneous and individual bundle mechanical properties were determined to be significantly different in both the AMB and PLB (Table 6.2).

6.3.2 Anterior tibial translation

The geometry, mechanical behavior, and inclusion of prestrain all had effects during anterior tibial loading. Their effects on joint motion and macroscopic ACL strains are shown in Fig. 6.4a and Fig. 6.4b, respectively. Without prestrain, both double bundle models (DBH and DBI) predicted increased joint motion and, consequently, larger macroscopic tissue strains compared to the single bundle (SBH) ACL geometric model (Fig. 6.4). By considering prestrain (DBPH and DBPI), predicted ATT was drastically reduced compared

Table 6.2: Summary of statistical analyses to determine the specific differences between assumed constitutive models (built with either homogeneous or individual mechanical properties) in each ACL bundle associated with prestrain. Bold values indicate $p < 0.05$. For MW tests, if significant differences are present an (H) or (I) denotes a larger median assuming homogeneous or individual bundle mechanical properties, respectively.

	KS Test (Distributions) p value		MW Test (Medians) p value		SR Test (Spatial variation) p value	
	Max principal	Tensile	Max principal	Tensile	Max principal	Tensile
AMB	0.195	**0.019**	0.217	0.603	**<0.001**	**<0.001**
PLB	**<0.001**	**<0.001**	**<0.001** (H)	**<0.001** (H)	**<0.001**	**<0.001**

to models without prestrain (Fig. 6.4a). ATT slightly increased in double bundle models when considering individual bundle mechanical properties both with (0.305 to 0.392 mm) and without (2.35 to 2.49 mm) prestrain at 134 N. Given the rigid bone assumption and the character of the boundary conditions, similar trends were observed with respect to macroscopic strains as with ATT. Even including the approximately 1% macroscopic ACL strain associated with the addition of prestrain, prestrained models predicted lower total macroscopic ACL strain than all ACL models without prestrain (Fig. 6.4b).

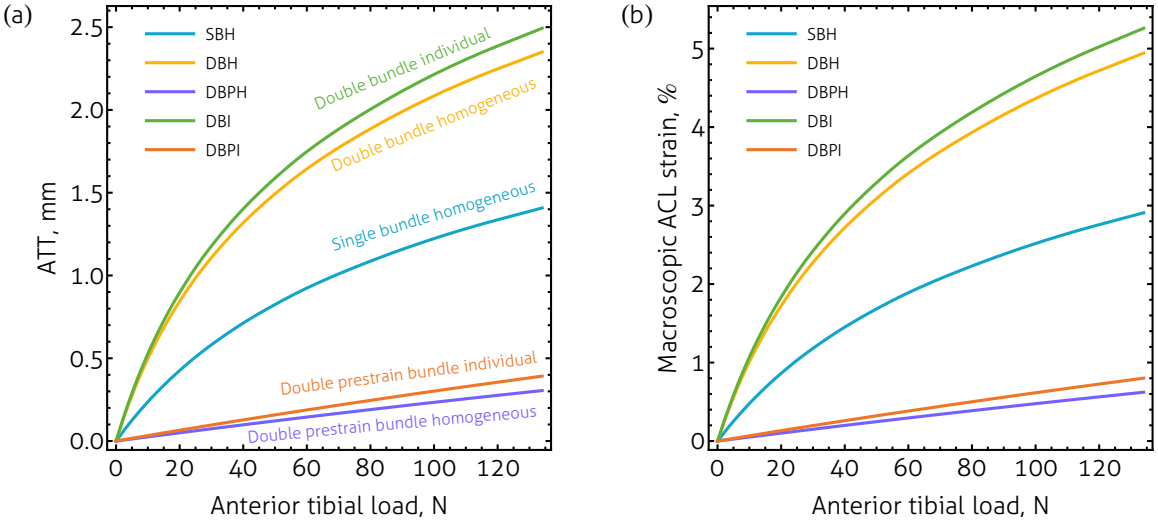

Figure 6.4: (a) Joint kinematics and (b) macroscopic tissue-level strains corresponding to anterior tibial loading.

Similar to the macroscopic measures, prestrain and bundle geometry, and to a lesser extent bundle mechanical properties, had noticeable effects on tissue-level deformation. A detailed breakdown of 99th percentile tensile and maximum principal strain differences

is shown in Fig. 6.5a and Fig. 6.5b, respectively. The inclusion of prestrain reduced both tensile and maximum principal strain differences an order of magnitude, from over 7.5% to below 0.75% (Fig. 6.5). As with joint motion and macroscopic ACL strains, considering the AMB and PLB geometrically separate without prestrain led to increases in predicted local tissue strains (Fig. 6.5). In agreement with the observed macroscopic trends, predicted deformation also increased with the inclusion of individual bundle mechanical properties. This increase was most noticeable in the PLB without prestrain, where local strain differences increased from 10.9% to 12.0% (Fig. 6.5).

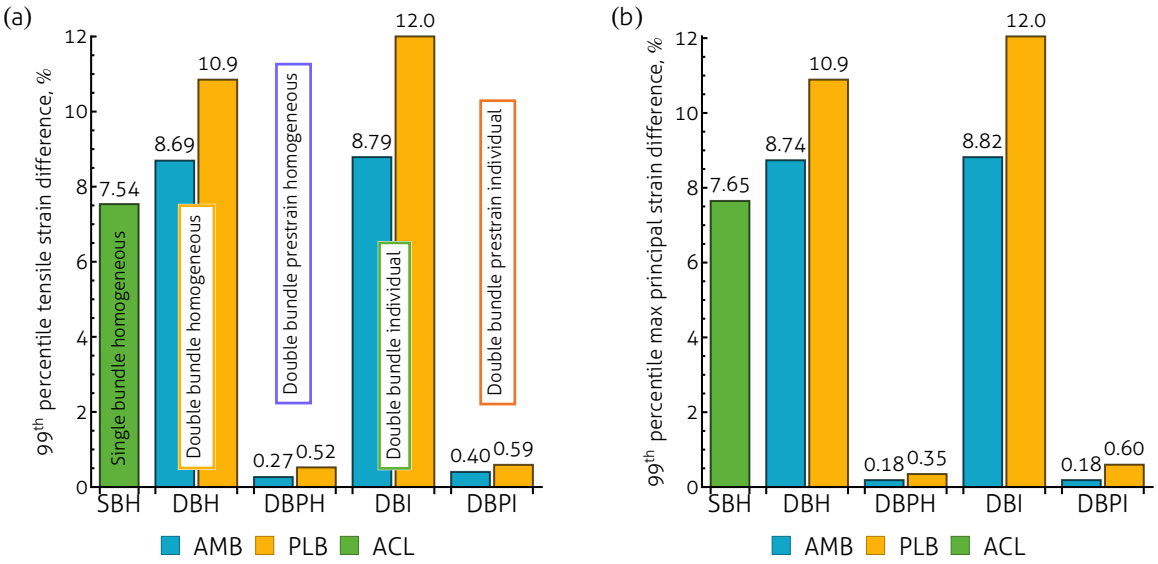

Figure 6.5: 99th percentile tissue-level maximum (a) tensile and (b) principal strain differences at maximum tibial displacement during anterior tibial loading.

Without prestrain, significant differences were found between the distributions, medians, and spatial variations of tensile and maximum principal strains in both bundles during ATT (Table 6.3). With prestrain in the PLB, significant differences between mechanically homogeneous and independent models were observed in every test, save for a failure to reject the null hypothesis of no difference between the medians of the maximum principal strain distributions (Table 6.3). There appears to be some effect of bundle mechanics in the AMB with prestrain, though the exact nature of the relationship is more complicated. Significant differences in the distributions of tensile strain and in the spatial variation of the maximum principal strains were observed in the AMB. However, there was insufficient evidence to reject the null hypotheses that the distributions of maximum principal strains, the tensile and maximum principal strain medians, and the spatial variation of tensile strains between homogeneous and independent mechanical bundle models in the AMB were not different (Table 6.3).

Table 6.3: Summary of statistical analyses to determine the specific differences between assumed constitutive models (built with either homogeneous or individual mechanical properties) in each ACL bundle associated with ATT. Bold values indicate $p < 0.05$. For MW tests, if significant differences are present an (H) or (I) denotes a larger median assuming homogeneous or individual bundle mechanical properties, respectively.

	KS Test (Distributions) p value		MW Test (Medians) p value		SR Test (Spatial variation) p value	
	Max principal	Tensile	Max principal	Tensile	Max principal	Tensile
AMB (Prestrain)	0.728	**0.003**	0.748	0.267	**<0.001**	0.177
PLB (Prestrain)	**<0.001**	**<0.001**	0.215	**<0.001** (I)	**<0.001**	**<0.001**
AMB	**<0.001**	**<0.001**	**<0.001** (I)	**<0.001** (I)	**<0.001**	**<0.001**
PLB	**<0.001**	**<0.001**	**<0.001** (I)	**<0.001** (I)	**<0.001**	**<0.001**

6.3.3 Internal tibial rotation

The joint-level torque response, 99th percentile tissue-level tensile strains, and 99th percentile tissue-level maximum principal strains are presented as a function of joint angle in Fig. 6.6a, Fig. 6.6b, and Fig. 6.6c, respectively. As with anterior tibial loading, including prestrain resulted in drastically increased joint stability (Fig. 6.6a) and reductions in local tissue deformation (Figs. 6.6b-c) compared to ACL models without prestrain. Double bundle ACL models without prestrain (DBH and DBI) yielded noticeably less rotational stiffness compared to a single bundle (SBH) ACL (Fig. 6.6a). While there were not consistently large differences in the tissue-level strains between the AMB and PLB during ATT (Fig. 6.5), ITR resulted in decidedly more strain predicted in the PLB compared to the AMB (Figs. 6.6b-c); this trend was consistent across all double bundle models and rotational angles (dashed compared to solid lines of the DBH, DBPH, DBI, and DBPI models in Figs. 6.6b-c). During ITR, individual mechanical properties in prestrained ACL bundles had an obvious effect on predicted joint laxity (3.45 N·m and 5.35 N·m at ITR $= 15^{\circ}$ with individual and homogeneous mechanical properties, respectively (Fig. 6.6a)), compared to anterior tibial loading where the effect was negligible (Fig. 6.4a).

Without prestrain, significant differences were observed between the distributions, medians, and locations of tensile and maximum principal strains assuming homogeneous and individual mechanical properties in the PLB (Table 6.4). Significant differences were similarly observed between the distributions, medians, and locations of tensile strains in the AMB without prestrain; however, there was insufficient evidence to reject the null hypotheses of no differences between the distributions and medians of maximum principal strains

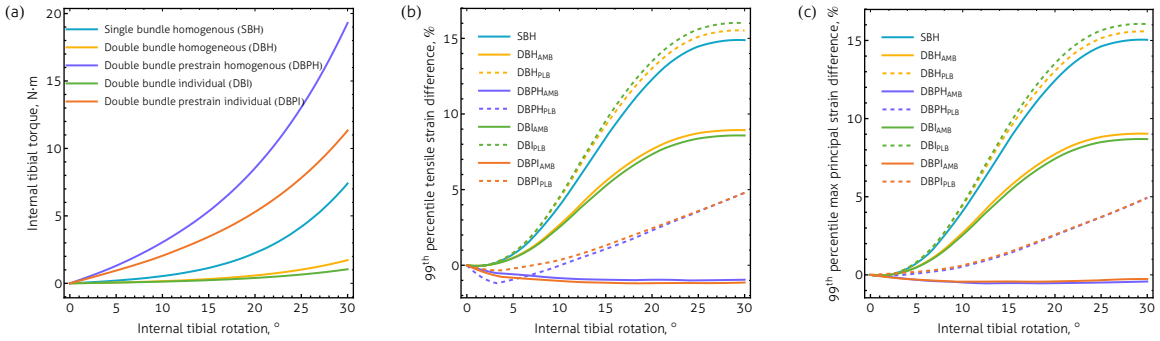

Figure 6.6: (a) Internal tibial torque-angle predicted responses, with associated 99th percentile tissue-level maximum (b) tensile and (c) principal strain differences as a function of tibial rotation angle. In (b,c) solid and dashed lines refer to 99th percentile maximum tissue-level strains in the AMB and PLB, respectively.

(Table 6.4). The distributions and existence of spatial variation in tensile strains between homogeneous and independent bundle property models were found to be significantly different in both the AMB and PLB with prestrain, but there lacked enough evidence to reject the null hypothesis that the medians of the tensile strain distributions were different (Table 6.4). In the AMB with prestrain, significant differences were also observed with respect to the medians and spatial variation in maximum principal strain distributions (Table 6.4). The distributions of maximum principal strains in the PLB with prestrain were found to be significantly different (Table 6.4).

Table 6.4: Summary of statistical analyses to determine the specific differences between assumed constitutive models (built with either homogeneous or individual mechanical properties) in each ACL bundle associated with ITR. Bold values indicate $p < 0.05$. For MW tests, if significant differences are present an (H) or (I) denotes a larger median assuming homogeneous or individual bundle mechanical properties, respectively.

	KS Test (Distributions) p value		MW Test (Medians) p value		SR Test (Spatial variation) p value	
	Max principal	Tensile	Max principal	Tensile	Max principal	Tensile
AMB (Prestrain)	0.095	**0.001**	**0.043** (H)	0.223	**<0.001**	**<0.001**
PLB (Prestrain)	**<0.001**	**0.021**	0.154	0.053	0.066	**<0.001**
AMB	0.069	**0.002**	0.767	**0.044** (H)	**<0.001**	**<0.001**
PLB	**<0.001**	**<0.001**	**<0.001** (H)	**0.028** (H)	**<0.001**	**<0.001**

6.4 Discussion

The ACL is critical in providing translational and rotational stability to the knee. In this work, the roles of specific ACL geometric features, mechanical properties, and intrinsic prestrain distributions were examined in the context of their respective effects on predicted joint motions during common clinical assessments of ACL integrity. Prestrain and double bundle geometric realizations of the ACL were developed from a homogeneous segmentation of the ACL at full extension. This procedure allows for a more general and faithful approximation of the true strain state within the ACL for arbitrary knee configurations. In addition to the response of the joint throughout the clinical assessments, macroscopic and tissue-level deformations of the ACL, or its constituent bundles, were also monitored.

6.4.1 ACL prestrain

Prestrain in the ACL exists for arbitrary, physiological knee configurations (Beynnon et al., 1992, 1995; Butler, 1989; Fleming et al., 1994; Howe et al., 1990; McLean et al., 2015). Previous attempts to quantify the exact nature of this deformation have been limited to bulk strain estimates (Beynnon et al., 1992, 1995; Fleming et al., 1994; Howe et al., 1990). Beynnon et al. (1992) found macroscopic ACL strains slightly less than 1% at full extension, in good agreement with approximately 1% attachment-to-attachment strains observed herein. Measurements of this type provide some broad context for the range of expected deformation in the ACL, but potentially fail to capture the true distribution of strain within each bundle. Understanding the locations of high deformation in the ACL may provide insights on mitigating ligament injury or designing improved reconstructive procedures. Prestrain predictions assuming both homogeneous and independent bundle mechanical properties showed elevated strains near the proximal attachment of the PLB and on the posterior aspect of the midsubstance (Fig. 6.3), coincident with a significant number of ACL failures (Beaulieu et al., 2014, 2015; Kennedy et al., 1974; Lipps et al., 2013; Meyer and Haut, 2008; Meyer et al., 2008).

The assumption of individual AMB/PLB mechanical properties led to an increased inequality between the maximum strains (both tensile and maximum principal) supported by each bundle (Fig. 6.3). Individual bundle mechanical properties also affected the distribution of strains within the bundles. There were significant differences in the distributions, medians, and spatial locations of strains (tensile and maximum principal) in the PLB assuming homogeneous and individual bundle mechanical properties (Table 6.2). In the AMB, significant locational shifts in both tensile and maximum principal strains were observed; however, there was insufficient evidence to reject the null hypothesis of differences

in the tensile and maximum principal median strains (Table 6.2). This suggests that while the locations of strains changed in the AMB with the introduction of individual bundle mechanical properties, there was no associated change in the median strains.

In all cases, the maximum strains manifesting from the prestrain procedure were largely aligned with the preferred material basis, with only small differences between the magnitudes of maximum tensile and maximum principal strains. Predicted strain fields were also highly heterogeneous (Fig. 6.3); this feature may contribute to large deviations in joint motion observed after ACL reconstruction (Deneweth et al., 2010; Salmon et al., 2006; Selmi et al., 2006; Tashman et al., 2004), especially given that traditionally graft prestrain is introduced via axial, end-to-end tensioning (Spindler and Wright, 2008).

While the prestrain quantification procedure outlined in Fig. 6.2 may have substantial implications with respect to understanding general ACL mechanics and optimizing surgical reconstruction, maximum prestrain values presented herein are high and potentially outside the physiological range. High predicted strain values were concentrated and predominately located near the attachments to rigid bones. In the body, there exist several mechanical strategies for mitigating the deformation concentrations that develop at the interface of bonded dissimilar materials. In real soft tissues, like ligaments and tendons, there exists a complex continuum of tissues spanning from ligament proper to calcified bone (Genin and Thomopoulos, 2017; Genin et al., 2009). These functionally graded tissues act to alleviate stress concentrations that might manifest from sharp gradients in material properties between bones and ligaments (Genin and Thomopoulos, 2017; Genin et al., 2009; Thomopoulos et al., 2006). Similarly, interdigitation of the bone with the ligament, gradual morphological transitions from bone to ligament, and optimal ligament insertion angles all contribute to suppressing potentially damaging free-edge deformations (Liu et al., 2011). Additionally, local strains observed in the prestrain distributions exceeded the range of the experimental data used in the fitting of the constitutive behavior of the ACL or its bundles (Fig. 6.1). Therefore, any nominal conclusions based on local tissue deformation may be limited.

6.4.2 Lachman (ATT) test

In general, failure to include prestrain resulted in significantly more joint motion and tissue-level strain differences. During ATT, predicted joint motions without prestrain increased by over 350% (Fig. 6.4a). These large increases in joint motion resulted in substantially more macroscopic and relative tissue-level deformation in ACL models without prestrain. Maximum strain differences increased by over a factor of 10 in ACL models without pre-

strain during ATT (Fig. 6.5). The individual mechanical properties of ACL bundles were shown to have a meaningful effect in certain loading configurations on the distribution of deformation within the bundles of the ACL (Table 6.3).

There is a large body of work investigating the resistive contribution of the ACL to anterior tibial displacements experimentally. At full extension, Furman et al. (1976) and Markolf et al. (1976) found that intact cadaver knees were limited—in the clinical sense—to 1.8 ± 0.2 mm and 2.0 ± 0.5 mm anterior drawer, respectively. Similarly, Haimes et al. (1994) observed approximately 1 and 7 mm ATT with the application of 100 N anterior tibial load in whole cadaver and ACL sectioned knees, respectively. Approximately 3 mm of ATT was observed by Draganich et al. (1990) at 50 N of anterior tibial load in intact knees. At 90 N, intact knee ATT has been reported at 1.8 ± 1.3 mm (Kondo et al., 2014). Also, at anterior tibial loads of 134 N, ATT of 2.9 ± 1.2 mm and 4.0 ± 1.7 mm have been found by Zantop et al. (2007b) and Zantop et al. (2007a), respectively. It is clear that there is tremendous variability in the anterior-posterior laxity of the knee. The findings presented herein are by no means comprehensive, but are representative of the range of ATT during anterior tibial loading.

Computational models of anterior tibial motion have been used to expand upon these experimental efforts. They have largely focused on predicting the consequences of ACL reconstructive procedures (Peña et al., 2005b; Suggs et al., 2003; Wan et al., 2017; Westermann et al., 2013, 2016), though the contributions and load sharing of the AMB and PLB during ATT have also been explored (Song et al., 2004). Suggs et al. (2003), using uniaxial spring approximations for ligaments, predicted 3.5 mm ATT at 134 N anterior tibial loading; Peña et al. (2005b) predicted slightly more ATT at 134 N, finding 5.8 mm ATT at full extension in a healthy joint using continuum ligament representations. In single bundle grafts, ATT at 89 and 134 N has been observed between 4.0 to 9.2 mm (Westermann et al., 2013, 2016) and 2.3 to 2.5 mm (Wan et al., 2017), respectively. In most cases, models that include grafts apply a pretensioning step (Suggs et al., 2003; Wan et al., 2017; Westermann et al., 2013, 2016); however, they often fail to make the same considerations in the native tissue (Song et al., 2004; Suggs et al., 2003).

Compared to previous computational efforts, models with and without prestrain predicted smaller amounts of ATT. At 134 N, the double bundle model without prestrain and with individual bundle mechanical properties produced the highest ATT at 2.5 mm. While within the range of ATT predicted by some graft based models (Wan et al., 2017), even at its most compliant, the ACL models examined herein all fall outside the previously reported numerical ATT range of native ACLs (Peña et al., 2005b; Suggs et al., 2003).

In the context of experimental investigations, comparisons of joint motion become more

complicated. Clinical evidence of limits on ATT suggest that maximum observable ATT should be less than 2 mm at full extension (Furman et al., 1976; Markolf et al., 1976). Only double bundle models with prestrain yielded predicted ATT within that limit at appropriate force levels. On the other hand, force-based, robotic measurements seem to indicate more compliance in the joint. Even considering only the low range of observed displacements in force-based experiments (1.8 mm at 90 N (Kondo et al., 2014) and 2.9 mm at 134 N (Zantop et al., 2007b)), prestrain in the ACL results in an overprediction of anterior joint stiffness; compared to double bundle models without prestrain, however, ATT predictions at 90 and 134 N (DBH: 2.0/2.3 mm; DBI: 2.1/2.5 mm) are in much better agreement. Even though the ACL supports a vast majority of the load during ATT (Haimes et al., 1994; Kondo et al., 2014; Loh et al., 2003; Zantop et al., 2007a,b), the high predicted joint stiffness of prestrained models was produced without the inclusion of numerous collateral structures. This feature may need to be considered when comprehensively assessing the exact role of prestrain in preventing excessive ATT.

Markolf et al. (1976) also provided data on the slope of the force-displacement curve associated with ATT. At 100 N and full extension, the anterior stiffness of the joint was reported at 118 ± 70 N/mm. The relevant measure can be obtained by taking the inverse of the slope of the displacement-force curves shown in Fig. 6.4a evaluated at 100 N. Similar to the comparison of displacements in the force-based experiments, ACLs with prestrain resulted in higher predicted anterior stiffness (DBPH: 452 N/mm; DBPI: 354 N/mm) compared to models without prestrain (DBH: 95 N/mm; DBI: 90 N/mm), which fall within the observed experimental range.

There also might be an overprediction of ligament-level deformation associated with the absence of prestrain. Though not in native tissue, Draganich et al. (1990) measured macroscopic ACL graft strains of approximately 1% at 50 N anterior tibial load. Both double bundle models without prestrain predicted macroscopic ACL strain greater than 3%, while prestrained models appeared substantially stiffer (Fig. 6.4b). The single bundle representation most closely matched graft strains (Draganich et al., 1990), with 1.7% ACL strain at 50 N.

Without prestrain, significant differences were observed with the incorporation of independent bundle mechanical properties between the distributions, medians, and locations of tensile and maximum principal strains in both the AMB and PLB (Table 6.3). The same ubiquitous effect of individual bundle mechanics was not present when considering models with prestrain. While significant differences between homogeneous and individual mechanical property assignments in the PLB were largely present, the same was not true in the AMB (Table 6.3). Similar to comparisons in the strain manifesting from the prestrain

procedure (Table 6.2), significant differences were not observed in the medians of tensile and maximum principal strains (Table 6.3). Therefore, in the case of ATT, the decision to include prestrain has direct consequences on assessing the role of tissue specific material properties with respect to tissue-level deformation predictions. It also shows an increased sensitivity of individual bundle mechanical properties in nonprestrained ACL models. This can also be observed at the joint-level, with increased variability between ATT and macroscopic strain comparing DBH and DBI, as opposed to DBPH and DBPI, model predictions (Fig. 6.4).

6.4.3 Pivot shift (ITR) test

Similar to ATT, lack of prestrain resulted in a reduction of predicted joint stiffness by at least 150% during ITR (Fig. 6.6a). This increased motion of nonprestrained models contributed to 2-fold increases in maximum strain differences overs prestrained ACL models during ITR (Fig. 6.6b-c). There were also increased disparities between maximum tissue-level strains within ACL bundles during ITR, with the PLB sustaining higher strains than the AMB (Fig. 6.6b-c). The influence of bundle-level mechanical properties during ITR on bundle strain distributions was more scattered compared to ATT (Tables 6.3-6.4), suggesting a more nuanced connection between joint loading and the evolution of tissue-level strains.

Again, similar to investigations into the role of the ACL in mitigating against excessive ATT, there is an enormous breadth of observed joint-level responses of the knee to ITR. For example, at an internal tibial torque of 3 N·m, ITR of approximately 12° was reported by Draganich et al. (1990), while under similar conditions Nielsen et al. (1984) observed ITR of less than 5°. With the application of 5 N·m internal tibial torque, Kondo et al. (2014) found 10.4 $\pm$ 7.1° ITR, and Kanamori et al. (2000) observed 12.9 $\pm$ 2.1° with 10 N·m internal tibial torque at full extension in intact cadaver knees; at 15 N·m internal tibial torque, mean ITR has also been reported at approximately 13° (Kiapour et al., 2014a,b).

There is some limited evidence of good agreement between experimental and computational investigations into the response of the knee to ITR. Kiapour et al. (2014a) showed a numerical prediction (approximately 12°) within the experimental range using a comprehensive, subject-specific FE model at full extension and 15 N·m internal tibial torque. However, other computational efforts have predicted substantially more rotational compliance. At 2 N·m internal tibial torque, Ramaniraka et al. (2007) found approximately 12° ITR at full extension with a native ACL. Examining various ACL grafts, Wan et al. (2017) observed ITR between 13-14° at full extension with 4 N·m applied internal tibial torque.

The inclusion of prestrain drastically increases the predicted rotational stiffness of the knee; this trend is consistent across internal tibial angles (Fig. 6.6a). Double bundle models without prestrain fail to produce greater than 2 N·m internal torque through 30° of ITR (Fig. 6.6a), with prestrained models achieving 2 N·m internal torque at 7.2 and 9.8° assuming homogeneous and individual bundle mechanical properties (Fig. 6.6a), respectively. At increasing torques, the importance of prestrain in matching experimental joint kinematics becomes more apparent. Prestrained ITR predictions at 5 N·m (14.3 and 19.3° for DBPH and DBPI, respectively) both fall within or just above the equivalent experimental range presented by Kondo et al. (2014). At even more severe internal tibial torques, even prestrained ACL models start to fall outside comparable experimental ranges (Kanamori et al., 2000; Kiapour et al., 2014a,b). ITR predictions assuming individual mechanical bundle properties increase past 20° for torques greater than 5 N·m, and homogeneous models surpass 20° ITR above 9 N·m internal tibial torque (Fig. 6.6a). The lack of supporting tissue structures, especially in this loading configuration, may be a significant contributor to reduced rotational joint compliance compared to experimental, intact knee observations.

Supporting tissues may have also provided increased joint stiffness in previous computational efforts. Using a single bundle ACL (assumed unloaded at full extension), the 12° ITR found by Ramaniraka et al. (2007) is less than the 19.1° predicted in the equivalent single bundle ACL model without prestrain and homogeneous mechanical properties (Fig. 6.6a). However, with prestrain, predicted joint ITR was significantly reduced, even without the presence of collateral tissues. Also, tension in grafts seems to drive predicted ITR into the same range as prestrained ACL models at 4 N·m (Fig. 6.6a, Wan et al. (2017)). This may indicate that graft tensioning, even if applied homogeneously, may act to replicate the innate, prestrained mechanics of the ACL more faithfully.

As with ATT, Markolf et al. (1976) provided data on the slope of the torque-angle curve associated with ITR. With approximately 8 N·m internal tibial torque and at full extension, the terminal internal stiffness of the knee was measured as 2.3 $\pm$ 0.6 N·m/°. Using Fig. 6.6a, the comparable quantities are the slopes of the curves shown and can be calculated directly. As opposed to anterior joint stiffness, all ACL models presented herein are more compliant than the range proposed by Markolf et al. (1976); only double bundle models with prestrain were sufficiently stiff to make the appropriate comparison. At 8 N·m, the rotational stiffness of prestrained ACLs (DBPH: 0.72 N·m/°; DBPI: 0.60 N·m/°) fell below the bottom of the experimental range. Again, collateral structures, like the medial/lateral collateral ligaments and capsule tissues, might be providing significant stiffening during ITR, potentially accounting for differences from cadaveric studies at large rotations.

While assigning independent bundle mechanical properties had a limited effect on both

joint motion and, consequently, macroscopic strain during ATT (Fig. 6.4), the same was not true during ITR. Clear differences in joint-level performance were observed between the homogeneously and individually defined bundle mechanics models (Fig. 6.6a). In particular, the addition of individual mechanical properties reduces joint resultant torques by 26.6% and 35.2% at 15° ITR in ACL models without and with prestrain, respectively.

During ITR, increased maximum tissue-level strain differences in double bundle models were observed in the PLB compared to the AMB (Fig. 6.6b-c). In all cases, not only were maximum strain values greater, but median tensile and maximum principal strains in the PLB were also found to be significantly greater than in the AMB—MW tests for significant differences in medians performed and in all cases $p < 0.001$. This agrees with previous evidence that the PLB is the primary resistive structure (Gabriel et al., 2004) and supports a larger fraction of total ACL load during ITR (Song et al., 2004). As with ATT, tissue-level strain difference predictions were substantially smaller in models incorporating prestrain (Figs. 6.5 and 6.6b-c). This implies that assuming the ACL is in its reference configuration at full extension, or some other physiological position, may lead to spurious and inflated conclusions regarding the true strain state of the tissue.

Bundle specific material properties significantly affected tissue-level strains during ITR. Differences in the strain distributions in the PLB without prestrain lead to significantly greater median tensile and maximum principal strains assuming homogeneous mechanical properties (Table 6.4). These increases were present even though the PLB was stiffer when considering it with averaged mechanics, and likely contributed to the increased torque of homogeneous over bundle specific models at a given angle (Fig. 6.6a). In nearly every bundle configuration, save for maximum principal strain in the prestrained PLB, significant variation in the spatial positions of strains were observed (Table 6.4). These differences were often found in the absence of significantly different strain distributions or medians. Therefore, the ability of the ACL bundles to rearrange strains spatially appears to be somewhat robust to variation in local mechanical properties during ITR.

6.5 Conclusion

The response of the knee to various assumptions of ACL geometry and mechanical properties was analyzed using representative, three-dimensional FE models. A commonly implemented, single bundle ACL was compared to more physiologically motivated, double bundle geometries. Differences in the mechanical properties of the ACL bundles were also considered in double bundle models. Given the inhomogeneous native loading of the ACL, prestrain distributions in the ACL were calculated and were used to assess the role of

ACL geometry, mechanical behavior, and prestrain in maintaining joint stability. Stability was quantified using two clinical procedures, the Lachman and pivot shift tests. Prestrain distributions, independent from bundle mechanical properties, showed high local strains in regions typically associated with ACL failure. Prestrain also had a substantial effect on predicted joint stability, with prestrained ACL models exhibiting increased translational and rotational stiffnesses. Prestrain also provides reasonable context for tissue-level strains. Since some portion of the ACL is always loaded during normal function, the effect of assuming the current configuration is the reference configuration is pronounced. Tissue-level strains that evolved during the clinical assessments in ACL models without prestrain were considerably higher then the prestrained equivalents. Individual bundle mechanical properties were also shown to have a meaningful impact on the distributions, medians, and locations of strains within each of the ACL bundles, although the exact relationship between macroscopic joint motion and the deformation within individual bundle structures as a function of assumed constitutive behavior is complex. It is clear that prestrain is an important, and often neglected, feature of ACL mechanics.

CHAPTER 7

Conclusions and future work

7.1 General conclusions

Soft tissue injuries and diseases are conspicuously common (Griffin et al., 2006; Peat et al., 2001) and often have substantial personal wellness (Butler et al., 2009; Elias et al., 1999; Hangody and Füles, 2003; Lawrence et al., 2008) and economic (Leigh et al., 2001; Spindler and Wright, 2008; Yelin et al., 2007) ramifications. There is compelling evidence suggesting a link between knee mechanics (both at the joint and tissue levels) and soft tissue injuries and diseases (Andriacchi et al., 2009; Astephen et al., 2008; Gao and Zheng, 2010; Griffin and Guilak, 2005; Setton et al., 1999; Tashman et al., 2004). Computational models can bridge the gap between the diversity of patient physiologies and anatomies and the physical limitations of experiments to explore the mechanical contributions of various healthy and abnormal tissue structures, but these models rely on accurate and representative material descriptions. In the abstract, these descriptions would be designed to provide a comprehensive picture of the real physics of the body; however, the sheer complexities of relevant biological structures are such that approximations are required. Yet, without fundamental knowledge of how tissues deform to general loading, critical insights into these mechanical mechanisms of injuries and diseases may remain out of reach. With the frequencies of conditions like OA and ligament rupture on the rise (Kim et al., 2011b; Woolf and Pfleger, 2003), there is a clear and present need for the development and validation of representative and implementable soft tissue constitutive theories, which may prove invaluable in delineating the mechanical pathways of injury and disease. The work presented herein begins to address some consequences of soft tissue constitutive theory selection in the context of computational investigations of knee mechanics.

In **Chapter 3**, the contributions of articular cartilage constitutive form on local tissue deformation and predicted joint motion were assessed. Specifically, increasing mechanical complexity was introduced into the constitutive descriptions of articular cartilage, from linear elasticity to directional, nonlinear, and spatially dependent elasticity. The sensitivities of each constitutive complexity level were also investigated. Joint kinematics and

tissue deformation were found to be sensitive to their assumed stiffness within the context of linear elastic cartilage constitutive models. With the inclusion of nonlinear and transversely isotropic cartilage constitutive models, local deformation was reduced compared to linear elastic models; joint kinematics and local cartilage deformations were also brought within physiologically reasonable ranges. Finally, with experimentally motivated, spatially heterogeneous cartilage constitutive models, the spatial distributions of local deformation predictions were refined compared to spatially homogeneous material models. With increased smoothness in the articular cartilage constitutive model property field, joint kinematics were minimally effected, while strain artifacts within the cartilage bulk were largely eliminated.

Chapter 4 used the insights gained from Chapter 3 to investigate the mechanical effects of full-thickness focal defects within the femoral cartilage. Defects of various sizes and locations were introduced into the femoral condyles. Regardless of defect size or location, the magnitudes of maximum compressive strains and contact stresses supported by the articular cartilage increased. Highest femoral cartilage compressive strains in defect containing models were observed near the perimeters of their defects. Substantial variations in predicted deformation were also found in the opposing, and unaffected, tibial cartilage. The relationship between femoral defects and tibial cartilage deformation has largely been unexplored. Maximum compressive strains increased with a small lateral defect, but decreased with medial defects. Even in cases where nominal differences between defect containing and healthy cartilage predicted strain fields were small, there existed meaningful differences in the spatial distributions of deformation. Variations in the locations of maximum loading are especially consequential in the context of heterogeneous articular cartilage mechanical properties, as these newly loaded tissues may be unsuited to withstand their altered mechanical environment.

Chapter 5 explored the directional mechanical behavior of structural ligaments. Within continuum soft tissue computational models, it is commonly assumed that knee ligaments can be represented by transversely isotropic constitutive theories. Various frequently employed transversely isotropic, hyperelastic constitutive theories were evaluated on their ability to describe two sets of quasi-static stress-strain data obtained in orthogonal directions. A general procedure for determining optimal material model parameters was developed using a stochastic, genetic optimization framework. Nonlinearity in the transverse direction (the direction normal to the mean collagen direction) was not faithfully represented by the pool of candidate phenomenological and mechanistic theories. Therefore, a novel constitutive theory was developed and applied to directional stress-strain data of the MCL. The new theory was built by augmenting an isotropic and compressible eight-

chain MacKintosh network model with stiff nonlinear fiber elements. This hybrid theory was shown to have superior performance in the representing the quasi-static stress-strain behavior of the MCL, particularly in the transverse direction.

Finally, in **Chapter 6**, lessons learned concerning the directional behavior of ligaments from Chapter 5 were applied to the ACL. Specifically, contribution of the ACL to knee stability was assessed. In the knee, understanding the role of the ACL is complicated by its nontrivial mechanics and geometry. These gross ACL features are complicated by the presence of the two macroscopic fiber bundles of the ACL (the AMB and PLB), which do not exist completely unloaded in any physiological knee configuration. Therefore, to understand the mechanical contribution of the ACL to knee stability, FE models containing various ACL bundle geometries, mechanical properties, and prestrain distributions were subjected to two clinical assessments of ACL integrity: the Lachman and pivot shift tests. Predicted prestrain distributions were found to be heterogeneous, with strain localizations in the posterior aspect of the proximal third and midsubstance of the PLB. The inclusion of prestrain resulted in decreased knee laxity compared to ACL models without prestrain. This resulted in large reductions of macroscopic joint motion and tissue-level strains, bringing levels within the expected bounds of healthy joints during clinical assessments.

7.2 Limitations

While the work presented herein represents a significant advancement in the understanding of soft tissue constitutive models in the context of knee FE models, there are a number of important limitations that should be considered when analyzing its specific outcomes.

First, with respect to the whole knee computational framework, only a single, representative knee geometry was investigated. There exists significant variation between the anatomies and physiologies of individuals (Boden et al., 1992; Hashemi et al., 2010b; Liu et al., 2010b); therefore, further work may be required to determine the appropriateness of applying the conclusions of the current work to a more general population. This limitation is somewhat mitigated by the comparison to results from other experimental and computational investigations, which used either real or different knee soft tissue geometric representations. Furthermore, only a single loading configuration was analyzed for the whole knee models. While the maximum loading observed during the stance phase of gait may be sufficient to differentiate between various constitutive and geometric features within the knee, diseases and injuries likely occur during abnormal activities (Maly, 2008; Powers, 2010). Additionally, the sensitivities and appropriateness of the constitutive forms of collateral soft tissues, like the menisci and collateral ligaments, were not investigated.

These tissues are important for maintaining healthy knee function (Kannus, 1988; Meister et al., 2000), and understanding the implications of constitutive assumptions certainly warrants further study, as there may be significant mechanic and geometric variation among populations (Gardiner and Weiss, 2003). Due to the loading configuration and the time scales over which deformations were occurring, intrinsic viscoelasticity of tissues was not considered. This will likely be a critical feature when investigating more dynamic, injury inducing events (Hayes and Mockros, 1971; Ma et al., 2010). There is also new evidence to suggest that bone deformation may be important even during low impact, repetitive loading (Venäläinen et al., 2016a), though the magnitude of this effect is still questionable (Donahue et al., 2002). Therefore, the assumption of rigid bones might need to be revisited. Additional limitations of the cartilage mechanical heterogeneity framework are discussed in **Chapter 3**.

When considering articular cartilage focal defects, only idealized, circular geometries were considered. The real morphologies of focal defects are complex and their size range vast (Ali et al., 2010; Bredella et al., 1999; Wong and Sah, 2010). While real defect anatomies are certainly an interesting direction to pursue in the future, it is important to note that the cartilage deformation trends around the defect perimeters observed in the current work are similar to those derived from a single, patient specific focal defect (Venäläinen et al., 2016b). Defects were also only considered in the midsubstance of weight bearing regions on the femoral condyles. The sensitivity of the current work to the construction of defects in this region was not assessed, but relative differences between various cartilage geometries is likely to be preserved independent from small locational deviations of focal defects. Additionally, loading was assumed to remain consistent between healthy and defect containing models. While knee loading has been shown to change with injury (Elias et al., 1999), identical loading conditions were incorporated as a first approximation to better understand the specific mechanical contributions of focal defects on the knee. Additional limitations of the investigation into the contributions of focal defects are discussed in **Chapter 4**.

Shifting to aspects of ligament constitutive theories and their implications, there are a number of limitations that should similarly be addressed. The most potentially problematic of these issues is the absence, or more appropriately the inability, of testing the efficacy of ligament constitutive theories against data not used in their construction. The lack of reliable mechanical characterization data in configurations other than along the mean collagen direction is a serious issue facing the ligament modeling community. While the availability of experimental data in new loading directions is certainly required, a more fundamental issue still needs to be addressed. Namely, whether experimental conventions

like the assumption of uniaxial deformation are of value. Ligaments are highly anisotropic (Henninger et al., 2013, 2015; Lujan et al., 2007; Quapp and Weiss, 1998), and specimen test geometry of ansiotropic materials has been shown to significantly affect apparent moduli (Choi and Horgan, 1977; Folkes and Arridge, 1975; Raumann, 1962). There are also important structural aspects of ligaments that further call into question the reliability of previous mechanical characterization data (Mallett and Arruda, 2017). Therefore, while there is clearly a need for a rigorous reexamination of ligament mechanical characterization methodologies, the directional stress-strain data used in the determination and evaluation of various transversely isotropic, hyperelastic constitutive theories in the current work provide an adequate platform for elucidating their differences and potential deficiencies. Additional limitations of the analysis of directional, hyperelastic constitutive models for ligaments are discussed in **Chapter 5**.

Finally, when assessing the role of the ACL in maintaining knee stability, again only a single individual served as the basis for the analysis. This geometry is an example of typical, healthy joint; however, as with many biological structures, significant anatomic variation at the population level may exist (Beaulieu et al., 2016; Hovinga and Lerner, 2009; Kopf et al., 2009). Similarly, only a single reconstruction of the individual bundle geometries of the ACL was performed. Specific realizations of the AMB and PLB are likely to affect prestrain distributions and local tissue deformation during joint motion, but the relative effects of the presence of prestrain are expected to be consistent independent from bundle geometries. There is some evidence to suggest that it may be possible to individually identify and segment each bundle directly from MRI (Steckel et al., 2006), which has the potential to reduce the uncertainty associated with AMB and PLB creation. Additional limitations of determining the roles of specific ACL bundle geometries, mechanical property assumptions, and prestrain distributions are discussed in **Chapter 6**.

7.3 Future work

As previously discussed, there is a clear opportunity to move the analyses performed herein to populations of individuals. The relative heterogeneity of articular cartilage has been shown to be consistent across patients (Deneweth et al., 2013a,b, 2015); therefore, applying the cartilage mechanical property mapping framework shown herein to a larger pool of knee geometries would be valuable in confirming current observations at the population level. A larger population of knee geometries would also prove invaluable in understanding the consequences of specific anatomic and physiologic features on the internal loading of soft tissues and joint motion. For example, increased tibial slope has been shown to be

correlated to ACL injury (Hashemi et al., 2010b; Marouane et al., 2014; McLean et al., 2011). Knee models containing various tibial slopes can potentially be used to determine mechanisms of and critical thresholds for ligament failure. There is also interesting work related to the building of joint mechanics statistical models to study the sensitivities of computational predictions to various input parameters (Guo et al., 2015, 2017). Creating a population of knee anatomies would be a critical first step in establishing these types of models. Potential applications include, but are not limited to, quantifying the sensitivities of local cartilage deformation to specific property mappings and building low-cost, predictive computational tools for use in clinical settings. Another interesting extension of the current work would be to investigate the response of the knee to more dynamic, injury-causing loading configurations. Understanding the consequences of cartilage mechanical heterogeneity during abrupt landings or large rotations may offer new insights into ligament injury.

Another meaningful and previously unexplored avenue would be to quantify the effects of including ligaments, like the ACL, with physiologically representative prestrain throughout the joint. When ligament prestrain is considered in computational models, it has largely been limited to homogeneous strain fields (Limbert et al., 2004; Peña et al., 2005b); however, the current work shows that assumption may not be representative. Comparing predictions from knee models containing ligaments without prestrain to both those with homogeneous and heterogeneous prestrain would be instrumental in determining the need of prestrain for faithfully representing the knee in computational models. Promising theoretical developments (Maas et al., 2016) have opened the door for including general prestrain distributions to arbitrary geometries in their physiologically imaged configurations. While previous work has investigated the effects of ligament reconstruction on joint mechanics (Bae et al., 2015; Huang et al., 2012; Kim et al., 2011a), the results presented herein show the importance of cartilage heterogeneity in predictions of local tissue deformation. Therefore, building computational models containing various ligament reconstructive procedures might provide new insights into the link between reconstruction and OA development. There have also been some recent efforts to include phenomenological approximations of cartilage wear in whole knee models to study the mechanisms of OA progression (Hosseini et al., 2014; Liukkonen et al., 2017; Mononen et al., 2016). It would be interesting to see how wear, in combination with spatially heterogeneous articular cartilage and ligament prestrain, manifests during normal and abnormal loading environments.

Finally, the defect containing knee models analyzed in the current work readily afford a platform for investigating possible interventions. Again, cartilage heterogeneity is likely an important consideration. During cartilaginous autograft transplantation procedures, car-

tilage tissue is relocated from elsewhere in the joint to the affected area (Brittberg et al., 1994; Magnussen et al., 2008). Consequently, the local mechanical properties of these transplanted tissues may be meaningfully different and may result in unexpected and detrimental knee motions and cartilage deformations.

APPENDIX A

Cartilage and ligament constitutive theory in defect models

The nonlinear, anisotropic strain energy density function used for articular cartilage, as well as the supporting ligaments, can be expressed as

$$\begin{aligned} U(\mathbf{x}) =& U_0 + \frac{C_r}{4}\left(N\sum_{i=1}^{4}\left[\frac{\rho^{(i)}}{N}\beta_\rho^{(i)} + \ln\frac{\beta_\rho^{(i)}}{\sinh\beta_\rho^{(i)}}\right]\right. \\ & \left. - \frac{\beta_P}{\sqrt{N}}\ln\left[\lambda_{\mathbf{a}}^{a^2}\lambda_{\mathbf{b}}^{b^2}\lambda_{\mathbf{c}}^{c^2}\right]\right) + \frac{B}{\alpha^2}\left\{\cosh\left[\alpha\left(J-1\right)\right]-1\right\}, \end{aligned} \tag{A.1}$$

where U_0 is a constant, C_r is the rubbery (or initial) modulus, $\sqrt{N}$ is the root mean square chain length in the reference configuration, $\rho^{(i)}$ is the deformed chain length in the current configuration of the i^{th} chain, $\lambda_{\mathbf{a}}$, $\lambda_{\mathbf{b}}$, $\lambda_{\mathbf{c}}$ are the stretches along the principal material axes **a**, **b**, **c**, respectively, a, b, c are the nondimensional edge lengths of the representative volume element, B is the bulk modulus, α describes curvature of the relationship between hydrostatic pressure and volume at large volume changes, and J is the determinant of the deformation gradient. From the properties of freely jointed chains,

$$\beta_\rho^{(i)} = \mathcal{L}^{-1}\left(\rho^{(i)}/N\right) \tag{A.2}$$

and

$$\beta_P = \mathcal{L}^{-1}\left(P/N\right), \tag{A.3}$$

where P is the undeformed chain length, and $\mathcal{L}^{-1}(\cdot)$ is the inverse Langevin function—note: $\mathcal{L}(x) = \coth(x) - 1/x$.

The general orthotropic form of the strain energy shown in Eq. A.1 can be reduced to describe transverse isotropic continua by setting two of the nondimensional lengths of the representative volume element to be equal ($a = b$, $a = c$, or $b = c$). Assuming that $b = c$ for transversely isotropic materials, the remaining ratio of nondimensional lengths, $a : b$, represents the degree of anisotropy in the material.

Using an approximate form of the inverse Langevin function (Marchi and Arruda,

Table A.1: ACL, MCL, PCL, and LCL material properties

	$\rho\,(\mathrm{g/cm^3})$	$C_r\,(\mathrm{MPa})$	a	$b = c$	$B\,(\mathrm{MPa})$	α
ACL	1	0.13765	1.5532	1.0049	100	1
PCL	1	0.93447	1.5996	0.96781	100	1
MCL/LCL	1	0.44865	1.6172	0.95308	100	1

2015), the material constants for each ligament type were determined using appropriate experimental data (Butler et al., 1990; Ma and Arruda, 2013; McLean et al., 2015; Quapp and Weiss, 1998). Due to the macromolecular construction of supporting ligaments (highly aligned collagen fibers in an extracellular matrix), the preferred material direction of each ligament emanated from and terminated at its bony attachments and followed its bulk geometric centerline.

The relative transverse isotropy in the cartilage constitutive model, where the material direction $\mathbf{a}$ was oriented parallel to the underlying bone surface normals, remained constant at $1 : 1.33$ and $1 : 1.348$ for the tibial and femoral cartilages, respectively (Deneweth et al., 2013a, 2015). Deneweth et al. (2013a, 2015) showed the ability of transversely isotropic, network based models to describe the continuum response of articular cartilage during physiologically relevant loading conditions. The model is also motivated by and contains physics representative of the various structural regions of articular cartilage. For the native tibial and femoral cartilages the mean initial moduli $\pm$ one standard deviation were determined to be 88.6 ± 51.7 kPa and 413 ± 157 kPa, respectively. The bulk moduli of tibial and femoral cartilages were assumed to be 1 GPa (Marchi and Arruda, 2017a).

APPENDIX B

Specific stress functions

Using Eqs. 5.34-5.36 it is possible to construct stress descriptions for each transversely isotropic constitutive model. Specifically, the Cauchy stresses for the Feng, Weiss_A, Weiss_B, cHGO, and dcHGO models are given by

$$\boldsymbol{\sigma}_{\text{feng}} = \frac{2C_1}{J^{5/3}}\left(\mathbf{B} - \frac{1}{3}I_1\mathbf{I}\right) + B\left(J-1\right)\mathbf{I} + 4J^{-1}C_1\zeta\left(I_4 - 1\right)\mathbf{a}\otimes\mathbf{a}, \tag{B.1}$$

$$\boldsymbol{\sigma}_{\text{weiss}_\text{A}} = \frac{2C_1}{J^{5/3}}\left(\mathbf{B} - \frac{1}{3}I_1\mathbf{I}\right) + B\left(J-1\right)\mathbf{I} + 2J^{-1}C_3\left(\exp\left[I_4 - 1\right] - 1\right)\mathbf{a}\otimes\mathbf{a}, \tag{B.2}$$

$$\begin{aligned}\boldsymbol{\sigma}_{\text{weiss}_\text{B}} = {} & \frac{2C_1}{J^{5/3}}\left(\mathbf{B} - \frac{1}{3}I_1\mathbf{I}\right) + B\left(J-1\right)\mathbf{I} \\ & + \left\{\begin{array}{ll} 0, & \sqrt{I_4} \leq 1 \\ \frac{C_3}{JI_4}\left(\exp\left[C_4\left(\sqrt{I_4}-1\right)\right]-1\right), & 1 < \sqrt{I_4} \leq \lambda^* \\ \frac{C_5\sqrt{I_4}+C_6}{JI_4} & \lambda^* < \sqrt{I_4} \end{array}\right\}\mathbf{a}\otimes\mathbf{a},\end{aligned} \tag{B.3}$$

$$\begin{aligned}\boldsymbol{\sigma}_{\text{cHGO}} = {} & \frac{2C_1}{J^{5/3}}\left(\mathbf{B} - \frac{1}{3}I_1\mathbf{I}\right) + B\left(J-1\right)\mathbf{I} \\ & + 2k_1J^{-1}\left(I_4-1\right)\exp\left[k_2(I_4-1)^2\right]\mathbf{a}\otimes\mathbf{a},\end{aligned} \tag{B.4}$$

and

$$\begin{aligned}\boldsymbol{\sigma}_{\text{dcHGO}} = {} & \frac{2C_1}{J^{5/3}}\left(\mathbf{B} - \frac{1}{3}I_1\mathbf{I}\right) + B\left(J-1\right)\mathbf{I} \\ & + 2k_1EJ^{-1}\exp\left[k_2E^2\right]\left(\kappa\mathbf{B} + \left(1-3\kappa\right)\mathbf{a}\otimes\mathbf{a}\right),\end{aligned} \tag{B.5}$$

where $E = \left(\kappa I_1 + \left(1-3\kappa\right)I_4 - 1\right)$, respectively.

Closed form solutions for the Cauchy stress corresponding to the oFJC, oWLC, and oMAC models are complex, and it is often convenient to calculate the second PK stress component-wise. Applying Eq. 5.33 to Eq. 5.16 yields an explicit definition of the second PK for an orthotropic RVE with arbitrary chain descriptions (Bischoff et al., 2002b).

Specifically, the second PK stress may be written as

$$S_{jk} = \frac{n}{4}\left\{\sum_{i=1}^{4}\left[\frac{P_j^{(i)}P_k^{(i)}}{\rho^{(i)}}\left(\frac{du_{\text{chain}}\left(\rho\right)}{d\rho}\bigg|_{\rho=\rho^{(i)}}\right)\right] - \frac{1}{P}\left(\frac{du_{\text{chain}}\left(\rho\right)}{d\rho}\bigg|_{\rho=P}\right)\left(\frac{a^2a_ja_k}{\lambda_{\mathbf{a}}^2}\right.\right. \\ \left.\left. + \frac{b^2b_jb_k}{\lambda_{\mathbf{b}}^2} + \frac{c^2c_jc_k}{\lambda_{\mathbf{c}}^2}\right)\right\} + \frac{B}{\alpha}\sinh\left(\alpha\left(J-1\right)\right)\frac{\partial J}{\partial E_{jk}}, \tag{B.6}$$

where

$$\frac{\partial J}{\partial E_{jk}} = \frac{\varepsilon_{jyz}}{J}\delta_{1k}C_{y2}C_{z3} + \frac{\varepsilon_{xjz}}{J}C_{x1}\delta_{2k}C_{z3} + \frac{\varepsilon_{xyj}}{J}C_{x1}C_{y2}\delta_{3k}, \tag{B.7}$$

$\boldsymbol{\varepsilon}$ is the permutation tensor, and $\boldsymbol{\delta}$ is the Kronecker delta. Following Eq. B.6, the second PK stresses for the oFJC, oWLC, and oMAC models can be expressed using index notation as,

$$S_{\text{oFJC}_{jk}} = \frac{C_r}{4}\left[\sum_{i=1}^{4}\left\{\frac{P_j^{(i)}P_k^{(i)}}{\rho^{(i)}}\beta_\rho^{(i)}\right\} - \frac{\beta_P}{\sqrt{N}}\left(\frac{a^2}{\lambda_{\mathbf{a}}^2}a_ja_k\right.\right. \\ \left.\left. + \frac{b^2}{\lambda_{\mathbf{b}}^2}b_jb_k + \frac{c^2}{\lambda_{\mathbf{c}}^2}c_jc_k\right)\right] + \frac{B}{\alpha}\sinh\left(\alpha\left(J-1\right)\right)\frac{\partial J}{\partial E_{jk}}, \tag{B.8}$$

$$S_{\text{oWLC}_{jk}} = \frac{C_r}{16}\left[\sum_{i=1}^{4}\left\{P_j^{(i)}P_k^{(i)}\frac{\left(6\Lambda^2 + 4{\rho^{(i)}}^2 - 9\Lambda\rho^{(i)}\right)}{\Lambda(\Lambda-\rho^{(i)})^2}\right\}\right. \\ \left. - \frac{\left(8+6\Lambda-9\sqrt{2\Lambda}\right)}{\Lambda\left(\sqrt{2}-\sqrt{\Lambda}\right)^2}\left(\frac{a^2}{\lambda_{\mathbf{a}}^2}a_ja_k + \frac{b^2}{\lambda_{\mathbf{b}}^2}b_jb_k + \frac{c^2}{\lambda_{\mathbf{c}}^2}c_jc_k\right)\right] \\ + \frac{B}{\alpha}\sinh\left(\alpha\left(J-1\right)\right)\frac{\partial J}{\partial E_{jk}}, \tag{B.9}$$

and

$$S_{\text{oMAC}_{jk}} = \frac{C_r}{16}\left[\sum_{i=1}^{4}\left\{P_j^{(i)}P_k^{(i)}\frac{\Lambda^2\left(\Lambda^2+6\left(\rho^{(i)}-\Lambda\right)\right)}{\rho^{(i)}(\Lambda-\rho^{(i)})^2\left(\Lambda^2+2\left(\rho^{(i)}-\Lambda\right)\right)}\right\}\right. \\ \left. - \frac{\Lambda^2\left(\Lambda^2+6\left(P-\Lambda\right)\right)}{P(P-\Lambda)^2\left(\Lambda^2+2\left(P-\Lambda\right)\right)}\left(\frac{a^2}{\lambda_{\mathbf{a}}^2}a_ja_k + \frac{b^2}{\lambda_{\mathbf{b}}^2}b_jb_k + \frac{c^2}{\lambda_{\mathbf{c}}^2}c_jc_k\right)\right] \\ + \frac{B}{\alpha}\sinh\left(\alpha\left(J-1\right)\right)\frac{\partial J}{\partial E_{jk}}, \tag{B.10}$$

respectively, which can readily be pushed forward numerically using Eq. 5.35 to obtain the Cauchy stress. It is important to note that while the total strain energy of the orthotropic eight-chain model built using MacKintosh chains contained a dependence on A (Eq. 5.24),

the stress (Eq. B.10) reduces to a function of only normalized parameters.

The Cauchy stress for the aMAC model can be obtained through a direct application of Eq. 5.36 as

$$\begin{aligned}\boldsymbol{\sigma}_{\text{aMAC}} = &\frac{9C_r\rho_0\Lambda^2\left(\sqrt{3}\Lambda\left(\Lambda-6\right)+6\rho_0\sqrt{I_1}\right)}{4\sqrt{I_1}J\left(\rho_0\sqrt{3I_1}-3\Lambda\right)^2\left(3\Lambda\left(\Lambda-2\right)+2\rho_0\sqrt{3I_1}\right)}\mathbf{B}\\ &+\left\{B\left(J-1\right)-\frac{C_r\rho_0\Lambda^2\left(\Lambda^2+6\left(\rho_0-\Lambda\right)\right)}{12J(\Lambda-\rho_0)^2\left(\Lambda^2+2\left(\rho_0-\Lambda\right)\right)}\right\}\mathbf{I}\\ &+2k_1J^{-1}\left(I_4-1\right)\exp\left[k_2(I_4-1)^2\right]\mathbf{a}\otimes\mathbf{a},\end{aligned} \tag{B.11}$$

where $\Lambda = L/A$ and $\rho_0 = r_0/A$. Again, note that the compressible MacKintosh strain energy function shown in Eq. 5.30, which is a function of both the contour, persistence, and reference lengths, reduces to depend simply on the ratio between the chain parameters in the description of the Cauchy stress (Eq. B.11).

APPENDIX C

FE implementation of directional materials

Once the constitutive form of a particular ligament has been determined, the next step is usually the integration of that description into a numerical framework. This section will summarize a simplified workflow that can be used to implement anisotropic, hyperelastic material models in the commonly used commercial FE code ABAQUS/Standard (SIMULA, Providence, Rhode Island, United States), an implicit FE code. User-defined materials in ABAQUS/Standard, UMAT subroutines, require determining the current consistent material Jacobian, Cauchy stress, and state variables at the end of each solution increment (Hibbett et al., 2016). To calculate these quantities, the deformation gradient is available, in a corotated basis, at the beginning and end of load increment, as well as any material state variables passed from the previous load increment.

While calculating the stress in the corotated basis at a particular $\mathbf{F}$ may be readily implemented, a closed form expression for the consistent material Jacobian may be substantially more complex or simply nonexistent. There has been some discussion related to the exact objective stress rate required by ABAQUS/Standard; however, there is now a clear consensus that the Juamann rate of the Kirchhoff stress, $\overset{\nabla}{\boldsymbol{\tau}}$, is required (Hibbett et al., 2016). Specifically, the objective rate may be written as

$$\overset{\nabla}{\boldsymbol{\tau}} = \dot{\boldsymbol{\tau}} - \mathbf{W}\boldsymbol{\tau} - \boldsymbol{\tau}\mathbf{W}^T = \mathbb{c}^{\tau J} : \mathbf{D}, \tag{C.1}$$

where $\boldsymbol{\tau}$ is the Kirchhoff stress ($\boldsymbol{\tau} = J\boldsymbol{\sigma}$), $\mathbf{W}$ is the spin tensor, $\mathbf{D}$ is the rate of deformation tensor, and $\mathbb{c}^{\tau J}$ is the tangent modulus tensor corresponding to the Jaumann rate of the Kirchhoff stress. The consistent tangent moduli required for an ABAQUS/Standard UMAT, $\mathbb{C}^J$, are related to the tangent modulus tensor corresponding to the Jaumann rate of the Kirchhoff stress through

$$\mathbb{C}^J = J^{-1}\mathbb{c}^{\tau J}. \tag{C.2}$$

Numeric approximations of tangent moduli

It is possible to numerically approximate the tangent modulus tensor required by ABAQUS/Standard, $\mathbb{C}^J$, through a linearization of Eq. C.1 using a combination of associated perturbations of the deformation gradient—note that detailed derivations of the following linearization procedure of Eq. C.1 can be found in Miehe (1996) and Sun et al. (2008). In particular, Eq. C.1 can be linearized as

$$\Delta\boldsymbol{\tau} - \Delta\mathbf{W}\boldsymbol{\tau} - \boldsymbol{\tau}\Delta\mathbf{W}^T = \mathbb{c}^{\tau J} : \Delta\mathbf{D}, \tag{C.3}$$

and through six independent perturbations of $\Delta\mathbf{D}$—which has six independent components due to structural symmetries—an approximation of $\mathbb{c}^{\tau J}$ can be obtained; each perturbation of $\Delta\mathbf{D}$, $\Delta\mathbf{D}^{(ij)}$, represents a perturbation along the $(i,j)^{\text{th}}$ component of $\Delta\mathbf{D}$. Expressing the perturbations in terms of the deformation gradient, following Miehe (1996),

$$\Delta\mathbf{F}^{(ij)} = \frac{\varepsilon}{2}\left(\mathbf{e}_i \otimes \mathbf{e}_j\mathbf{F} + \mathbf{e}_j \otimes \mathbf{e}_i\mathbf{F}\right), \tag{C.4}$$

where $\Delta\mathbf{F}^{(ij)}$ is a perturbation of $\mathbf{F}$ along its $(i,j)^{\text{th}}$ component, ε is a small scalar perturbation factor, and $\mathbf{e}$ is the current configuration basis. Note that in ABAQUS/Standard $\mathbf{e}$ is coincident with the corotated basis used within the UMAT framework; therefore, $\mathbf{e}_1 = \{1,0,0\}$, $\mathbf{e}_2 = \{0,1,0\}$, $\mathbf{e}_3 = \{0,0,1\}$ in the current configuration with respect to the corotated basis.

Sun et al. (2008) proposed a forward difference method, and later a central difference method (Liu and Sun, 2015), based on a total, perturbed deformation gradient,

$$\hat{\mathbf{F}}^{(ij)} = \mathbf{F} + \Delta\mathbf{F}^{(ij)}, \tag{C.5}$$

and major tensoral symmetries, to approximate the consistent tangent moduli tensor as

$$\mathbb{C}^{J^{(ij)}} \approx \frac{1}{J\varepsilon}\left(\boldsymbol{\tau}\left(\hat{\mathbf{F}}^{(ij)}\right) - \boldsymbol{\tau}\left(\mathbf{F}\right)\right), \tag{C.6}$$

where J is the determinant of $\mathbf{F}$ and $\mathbb{C}^{J^{(ij)}}$ are the components of the consistent tangent moduli tensor corresponding to the perturbation $\Delta\mathbf{F}^{(ij)}$. Due to the major symmetries of $\mathbb{C}^J$, it can be shown, using the indexing conventions of ABAQUS/Standard, to have the

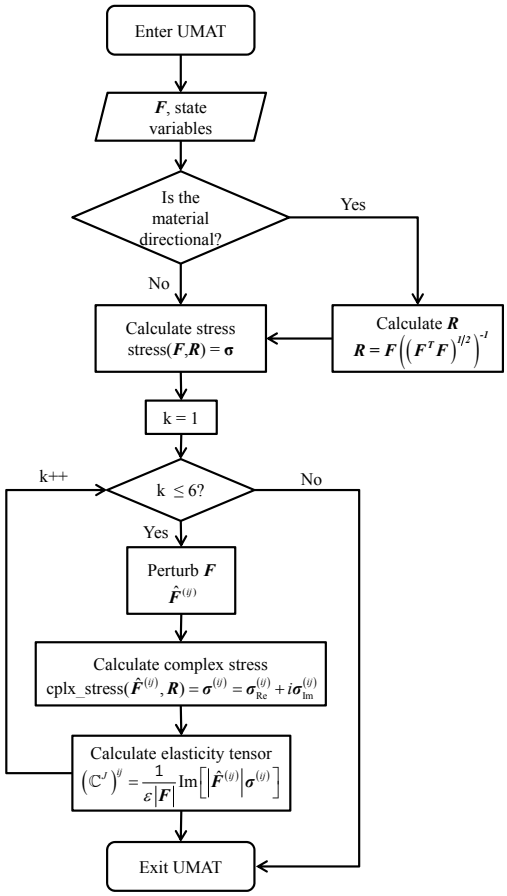

Figure C.1: Numerical algorithm for the implementation of anisotropic hyperelastic constitutive models within an ABAQUS/Standard UMAT.

following structure:

$$\mathbb{C}^J \approx \frac{1}{J\varepsilon}\begin{bmatrix} \tau_{11}\left(\widehat{\mathbf{F}}^{(11)}\right)-\tau_{11}(\mathbf{F}) & \tau_{11}\left(\widehat{\mathbf{F}}^{(22)}\right)-\tau_{11}(\mathbf{F}) & \tau_{11}\left(\widehat{\mathbf{F}}^{(33)}\right)-\tau_{11}(\mathbf{F}) & \tau_{11}\left(\widehat{\mathbf{F}}^{(12)}\right)-\tau_{11}(\mathbf{F}) & \tau_{11}\left(\widehat{\mathbf{F}}^{(13)}\right)-\tau_{11}(\mathbf{F}) & \tau_{11}\left(\widehat{\mathbf{F}}^{(23)}\right)-\tau_{11}(\mathbf{F}) \\ \tau_{22}\left(\widehat{\mathbf{F}}^{(11)}\right)-\tau_{22}(\mathbf{F}) & \tau_{22}\left(\widehat{\mathbf{F}}^{(22)}\right)-\tau_{22}(\mathbf{F}) & \tau_{22}\left(\widehat{\mathbf{F}}^{(33)}\right)-\tau_{22}(\mathbf{F}) & \tau_{22}\left(\widehat{\mathbf{F}}^{(12)}\right)-\tau_{22}(\mathbf{F}) & \tau_{22}\left(\widehat{\mathbf{F}}^{(13)}\right)-\tau_{22}(\mathbf{F}) & \tau_{22}\left(\widehat{\mathbf{F}}^{(23)}\right)-\tau_{22}(\mathbf{F}) \\ \tau_{33}\left(\widehat{\mathbf{F}}^{(11)}\right)-\tau_{33}(\mathbf{F}) & \tau_{33}\left(\widehat{\mathbf{F}}^{(22)}\right)-\tau_{33}(\mathbf{F}) & \tau_{33}\left(\widehat{\mathbf{F}}^{(33)}\right)-\tau_{33}(\mathbf{F}) & \tau_{33}\left(\widehat{\mathbf{F}}^{(12)}\right)-\tau_{33}(\mathbf{F}) & \tau_{33}\left(\widehat{\mathbf{F}}^{(13)}\right)-\tau_{33}(\mathbf{F}) & \tau_{33}\left(\widehat{\mathbf{F}}^{(23)}\right)-\tau_{33}(\mathbf{F}) \\ \tau_{12}\left(\widehat{\mathbf{F}}^{(11)}\right)-\tau_{12}(\mathbf{F}) & \tau_{12}\left(\widehat{\mathbf{F}}^{(22)}\right)-\tau_{12}(\mathbf{F}) & \tau_{12}\left(\widehat{\mathbf{F}}^{(33)}\right)-\tau_{12}(\mathbf{F}) & \tau_{12}\left(\widehat{\mathbf{F}}^{(12)}\right)-\tau_{12}(\mathbf{F}) & \tau_{12}\left(\widehat{\mathbf{F}}^{(13)}\right)-\tau_{12}(\mathbf{F}) & \tau_{12}\left(\widehat{\mathbf{F}}^{(23)}\right)-\tau_{12}(\mathbf{F}) \\ \tau_{13}\left(\widehat{\mathbf{F}}^{(11)}\right)-\tau_{13}(\mathbf{F}) & \tau_{13}\left(\widehat{\mathbf{F}}^{(22)}\right)-\tau_{13}(\mathbf{F}) & \tau_{13}\left(\widehat{\mathbf{F}}^{(33)}\right)-\tau_{13}(\mathbf{F}) & \tau_{13}\left(\widehat{\mathbf{F}}^{(12)}\right)-\tau_{13}(\mathbf{F}) & \tau_{13}\left(\widehat{\mathbf{F}}^{(13)}\right)-\tau_{13}(\mathbf{F}) & \tau_{13}\left(\widehat{\mathbf{F}}^{(23)}\right)-\tau_{13}(\mathbf{F}) \\ \tau_{23}\left(\widehat{\mathbf{F}}^{(11)}\right)-\tau_{23}(\mathbf{F}) & \tau_{23}\left(\widehat{\mathbf{F}}^{(22)}\right)-\tau_{23}(\mathbf{F}) & \tau_{23}\left(\widehat{\mathbf{F}}^{(33)}\right)-\tau_{23}(\mathbf{F}) & \tau_{23}\left(\widehat{\mathbf{F}}^{(12)}\right)-\tau_{23}(\mathbf{F}) & \tau_{23}\left(\widehat{\mathbf{F}}^{(13)}\right)-\tau_{23}(\mathbf{F}) & \tau_{23}\left(\widehat{\mathbf{F}}^{(23)}\right)-\tau_{23}(\mathbf{F}) \end{bmatrix}. \quad \text{(C.7)}$$

While Eq. C.6 provides a convenient approach for determining consistent tangent moduli, a pair of major limitations are unavoidable in finite difference methods, like the one used in the construction of Eq. C.6. Namely, the accumulation of floating pointing errors due to limited numerical precision for small perturbations, ε, and insufficient accuracy for large ε. The complex-step derivative approximation (CSDA)—originally proposed by Lyness (1968)—avoids floating pointing error accumulation by directing perturbations along the imaginary axis, and, for sufficiently small ε, directional derivatives of a tensor valued

tensor function may, to nearly the accuracy of the precision of the arithmetic, be approximated as

$$\frac{\partial \mathbf{f}}{\partial \mathbf{A}} : \mathbf{Z} \approx \frac{\Im\left[\mathbf{f}\left(\mathbf{A} + i\varepsilon\mathbf{Z}\right)\right]}{\varepsilon}, \tag{C.8}$$

where the derivative of the tensor valued function $\mathbf{f}$ is evaluated at the point $\mathbf{A}$ in the direction of $\mathbf{Z}$ and $\Im\left[\cdot\right]$ is the imaginary component of a complex argument.

Tanaka et al. (2014) provides a rigorous derivation of consistent tangent moduli in a variety of spatial settings, though there is no explicit discussion of the form of the perturbation scheme required to determine the consistent tangent moduli tensor specified by ABAQUS/Standard in an efficient manner. A close reading of Hürkamp et al. (2015), in combination with an adaptation of some results for hyper-dual numbers presented in Tanaka et al. (2015), begins to clearly define the requisite mathematical formulation for $\mathbb{C}^J$. In particular, it can be shown that

$$\mathbb{C}^{J^{(ij)}} \approx \frac{1}{J\varepsilon}\Im\left[\boldsymbol{\tau}\left(\mathbf{F} + i\varepsilon\Delta\mathbf{F}^{(ij)}\right)\right], \tag{C.9}$$

where $\Delta\mathbf{F}^{(ij)}$ takes the form of Eq. C.4. With Eq. C.9 it is possible to algorithmically define a general anisotropic, hyperelastic material within the ABAQUS/Standard UMAT framework. Figure C.1 details a possible step-by-step procedure for defining UMAT calculations. In Fig. C.1 $|\cdot|$ refers to the determinant of the argument matrix and $\mathbf{R}$ is the rotation associated with the deformation.

BIBLIOGRAPHY

E. M. Abdel-Rahman and M. S. Hefzy. Three-dimensional dynamic behaviour of the human knee joint under impact loading. *Medical Engineering & Physics*, 20(4):276–290, 1998.

S. D. Abramowitch and S. L.-Y. Woo. An improved method to analyze the stress relaxation of ligaments following a finite ramp time based on the quasi-linear viscoelastic theory. *Journal of biomechanical engineering*, 126(1):92–97, 2004.

M. Adouni, A. Shirazi-Adl, and R. Shirazi. Computational biodynamics of human knee joint in gait: from muscle forces to cartilage stresses. *Journal of Biomechanics*, 45(12): 2149–2156, 2012.

J. Agel, E. A. Arendt, and B. Bershadsky. Anterior cruciate ligament injury in national collegiate athletic association basketball and soccer. *The American journal of sports medicine*, 33(4):524–531, 2005.

P. Aglietti, R. Buzzi, F. Giron, A. Simeone, and G. Zaccherotti. Arthroscopic-assisted anterior cruciate ligament reconstruction with the central third patellar tendon a 5–8-year follow-up. *Knee Surgery, Sports Traumatology, Arthroscopy*, 5(3):138–144, 1997.

A. Ahmed and D. Burke. In-vitro of measurement of static pressure distribution in synovial joints-part 1: Tibial surface of the knee. *Journal of biomechanical engineering*, 105(3): 216–225, 1983.

E. Alentorn-Geli, G. D. Myer, H. J. Silvers, G. Samitier, D. Romero, C. Lázaro-Haro, and R. Cugat. Prevention of non-contact anterior cruciate ligament injuries in soccer players. part 1: Mechanisms of injury and underlying risk factors. *Knee Surgery, Sports Traumatology, Arthroscopy*, 17(7):705–729, 2009.

S. A. Ali, R. Helmer, and M. R. Terk. Analysis of the patellofemoral region on mri: association of abnormal trochlear morphology with severe cartilage defects. *American Journal of Roentgenology*, 194(3):721–727, 2010.

D. Amiel, C. Frank, F. Harwood, J. Fronek, and W. Akeson. Tendons and ligaments: a morphological and biochemical comparison. *Journal of Orthopaedic Research*, 1(3): 257–265, 1983.

A. Amis and G. Dawkins. Functional anatomy of the anterior cruciate ligament. fibre bundle actions related to ligament replacements and injuries. *Journal of Bone & Joint Surgery, British Volume*, 73(2):260–267, 1991.

A. A. Amis, A. M. Bull, and D. T. Lie. Biomechanics of rotational instability and anatomic anterior cruciate ligament reconstruction. *Operative Techniques in Orthopaedics*, 15(1): 29–35, 2005.

H. Andersen and P. Dyhre-Poulsen. The anterior cruciate ligament does play a role in controlling axial rotation in the knee. *Knee Surgery, Sports Traumatology, Arthroscopy*, 5(3):145–149, 1997.

A. F. Anderson, R. B. Snyder, and A. B. Lipscomb. Anterior cruciate ligament reconstruction. *The American journal of sports medicine*, 29(3):272–279, 2001.

C. Andersson, M. Odensten, L. Good, and J. Gillquist. Surgical or non-surgical treatment of acute rupture of the anterior cruciate ligament. a randomized study with long-term follow-up. *JBJS*, 71(7):965–974, 1989.

T. P. Andriacchi and A. Mündermann. The role of ambulatory mechanics in the initiation and progression of knee osteoarthritis. *Current opinion in rheumatology*, 18(5):514–518, 2006.

T. P. Andriacchi, S. Koo, and S. F. Scanlan. Gait mechanics influence healthy cartilage morphology and osteoarthritis of the knee. *The Journal of Bone & Joint Surgery*, 91 (Supplement 1):95–101, 2009.

R. Appleyard, D. Burkhardt, P. Ghosh, R. Read, M. Cake, M. Swain, and G. Murrell. Topographical analysis of the structural, biochemical and dynamic biomechanical properties of cartilage in an ovine model of osteoarthritis. *Osteoarthritis and Cartilage*, 11(1): 65–77, 2003.

R. C. Appleyard, M. V. Swain, S. Khanna, and G. A. Murrell. The accuracy and reliability of a novel handheld dynamic indentation probe for analysing articular cartilage. *Physics in medicine and biology*, 46(2):541, 2001.

E. A. Arendt, J. Agel, and R. Dick. Anterior cruciate ligament injury patterns among collegiate men and women. *Journal of athletic training*, 34(2):86, 1999.

C. Armstrong and V. Mow. Variations in the intrinsic mechanical properties of human articular cartilage with age, degeneration, and water content. *JBJS*, 64(1):88–94, 1982.

C. Armstrong, W. Lai, and V. Mow. An analysis of the unconfined compression of articular cartilage. *Journal of biomechanical engineering*, 106(2):165–173, 1984.

S. P. Arnoczky. Anatomy of the anterior cruciate ligament. *Clinical orthopaedics and related research*, (172):19–25, 1982.

A. Årøen, S. Løken, S. Heir, E. Alvik, A. Ekeland, O. G. Granlund, and L. Engebretsen. Articular cartilage lesions in 993 consecutive knee arthroscopies. *The American Journal of Sports Medicine*, 32(1):211–215, 2004.

J. Arokoski, M. M. Hyttinen, H. J. Helminen, and J. S. Jurvelin. Biomechanical and structural characteristics of canine femoral and tibial cartilage. *Journal of Biomedical Materials Research Part A*, 48(2):99–107, 1999.

E. M. Arruda and M. C. Boyce. A three-dimensional constitutive model for the large stretch behavior of rubber elastic materials. *Journal of the Mechanics and Physics of Solids*, 41 (2):389–412, 1993.

J. L. Astephen, K. J. Deluzio, G. E. Caldwell, M. J. Dunbar, and C. L. Hubley-Kozey. Gait and neuromuscular pattern changes are associated with differences in knee osteoarthritis severity levels. *Journal of biomechanics*, 41(4):868–876, 2008.

G. Ateshian, L. Soslowsky, and V. Mow. Quantitation of articular surface topography and cartilage thickness in knee joints using stereophotogrammetry. *Journal of biomechanics*, 24(8):761–776, 1991.

G. Ateshian, W. Warden, J. Kim, R. Grelsamer, and V. Mow. Finite deformation biphasic material properties of bovine articular cartilage from confined compression experiments. *Journal of biomechanics*, 30(11):1157–1164, 1997.

K. Athanasiou, M. Rosenwasser, J. Buckwalter, T. Malinin, and V. Mow. Interspecies comparisons of in situ intrinsic mechanical properties of distal femoral cartilage. *Journal of Orthopaedic Research*, 9(3):330–340, 1991.

P. Atkinson, T. Atkinson, C. Huang, and R. Doane. A comparison of the mechanical and dimensional properties of the human medial and lateral patellofemoral ligaments. In *Proceedings of the 46th Annual Meeting of the Orthopaedic Research Society, Orlando, FL*, 2000.

H. Atmaca, C. C. Kesemenli, K. Memişoğlu, A. Özkan, and Y. Celik. Changes in the loading of tibial articular cartilage following medial meniscectomy: a finite element analysis study. *Knee Surgery, Sports Traumatology, Arthroscopy*, 21(12):2667–2673, 2013.

B. R. Bach, S. Tradonsky, J. Bojchuk, M. E. Levy, C. A. Bush-Joseph, and N. H. Khan. Arthroscopically assisted anterior cruciate ligament reconstruction using patellar tendon autograft. *The American journal of sports medicine*, 26(1):20–29, 1998.

N. M. Bachrach, V. C. Mow, and F. Guilak. Incompressibility of the solid matrix of articular cartilage under high hydrostatic pressures. *Journal of biomechanics*, 31(5):445–451, 1998.

D. Bader and G. Kempson. The short-term compressive properties of adult human articular cartilage. *Bio-medical materials and engineering*, 4(3):245–256, 1994.

J. Y. Bae, G.-H. Kim, J. K. Seon, and I. Jeon. Finite element study on the anatomic transtibial technique for single-bundle anterior cruciate ligament reconstruction. *Medical & Biological Engineering & Computing*, pages 1–10, 2015.

R. Bakker, S. Tomescu, E. Brenneman, G. Hangalur, A. Laing, and N. Chandrashekar. Effect of sagittal plane mechanics on acl strain during jump landing. *Journal of Orthopaedic Research*, 34(9):1636–1644, 2016.

M. A. Baldwin, C. W. Clary, C. K. Fitzpatrick, J. S. Deacy, L. P. Maletsky, and P. J. Rullkoetter. Dynamic finite element knee simulation for evaluation of knee replacement mechanics. *Journal of Biomechanics*, 45(3):474–483, 2012.

M. Barker and B. Seedhom. The relationship of the compressive modulus of articular cartilage with its deformation response to cyclic loading: does cartilage optimize its modulus so as to minimize the strains arising in it due to the prevalent loading regime? *Rheumatology*, 40(3):274–284, 2001.

M. L. Beaulieu, Y. K. Oh, A. Bedi, J. A. Ashton-Miller, and E. M. Wojtys. Does limited internal femoral rotation increase peak anterior cruciate ligament strain during a simulated pivot landing? *The American Journal of Sports Medicine*, page 0363546514549446, 2014.

M. L. Beaulieu, E. M. Wojtys, and J. A. Ashton-Miller. Risk of anterior cruciate ligament fatigue failure is increased by limited internal femoral rotation during in vitro repeated pivot landings. *The American Journal of Sports Medicine*, 43(9):2233–2241, 2015.

M. L. Beaulieu, G. E. Carey, S. H. Schlecht, E. M. Wojtys, and J. A. Ashton-Miller. On the heterogeneity of the femoral enthesis of the human acl: microscopic anatomy and clinical implications. *Journal of experimental orthopaedics*, 3(1):1–9, 2016.

P. R. Beck, A. L. Thomas, J. Farr, P. B. Lewis, and B. J. Cole. Trochlear contact pressures after anteromedialization of the tibial tubercle. *The American journal of sports medicine*, 33(11):1710–1715, 2005.

A. Bedi, R. F. Warren, E. M. Wojtys, Y. K. Oh, J. A. Ashton-Miller, H. Oltean, and B. T. Kelly. Restriction in hip internal rotation is associated with an increased risk of acl injury. *Knee Surgery, Sports Traumatology, Arthroscopy*, pages 1–8, 2014.

O. Behery, R. A. Siston, J. D. Harris, and D. C. Flanigan. Treatment of cartilage defects of the knee: expanding on the existing algorithm. *Clinical Journal of Sport Medicine*, 24 (1):21–30, 2014.

P. Beillas, G. Papaioannou, S. Tashman, and K. Yang. A new method to investigate in vivo knee behavior using a finite element model of the lower limb. *Journal of Biomechanics*, 37(7):1019–1030, 2004.

S. Below, S. P. Arnoczky, J. Dodds, C. Kooima, and N. Walter. The split-line pattern of the distal femur: a consideration in the orientation of autologous cartilage grafts. *Arthroscopy: The Journal of Arthroscopic & Related Surgery*, 18(6):613–617, 2002.

M. Z. Bendjaballah, A. Shirazi-Adl, and D. Zukor. Finite element analysis of human knee joint in varus-valgus. *Clinical Biomechanics*, 12(3):139–148, 1997.

M. Benjamin and J. Ralphs. Fibrocartilage in tendons and ligamentsâĂŤan adaptation to compressive load. *The Journal of Anatomy*, 193(4):481–494, 1998.

M. Benjamin, E. Evans, and L. Copp. The histology of tendon attachments to bone in man. *Journal of anatomy*, 149:89, 1986.

M. Benjamin, T. Kumai, S. Milz, B. Boszczyk, A. Boszczyk, and J. Ralphs. The skeletal attachment of tendonsâĂŤtendon âĂŸenthesesâĂŹ. *Comparative Biochemistry and Physiology Part A: Molecular & Integrative Physiology*, 133(4):931–945, 2002.

M. Berchuck, T. P. Andriacchi, B. R. Bach, and B. Reider. Gait adaptations by patients who have a deficient anterior cruciate ligament. *J Bone Joint Surg Am*, 72(6):871–877, 1990.

T. F. Besier, M. Fredericson, G. E. Gold, G. S. Beaupré, and S. L. Delp. Knee muscle forces during walking and running in patellofemoral pain patients and pain-free controls. *Journal of Biomechanics*, 42(7):898–905, 2009.

B. Beynnon, J. Howe, M. H. Pope, R. J. Johnson, and B. Fleming. The measurement of anterior cruciate ligament strain in vivo. *International orthopaedics*, 16(1):1–12, 1992.

B. D. Beynnon, B. C. Fleming, R. J. Johnson, C. E. Nichols, P. A. Renström, and M. H. Pope. Anterior cruciate ligament strain behavior during rehabilitation exercises in vivo. *The American Journal of Sports Medicine*, 23(1):24–34, 1995.

A. M. Bhosale and J. B. Richardson. Articular cartilage: structure, injuries and review of management. *British medical bulletin*, 87(1):77–95, 2008.

D. Bingham and P. DeHoff. A constitutive equation for the canine anterior cruciate ligament. *ASME J Biomech Eng*, 101:15–22, 1979.

D. Birk and R. Mayne. Localization of collagen types i, iii and v during tendon development. changes in collagen types i and iii are correlated with changes in fibril diameter. *European journal of cell biology*, 72(4):352–361, 1997.

D. E. Birk and R. L. Trelstad. Extracellular compartments in matrix morphogenesis: collagen fibril, bundle, and lamellar formation by corneal fibroblasts. *The Journal of cell biology*, 99(6):2024–2033, 1984.

J. Bischoff, E. Arruda, and K. Grosh. A microstructurally based orthotropic hyperelastic constitutive law. *Journal of Applied Mechanics*, 69(5):570–579, 2002a.

J. Bischoff, E. Arruda, and K. Grosh. Orthotropic hyperelasticity in terms of an arbitrary molecular chain model. *Journal of Applied Mechanics*, 69(2):198–201, 2002b.

J. E. Bischoff, E. M. Arruda, and K. Grosh. Finite element simulations of orthotropic hyperelasticity. *Finite Elements in Analysis and Design*, 38(10):983–998, 2002c.

J. E. Bischoff, E. M. Arruda, and K. Grosh. A rheological network model for the continuum anisotropic and viscoelastic behavior of soft tissue. *Biomechanics and modeling in mechanobiology*, 3(1):56–65, 2004.

T. A. Blackburn and E. Craig. Knee anatomy: a brief review. *Physical therapy*, 60(12): 1556–1560, 1980.

L. Blankevoort and R. Huiskes. Validation of a three-dimensional model of the knee. *Journal of Biomechanics*, 29(7):955–961, 1996.

V. Bobić. Arthroscopic osteochondral autograft transplantation in anterior cruciate ligament reconstruction: a preliminary clinical study. *Knee Surgery, Sports Traumatology, Arthroscopy*, 3(4):262–264, 1996.

B. P. Boden, G. S. Dean, J. A. Feagin, and W. E. Garrett. Mechanisms of anterior cruciate ligament injury. *Orthopedics*, 23(6):573–578, 2000.

S. D. Boden, D. O. Davis, T. S. Dina, D. W. Stoller, S. D. Brown, J. C. Vailas, and P. A. Labropoulos. A prospective and blinded investigation of magnetic resonance imaging of the knee: abnormal findings in asymptomatic subjects. *Clinical orthopaedics and related research*, 282:177–185, 1992.

S. Bollen. Epidemiology of knee injuries: diagnosis and triage. *British journal of sports medicine*, 34(3):227–228, 2000.

C. Bonifasi-Lista, S. P. Lake, M. S. Small, and J. A. Weiss. Viscoelastic properties of the human medial collateral ligament under longitudinal, transverse and shear loading. *Journal of Orthopaedic Research*, 23(1):67–76, 2005.

T. J. Bonner, N. Newell, A. Karunaratne, A. D. Pullen, A. A. Amis, A. M. Bull, and S. D. Masouros. Strain-rate sensitivity of the lateral collateral ligament of the knee. *journal of the mechanical behavior of biomedical materials*, 41:261–270, 2015.

J. R. Borchers, C. C. Kaeding, A. D. Pedroza, L. J. Huston, K. P. Spindler, R. W. Wright, M. Consortium, and the MARS Group. Intra-articular findings in primary and revision anterior cruciate ligament reconstruction surgery: a comparison of the moon and mars study groups. *The American journal of sports medicine*, 39(9):1889–1893, 2011.

F. Boschetti, G. Pennati, F. Gervaso, G. M. Peretti, and G. Dubini. Biomechanical properties of human articular cartilage under compressive loads. *Biorheology*, 41(3-4):159–166, 2004.

M. C. Boyce and E. M. Arruda. Constitutive models of rubber elasticity: a review. *Rubber chemistry and technology*, 73(3):504–523, 2000.

P. Brama, J. Tekoppele, R. Bank, A. Barneveld, and P. Weeren. Functional adaptation of equine articular cartilage: the formation of regional biochemical characteristics up to age one year. *Equine veterinary journal*, 32(3):217–221, 2000a.

P. Brama, J. Tekoppele, R. Bank, D. Karssenberg, A. Barneveld, and P. Weeren. Topographical mapping of biochemical properties of articular cartilage in the equine fetlock joint. *Equine veterinary journal*, 32(1):19–26, 2000b.

J. P. Braman, J. D. Bruckner, J. M. Clark, A. G. Norman, and H. A. Chansky. Articular cartilage adjacent to experimental defects is subject to atypical strains. *Clinical orthopaedics and related research*, 430:202–207, 2005.

O. C. Brantigan and A. F. Voshell. The mechanics of the ligaments and menisci of the knee joint. *JBJS*, 23(1):44–66, 1941.

M. Bredella, P. Tirman, C. Peterfy, M. Zarlingo, J. Feller, F. Bost, J. Belzer, T. Wischer, and H. Genant. Accuracy of t2-weighted fast spin-echo mr imaging with fat saturation in detecting cartilage defects in the knee: comparison with arthroscopy in 130 patients. *AJR. American journal of roentgenology*, 172(4):1073–1080, 1999.

P. Briant, S. Bevill, and T. Andriacchi. Cartilage strain distributions are different under the same load in the central and peripheral tibial plateau regions. *Journal of biomechanical engineering*, 137(12):121009, 2015.

T. Brindle, J. Nyland, and D. L. Johnson. The meniscus: review of basic principles with application to surgery and rehabilitation. *Journal of athletic training*, 36(2):160, 2001.

M. Brittberg and C. S. Winalski. Evaluation of cartilage injuries and repair. *JBJS*, 85 (suppl_2):58–69, 2003.

M. Brittberg, A. Lindahl, A. Nilsson, C. Ohlsson, O. Isaksson, and L. Peterson. Treatment of deep cartilage defects in the knee with autologous chondrocyte transplantation. *New england journal of medicine*, 331(14):889–895, 1994.

C. Brown, T. Nguyen, H. Moody, R. Crawford, and A. Oloyede. Assessment of common hyperelastic constitutive equations for describing normal and osteoarthritic articular cartilage. *Proceedings of the Institution of Mechanical Engineers, Part H: Journal of Engineering in Medicine*, 223(6):643–652, 2009.

T. D. Brown and R. J. Singerman. Experimental determination of the linear biphasic constitutive coefficients of human fetal proximal femoral chondroepiphysis. *Journal of biomechanics*, 19(8):597–605, 1986.

T. D. Brown, D. F. Pope, J. E. Hale, J. A. Buckwalter, and R. A. Brand. Effects of osteochondral defect size on cartilage contact stress. *Journal of Orthopaedic Research*, 9(4): 559–567, 1991.

J. C. Buckland-Wright, D. G. Macfarlane, J. A. Lynch, M. K. Jasani, and C. R. Bradshaw. Joint space width measures cartilage thickness in osteoarthritis of the knee: high resolution plain film and double contrast macroradiographic investigation. *Annals of the rheumatic diseases*, 54(4):263–268, 1995.

M. R. Buckley, J. P. Gleghorn, L. J. Bonassar, and I. Cohen. Mapping the depth dependence of shear properties in articular cartilage. *Journal of biomechanics*, 41(11):2430–2437, 2008.

J. Buckwalter. Articular cartilage; composition, structure, response to injury, and methods of facilating repair. *Articular Cartilage and Knee Joint Function; Basic Science and Arthroscopy*, pages 19–56, 1990.

J. Buckwalter and H. Mankin. Instructional course lectures, the american academy of orthopaedic surgeons-articular cartilage. part i: Tissue design and chondrocyte-matrix interactions. *JBJS*, 79(4):600–611, 1997.

J. A. Buckwalter and T. D. Brown. Joint injury, repair, and remodeling: roles in post-traumatic osteoarthritis. *Clinical orthopaedics and related research*, 423:7–16, 2004.

J. A. Buckwalter, V. C. Mow, and A. Ratcliffe. Restoration of injured or degenerated articular cartilage. *Journal of the American Academy of Orthopaedic Surgeons*, 2(4): 192–201, 1994.

M. J. Buehler. Atomistic and continuum modeling of mechanical properties of collagen: elasticity, fracture, and self-assembly. *Journal of Materials Research*, 21(8):1947–1961, 2006.

D. Butler, F. Noyes, and E. Grood. Ligamentous restraints to anterior-posterior drawer in the human knee. *J Bone Joint Surg Am*, 62(2):259–270, 1980.

D. Butler, M. Sheh, D. Stouffer, V. Samaranayake, and M. S. Levy. Surface strain variation in human patellar tendon and knee cruciate ligaments. *Journal of Biomechanical Engineering*, 112(1):38–45, 1990.

D. L. Butler. Anterior cruciate ligament: its normal response and replacement. *Journal of Orthopaedic Research*, 7(6):910–921, 1989.

D. L. Butler, Y. Guan, M. D. Kay, J. F. Cummings, S. M. Feder, and M. S. Levy. Location-dependent variations in the material properties of the anterior cruciate ligament. *Journal of biomechanics*, 25(5):511–518, 1992.

R. J. Butler, K. I. Minick, R. Ferber, and F. Underwood. Gait mechanics after acl reconstruction: implications for the early onset of knee osteoarthritis. *British journal of sports medicine*, 43(5):366–370, 2009.

D. R. Carter, G. S. Beaupré, M. Wong, R. L. Smith, T. P. Andriacchi, and D. J. Schurman. The mechanobiology of articular cartilage development and degeneration. *Clinical orthopaedics and related research*, 427:S69–S77, 2004.

D. Chan, C. Neu, and M. Hull. In situ deformation of cartilage in cyclically loaded tibiofemoral joints by displacement-encoded mri. *Osteoarthritis and cartilage*, 17(11): 1461–1468, 2009.

N. Chandrashekar, H. Mansouri, J. Slauterbeck, and J. Hashemi. Sex-based differences in the tensile properties of the human anterior cruciate ligament. *Journal of biomechanics*, 39(16):2943–2950, 2006.

A. H. Chang, K. C. Moisio, J. S. Chmiel, F. Eckstein, A. Guermazi, P. V. Prasad, Y. Zhang, O. Almagor, L. Belisle, K. Hayes, et al. External knee adduction and flexion moments during gait and medial tibiofemoral disease progression in knee osteoarthritis. *Osteoarthritis and cartilage*, 23(7):1099–1106, 2015.

M. Charlebois, M. D. McKee, and M. D. Buschmann. Nonlinear tensile properties of bovine articular cartilage and their variation with age and depth. *Journal of Biomechanical Engineering*, 126(2):129–137, 2004.

S. Chatelin, C. Deck, and R. Willinger. An anisotropic viscous hyperelastic constitutive law for brain material finite-element modeling. *Journal of biorheology*, 27(1-2):26–37, 2013.

A. Chaudhari, P. L. Briant, S. L. Bevill, S. Koo, and T. P. Andriacchi. Knee kinematics, cartilage morphology, and osteoarthritis after acl injury. *Medicine and science in sports and exercise*, 40(2):215–222, 2008.

S. Chegini and S. J. Ferguson. Time and depth dependent poissonâĂŹs ratio of cartilage explained by an inhomogeneous orthotropic fiber embedded biphasic model. *Journal of biomechanics*, 43(9):1660–1666, 2010.

A. Chen, W. Bae, R. Schinagl, and R. Sah. Depth-and strain-dependent mechanical and electromechanical properties of full-thickness bovine articular cartilage in confined compression. *Journal of biomechanics*, 34(1):1–12, 2001.

C. T. Chen and P. A. Torzilli. In vitro cartilage explant injury models. In *Post-Traumatic Arthritis*, pages 29–40. Springer, 2015.

I. Choi and C. Horgan. Saint-venantâĂŹs principle and end effects in anisotropic elasticity. *Journal of Applied Mechanics*, 44(3):424–430, 1977.

W. J. Choi, K. K. Park, B. S. Kim, and J. W. Lee. Osteochondral lesion of the talus: is there a critical defect size for poor outcome? *The American journal of sports medicine*, 37(10):1974–1980, 2009.

V. Chouliaras, S. Ristanis, C. Moraiti, V. Tzimas, N. Stergiou, and A. Georgoulis. Anterior cruciate ligament reconstruction with a quadrupled hamstrings tendon autograft does not restore tibial rotation to normative levels during landing from a jump and subsequent pivoting. *Journal of Sports Medicine and Physical Fitness*, 49(1):64, 2009.

A. Cohen. A padé approximant to the inverse langevin function. *Rheologica acta*, 30(3): 270–273, 1991.

Z. A. Cohen, D. M. Mccarthy, S. D. Kwak, P. Legrand, F. Fogarasi, E. J. Ciaccio, and G. A. Ateshian. Knee cartilage topography, thickness, and contact areas from mri: in-vitro calibration and in-vivo measurements. *Osteoarthritis and cartilage*, 7(1):95–109, 1999.

F. R. Convery, W. H. Akeson, and G. H. Keown. The repair of large osteochondral defects an experimental study in horses. *Clinical Orthopaedics and Related Research*, 82:253–262, 1972.

R. R. Cooper, S. Misol, and P. Stimmel. Tendon and ligament insertion: A light and election microscopic study. *JBJS*, 52(1):1–170, 1970.

C. L. Cox, L. J. Huston, W. R. Dunn, E. K. Reinke, S. K. Nwosu, R. D. Parker, R. W. Wright, C. C. Kaeding, R. G. Marx, A. Amendola, et al. Are articular cartilage lesions and meniscus tears predictive of ikdc, koos, and marx activity level outcomes after anterior cruciate ligament reconstruction? a 6-year multicenter cohort study. *The American journal of sports medicine*, 42(5):1058–1067, 2014.

G. Cox, E. Kable, A. Jones, I. Fraser, F. Manconi, and M. D. Gorrell. 3-dimensional imaging of collagen using second harmonic generation. *Journal of structural biology*, 141(1):53–62, 2003.

W. W. Curl, J. Krome, E. S. Gordon, J. Rushing, B. P. Smith, and G. G. Poehling. Cartilage injuries: a review of 31,516 knee arthroscopies. *Arthroscopy: The Journal of Arthroscopic & Related Surgery*, 13(4):456–460, 1997.

D. D D'Lima, P. C Chen, et al. Osteochondral grafting: effect of graft alignment, material properties, and articular geometry. *The open orthopaedics journal*, 3(1), 2009.

Y. Dabiri and L. Li. Focal cartilage defect compromises fluid-pressure dependent load support in the knee joint. *International journal for numerical methods in biomedical engineering*, 31(6), 2015.

D. M. Daniel, W. H. Akeson, and J. J. O'Connor. *Knee ligaments: structure, function, injury, and repair*. Raven Pr, 1990.

K. D. Danylchuk, J. B. Finlay, and J. Krcek. Microstructural organization of human and bovine cruciate ligaments. *Clinical orthopaedics and related research*, 131:294–298, 1978.

E. Darabi and M. Itskov. A simple and accurate approximation of the inverse langevin function. *Rheologica Acta*, 54(5):455–459, 2015.

R. E. Debski, S. M. Moore, J. L. Mercer, M. S. Sacks, and P. J. McMahon. The collagen fibers of the anteroinferior capsulolabrum have multiaxial orientation to resist shoulder dislocation. *Journal of Shoulder and Elbow Surgery*, 12(3):247–252, 2003.

W. Decraemer, M. Maes, V. Vanhuyse, and P. Vanpeperstraete. A non-linear viscoelastic constitutive equation for soft biological tissues, based upon a structural model. *Journal of biomechanics*, 13(7):559–564, 1980.

P. Dehoff. On the nonlinear viscoelastic behavior of soft biological tissues. *Journal of Biomechanics*, 11(1-2):35–40, 1978.

J. M. Deneweth, M. J. Bey, S. G. McLean, T. R. Lock, P. A. Kolowich, and S. Tashman. Tibiofemoral joint kinematics of the anterior cruciate ligament-reconstructed knee during a single-legged hop landing. *The American Journal of Sports Medicine*, 38(9): 1820–1828, 2010.

J. M. Deneweth, S. G. McLean, and E. M. Arruda. Evaluation of hyperelastic models for the non-linear and non-uniform high strain-rate mechanics of tibial cartilage. *Journal of Biomechanics*, 46(10):1604–1610, 2013a.

J. M. Deneweth, K. E. Newman, S. M. Sylvia, S. G. McLean, and E. M. Arruda. Heterogeneity of tibial plateau cartilage in response to a physiological compressive strain rate. *Journal of Orthopaedic Research*, 31(3):370–375, 2013b.

J. M. Deneweth, E. M. Arruda, and S. G. McLean. Hyperelastic modeling of location-dependent human distal femoral cartilage mechanics. *International Journal of Non-Linear Mechanics*, 68:146–156, 2015.

Y. Y. Dhaher, T.-H. Kwon, and M. Barry. The effect of connective tissue material uncertainties on knee joint mechanics under isolated loading conditions. *Journal of Biomechanics*, 43(16):3118–3125, 2010.

M. Dienst, R. T. Burks, and P. E. Greis. Anatomy and biomechanics of the anterior cruciate ligament. *Orthopedic Clinics of North America*, 33(4):605–620, 2002.

N. Diermann, T. Schumacher, S. Schanz, M. J. Raschke, W. Petersen, and T. Zantop. Rotational instability of the knee: internal tibial rotation under a simulated pivot shift test. *Archives of orthopaedic and trauma surgery*, 129(3):353–358, 2009.

M. R. DiSilvestro and J.-K. F. Suh. A cross-validation of the biphasic poroviscoelastic model of articular cartilage in unconfined compression, indentation, and confined compression. *Journal of biomechanics*, 34(4):519–525, 2001.

M. R. DiSilvestro and J.-K. F. Suh. Biphasic poroviscoelastic characteristics of proteoglycan-depleted articular cartilage: simulation of degeneration. *Annals of biomedical engineering*, 30(6):792–800, 2002.

M. R. DiSilvestro, Q. Zhu, and J.-K. F. Suh. Biphasic poroviscoelastic simulation of the unconfined compression of articular cartilage: IiâĂŤeffect of variable strain rates. *Journal of biomechanical engineering*, 123(2):198–200, 2001a.

M. R. DiSilvestro, Q. Zhu, and J.-K. F. Suh. Biphasic poroviscoelastic simulation of the unconfined compression of articular cartilage: IiâĂŤeffect of variable strain rates. *Journal of biomechanical engineering*, 123(2):198–200, 2001b.

M. R. DiSilvestro, Q. Zhu, M. Wong, J. S. Jurvelin, and J.-K. F. Suh. Biphasic poroviscoelastic simulation of the unconfined compression of articular cartilage: IâĂŤsimultaneous prediction of reaction force and lateral displacement. *Journal of biomechanical engineering*, 123(2):191–197, 2001c.

J. A. Dodds and S. P. Arnoczky. Anatomy of the anterior cruciate ligament: a blueprint for repair and reconstruction. *Arthroscopy: The Journal of Arthroscopic & Related Surgery*, 10(2):132–139, 1994.

T. L. H. Donahue, M. Hull, M. M. Rashid, and C. R. Jacobs. A finite element model of the human knee joint for the study of tibio-femoral contact. *Journal of Biomechanical Engineering*, 124(3):273–280, 2002.

T. L. H. Donahue, M. Hull, M. M. Rashid, and C. R. Jacobs. How the stiffness of meniscal attachments and meniscal material properties affect tibio-femoral contact pressure computed using a validated finite element model of the human knee joint. *Journal of Biomechanics*, 36(1):19–34, 2003.

Y.-f. Dong, G.-h. Hu, L.-l. Zhang, Y. Hu, Y.-h. Dong, and Q.-r. Xu. Accurate 3d reconstruction of subject-specific knee finite element model to simulate the articular cartilage defects. *Journal of Shanghai Jiaotong University (Science)*, 16(5):620–627, 2011.

M. Doweidar, B. Calvo, I. Alfaro, P. Groenenboom, and M. Doblaré. A comparison of implicit and explicit natural element methods in large strains problems: Application to soft biological tissues modeling. *Computer methods in applied mechanics and engineering*, 199(25):1691–1700, 2010.

L. F. Draganich, B. Reider, M. Ling, and M. Samuelson. An in vitro study of an intraarticular and extraarticular reconstruction in the anterior cruciate ligament deficient knee. *The American journal of sports medicine*, 18(3):262–266, 1990.

V. Duthon, C. Barea, S. Abrassart, J. Fasel, D. Fritschy, and J. Ménétrey. Anatomy of the anterior cruciate ligament. *Knee surgery, sports traumatology, arthroscopy*, 14(3): 204–213, 2006.

A. Eberhardt, L. Keer, J. Lewis, and V. Vithoontien. An analytical model of joint contact. *Journal of biomechanical engineering*, 112(4):407–413, 1990.

A. Edwards, A. M. Bull, and A. A. Amis. The attachments of the anteromedial and posterolateral fibre bundles of the anterior cruciate ligament. *Knee Surgery, Sports Traumatology, Arthroscopy*, 15(12):1414–1421, 2007.

A. Edwards, A. M. Bull, and A. A. Amis. The attachments of the anteromedial and posterolateral fibre bundles of the anterior cruciate ligament. *Knee Surgery, Sports Traumatology, Arthroscopy*, 16(1):29–36, 2008.

P. S. Eggli, E. B. Hunzinker, and R. K. Schenk. Quantitation of structural features characterizing weight-and less-weight-bearing regions in articular cartilage: A stereological

analysis of medical femoral condyles in young adult rabbits. *The Anatomical Record*, 222(3):217–227, 1988.

W. Ehlers and B. Markert. A linear viscoelastic biphasic model for soft tissues based on the theory of porous media. *Transactions-American Society of Mechanical Engineers Journal of biomechanical Engineering*, 123(5):418–424, 2001.

J. J. Elias, J. D. DesJardins, A. F. Faust, S. A. Lietman, and E. Chao. Size and position of a single condyle allograft influence knee kinematics. *Journal of orthopaedic research*, 17 (4):540–545, 1999.

D. M. Elliott, D. A. Narmoneva, and L. A. Setton. Direct measurement of the poisson's ratio of human patella cartilage in tension. *TRANSACTIONS-AMERICAN SOCIETY OF MECHANICAL ENGINEERS JOURNAL OF BIOMECHANICAL ENGINEERING*, 124 (2):223–228, 2002.

B. J. Ellis, T. J. Lujan, M. S. Dalton, and J. A. Weiss. Medial collateral ligament insertion site and contact forces in the acl-deficient knee. *Journal of orthopaedic research*, 24(4): 800–810, 2006.

B. J. Ellis, R. E. Debski, S. M. Moore, P. J. McMahon, and J. A. Weiss. Methodology and sensitivity studies for finite element modeling of the inferior glenohumeral ligament complex. *Journal of biomechanics*, 40(3):603–612, 2007.

L. Engebretsen, E. Arendt, and H. M. Fritts. Osteochondral lesions and cruciate ligament injuries: Mri in 18 knees. *Acta orthopaedica Scandinavica*, 64(4):434–436, 1993.

D. R. Eyre, M. A. Weis, and J.-J. Wu. Articular cartilage collagen: an irreplaceable framework. *Eur Cell Mater*, 12(1):57–63, 2006.

S. Federico and W. Herzog. On the anisotropy and inhomogeneity of permeability in articular cartilage. *Biomechanics and modeling in mechanobiology*, 7(5):367–378, 2008.

D. T. Felson, R. C. Lawrence, P. A. Dieppe, R. Hirsch, C. G. Helmick, J. M. Jordan, R. S. Kington, N. E. Lane, M. C. Nevitt, Y. Zhang, et al. Osteoarthritis: new insights. part 1: the disease and its risk factors. *Annals of internal medicine*, 133(8):635–646, 2000.

Y. Feng, R. J. Okamoto, R. Namani, G. M. Genin, and P. V. Bayly. Measurements of mechanical anisotropy in brain tissue and implications for transversely isotropic material models of white matter. *Journal of the mechanical behavior of biomedical materials*, 23: 117–132, 2013.

J. Fick, A. Ronkainen, W. Herzog, and R. Korhonen. Site-dependent biomechanical responses of chondrocytes in the rabbit knee joint. *Journal of biomechanics*, 48(15):4010–4019, 2015.

B. Fleming, B. Beynnon, H. Tohyama, R. Johnson, C. Nichols, P. Renström, and M. Pope. Determination of a zero strain reference for the anteromedial band of the anterior cruciate ligament. *Journal of Orthopaedic Research*, 12(6):789–795, 1994.

M. Folkes and R. Arridge. The measurement of shear modulus in highly anisotropic materials: the validity of st. venant's principle. *Journal of Physics D: Applied Physics*, 8(9): 1053, 1975.

M. Fortin, J. Soulhat, A. Shirazi-Adl, E. Hunziker, and M. Buschmann. Unconfined compression of articular cartilage: nonlinear behavior and comparison with a fibril-reinforced biphasic model. *Journal of biomechanical engineering*, 122(2):189–195, 2000.

A. J. Fox, F. Wanivenhaus, A. J. Burge, R. F. Warren, and S. A. Rodeo. The human meniscus: a review of anatomy, function, injury, and advances in treatment. *Clinical Anatomy*, 28(2):269–287, 2015.

M. Franchi, A. Trirè, M. Quaranta, E. Orsini, and V. Ottani. Collagen structure of tendon relates to function. *The Scientific World Journal*, 7:404–420, 2007.

C. Frank, S.-Y. Woo, D. Amiel, F. Harwood, M. Gomez, and W. Akeson. Medial collateral ligament healing: a multidisciplinary assessment in rabbits. *The American journal of sports medicine*, 11(6):379–389, 1983.

K. B. Freedman, M. J. D'Amato, D. D. Nedeff, A. Kaz, and B. R. Bach. Arthroscopic anterior cruciate ligament reconstruction: a metaanalysis comparing patellar tendon and hamstring tendon autografts. *The American journal of sports medicine*, 31(1):2–11, 2003.

M. I. Froimson, A. Ratcliffe, T. R. Gardner, and V. C. Mow. Differences in patellofemoral joint cartilage material properties and their significance to the etiology of cartilage surface fibrillation. *Osteoarthritis and Cartilage*, 5(6):377–386, 1997.

H. M. Frost. From wolff's law to the utah paradigm: insights about bone physiology and its clinical applications. *The Anatomical Record*, 262(4):398–419, 2001.

F. H. Fu, C. D. Harner, D. L. Johnson, M. D. Miller, and S. L.-y. Woo. Biomechanics of knee ligaments: basic concepts and clinical application. *JBJS*, 75(11):1716–1727, 1993.

T. Fukubayashi, P. Torzilli, M. Sherman, and R. Warren. An in vitro biomechanical evaluation of anterior-posterior motion of the knee. tibial displacement, rotation, and torque. *The Journal of Bone & Joint Surgery*, 64(2):258–264, 1982.

S. Fukuta, M. Oyama, K. Kavalkovich, F. H. Fu, and C. Niyibizi. Identification of types ii, ix and x collagens at the insertion site of the bovine achilles tendon. *Matrix Biology*, 17 (1):65–73, 1998.

W. Furman, J. Marshall, and F. Girgis. The anterior cruciate ligament. a functional analysis based on postmortem studies. *JBJS*, 58(2):179–185, 1976.

M. T. Gabriel, E. K. Wong, S. L.-Y. Woo, M. Yagi, and R. E. Debski. Distribution of in situ forces in the anterior cruciate ligament in response to rotatory loads. *Journal of Orthopaedic Research*, 22(1):85–89, 2004.

A. R. Gannon, T. Nagel, and D. J. Kelly. The role of the superficial region in determining the dynamic properties of articular cartilage. *Osteoarthritis and cartilage*, 20(11):1417–1425, 2012.

B. Gao and N. N. Zheng. Alterations in three-dimensional joint kinematics of anterior cruciate ligament-deficient and-reconstructed knees during walking. *Clinical Biomechanics*, 25(3):222–229, 2010.

J. Garcia, N. Altiero, and R. Haut. An approach for the stress analysis of transversely isotropic biphasic cartilage under impact load. *Journal of biomechanical engineering*, 120(5):608–613, 1998.

J. C. Gardiner and J. A. Weiss. Subject-specific finite element analysis of the human medial collateral ligament during valgus knee loading. *Journal of Orthopaedic Research*, 21(6): 1098–1106, 2003.

S. Gasser and R. Uppal. Anterior cruciate ligament reconstruction: a new technique for achilles tendon allograft preparation. *Arthroscopy: The Journal of Arthroscopic & Related Surgery*, 22(12):1365–e1, 2006.

T. C. Gasser, R. W. Ogden, and G. A. Holzapfel. Hyperelastic modelling of arterial layers with distributed collagen fibre orientations. *Journal of the royal society interface*, 3(6): 15–35, 2006.

G. M. Genin and S. Thomopoulos. The tendon-to-bone attachment: Unification through disarray. *Nature Materials*, 16(6):607–608, 2017.

G. M. Genin, A. Kent, V. Birman, B. Wopenka, J. D. Pasteris, P. J. Marquez, and S. Thomopoulos. Functional grading of mineral and collagen in the attachment of tendon to bone. *Biophysical journal*, 97(4):976–985, 2009.

M. S. George, L. J. Huston, and K. P. Spindler. Endoscopic versus rear-entry acl reconstruction: a systematic review. *Clinical orthopaedics and related research*, 455:158–161, 2007.

A. Georgoulis, S. Ristanis, C. Moraiti, N. Paschos, F. Zampeli, S. Xergia, S. Georgiou, K. Patras, H. Vasiliadis, and G. Mitsionis. Acl injury and reconstruction: Clinical related in vivo biomechanics. *Orthopaedics & Traumatology: Surgery & Research*, 96(8):S119–S128, 2010.

A. D. Georgoulis, A. Papadonikolakis, C. D. Papageorgiou, A. Mitsou, and N. Stergiou. Three-dimensional tibiofemoral kinematics of the anterior cruciate ligament-deficient and reconstructed knee during walking. *The American journal of sports medicine*, 31(1): 75–79, 2003.

S. M. Gianotti, S. W. Marshall, P. A. Hume, and L. Bunt. Incidence of anterior cruciate ligament injury and other knee ligament injuries: a national population-based study. *Journal of Science and Medicine in Sport*, 12(6):622–627, 2009.

C. Gillis, N. Sharkey, S. Stover, R. Pool, D. Meagher, and N. Willits. Effect of maturation and aging on material and ultrasonographic properties of equine superficial digital flexor tendon. *American journal of veterinary research*, 56(10):1345–1350, 1995.

F. G. Girgis, J. L. Marshall, and A. A. M. Jem. The cruciate ligaments of the knee joint: Anatomical. functional and experimental analysis. *Clinical orthopaedics and related research*, 106:216–231, 1975.

A. Godest, M. Beaugonin, E. Haug, M. Taylor, and P. Gregson. Simulation of a knee joint replacement during a gait cycle using explicit finite element analysis. *Journal of Biomechanics*, 35(2):267–275, 2002.

J. P. Goldblatt and J. C. Richmond. Anatomy and biomechanics of the knee. *Operative Techniques in Sports Medicine*, 11(3):172–186, 2003.

S. R. Goldring and M. B. Goldring. The role of cytokines in cartilage matrix degeneration in osteoarthritis. *Clinical Orthopaedics and Related Research*, 427:S27–S36, 2004.

S. A. Goldstein. The mechanical properties of trabecular bone: dependence on anatomic location and function. *Journal of biomechanics*, 20(11-12):1055–1061, 1987.

M. A. Gomez and A. M. Nahum. Biomechanics of bone. In *Accidental injury*, pages 206–227. Springer, 2002.

A. H. Gomoll, H. Madry, G. Knutsen, N. van Dijk, R. Seil, M. Brittberg, and E. Kon. The subchondral bone in articular cartilage repair: current problems in the surgical management. *Knee Surgery, Sports Traumatology, Arthroscopy*, 18(4):434–447, 2010.

F. Gottsauner-Wolf, J. J. Grabowski, E. Chao, and K.-N. An. Effects of freeze/thaw conditioning on the tensile properties and failure mode of bone-muscle-bone units: A biomechanical and histological study in dogs. *Journal of orthopaedic research*, 13(1):90–95, 1995.

K. R. Gratz, B. L. Wong, W. C. Bae, and R. L. Sah. The effects of focal articular defects on intra-tissue strains in the surrounding and opposing cartilage. *Biorheology*, 45(3-4): 193–207, 2008.

K. R. Gratz, B. L. Wong, W. C. Bae, and R. L. Sah. The effects of focal articular defects on cartilage contact mechanics. *Journal of Orthopaedic Research: official publication of the Orthopaedic Research Society*, 27(5):584, 2009.

L. Y. Griffin, M. J. Albohm, E. A. Arendt, R. Bahr, B. D. Beynnon, M. DeMaio, R. W. Dick, L. Engebretsen, W. E. Garrett, J. A. Hannafin, et al. Understanding and preventing noncontact anterior cruciate ligament injuries. *The American journal of sports medicine*, 34(9):1512–1532, 2006.

T. M. Griffin and F. Guilak. The role of mechanical loading in the onset and progression of osteoarthritis. *Exercise and sport sciences reviews*, 33(4):195–200, 2005.

E. S. Grood and F. R. Noyes. Cruciate ligament prosthesis: strength, creep, and fatigue properties. *J Bone Joint Surg Am*, 58(8):1083–1088, 1976.

E. S. Grood and W. J. Suntay. A joint coordinate system for the clinical description of three-dimensional motions: application to the knee. *Journal of biomechanical engineering*, 105(2):136–144, 1983.

W. Gu, W. Lai, and V. Mow. A mixture theory for charged-hydrated soft tissues containing multi-electrolytes: passive transport and swelling behaviors. *Journal of biomechanical engineering*, 120(2):169–180, 1998.

T. M. Guess, G. Thiagarajan, M. Kia, and M. Mishra. A subject specific multibody model of the knee with menisci. *Medical engineering & physics*, 32(5):505–515, 2010.

J. H. Guettler, C. K. Demetropoulos, K. H. Yang, and K. A. Jurist. Osteochondral defects in the human knee influence of defect size on cartilage rim stress and load redistribution to surrounding cartilage. *The American Journal of Sports Medicine*, 32(6):1451–1458, 2004.

H. Guo, T. J. Santner, T. Chen, H. Wang, C. Brial, S. L. Gilbert, M. F. Koff, A. L. Lerner, and S. A. Maher. A statistically-augmented computational platform for evaluating meniscal function. *Journal of biomechanics*, 48(8):1444–1453, 2015.

H. Guo, T. J. Santner, A. L. Lerner, and S. A. Maher. Reducing uncertainty when using knee-specific finite element models by assessing the effect of input parameters. *Journal of Orthopaedic Research*, 2017.

Y. Guo, X. Zhang, and W. Chen. Three-dimensional finite element simulation of total knee joint in gait cycle. *Acta mechanica solida sinica*, 22(4):347–351, 2009.

J. L. Haimes, R. R. Wroble, E. S. Grood, and F. R. Noyes. Role of the medial structures in the intact and anterior cruciate ligament-deficient knee: limits of motion in the human knee. *The American journal of sports medicine*, 22(3):402–409, 1994.

J. P. Halloran, A. J. Petrella, and P. J. Rullkoetter. Explicit finite element modeling of total knee replacement mechanics. *Journal of Biomechanics*, 38(2):323–331, 2005.

K. Halonen, M. Mononen, J. Jurvelin, J. Töyräs, J. Salo, and R. Korhonen. Deformation of articular cartilage during static loading of a knee joint–experimental and finite element analysis. *Journal of biomechanics*, 47(10):2467–2474, 2014.

K. Halonen, M. E. Mononen, J. S. Jurvelin, J. Töyräs, A. Kłodowski, J.-P. Kulmala, and R. K. Korhonen. Importance of patella, quadriceps forces, and depthwise cartilage structure on knee joint motion and cartilage response during gait. *Journal of biomechanical engineering*, 138(7):071002, 2016.

H. S. Han, S. C. Seong, S. Lee, and M. C. Lee. Anterior cruciate ligament reconstruction. *Clinical orthopaedics and related research*, 466(1):198–204, 2008.

S.-K. Han, R. Madden, Z. Abusara, and W. Herzog. In situ chondrocyte viscoelasticity. *Journal of biomechanics*, 45(14):2450–2456, 2012.

L. Hangody and P. Füles. Autologous osteochondral mosaicplasty for the treatment of full-thickness defects of weight-bearing joints: ten years of experimental and clinical experience. *JBJS*, 85(suppl_2):25–32, 2003.

C. D. Harner, G. H. Baek, T. M. Vogrin, G. J. Carlin, S. Kashiwaguchi, and S. L. Woo. Quantitative analysis of human cruciate ligament insertions. *Arthroscopy: The Journal of Arthroscopic & Related Surgery*, 15(7):741–749, 1999.

R. Hart, S. Woo, P. Newton, et al. Ultrastructural morphometry of anterior cruciate and medial collateral ligaments: an experimental study in rabbits. *Journal of orthopaedic research*, 10(1):96–103, 1992.

J. Hashemi, R. Breighner, T.-H. Jang, N. Chandrashekar, S. Ekwaro-Osire, and J. R. Slauterbeck. Increasing pre-activation of the quadriceps muscle protects the anterior cruciate ligament during the landing phase of a jump: an in vitro simulation. *The Knee*, 17(3):235–241, 2010a.

J. Hashemi, N. Chandrashekar, H. Mansouri, B. Gill, J. R. Slauterbeck, R. C. Schutt, E. Dabezies, and B. D. Beynnon. Shallow medial tibial plateau and steep medial and lateral tibial slopes. *The American journal of sports medicine*, 38(1):54–62, 2010b.

B. Haughom, W. Schairer, R. B. Souza, D. Carpenter, C. B. Ma, and X. Li. Abnormal tibiofemoral kinematics following acl reconstruction are associated with early cartilage matrix degeneration measured by mri t1rho. *The Knee*, 19(4):482–487, 2012.

W. Hayes and L. Mockros. Viscoelastic properties of human articular cartilage. *Journal of applied physiology*, 31(4):562–568, 1971.

W. Hayes, L. Keer, G. Herrmann, and L. Mockros. A mathematical analysis for indentation tests of articular cartilage. *Journal of biomechanics*, 5(5):541–551, 1972.

W. C. Hayes and A. Bodine. Flow-independent viscoelastic properties of articular cartilage matrix. *Journal of biomechanics*, 11(8-9):407–419, 1978.

H. B. Henninger, C. J. Underwood, S. J. Romney, G. L. Davis, and J. A. Weiss. Effect of elastin digestion on the quasi-static tensile response of medial collateral ligament. *Journal of Orthopaedic Research*, 31(8):1226–1233, 2013.

H. B. Henninger, W. R. Valdez, S. A. Scott, and J. A. Weiss. Elastin governs the mechanical response of medial collateral ligament under shear and transverse tensile loading. *Acta biomaterialia*, 25:304–312, 2015.

W. Herzog and S. Federico. Considerations on joint and articular cartilage mechanics. *Biomechanics and modeling in mechanobiology*, 5(2):64–81, 2006.

W. Herzog, S. Diet, E. Suter, P. Mayzus, T. Leonard, C. Müller, J. Wu, and M. Epstein. Material and functional properties of articular cartilage and patellofemoral contact mechanics in an experimental model of osteoarthritis. *Journal of Biomechanics*, 31(12): 1137–1145, 1998.

A. Heuijerjans, W. Wilson, K. Ito, and C. van Donkelaar. The critical size of focal articular cartilage defects is associated with strains in the collagen fibers. *Clinical Biomechanics*, 2017.

T. E. Hewett, G. D. Myer, K. R. Ford, R. S. Heidt, A. J. Colosimo, S. G. McLean, A. J. Van den Bogert, M. V. Paterno, and P. Succop. Biomechanical measures of neuromuscular control and valgus loading of the knee predict anterior cruciate ligament injury risk in female athletes a prospective study. *The American Journal of Sports Medicine*, 33(4): 492–501, 2005.

Hibbett, Karlsson, and Sorensen. *ABAQUS: User's Manual*. Hibbitt, Karlsson & Sorensen, Incorporated, 2016.

R. V. Hingorani, P. P. Provenzano, R. S. Lakes, A. Escarcega, and R. Vanderby. Nonlinear viscoelasticity in rabbit medial collateral ligament. *Annals of biomedical engineering*, 32(2):306–312, 2004.

R. S. Hinman, K. A. Bowles, B. B. Metcalf, T. V. Wrigley, and K. L. Bennell. Lateral wedge insoles for medial knee osteoarthritis: effects on lower limb frontal plane biomechanics. *Clinical Biomechanics*, 27(1):27–33, 2012.

S. Hirokawa and R. Tsuruno. Three-dimensional deformation and stress distribution in an analytical/computational model of the anterior cruciate ligament. *Journal of Biomechanics*, 33(9):1069–1077, 2000.

K. Hjelle, E. Solheim, T. Strand, R. Muri, and M. Brittberg. Articular cartilage defects in 1,000 knee arthroscopies. *Arthroscopy: The Journal of Arthroscopic & Related Surgery*, 18(7):730–734, 2002.

M. Holmes and V. Mow. The nonlinear characteristics of soft gels and hydrated connective tissues in ultrafiltration. *Journal of biomechanics*, 23(11):1145–1156, 1990.

G. A. Holzapfel, T. C. Gasser, and R. W. Ogden. A new constitutive framework for arterial wall mechanics and a comparative study of material models. *Journal of elasticity and the physical science of solids*, 61(1-3):1–48, 2000.

G. A. Holzapfel, T. C. Gasser, and M. Stadler. A structural model for the viscoelastic behavior of arterial walls: continuum formulation and finite element analysis. *European Journal of Mechanics-A/Solids*, 21(3):441–463, 2002.

R. Y. Hori and L. Mockros. Indentation tests of human articular cartilage. *Journal of Biomechanics*, 9(4):259–268, 1976.

S. Hosseini, W. Wilson, K. Ito, and C. van Donkelaar. A numerical model to study mechanically induced initiation and progression of damage in articular cartilage. *Osteoarthritis and Cartilage*, 22(1):95–103, 2014.

K. R. Hovinga and A. L. Lerner. Anatomic variations between japanese and caucasian populations in the healthy young adult knee joint. *Journal of Orthopaedic Research*, 27 (9):1191–1196, 2009.

J. G. Howe, C. Wertheimer, R. J. Johnson, C. E. Nichols, M. H. Pope, and B. Beynnon. Arthroscopic strain gauge measurement of the normal anterior cruciate ligament. *Arthroscopy: The Journal of Arthroscopic & Related Surgery*, 6(3):198–204, 1990.

C.-Y. Huang, V. C. Mow, and G. A. Ateshian. The role of flow-independent viscoelasticity in the biphasic tensile and compressive responses of articular cartilage. *Transactions-American Society of Mechanical Engineers Journal of Biomechanical Engineering*, 123 (5):410–417, 2001.

C.-Y. Huang, M. A. Soltz, M. Kopacz, V. C. Mow, G. A. Ateshian, et al. Experimental verification of the roles of intrinsic matrix viscoelasticity and tension-compression nonlinearity in the biphasic response of cartilage. *Transactions-American Society of Mechanical Engineers Journal of Biomechanical Engineering*, 125(1):84–93, 2003.

R. Y. Huang, H. G. Zheng, and Q. Xu. Biomechanical evaluation of different techniques in double bundle anterior cruciate ligament reconstruction using finite element analysis. *Journal of Biomimetics, Biomaterials, and Biomedical Engineering*, 13:55, 2012.

M. Huber, S. Trattnig, and F. Lintner. Anatomy, biochemistry, and physiology of articular cartilage. *Investigative radiology*, 35(10):573–580, 2000.

J. C. Hughston and A. F. Eilers. The role of the posterior oblique ligament in repairs of acute medial (collateral) ligament tears of the knee. *J Bone Joint Surg Am*, 55(5):923–940, 1973.

R. Huiskes, R. Ruimerman, G. H. Van Lenthe, and J. D. Janssen. Effects of mechanical forces on maintenance and adaptation of form in trabecular bone. *Nature*, 405(6787): 704, 2000.

Human Kinetics. Many ligaments make up kneeâĂŹs structure. http://www.humankinetics.com/excerpts/excerpts/many-ligaments-make-up-knees-structure, 2017. Accessed: 2017-10-10.

D. S. Hungerford and M. Barry. Biomechanics of the patellofemoral joint. *Clinical orthopaedics and related research*, 144:9–15, 1979.

E. B. Hunziker, E. Kapfinger, and J. Geiss. The structural architecture of adult mammalian articular cartilage evolves by a synchronized process of tissue resorption and neoformation during postnatal development. *Osteoarthritis and cartilage*, 15(4):403–413, 2007.

A. Hürkamp, M. Tanaka, and M. Kaliske. Complex step derivative approximation of consistent tangent operators for viscoelasticity based on fractional calculus. *Computational Mechanics*, 56(6):1055–1071, 2015.

J. G. Ingram, S. K. Fields, E. E. Yard, and R. D. Comstock. Epidemiology of knee injuries among boys and girls in us high school athletics. *The American Journal of Sports Medicine*, 36(6):1116–1122, 2008.

T. Iwahashi, K. Shino, K. Nakata, H. Otsubo, T. Suzuki, H. Amano, and N. Nakamura. Direct anterior cruciate ligament insertion to the femur assessed by histology and 3-dimensional volume-rendered computed tomography. *Arthroscopy: The Journal of Arthroscopic & Related Surgery*, 26(9):S13–S20, 2010.

D. W. Jackson, E. S. Grood, J. D. Goldstein, M. A. Rosen, P. R. Kurzweil, J. F. Cummings, and T. M. Simon. A comparison of patellar tendon autograft and allograft used for anterior cruciate ligament reconstruction in the goat model. *The American Journal of Sports Medicine*, 21(2):176–185, 1993.

D. W. Jackson, P. A. Lalor, H. M. Aberman, and T. M. Simon. Spontaneous repair of full-thickness defects of articular cartilage in a goat model. *The Journal of Bone & Joint Surgery*, 83(1):53–53, 2001.

R. Jedynak. Approximation of the inverse langevin function revisited. *Rheologica Acta*, 54 (1):29–39, 2015.

H. Jin and J. L. Lewis. Determination of poissonâĂŹs ratio of articular cartilage by indentation using different-sized indenters. *Journal of biomechanical engineering*, 126(2): 138–145, 2004.

G. Johnson, G. Livesay, S. L. Woo, and K. Rajagopal. A single integral finite strain viscoelastic model of ligaments and tendons. *Journal of biomechanical engineering*, 118 (2):221–226, 1996.

B. Jones, C. T. Hung, and G. Ateshian. Biphasic analysis of cartilage stresses in the patellofemoral joint. *The journal of knee surgery*, 2015.

R. Jones, N. Nawana, M. Pearcy, D. Learmonth, D. Bickerstaff, J. Costi, and R. Paterson. Mechanical properties of the human anterior cruciate ligament. *Clinical Biomechanics*, 10(7):339–344, 1995.

K. P. Jordan, A. Jöud, C. Bergknut, P. Croft, J. J. Edwards, G. Peat, I. F. Petersson, A. Turkiewicz, R. Wilkie, and M. Englund. International comparisons of the consultation prevalence of musculoskeletal conditions using population-based healthcare data from england and sweden. *Annals of the rheumatic diseases*, pages annrheumdis–2012, 2013.

P. Julkunen, R. Korhonen, M. Nissi, and J. Jurvelin. Mechanical characterization of articular cartilage by combining magnetic resonance imaging and finite-element analysisâĂŤa

potential functional imaging technique. *Physics in medicine and biology*, 53(9):2425, 2008.

J. Jurvelin, M. Buschmann, and E. Hunziker. Optical and mechanical determination of poisson's ratio of adult bovine humeral articular cartilage. *Journal of biomechanics*, 30 (3):235–241, 1997.

J. Jurvelin, M. Buschmann, and E. Hunziker. Mechanical anisotropy of the human knee articular cartilage in compression. *Proceedings of the Institution of Mechanical Engineers, Part H: Journal of Engineering in Medicine*, 217(3):215–219, 2003.

J. S. Jurvelin, J. P. Arokoski, E. B. Hunziker, and H. J. Helminen. Topographical variation of the elastic properties of articular cartilage in the canine knee. *Journal of biomechanics*, 33(6):669–675, 2000.

A. Kanamori, S. L. Woo, C. B. Ma, J. Zeminski, T. W. Rudy, G. Li, and G. A. Livesay. The forces in the anterior cruciate ligament and knee kinematics during a simulated pivot shift test: a human cadaveric study using robotic technology. *Arthroscopy: The Journal of Arthroscopic & Related Surgery*, 16(6):633–639, 2000.

I. Kang, D. Panneerselvam, V. P. Panoskaltsis, S. J. Eppell, R. E. Marchant, and C. M. Doerschuk. Changes in the hyperelastic properties of endothelial cells induced by tumor necrosis factor-α. *Biophysical journal*, 94(8):3273–3285, 2008.

K.-T. Kang, S.-H. Kim, J. Son, Y. H. Lee, and H.-J. Chun. In vivo evaluation of the subject-specific finite element model for knee joint cartilage contact area. *International Journal of Precision Engineering and Manufacturing*, 16(6):1171–1177, 2015.

P. Kannus. Long-term results of conservatively treated medial collateral ligament injuries of the knee joint. *Clinical orthopaedics and related research*, 226:103–112, 1988.

J. Kastelic, A. Galeski, and E. Baer. The multicomposite structure of tendon. *Connective tissue research*, 6(1):11–23, 1978.

T. M. Keaveny, E. F. Morgan, G. L. Niebur, and O. C. Yeh. Biomechanics of trabecular bone. *Annual review of biomedical engineering*, 3(1):307–333, 2001.

J. C. Kennedy, H. W. Weinberg, and A. S. Wilson. The anatomy and function of the anterior cruciate ligament: as determined by clinical and morphological studies. *JBJS*, 56(2):223–235, 1974.

M. Kessler, H. Behrend, S. Henz, G. Stutz, A. Rukavina, and M. Kuster. Function, osteoarthritis and activity after acl-rupture: 11 years follow-up results of conservative versus reconstructive treatment. *Knee Surgery, Sports Traumatology, Arthroscopy*, 16(5): 442–448, 2008.

A. Kiapour, A. M. Kiapour, V. Kaul, C. E. Quatman, S. C. Wordeman, T. E. Hewett, C. K. Demetropoulos, and V. K. Goel. Finite element model of the knee for investigation of injury mechanisms: development and validation. *Journal of Biomechanical Engineering*, 136(1):011002, 2014a.

A. M. Kiapour, V. Kaul, A. Kiapour, C. E. Quatman, S. C. Wordeman, T. E. Hewett, C. K. Demetropoulos, and V. K. Goel. The effect of ligament modeling technique on knee joint kinematics: a finite element study. *Applied Mathematics*, 4(5A):91, 2014b.

H. Y. Kim, Y.-J. Seo, H.-J. Kim, T. Nguyenn, N. S. Shetty, and Y.-S. Yoo. Tension changes within the bundles of anatomic double-bundle anterior cruciate ligament reconstruction at different knee flexion angles: a study using a 3-dimensional finite element model. *Arthroscopy: The Journal of Arthroscopic & Related Surgery*, 27(10):1400–1408, 2011a.

S. Kim, J. Bosque, J. P. Meehan, A. Jamali, and R. Marder. Increase in outpatient knee arthroscopy in the united states: a comparison of national surveys of ambulatory surgery, 1996 and 2006. *The Journal of Bone and Joint Surgery. American volume*, 93(11):994–1000, 2011b.

P. Kiviranta, E. Lammentausta, J. Töyräs, I. Kiviranta, and J. Jurvelin. Indentation diagnostics of cartilage degeneration. *Osteoarthritis and Cartilage*, 16(7):796–804, 2008.

T. J. Klein, M. Chaudhry, W. C. Bae, and R. L. Sah. Depth-dependent biomechanical and biochemical properties of fetal, newborn, and tissue-engineered articular cartilage. *Journal of biomechanics*, 40(1):182–190, 2007.

O. Klets, M. E. Mononen, P. Tanska, M. T. Nieminen, R. K. Korhonen, and S. Saarakkala. Comparison of different material models of articular cartilage in 3d computational modeling of the knee: Data from the osteoarthritis initiative (oai). *Journal of Biomechanics*, 2016.

E. Kondo, A. M. Merican, K. Yasuda, and A. A. Amis. Biomechanical analysis of knee laxity with isolated anteromedial or posterolateral bundle–deficient anterior cruciate ligament. *Arthroscopy: The Journal of Arthroscopic & Related Surgery*, 30(3):335–343, 2014.

S. Kopf, V. Musahl, S. Tashman, M. Szczodry, W. Shen, and F. H. Fu. A systematic review of the femoral origin and tibial insertion morphology of the acl. *Knee Surgery, Sports Traumatology, Arthroscopy*, 17(3):213–219, 2009.

R. Korhonen, M. Laasanen, J. Töyräs, J. Rieppo, J. Hirvonen, H. Helminen, and J. Jurvelin. Comparison of the equilibrium response of articular cartilage in unconfined compression, confined compression and indentation. *Journal of biomechanics*, 35(7):903–909, 2002a.

R. Korhonen, M. Wong, J. Arokoski, R. Lindgren, H. Helminen, E. Hunziker, and J. Jurvelin. Importance of the superficial tissue layer for the indentation stiffness of articular cartilage. *Medical engineering & physics*, 24(2):99–108, 2002b.

M. Kozanek, A. Hosseini, F. Liu, S. K. Van de Velde, T. J. Gill, H. E. Rubash, and G. Li. Tibiofemoral kinematics and condylar motion during the stance phase of gait. *Journal of biomechanics*, 42(12):1877–1884, 2009.

T. Krosshaug, A. Nakamae, B. P. Boden, L. Engebretsen, G. Smith, J. R. Slauterbeck, T. E. Hewett, and R. Bahr. Mechanisms of anterior cruciate ligament injury in basketball video analysis of 39 cases. *The American Journal of Sports Medicine*, 35(3):359–367, 2007a.

T. Krosshaug, J. R. Slauterbeck, L. Engebretsen, and R. Bahr. Biomechanical analysis of anterior cruciate ligament injury mechanisms: three-dimensional motion reconstruction from video sequences. *Scandinavian journal of medicine & science in sports*, 17(5): 508–519, 2007b.

E. Kuhl, K. Garikipati, E. M. Arruda, and K. Grosh. Remodeling of biological tissue: mechanically induced reorientation of a transversely isotropic chain network. *Journal of the Mechanics and Physics of Solids*, 53(7):1552–1573, 2005.

K. Kühn, D. DâĂŹLima, S. Hashimoto, and M. Lotz. Cell death in cartilage. *Osteoarthritis and Cartilage*, 12(1):1–16, 2004.

M. Kurosaka, S. Yoshiya, J. T. Andrish, et al. A biomechanical comparison of different surgical techniques of graft fixation in anterior cruciate ligament reconstruction. *The American Journal of Sports Medicine*, 15(3):225–229, 1987.

B. Kurz, M. Jin, P. Patwari, D. M. Cheng, M. W. Lark, and A. J. Grodzinsky. Biosynthetic response and mechanical properties of articular cartilage after injurious compression. *Journal of Orthopaedic Research*, 19(6):1140–1146, 2001.

M. K. Kwan, W. M. Lai, and V. C. Mow. A finite deformation theory for cartilage and other soft hydrated connective tissuesâĂŤi. equilibrium results. *Journal of biomechanics*, 23 (2):145–155, 1990.

M. K. Kwan, T. H. Lin, and S. L. Woo. On the viscoelastic properties of the anteromedial bundle of the anterior cruciate ligament. *Journal of biomechanics*, 26(4-5):447–452, 1993.

J. H. Lai and M. E. Levenston. Meniscus and cartilage exhibit distinct intra-tissue strain distributions under unconfined compression. *Osteoarthritis and cartilage*, 18(10):1291–1299, 2010.

W. Lai, V. C. Mow, and V. Roth. Effects of nonlinear strain-dependent permeability and rate of compression on the stress behavior of articular cartilage. *Journal of biomechanical engineering*, 103:61, 1981.

W. M. Lai and V. C. Mow. Drag-induced compression of articular cartilage during a permeation experiment 1. *Biorheology*, 17(1-2):111–123, 1980.

W. M. Lai, J. Hou, and V. C. Mow. A triphasic theory for the swelling and deformation behaviors of articular cartilage. *J Biomech Eng*, 113(3):245–258, 1991.

R. Lakes and R. Vanderby. Interrelation of creep and relaxation: a modeling approach for ligaments. *TRANSACTIONS-AMERICAN SOCIETY OF MECHANICAL ENGINEERS JOURNAL OF BIOMECHANICAL ENGINEERING*, 121(6):612–615, 1999.

J. G. Lane, S. E. Irby, K. Kaufman, C. Rangger, and D. M. Daniel. The anterior cruciate ligament in controlling axial rotation: an evaluation of its effect. *The American journal of sports medicine*, 22(2):289–293, 1994.

J. M. Lane and C. Weiss. Review of articular cartilage collagen research. *Arthritis & Rheumatology*, 18(6):553–562, 1975.

E. Langelier and M. D. Buschmann. Increasing strain and strain rate strengthen transient stiffness but weaken the response to subsequent compression for articular cartilage in unconfined compression. *Journal of biomechanics*, 36(6):853–859, 2003.

Y. Lanir. A structural theory for the homogeneous biaxial stress-strain relationships in flat collagenous tissues. *Journal of biomechanics*, 12(6):423–436, 1979.

Y. Lanir. Constitutive equations for fibrous connective tissues. *Journal of biomechanics*, 16(1):1–12, 1983.

R. F. LaPrade, A. H. Engebretsen, T. V. Ly, S. Johansen, F. A. Wentorf, and L. Engebretsen. The anatomy of the medial part of the knee. *JBJS*, 89(9):2000–2010, 2007.

R. C. Lawrence, D. T. Felson, C. G. Helmick, L. M. Arnold, H. Choi, R. A. Deyo, S. Gabriel, R. Hirsch, M. C. Hochberg, G. G. Hunder, et al. Estimates of the prevalence of arthritis and other rheumatic conditions in the united states: Part ii. *Arthritis & Rheumatism*, 58(1):26–35, 2008.

T. P. Lefkoe, P. G. Trafton, M. G. Ehrlich, W. R. Walsh, D. T. Dennehy, H.-J. Barrach, and E. Akelman. An experimental model of femoral condylar defect leading to osteoarthrosis. *Journal of Orthopaedic Trauma*, 7(5):458–467, 1993.

J. P. Leigh, W. Seavey, and B. Leistikow. Estimating the costs of job related arthritis. *The Journal of rheumatology*, 28(7):1647–1654, 2001.

G. Li, J. Gil, A. Kanamori, and S.-Y. Woo. A validated three-dimensional computational model of a human knee joint. *Journal of Biomechanical Engineering*, 121(6):657–662, 1999a.

G. Li, J. Suggs, and T. Gill. The effect of anterior cruciate ligament injury on knee joint function under a simulated muscle load: a three-dimensional computational simulation. *Annals of Biomedical Engineering*, 30(5):713–720, 2002.

L. Li, J. Soulhat, M. Buschmann, and A. Shirazi-Adl. Nonlinear analysis of cartilage in unconfined ramp compression using a fibril reinforced poroelastic model. *Clinical Biomechanics*, 14(9):673–682, 1999b.

L. Li, M. Buschmann, and A. Shirazi-Adl. A fibril reinforced nonhomogeneous poroelastic model for articular cartilage: inhomogeneous response in unconfined compression. *Journal of biomechanics*, 33(12):1533–1541, 2000.

L. Li, M. Buschmann, and A. Shirazi-Adl. Strain-rate dependent stiffness of articular cartilage in unconfined compression. *Journal of biomechanical engineering*, 125(2): 161–168, 2003.

G. Limbert, M. Taylor, and J. Middleton. Three-dimensional finite element modelling of the human acl: simulation of passive knee flexion with a stressed and stress-free acl. *Journal of Biomechanics*, 37(11):1723–1731, 2004.

D. C. Lin, D. I. Shreiber, E. K. Dimitriadis, and F. Horkay. Spherical indentation of soft matter beyond the hertzian regime: numerical and experimental validation of hyperelastic models. *Biomechanics and modeling in mechanobiology*, 8(5):345, 2009.

B. Linden. Osteochondritis dissecans of the femoral condyles: a long-term follow-up study. *The Journal of Bone & Joint Surgery*, 59(6):769–776, 1977.

T. F. Linsenmayer, E. Gibney, F. Igoe, M. K. Gordon, J. M. Fitch, L. I. Fessler, and D. E. Birk. Type v collagen: molecular structure and fibrillar organization of the chicken alpha 1 (v) nh2-terminal domain, a putative regulator of corneal fibrillogenesis. *The Journal of Cell Biology*, 121(5):1181–1189, 1993.

J. Lipke, C. Janecki, C. Nelson, P. McLeod, C. Thompson, J. Thompson, and D. Haynes. The role of incompetence of the anterior cruciate and lateral ligaments in anterolateral and anteromedial instability. a biomechanical study of cadaver knees. *JBJS*, 63(6):954–960, 1981.

D. B. Lipps, Y. K. Oh, J. A. Ashton-Miller, and E. M. Wojtys. Morphologic characteristics help explain the gender difference in peak anterior cruciate ligament strain during a simulated pivot landing. *The American Journal of Sports Medicine*, 40(1):32–40, 2012.

D. B. Lipps, E. M. Wojtys, and J. A. Ashton-Miller. Anterior cruciate ligament fatigue failures in knees subjected to repeated simulated pivot landings. *The American journal of sports medicine*, 41(5):1058–1066, 2013.

F. Liu, M. Kozanek, A. Hosseini, S. K. Van de Velde, T. J. Gill, H. E. Rubash, and G. Li. In vivo tibiofemoral cartilage deformation during the stance phase of gait. *Journal of biomechanics*, 43(4):658–665, 2010a.

F. Liu, B. Yue, H. R. Gadikota, M. Kozanek, W. Liu, T. J. Gill, H. E. Rubash, and G. Li. Morphology of the medial collateral ligament of the knee. *Journal of orthopaedic surgery and research*, 5(1):69, 2010b.

H. Liu and W. Sun. Computational efficiency of numerical approximations of tangent moduli for finite element implementation of a fiber-reinforced hyperelastic material model. *Computer methods in biomechanics and biomedical engineering*, pages 1–10, 2015.

S. H. Liu, R.-S. Yang, R. Al-Shaikh, and J. M. Lane. Collagen in tendon, ligament, and bone healing: A current review. *Clinical orthopaedics and related research*, 318:265–278, 1995.

Y. Liu, V. Birman, C. Chen, S. Thomopoulos, and G. M. Genin. Mechanisms of bimaterial attachment at the interface of tendon to bone. *Journal of engineering materials and technology*, 133(1):011006, 2011.

Y. Liu, S. Thomopoulos, C. Chen, V. Birman, M. J. Buehler, and G. M. Genin. Modelling the mechanics of partially mineralized collagen fibrils, fibres and tissue. *Journal of The Royal Society Interface*, 11(92):20130835, 2014.

M. K. Liukkonen, M. E. Mononen, O. Klets, J. P. Arokoski, S. Saarakkala, and R. K. Korhonen. Simulation of subject-specific progression of knee osteoarthritis and comparison to experimental follow-up data: Data from the osteoarthritis initiative. *Scientific Reports*, 7, 2017.

J. C. Loh, Y. Fukuda, E. Tsuda, R. J. Steadman, F. H. Fu, and S. L. Woo. Knee stability and graft function following anterior cruciate ligament reconstruction: Comparison between 11 o'clock and 10 o'clock femoral tunnel placement. *Arthroscopy: The Journal of Arthroscopic & Related Surgery*, 19(3):297–304, 2003.

L. Lohmander, A. Östenberg, M. Englund, and H. Roos. High prevalence of knee osteoarthritis, pain, and functional limitations in female soccer players twelve years after anterior cruciate ligament injury. *Arthritis & Rheumatism*, 50(10):3145–3152, 2004.

L. S. Lohmander, P. M. Englund, L. L. Dahl, and E. M. Roos. The long-term consequence of anterior cruciate ligament and meniscus injuries. *The American journal of sports medicine*, 35(10):1756–1769, 2007.

X. L. Lu and V. C. Mow. Biomechanics of articular cartilage and determination of material properties. *Medicine & Science in Sports & Exercise*, 40(2):193–199, 2008.

J. W. Luites, A. B. Wymenga, L. Blankevoort, and J. G. Kooloos. Description of the attachment geometry of the anteromedial and posterolateral bundles of the acl from arthroscopic perspective for anatomical tunnel placement. *Knee Surgery, Sports Traumatology, Arthroscopy*, 15(12):1422–1431, 2007.

T. J. Lujan, C. J. Underwood, H. B. Henninger, B. M. Thompson, and J. A. Weiss. Effect of dermatan sulfate glycosaminoglycans on the quasi-static material properties of the human medial collateral ligament. *Journal of orthopaedic research*, 25(7):894–903, 2007.

J. Lyness. Differentiation formulas for analytic functions. *Mathematics of Computation*, pages 352–362, 1968.

R. M. Lyon, W. H. Akeson, D. Amiel, L. R. Kitabayashi, and L.-Y. Savio. Ultrastructural differences between the cells of the medial collateral and the anterior cruciate ligaments. *Clinical orthopaedics and related research*, 272:279–286, 1991.

J. Ma and E. M. Arruda. A micromechanical viscoelastic constitutive model for native and engineered anterior cruciate ligaments. In *Computer Models in Biomechanics*, pages 351–363. Springer, 2013.

J. Ma, H. Narayanan, K. Garikipati, K. Grosh, and E. Arruda. Experimental and computational investigation of viscoelasticity of native and engineered ligament and tendon. In *IUTAM Symposium on Cellular, Molecular and Tissue Mechanics*, pages 3–17. Springer, 2010.

S. A. Maas, A. Erdemir, J. P. Halloran, and J. A. Weiss. A general framework for application of prestrain to computational models of biological materials. *journal of the mechanical behavior of biomedical materials*, 61:499–510, 2016.

C. Machiraju, A.-V. Phan, A. Pearsall, and S. Madanagopal. Viscoelastic studies of human subscapularis tendon: relaxation test and a wiechert model. *Computer methods and programs in biomedicine*, 83(1):29–33, 2006.

F. MacKintosh, J. Käs, and P. Janmey. Elasticity of semiflexible biopolymer networks. *Physical review letters*, 75(24):4425, 1995.

R. A. Magnussen, W. R. Dunn, J. L. Carey, and K. P. Spindler. Treatment of focal articular cartilage defects in the knee. *Clinical orthopaedics and related research*, 466(4):952–962, 2008.

N. R. Maiden and R. W. Byard. Unpredictable tensile strength biomechanics may limit thawed cadaver use for simulant research. *Australian Journal of Forensic Sciences*, 48 (1):54–58, 2016.

M. Majewski, H. Susanne, and S. Klaus. Epidemiology of athletic knee injuries: A 10-year study. *The knee*, 13(3):184–188, 2006.

A. Mak. The apparent viscoelastic behavior of articular cartilageâĂŤthe contributions from the intrinsic matrix viscoelasticity and interstitial fluid flows. *Journal of biomechanical engineering*, 108(2):123–130, 1986a.

A. Mak, W. Lai, and V. Mow. Biphasic indentation of articular cartilageâĂŤi. theoretical analysis. *Journal of biomechanics*, 20(7):703–714, 1987.

A. F. Mak. Unconfined compression of hydrated viscoelastic tissues: a biphasic poroviscoelastic analysis. *Biorheology*, 23(4):371–383, 1986b.

K. F. Mallett and E. M. Arruda. Digital image correlation-aided mechanical characterization of the anteromedial and posterolateral bundles of the anterior cruciate ligament. *Acta Biomaterialia*, 2017.

M. R. Maly. Abnormal and cumulative loading in knee osteoarthritis. *Current opinion in rheumatology*, 20(5):547–552, 2008.

K. Manda, L. Ryd, and A. Eriksson. Finite element simulations of a focal knee resurfacing implant applied to localized cartilage defects in a sheep model. *Journal of Biomechanics*, 44(5):794–801, 2011.

H. J. Mankin. The reaction of articular cartilage to injury and osteoarthritis. *New England Journal of Medicine*, 291(24):1285–1292, 1974.

H. B. Mann and D. R. Whitney. On a test of whether one of two random variables is stochastically larger than the other. *The annals of mathematical statistics*, pages 50–60, 1947.

R. A. Mann and J. Hagy. Biomechanics of walking, running, and sprinting. *The American journal of sports medicine*, 8(5):345–350, 1980.

B. C. Marchi and E. M. Arruda. An error-minimizing approach to inverse langevin approximations. *Rheologica Acta*, 54(11-12):887–902, 2015.

B. C. Marchi and E. M. Arruda. A study on the role of articular cartilage soft tissue constitutive form in models of whole knee biomechanics. *Biomechanics and Modeling in Mechanobiology*, 16(1):117–138, 2017a.

B. C. Marchi and E. M. Arruda. Stability in computational knee models driven by physiologically and anatomically representative ligaments. *In Review*, 2017b.

B. C. Marchi, E. M. Arruda, and R. M. Coleman. The effect of articular cartilage focal defect size and location in whole knee biomechanics models. *In Review*, 2017a.

B. C. Marchi, C. M. Luetkemeyer, and E. M. Arruda. Evaluating continuum level descriptions of the medial collateral ligament. *In Review*, 2017b.

R. A. Marder, J. R. Raskind, and M. Carroll. Prospective evaluation of arthroscopically assisted anterior cruciate ligament reconstruction: patellar tendon versus semitendinosus and gracilis tendons. *The American journal of sports medicine*, 19(5):478–484, 1991.

K. L. Markolf, J. Mensch, and H. Amstutz. Stiffness and laxity of the knee–the contributions of the supporting structures. a quantitative in vitro study. *The Journal of Bone & Joint Surgery*, 58(5):583–594, 1976.

K. L. Markolf, J. R. Zemanovic, and D. R. McAllister. Cyclic loading of posterior cruciate ligament replacements fixed with tibial tunnel and tibial inlay methods. *JBJS*, 84(4): 518–524, 2002.

H. Marouane, A. Shirazi-Adl, M. Adouni, and J. Hashemi. Steeper posterior tibial slope markedly increases acl force in both active gait and passive knee joint under compression. *Journal of Biomechanics*, 47(6):1353–1359, 2014.

F. J. Massey Jr. The kolmogorov-smirnov test for goodness of fit. *Journal of the American statistical Association*, 46(253):68–78, 1951.

K. Matsuki, K. O. Matsuki, T. Kenmoku, S. Yamaguchi, T. Sasho, and S. A. Banks. In vivo kinematics of early-stage osteoarthritic knees during pivot and squat activities. *Gait & Posture*, 58:214–219, 2017.

Y. Matsusue, T. Yamamuro, and H. Hama. Arthroscopic multiple osteochondral transplantation to the chondral defect in the knee associated with anterior cruciate ligament disruption. *Arthroscopy: The Journal of Arthroscopic & Related Surgery*, 9(3):318–321, 1993.

S. G. McLean, Y. K. Oh, M. L. Palmer, S. M. Lucey, D. G. Lucarelli, J. A. Ashton-Miller, and E. M. Wojtys. The relationship between anterior tibial acceleration, tibial slope, and acl strain during a simulated jump landing task. *The Journal of Bone & Joint Surgery*, 93(14):1310–1317, 2011.

S. G. McLean, K. F. Mallett, and E. M. Arruda. Deconstructing the anterior cruciate ligament: What we know and do not know about function, material properties, and injury mechanics. *Journal of Biomechanical Engineering*, 137(2):020906, 2015.

G. Meachim, D. Denham, I. Emery, and P. Wilkinson. Collagen alignments and artificial splits at the surface of human articular cartilage. *Journal of anatomy*, 118(Pt 1):101, 1974.

B. R. Meister, S. P. Michael, R. A. Moyer, J. D. Kelly, and C. D. Schneck. Anatomy and kinematics of the lateral collateral ligament of the knee. *The American journal of sports medicine*, 28(6):869–878, 2000.

W. Mesfar and A. Shirazi-Adl. Biomechanics of the knee joint in flexion under various quadriceps forces. *The Knee*, 12(6):424–434, 2005.

E. G. Meyer and R. C. Haut. Anterior cruciate ligament injury induced by internal tibial torsion or tibiofemoral compression. *Journal of Biomechanics*, 41(16):3377–3383, 2008.

E. G. Meyer, T. G. Baumer, J. M. Slade, W. E. Smith, and R. C. Haut. Tibiofemoral contact pressures and osteochondral microtrauma during anterior cruciate ligament rupture due to excessive compressive loading and internal torque of the human knee. *The American journal of sports medicine*, 36(10):1966–1977, 2008.

C. Miehe. Numerical computation of algorithmic (consistent) tangent moduli in large-strain computational inelasticity. *Computer methods in applied mechanics and engineering*, 134(3):223–240, 1996.

G. J. Miller and E. F. Morgan. Use of microindentation to characterize the mechanical properties of articular cartilage: comparison of biphasic material properties across length scales. *Osteoarthritis and cartilage*, 18(8):1051–1057, 2010.

R. Minns and F. Steven. The collagen fibril organization in human articular cartilage. *Journal of anatomy*, 123(Pt 2):437, 1977.

K. Miyasaka, D. Daniel, M. Stone, and P. Hirshman. The incidence of knee ligament injuries in the general population. *Am J Knee Surg*, 1:43–48, 1991.

J. Mizrahi, A. Maroudas, Y. Lanir, I. Ziv, and T. Webber. The "instantaneous" deformation of cartilage: effects of collagen fiber orientation and osmotic stress. *Biorheology*, 23(4): 311–330, 1986.

K. L. Moffat, W.-H. S. Sun, P. E. Pena, N. O. Chahine, S. B. Doty, G. A. Ateshian, C. T. Hung, and H. H. Lu. Characterization of the structure–function relationship at the ligament-to-bone interface. *Proceedings of the National Academy of Sciences*, 105 (23):7947–7952, 2008.

A. B. Moghaddam and A. Torkaman. A cadaver study of the structures and positions of the anterior cruciate ligament in humans. *International journal of preventive medicine*, 4(Suppl 1):S85, 2013.

M. Mononen, M. Mikkola, P. Julkunen, R. Ojala, M. Nieminen, J. Jurvelin, and R. Korhonen. Effect of superficial collagen patterns and fibrillation of femoral articular cartilage on knee joint mechanicsâĂŤa 3d finite element analysis. *Journal of Biomechanics*, 45 (3):579–587, 2012.

M. E. Mononen, J. S. Jurvelin, and R. K. Korhonen. Implementation of a gait cycle loading into healthy and meniscectomised knee joint models with fibril-reinforced articular cartilage. *Computer methods in biomechanics and biomedical engineering*, 18(2):141–152, 2015.

M. E. Mononen, P. Tanska, H. Isaksson, and R. K. Korhonen. A novel method to simulate the progression of collagen degeneration of cartilage in the knee: Data from the osteoarthritis initiative. *Scientific reports*, 6, 2016.

R. Mootanah, C. Imhauser, F. Reisse, D. Carpanen, R. Walker, M. Koff, M. Lenhoff, S. Rozbruch, A. Fragomen, Z. Dewan, et al. Development and validation of a computational model of the knee joint for the evaluation of surgical treatments for osteoarthritis. *Computer Methods in Biomechanics and Biomedical Engineering*, 17(13):1502–1517, 2014.

J. Morrison. The mechanics of the knee joint in relation to normal walking. *Journal of biomechanics*, 3(1):51–61, 1970.

T. J. Mosher and B. J. Dardzinski. Cartilage mri t2 relaxation time mapping: overview and applications. In *Seminars in musculoskeletal radiology*, volume 8, pages 355–368. Copyright© 2004 by Thieme Medical Publishers, Inc., 333 Seventh Avenue, New York, NY 10001 USA., 2004.

P. R. Moshtagh, B. Pouran, N. M. Korthagen, A. A. Zadpoor, and H. Weinans. Guidelines for an optimized indentation protocol for measurement of cartilage stiffness: The effects of spatial variation and indentation parameters. *Journal of biomechanics*, 49(14):3602–3607, 2016.

M. Motavalli, O. Akkus, and J. M. Mansour. Depth-dependent shear behavior of bovine articular cartilage: relationship to structure. *Journal of anatomy*, 225(5):519–526, 2014.

S. G. Moulton, B. D. Steineman, T. L. H. Donahue, C. A. Fontboté, T. R. Cram, and R. F. LaPrade. Direct versus indirect acl femoral attachment fibres and their implications on acl graft placement. *Knee Surgery, Sports Traumatology, Arthroscopy*, 25(1):165–171, 2017.

V. Mow and M. Rosenwasser. Articular cartilage: biomechanics. *Injury and Repair of the Musculoskeletal Soft Tissues*, 1:427–463, 1988.

V. Mow, L. Setton, F. Guilak, and A. Ratcliffe. Mechanical factors in articular cartilage and their role in osteoarthritis. *Osteoarthritic disorders*, pages 147–171, 1995.

V. C. Mow and X. E. Guo. Mechano-electrochemical properties of articular cartilage: their inhomogeneities and anisotropies. *Annual Review of Biomedical Engineering*, 4(1):175–209, 2002.

V. C. Mow and J. M. Mansour. The nonlinear interaction between cartilage deformation and interstitial fluid flow. *Journal of Biomechanics*, 10(1):31–39, 1977.

V. C. Mow, S. Kuei, W. M. Lai, C. G. Armstrong, et al. Biphasic creep and stress relaxation of articular cartilage in compression: theory and experiments. *J Biomech Eng*, 102(1): 73–84, 1980.

V. C. Mow, M. H. Holmes, and W. M. Lai. Fluid transport and mechanical properties of articular cartilage: a review. *Journal of Biomechanics*, 17(5):377–394, 1984.

V. C. Mow, M. Gibbs, W. M. Lai, W. Zhu, and K. A. Athanasiou. Biphasic indentation of articular cartilageâĂŤii. a numerical algorithm and an experimental study. *Journal of biomechanics*, 22(8-9):853–861, 1989.

V. C. Mow, G. A. Ateshian, and R. L. Spilker. Biomechanics of diarthrodial joints: a review of twenty years of progress. *Journal of biomechanical engineering*, 115(4B):460–467, 1993.

H. Muir. The chemistry of the ground substance of joint cartilage. *The joints and synovial fluid*, 2:27–94, 1980.

G. A. Murrell, S. Maddali, L. Horovitz, S. P. Oakley, and R. F. Warren. The effects of time course after anterior cruciate ligament injury in correlation with meniscal and cartilage loss. *The American Journal of Sports Medicine*, 29(1):9–14, 2001.

C. Neu, M. Hull, and J. Walton. Heterogeneous three-dimensional strain fields during unconfined cyclic compression in bovine articular cartilage explants. *Journal of orthopaedic research*, 23(6):1390–1398, 2005.

W. J. Newman, R. E. Debski, S. M. Moore, and J. A. Weiss. Development of a finite element model of the inferior glenohumeral ligament of the glenohumeral joint. In *ASME 2003 International Mechanical Engineering Congress and Exposition*, pages 243–244. American Society of Mechanical Engineers, 2003.

S. Nielsen, O. Rasmussen, J. Ovesen, and K. Andersen. Rotatory instability of cadaver knees after transection of collateral ligaments and capsule. *Archives of orthopaedic and traumatic surgery*, 103(3):165–169, 1984.

C. Niyibizi, C. S. Visconti, G. Gibson, and K. Kavalkovich. Identification and immunolocalization of type x collagen at the ligament–bone interface. *Biochemical and biophysical research communications*, 222(2):584–589, 1996.

C. Niyibizi, K. Kavalkovich, T. Yamaji, and S. L. Woo. Type v collagen is increased during rabbit medial collateral ligament healing. *Knee Surgery, Sports Traumatology, Arthroscopy*, 8(5):281–285, 2000.

D. Nolan and J. McGarry. On the compressibility of arterial tissue. *Annals of biomedical engineering*, pages 1–15, 2015.

D. Nolan, A. Gower, M. Destrade, R. Ogden, and J. McGarry. A robust anisotropic hyperelastic formulation for the modelling of soft tissue. *Journal of the mechanical behavior of biomedical materials*, 39:48–60, 2014.

F. R. Noyes and E. S. Grood. The strength of the anterior cruciate ligament in humans and rhesus monkeys. *The Journal of Bone & Joint Surgery*, 58(8):1074–1082, 1976.

F. R. Noyes, J. L. DeLucas, and P. J. Torvik. Biomechanics of anterior cruciate ligament failure: An analysis of. *J. Bone Joint Surg. Am*, 56:236–253, 1974.

F. R. Noyes, O. D. Schipplein, T. P. Andriacchi, S. R. Saddemi, and M. Weise. The anterior cruciate ligament-deficient knee with varus alignment an analysis of gait adaptations and dynamic joint loadings. *The American journal of sports medicine*, 20(6):707–716, 1992.

F. R. Noyes, L. E. Huser, and M. S. Levy. Rotational knee instability in acl-deficient knees: role of the anterolateral ligament and iliotibial band as defined by tibiofemoral compartment translations and rotations. *JBJS*, 99(4):305–314, 2017.

M. A. Oberlander, R. M. Shalvoy, and J. C. Hughston. The accuracy of the clinical knee examination documented by arthroscopy: a prospective study. *The American journal of sports medicine*, 21(6):773–778, 1993.

M. Odensten and J. Gillquist. Functional anatomy of the anterior cruciate ligament and a rationale for reconstruction. *JBJS*, 67(2):257–262, 1985.

Y. K. Oh, J. L. Kreinbrink, J. A. Ashton-Miller, and E. M. Wojtys. Effect of acl transection on internal tibial rotation in an in vitro simulated pivot landing. *J Bone Joint Surg Am*, 93(4):372–380, 2011.

Y. K. Oh, D. B. Lipps, J. A. Ashton-Miller, and E. M. Wojtys. What strains the anterior cruciate ligament during a pivot landing? *The American Journal of Sports Medicine*, 40 (3):574–583, 2012.

A. Oloyede, R. Flachsmann, and N. D. Broom. The dramatic influence of loading velocity on the compressive response of articular cartilage. *Connective Tissue Research*, 27(4): 211–224, 1992.

O.-E. Olsen, G. Myklebust, L. Engebretsen, and R. Bahr. Injury mechanisms for anterior cruciate ligament injuries in team handball a systematic video analysis. *The American journal of sports medicine*, 32(4):1002–1012, 2004.

A. D. Orsi, S. Chakravarthy, P. K. Canavan, E. Peña, R. Goebel, A. Vaziri, and H. Nayeb-Hashemi. The effects of knee joint kinematics on anterior cruciate ligament injury and articular cartilage damage. *Computer methods in biomechanics and biomedical engineering*, pages 1–14, 2015.

V. Ottani, M. Raspanti, and A. Ruggeri. Collagen structure and functional implications. *Micron*, 32(3):251–260, 2001.

J. S. Palmer and M. C. Boyce. Constitutive modeling of the stress–strain behavior of f-actin filament networks. *Acta Biomaterialia*, 4(3):597–612, 2008.

G. Pande, D. Owen, and O. Zienkiewicz. Overlay models in time-dependent non-linear material analysis. *Computers & Structures*, 7(3):435–443, 1977.

G. Papaioannou, C. K. Demetropoulos, and Y. H. King. Predicting the effects of knee focal articular surface injury with a patient-specific finite element model. *The Knee*, 17(1): 61–68, 2010.

R. Papannagari, T. J. Gill, L. E. DeFrate, J. M. Moses, A. J. Petruska, and G. Li. In vivo kinematics of the knee after anterior cruciate ligament reconstruction. *The American journal of sports medicine*, 34(12):2006–2012, 2006.

S. Park and G. A. Ateshian. Dynamic response of immature bovine articular cartilage in tension and compression, and nonlinear viscoelastic modeling of the tensile response. *Journal of biomechanical engineering*, 128(4):623–630, 2006.

N. K. Paschos, D. Gartzonikas, N.-M. Barkoula, C. Moraiti, A. Paipetis, T. E. Matikas, and A. D. Georgoulis. Cadaveric study of anterior cruciate ligament failure patterns under uniaxial tension along the ligament. *Arthroscopy: The Journal of Arthroscopic & Related Surgery*, 26(7):957–967, 2010.

G. Peat, R. McCarney, and P. Croft. Knee pain and osteoarthritis in older adults: a review of community burden and current use of primary health care. *Annals of the rheumatic diseases*, 60(2):91–97, 2001.

R. R. Pelker, G. E. Friedlaender, T. C. Markham, M. M. Panjabi, and C. J. Moen. Effects of freezing and freeze-drying on the biomechanical properties of rat bone. *Journal of Orthopaedic Research*, 1(4):405–411, 1983.

E. Peña, B. Calvo, M. Martinez, D. Palanca, and M. Doblaré. Finite element analysis of the effect of meniscal tears and meniscectomies on human knee biomechanics. *Clinical Biomechanics*, 20(5):498–507, 2005a.

E. Peña, M. Martinez, B. Calvo, D. Palanca, and M. Doblaré. A finite element simulation of the effect of graft stiffness and graft tensioning in acl reconstruction. *Clinical Biomechanics*, 20(6):636–644, 2005b.

E. Peña, B. Calvo, M. Martinez, and M. Doblaré. A three-dimensional finite element analysis of the combined behavior of ligaments and menisci in the healthy human knee joint. *Journal of Biomechanics*, 39(9):1686–1701, 2006a.

E. Peña, B. Calvo, M. Martinez, D. Palanca, and M. Doblaré. Influence of the tunnel angle in acl reconstructions on the biomechanics of the knee joint. *Clinical Biomechanics*, 21 (5):508–516, 2006b.

E. Peña, B. Calvo, M. A. Martínez, and M. Doblaré. Effect of the size and location of osteochondral defects in degenerative arthritis. a finite element simulation. *Computers in Biology and Medicine*, 37(3):376–387, 2007.

J. Penrose, G. Holt, M. Beaugonin, and D. Hose. Development of an accurate three-dimensional finite element knee model. *Computer Methods in Biomechanics & Biomedical Engineering*, 5(4):291–300, 2002.

A. E. Peters, E. J. Comerford, S. Macaulay, K. T. Bates, and R. Akhtar. Micromechanical properties of canine femoral articular cartilage following multiple freeze-thaw cycles. *Journal of the mechanical behavior of biomedical materials*, 71:114–121, 2017.

W. Petersen and B. Tillmann. Structure and vascularization of the cruciate ligaments of the human knee joint. *Anatomy and embryology*, 200(3):325–334, 1999.

W. Petersen and B. Tillmann. Anatomy and function of the anterior cruciate ligament. *Der Orthopade*, 31(8):710–718, 2002.

W. Petersen and T. Zantop. Anatomy of the anterior cruciate ligament with regard to its two bundles. *Clinical orthopaedics and related research*, 454:35–47, 2007.

I. F. Petersson and L. T. Jacobsson. Osteoarthritis of the peripheral joints. *Best Practice & Research Clinical Rheumatology*, 16(5):741–760, 2002.

M. A. Pflum, K. B. Shelburne, M. R. Torry, M. J. Decker, and M. G. Pandy. Model prediction of anterior cruciate ligament force during drop-landings. *Medicine and science in sports and exercise*, 36(11):1949–1958, 2004.

D. P. Pioletti, L. Rakotomanana, J.-F. Benvenuti, and P.-F. Leyvraz. Viscoelastic constitutive law in large deformations: application to human knee ligaments and tendons. *Journal of biomechanics*, 31(8):753–757, 1998.

D. P. Pioletti, L. R. Rakotomanana, and P.-F. Leyvraz. Strain rate effect on the mechanical behavior of the anterior cruciate ligament–bone complex. *Medical Engineering & Physics*, 21(2):95–100, 1999.

R. Piziali, J. Rastegar, D. Nagel, and D. Schurman. The contribution of the cruciate ligaments to the load-displacement characteristics of the human knee joint. *Journal of biomechanical engineering*, 102(4):277–283, 1980a.

R. L. Piziali, W. P. Seering, D. A. Nagel, and D. J. Schurman. The function of the primary ligaments of the knee in anterior-posterior and medial-lateral motions. *Journal of Biomechanics*, 13(9):777–784, 1980b.

C. A. Poole. Articular cartilage chondrons: form, function and failure. *The Journal of Anatomy*, 191(1):1–13, 1997.

C. M. Powers. The influence of abnormal hip mechanics on knee injury: a biomechanical perspective. *journal of orthopaedic & sports physical therapy*, 40(2):42–51, 2010.

P. Provenzano, R. Lakes, T. Keenan, et al. Nonlinear ligament viscoelasticity. *Annals of biomedical engineering*, 29(10):908–914, 2001.

P. P. Provenzano and R. Vanderby. Collagen fibril morphology and organization: implications for force transmission in ligament and tendon. *Matrix Biology*, 25(2):71–84, 2006.

S.-h. Qian, S.-r. Ge, and Q.-l. Wang. The frictional coefficient of bovine knee articular cartilage. *Journal of Bionic Engineering*, 3(2):79–85, 2006.

K. Quapp and J. Weiss. Material characterization of human medial collateral ligament. *Journal of Biomechanical Engineering*, 120(6):757–763, 1998.

C. E. Quatman, A. Kiapour, G. D. Myer, K. R. Ford, C. K. Demetropoulos, V. K. Goel, and T. E. Hewett. Cartilage pressure distributions provide a footprint to define female anterior cruciate ligament injury mechanisms. *The American Journal of Sports Medicine*, 39(8):1706–1713, 2011.

K. P. Quinn and B. A. Winkelstein. Preconditioning is correlated with altered collagen fiber alignment in ligament. *Journal of biomechanical engineering*, 133(6):064506, 2011.

T. Quinn, R. Allen, B. Schalet, P. Perumbuli, and E. Hunziker. Matrix and cell injury due to sub-impact loading of adult bovine articular cartilage explants: effects of strain rate and peak stress. *Journal of orthopaedic research*, 19(2):242–249, 2001.

A. Race and A. A. Amis. The mechanical properties of the two bundles of the human posterior cruciate ligament. *Journal of biomechanics*, 27(1):13–24, 1994.

R. M. Radasch. Biomechanics of bone and fractures. *Veterinary Clinics of North America: Small Animal Practice*, 29(5):1045–1082, 1999.

E. L. Radin and R. M. Rose. Role of subchondral bone in the initiation and progression of cartilage damage. *Clinical orthopaedics and related research*, 213:34–40, 1986.

N. Ramaniraka, P. Saunier, O. Siegrist, and D. P. Pioletti. Biomechanical evaluation of intra-articular and extra-articular procedures in anterior cruciate ligament reconstruction: a finite element analysis. *Clinical Biomechanics*, 22(3):336–343, 2007.

G. Raumann. The anisotropy of the shear moduli of drawn polyethylene. *Proceedings of the Physical Society*, 79(6):1221, 1962.

M. Recht, J. Kramer, S. Marcelis, M. Pathria, D. Trudell, P. Haghighi, D. Sartoris, and D. Resnick. Abnormalities of articular cartilage in the knee: analysis of available mr techniques. *Radiology*, 187(2):473–478, 1993.

J. D. Reuben, J. S. Rovick, R. J. Schrager, P. S. Walker, and A. L. Boland. Three-dimensional dynamic motion analysis of the anterior cruciate ligament deficient knee joint. *The American journal of sports medicine*, 17(4):463–471, 1989.

F. Richard, M. Villars, and S. Thibaud. Viscoelastic modeling and quantitative experimental characterization of normal and osteoarthritic human articular cartilage using indentation. *Journal of the mechanical behavior of biomedical materials*, 24:41–52, 2013.

J. Rieppo, J. Töyräs, M. T. Nieminen, V. Kovanen, M. M. Hyttinen, R. K. Korhonen, J. S. Jurvelin, and H. J. Helminen. Structure-function relationships in enzymatically modified articular cartilage. *Cells Tissues Organs*, 175(3):121–132, 2003.

D. L. Robinson, M. E. Kersh, N. C. Walsh, D. C. Ackland, R. N. de Steiger, and M. G. Pandy. Mechanical properties of normal and osteoarthritic human articular cartilage. *Journal of the mechanical behavior of biomedical materials*, 61:96–109, 2016.

H. Roesler. The history of some fundamental concepts in bone biomechanics. *Journal of biomechanics*, 20(11-12):1025–1034, 1987.

A. Ronkainen, J. Fick, W. Herzog, and R. Korhonen. Site-specific cell-tissue interactions in rabbit knee joint articular cartilage. *Journal of Biomechanics*, 49(13):2882–2890, 2016.

S. Saarakkala, P. Julkunen, P. Kiviranta, J. Mäkitalo, J. Jurvelin, and R. Korhonen. Depth-wise progression of osteoarthritis in human articular cartilage: investigation of composition, structure and biomechanics. *Osteoarthritis and Cartilage*, 18(1):73–81, 2010.

M. Sakamoto, G. Li, T. Hara, and E. Y. Chao. A new method for theoretical analysis of static indentation test. *Journal of biomechanics*, 29(5):679–685, 1996.

M. Sakane, R. J. Fox, S. L.-Y. W. Glen, A. Livesay, G. Li, and F. H. Fu. In situ forces in the anterior cruciate ligament and its bundles in response to anterior tibial loads. *Journal of Orthopaedic Research*, 15(2):285–293, 1997.

G. J. Salem, R. Salinas, and F. V. Harding. Bilateral kinematic and kinetic analysis of the squat exercise after anterior cruciate ligament reconstruction. *Archives of physical medicine and rehabilitation*, 84(8):1211–1216, 2003.

L. J. Salmon, V. J. Russell, K. Refshauge, D. Kader, C. Connolly, J. Linklater, and L. A. Pinczewski. Long-term outcome of endoscopic anterior cruciate ligament reconstruction with patellar tendon autograft. *The American journal of sports medicine*, 34(5):721–732, 2006.

R. Sanjeevi. A viscoelastic model for the mechanical properties of biological materials. *Journal of biomechanics*, 15(2):107–109, 1982.

R. M. Schinagl, D. Gurskis, A. C. Chen, and R. L. Sah. Depth-dependent confined compression modulus of full-thickness bovine articular cartilage. *Journal of Orthopaedic Research*, 15(4):499–506, 1997.

A. G. Schwartz, J. D. Pasteris, G. M. Genin, T. L. Daulton, and S. Thomopoulos. Mineral distributions at the developing tendon enthesis. *PloS one*, 7(11):e48630, 2012.

M. Schwartz, P. Leo, and J. Lewis. A microstructural model for the elastic response of articular cartilage. *Journal of biomechanics*, 27(7):865–873, 1994.

H. R. Screen. Hierarchical approaches to understanding tendon mechanics. *Journal of Biomechanical Science and Engineering*, 4(4):481–499, 2009.

T. A. S. Selmi, D. Fithian, and P. Neyret. The evolution of osteoarthritis in 103 patients with acl reconstruction at 17 years follow-up. *The Knee*, 13(5):353–358, 2006.

L. Setton, V. Mow, F. Müller, J. Pita, and D. Howell. Mechanical properties of canine articular cartilage are significantly altered following transection of the anterior cruciate ligament. *Journal of Orthopaedic Research*, 12(4):451–463, 1994.

L. A. Setton, D. M. Elliott, and V. C. Mow. Altered mechanics of cartilage with osteoarthritis: human osteoarthritis and an experimental model of joint degeneration. *Osteoarthritis and Cartilage*, 7(1):2–14, 1999.

L. Sharma, J. Song, D. T. Felson, E. Shamiyeh, and D. D. Dunlop. The role of knee alignment in disease progression and functional decline in knee osteoarthritis. *Jama*, 286(2):188–195, 2001.

K. D. Shelbourne and P. Nitz. Accelerated rehabilitation after anterior cruciate ligament reconstruction. *The American journal of sports medicine*, 18(3):292–299, 1990.

K. D. Shelbourne, T. E. Klootwyk, J. H. Wilckens, and M. S. De Carlo. Ligament stability two to six years after anterior cruciate ligament reconstruction with autogenous patellar tendon graft and participation in accelerated rehabilitation program. *The American journal of sports medicine*, 23(5):575–579, 1995.

K. D. Shelbourne, T. Gray, and M. Haro. Incidence of subsequent injury to either knee within 5 years after anterior cruciate ligament reconstruction with patellar tendon autograft. *The American journal of sports medicine*, 37(2):246–251, 2009.

K. B. Shelburne, M. R. Torry, and M. G. Pandy. Muscle, ligament, and joint-contact forces at the knee during walking. *Medicine and Science in Sports and Exercise*, 37(11):1948, 2005.

K. B. Shelburne, M. R. Torry, and M. G. Pandy. Contributions of muscles, ligaments, and the ground-reaction force to tibiofemoral joint loading during normal gait. *Journal of Orthopaedic Research*, 24(10):1983–1990, 2006.

C. S. Shin, A. M. Chaudhari, and T. P. Andriacchi. The influence of deceleration forces on acl strain during single-leg landing: a simulation study. *Journal of Biomechanics*, 40(5): 1145–1152, 2007.

R. Shirazi and A. Shirazi-Adl. Analysis of partial meniscectomy and acl reconstruction in knee joint biomechanics under a combined loading. *Clinical Biomechanics*, 24(9): 755–761, 2009a.

R. Shirazi and A. Shirazi-Adl. Computational biomechanics of articular cartilage of human knee joint: effect of osteochondral defects. *Journal of Biomechanics*, 42(15):2458–2465, 2009b.

R. Shirazi, A. Shirazi-Adl, and M. Hurtig. Role of cartilage collagen fibrils networks in knee joint biomechanics under compression. *Journal of biomechanics*, 41(16):3340–3348, 2008.

J. L. Silverberg, S. Dillavou, L. Bonassar, and I. Cohen. Anatomic variation of depth-dependent mechanical properties in neonatal bovine articular cartilage. *Journal of Orthopaedic Research*, 31(5):686–691, 2013.

D. Skaggs, W. Warden, and V. Mow. Radial tie fibers influence the tensile properties of the bovine medial meniscus. *Journal of Orthopaedic Research*, 12(2):176–185, 1994.

N. W. Skelley, R. M. Castile, T. E. York, V. Gruev, S. P. Lake, and R. H. Brophy. Differences in the microstructural properties of the anteromedial and posterolateral bundles of the anterior cruciate ligament. *The American journal of sports medicine*, 43(4):928–936, 2015.

N. W. Skelley, R. M. Castile, P. C. Cannon, C. I. Weber, R. H. Brophy, and S. P. Lake. Regional variation in the mechanical and microstructural properties of the human anterior cruciate ligament. *The American journal of sports medicine*, 44(11):2892–2899, 2016.

C. Smith, I. Young, and J. Kearney. Mechanical properties of tendons: changes with sterilization and preservation. *TRANSACTIONS-AMERICAN SOCIETY OF MECHANICAL ENGINEERS JOURNAL OF BIOMECHANICAL ENGINEERING*, 118:56–61, 1996.

H. E. Smith, T. J. Mosher, B. J. Dardzinski, B. G. Collins, C. M. Collins, Q. X. Yang, V. J. Schmithorst, and M. B. Smith. Spatial variation in cartilage t2 of the knee. *Journal of Magnetic Resonance Imaging*, 14(1):50–55, 2001.

M. A. Soltz and G. A. Ateshian. Experimental verification and theoretical prediction of cartilage interstitial fluid pressurization at an impermeable contact interface in confined compression. *Journal of biomechanics*, 31(10):927–934, 1998.

M. A. Soltz and G. A. Ateshian. A conewise linear elasticity mixture model for the analysis of tension-compression nonlinearity in articular cartilage. *TRANSACTIONS-AMERICAN SOCIETY OF MECHANICAL ENGINEERS JOURNAL OF BIOMECHANICAL ENGINEERING*, 122(6):576–586, 2000.

Y. Song, R. E. Debski, V. Musahl, M. Thomas, and S. L.-Y. Woo. A three-dimensional finite element model of the human anterior cruciate ligament: a computational analysis with experimental validation. *Journal of Biomechanics*, 37(3):383–390, 2004.

J. Soulhat, M. Buschmann, and A. Shirazi-Adl. A fibril-network-reinforced biphasic iviodel of cartilage in unconfined compression. *Journal of biomechanical engineering*, 1999.

R. Spilker and J.-K. Suh. Formulation and evaluation of a finite element model for the biphasic model of hydrated soft tissues. *Computers & Structures*, 35(4):425–439, 1990.

R. L. Spilker, J.-K. Suh, and V. C. Mow. A finite element analysis of the indentation stress-relaxation response of linear biphasic articular cartilage. *ASME J. Biomech. Eng*, 114 (2):191–201, 1992.

K. P. Spindler and R. W. Wright. Anterior cruciate ligament tear. *New England Journal of Medicine*, 359(20):2135–2142, 2008.

H. Steckel, G. Vadala, D. Davis, and F. H. Fu. 2d and 3d 3-tesla magnetic resonance imaging of the double bundle structure in anterior cruciate ligament anatomy. *Knee Surgery, Sports Traumatology, Arthroscopy*, 14(11):1151–1158, 2006.

B. D. Stemper, N. Yoganandan, M. R. Stineman, T. A. Gennarelli, J. L. Baisden, and F. A. Pintar. Mechanics of fresh, refrigerated, and frozen arterial tissue. *Journal of Surgical Research*, 139(2):236–242, 2007.

N. Stergiou, S. Ristanis, C. Moraiti, and A. D. Georgoulis. Tibial rotation in anterior cruciate ligament (acl)-deficient and acl-reconstructed knees. *Sports medicine*, 37(7): 601–613, 2007.

R. Storn and K. Price. Differential evolution–a simple and efficient heuristic for global optimization over continuous spaces. *Journal of Global Optimization*, 11(4):341–359, 1997.

J. Suggs, C. Wang, and G. Li. The effect of graft stiffness on knee joint biomechanics after acl reconstruction—-a 3d computational simulation. *Clinical Biomechanics*, 18(1): 35–43, 2003.

J.-K. Suh and S. Bai. Finite element formulation of biphasic poroviscoelastic model for articular cartilage. *Transactions-American Society of Mechanical Engineers Journal of biomechanical Engineering*, 120:195–201, 1998.

J.-K. Suh and R. L. Spilker. Indentation analysis of biphasic articular cartilage: nonlinear phenomena under finite deformation. *TRANSACTIONS-AMERICAN SOCIETY OF MECHANICAL ENGINEERS JOURNAL OF BIOMECHANICAL ENGINEERING*, 116: 1–1, 1994.

J.-K. Suh, R. Spilker, and M. Holmes. A penalty finite element analysis for nonlinear mechanics of biphasic hydrated soft tissue under large deformation. *International journal for numerical methods in engineering*, 32(7):1411–1439, 1991.

H. B. Sun. Mechanical loading, cartilage degradation, and arthritis. *Annals of the New York Academy of Sciences*, 1211(1):37–50, 2010.

W. Sun, E. L. Chaikof, and M. E. Levenston. Numerical approximation of tangent moduli for finite element implementations of nonlinear hyperelastic material models. *Journal of biomechanical engineering*, 130(6):061003, 2008.

A. Swann and B. Seedhom. The stiffness of normal articular cartilage and the predominant acting stress levels: implications for the aetiology of osteoarthrosis. *Rheumatology*, 32 (1):16–25, 1993.

W. Świeszkowski, D. N. Ku, H. E. Bersee, and K. J. Kurzydlowski. An elastic material for cartilage replacement in an arthritic shoulder joint. *Biomaterials*, 27(8):1534–1541, 2006.

M. Takahashi, M. Doi, M. Abe, D. Suzuki, and A. Nagano. Anatomical study of the femoral and tibial insertions of the anteromedial and posterolateral bundles of human anterior cruciate ligament. *The American journal of sports medicine*, 34(5):787–792, 2006.

S. Takai, S. L.-Y. Woo, G. A. Livesay, D. J. Adams, and F. H. Fu. Determination of the in situ loads on the human anterior cruciate ligament. *Journal of Orthopaedic Research*, 11 (5):686–695, 1993.

M. Tanaka, M. Fujikawa, D. Balzani, and J. Schröder. Robust numerical calculation of tangent moduli at finite strains based on complex-step derivative approximation and its application to localization analysis. *Computer Methods in Applied Mechanics and Engineering*, 269:454–470, 2014.

M. Tanaka, T. Sasagawa, R. Omote, M. Fujikawa, D. Balzani, and J. Schröder. A highly accurate 1st-and 2nd-order differentiation scheme for hyperelastic material models based on hyper-dual numbers. *Computer Methods in Applied Mechanics and Engineering*, 283: 22–45, 2015.

P. Tanska, M. E. Mononen, and R. K. Korhonen. A multi-scale finite element model for investigation of chondrocyte mechanics in normal and medial meniscectomy human knee joint during walking. *Journal of biomechanics*, 48(8):1397–1406, 2015.

S. Tashman, W. Anderst, P. Kolowich, S. Havstad, and S. Arnoczky. Kinematics of the acl-deficient canine knee during gait: Serial changes over two years. *Journal of Orthopaedic Research*, 22(5):931–941, 2004.

S. Tashman, P. Kolowich, D. Collon, K. Anderson, and W. Anderst. Dynamic function of the acl-reconstructed knee during running. *Clinical orthopaedics and related research*, 454:66–73, 2007.

A. Thambyah, A. Nather, and J. Goh. Mechanical properties of articular cartilage covered by the meniscus. *Osteoarthritis and cartilage*, 14(6):580–588, 2006.

L. M. Thoma, M. P. Mcnally, A. M. Chaudhari, T. Best, D. C. Flanigan, R. A. Siston, and L. C. Schmitt. Differential knee joint loading patterns during gait for individuals with tibiofemoral and patellofemoral articular cartilage defects in the knee. *Osteoarthritis and Cartilage*, 2017.

S. Thomopoulos, J. P. Marquez, B. Weinberger, V. Birman, and G. M. Genin. Collagen fiber orientation at the tendon to bone insertion and its influence on stress concentrations. *Journal of biomechanics*, 39(10):1842–1851, 2006.

J. B. Thorlund, M. Englund, U. Jørgensen, N. Nissen, J. Schjerning, and L. Lohmander. Prevalence of early or established knee osteoarthritis among middle-aged and older patients undergoing knee arthroscopy for meniscal tear. *Osteoarthritis and Cartilage*, 24: S206, 2016.

G. Thornton, A. Oliynyk, C. Frank, and N. Shrive. Ligament creep cannot be predicted from stress relaxation at low stress: a biomechanical study of the rabbit medial collateral ligament. *Journal of Orthopaedic Research*, 15(5):652–656, 1997.

M. Tissakht and A. Ahmed. Tensile stress-strain characteristics of the human meniscal material. *Journal of Biomechanics*, 28(4):411–422, 1995.

S. Tomkoria, R. V. Patel, and J. J. Mao. Heterogeneous nanomechanical properties of superficial and zonal regions of articular cartilage of the rabbit proximal radius condyle by atomic force microscopy. *Medical engineering & physics*, 26(10):815–822, 2004.

J. S. Torg, W. Conrad, and V. Kalen. Clinical i diagnosis of anterior cruciate ligament instability in the athlete. *The American journal of sports medicine*, 4(2):84–93, 1976.

P. Torzilli and V. C. Mow. On the fundamental fluid transport mechanisms through normal and pathological articular cartilage during functionâĂŤi the formulation. *Journal of biomechanics*, 9(8):541–552, 1976a.

P. Torzilli and V. C. Mow. On the fundamental fluid transport mechanisms through normal and pathological articular cartilage during functionâĂŤii. the analysis, solution and conclusions. *Journal of Biomechanics*, 9(9):587–606, 1976b.

P. Torzilli, R. Grigiene, J. Borrelli, and D. Helfet. Effect of impact load on articular cartilage: cell metabolism and viability, and matrix water content. *Journal of biomechanical engineering*, 121(5):433–441, 1999.

J. Töyräs, T. Lyyra-Laitinen, M. Niinimäki, R. Lindgren, M. Nieminen, I. Kiviranta, and J. Jurvelin. Estimation of the young's modulus of articular cartilage using an arthroscopic indentation instrument and ultrasonic measurement of tissue thickness. *Journal of Biomechanics*, 34(2):251–256, 2001.

S. Treppo, H. Koepp, E. C. Quan, A. A. Cole, K. E. Kuettner, and A. J. Grodzinsky. Comparison of biomechanical and biochemical properties of cartilage from human knee and ankle pairs. *Journal of Orthopaedic Research*, 18(5):739–748, 2000.

C. H. Turner, J. Rho, Y. Takano, T. Y. Tsui, and G. M. Pharr. The elastic properties of trabecular and cortical bone tissues are similar: results from two microscopic measurement techniques. *Journal of biomechanics*, 32(4):437–441, 1999.

A. Unsworth, D. Dowson, and V. Wright. The frictional behavior of human synovial jointsâĂŤpart i: Natural joints. *Journal of Tribology*, 97(3):369–376, 1975.

B. A. Van Dommelen and P. J. Fowler. Anatomy of the posterior cruciate ligament: a review. *The American journal of sports medicine*, 17(1):24–29, 1989.

E. E. van Haaften, K. Ito, and C. C. van Donkelaar. The initial repair response of articular cartilage after mechanically induced damage. *Journal of Orthopaedic Research*, 35(6): 1265–1273, 2017.

M. Venäläinen, M. Mononen, S. Väänänen, J. Jurvelin, J. Töyräs, T. Virén, and R. Korhonen. Effect of bone inhomogeneity on tibiofemoral contact mechanics during physiological loading. *Journal of biomechanics*, 49(7):1111–1120, 2016a.

M. S. Venäläinen, M. E. Mononen, J. Salo, L. P. Räsänen, J. S. Jurvelin, J. Töyräs, T. Virén, and R. K. Korhonen. Quantitative evaluation of the mechanical risks caused by focal cartilage defects in the knee. *Scientific Reports*, 6, 2016b.

L. Vergori, M. Destrade, P. McGarry, and R. W. Ogden. On anisotropic elasticity and questions concerning its finite element implementation. *Computational Mechanics*, 52 (5):1185–1197, 2013.

A. Verteramo and B. Seedhom. Zonal and directional variations in tensile properties of bovine articular cartilage with special reference to strain rate variation. *Biorheology*, 41 (3-4):203–213, 2004.

A. Verteramo and B. B. Seedhom. Effect of a single impact loading on the structure and mechanical properties of articular cartilage. *Journal of biomechanics*, 40(16):3580–3589, 2007.

D. F. Villegas, J. A. Maes, S. D. Magee, and T. L. H. Donahue. Failure properties and strain distribution analysis of meniscal attachments. *Journal of Biomechanics*, 40(12): 2655–2662, 2007.

C. S. Visconti, K. Kavalkovich, J.-J. Wu, and C. Niyibizi. Biochemical analysis of collagens at the ligament–bone interface reveals presence of cartilage-specific collagens. *Archives of biochemistry and biophysics*, 328(1):135–142, 1996.

M. Waldén, M. Hägglund, J. Werner, and J. Ekstrand. The epidemiology of anterior cruciate ligament injury in football (soccer): a review of the literature from a gender-related perspective. *Knee surgery, sports traumatology, arthroscopy*, 19(1):3–10, 2011.

S. J. Wall, D. M. Rose, E. G. Sutter, S. M. Belkoff, and B. P. Boden. The role of axial compressive and quadriceps forces in noncontact anterior cruciate ligament injury a cadaveric study. *The American Journal of Sports Medicine*, 40(3):568–573, 2012.

C. Wan, Z. Hao, and S. Wen. The effect of the variation in acl constitutive model on joint kinematics and biomechanics under different loads: a finite element study. *Journal of biomechanical engineering*, 135(4):041002, 2013.

C. Wan, Z. Hao, and S. Wen. A comparison of material characterizations in frequently used constitutive models of ligaments. *International journal for numerical methods in biomedical engineering*, 30(6):605–615, 2014.

C. Wan, Z. Hao, Z. Li, and J. Lin. Finite element simulations of different hamstring tendon graft lengths and related fixations in anterior cruciate ligament reconstruction. *Medical & Biological Engineering & Computing*, pages 1–10, 2017.

C. C. Wang, C. T. Hung, and V. C. Mow. An analysis of the effects of depth-dependent aggregate modulus on articular cartilage stress-relaxation behavior in compression. *Journal of Biomechanics*, 34(1):75–84, 2001.

J. H.-C. Wang. Mechanobiology of tendon. *Journal of biomechanics*, 39(9):1563–1582, 2006.

Y. Wang, C. Ding, A. Wluka, S. Davis, P. Ebeling, G. Jones, and F. Cicuttini. Factors affecting progression of knee cartilage defects in normal subjects over 2 years. *Rheumatology*, 45(1):79–84, 2006.

Y. Wang, Y. Fan, and M. Zhang. Comparison of stress on knee cartilage during kneeling and standing using finite element models. *Medical Engineering & Physics*, 36(4):439–447, 2014.

S. J. Warden, L. K. Saxon, A. B. Castillo, and C. H. Turner. Knee ligament mechanical properties are not influenced by estrogen or its receptors. *American Journal of Physiology-Endocrinology and Metabolism*, 290(5):E1034–E1040, 2006.

J. Weidow, J. Kärrholm, T. Saari, and A. McPherson. Abnormal motion of the medial femoral condyle in lateral knee osteoarthritis. *Clinical orthopaedics and related research*, 454:27–34, 2007.

C. Weiss, L. Rosenberg, and A. J. Helfet. An ultrastructural study of normal young adult human articular cartilage. *The Journal of Bone & Joint Surgery*, 50(4):663–674, 1968.

J. A. Weiss and J. C. Gardiner. Computational modeling of ligament mechanics. *Critical Reviews in Biomedical Engineering*, 29(3), 2001.

J. A. Weiss, S. L.-Y. Woo, K. J. Ohland, S. Horibe, and P. O. Newton. Evaluation of a new injury model to study medial collateral ligament healing: primary repair versus nonoperative treatment. *Journal of Orthopaedic Research*, 9(4):516–528, 1991.

J. A. Weiss, B. N. Maker, and S. Govindjee. Finite element implementation of incompressible, transversely isotropic hyperelasticity. *Computer methods in applied mechanics and engineering*, 135(1):107–128, 1996.

J. A. Weiss, P. M. Moulis, H. E. Ayliffe, T. D. Rosenberg, and V. J. Cooley. Finite element simulation of stresses in healing cartilage defects. *ASME-PUBLICATIONS-BED*, 39: 263–264, 1998.

J. A. Weiss, J. C. Gardiner, B. J. Ellis, T. J. Lujan, and N. S. Phatak. Three-dimensional finite element modeling of ligaments: technical aspects. *Medical Engineering & Physics*, 27(10):845–861, 2005.

R. W. Westermann, B. R. Wolf, and J. M. Elkins. Effect of acl reconstruction graft size on simulated lachman testing: a finite element analysis. *The Iowa orthopaedic journal*, 33: 70, 2013.

R. W. Westermann, B. R. Wolf, and J. Elkins. Optimizing graft placement in anterior cruciate ligament reconstruction: A finite element analysis. *Journal of Knee Surgery*, 2016.

W. Widuchowski, J. Widuchowski, and T. Trzaska. Articular cartilage defects: study of 25,124 knee arthroscopies. *The Knee*, 14(3):177–182, 2007.

F. Wilcoxon. Individual comparisons by ranking methods. *Biometrics bulletin*, 1(6):80–83, 1945.

M. Williams. Stress singularities resulting from various boundary conditions in angular corners of plates in extension. *Journal of applied mechanics*, 19(4):526–528, 1952.

R. M. Williams, W. R. Zipfel, and W. W. Webb. Interpreting second-harmonic generation images of collagen i fibrils. *Biophysical journal*, 88(2):1377–1386, 2005.

W. Wilson, C. Van Donkelaar, and J. M. Huyghe. A comparison between mechano-electrochemical and biphasic swelling theories for soft hydrated tissues. *Transactions of the ASME-K-Journal of Biomechanical Engineering*, 127(1):158–165, 2005a.

W. Wilson, C. Van Donkelaar, B. Van Rietbergen, and R. Huiskes. A fibril-reinforced poroviscoelastic swelling model for articular cartilage. *Journal of biomechanics*, 38(6): 1195–1204, 2005b.

W. Wilson, C. van Burken, C. van Donkelaar, P. Buma, B. van Rietbergen, and R. Huiskes. Causes of mechanically induced collagen damage in articular cartilage. *Journal of Orthopaedic Research*, 24(2):220–228, 2006.

T. J. Withrow, L. J. Huston, E. M. Wojtys, and J. A. Ashton-Miller. The relationship between quadriceps muscle force, knee flexion, and anterior cruciate ligament strain in an in vitro simulated jump landing. *The American Journal of Sports Medicine*, 34(2): 269–274, 2006.

T. J. Withrow, L. J. Huston, E. M. Wojtys, and J. A. Ashton-Miller. Effect of varying hamstring tension on anterior cruciate ligament strain during in vitro impulsive knee flexion and compression loading. *The Journal of Bone & Joint Surgery*, 90(4):815–823, 2008.

A. Wittek, N. M. Grosland, G. R. Joldes, V. Magnotta, and K. Miller. From finite element meshes to clouds of points: A review of methods for generation of computational biomechanics models for patient-specific applications. *Annals of Biomedical Engineering*, pages 1–13, 2015.

M. Woiczinski, A. Steinbrück, P. Weber, P. Müller, V. Jansson, and C. Schröder. Development and validation of a weight-bearing finite element model for total knee replacement. *Computer methods in biomechanics and biomedical engineering*, 19(10): 1033–1045, 2016.

E. M. Wojtys, M. L. Beaulieu, and J. A. Ashton-Miller. New perspectives on acl injury: On the role of repetitive sub-maximal knee loading in causing acl fatigue failure. *Journal of Orthopaedic Research*, 34(12):2059–2068, 2016.

B. L. Wong and R. L. Sah. Effect of a focal articular defect on cartilage deformation during patello-femoral articulation. *Journal of Orthopaedic Research*, 28(12):1554–1561, 2010.

S. Woo, M. Gomez, Y. Seguchi, C. Endo, W. Akeson, et al. Measurement of mechanical properties of ligament substance from a bone-ligament-bone preparation. *Journal of Orthopaedic Research*, 1(1):22–29, 1983.

S. L. Woo and M. K. Kwan. Application of the up finite element method to the study of articular cartilage. *Journal of biomechanical engineering*, 113:397, 1991.

S. L. Woo, P. O. Newton, D. A. MacKenna, and R. M. Lyon. A comparative evaluation of the mechanical properties of the rabbit medial collateral and anterior cruciate ligaments. *Journal of biomechanics*, 25(4):377–386, 1992.

S. L. Woo, R. E. Debski, J. D. Withrow, and M. A. Janaushek. Biomechanics of knee ligaments. *The American journal of sports medicine*, 27(4):533–543, 1999.

S. L.-Y. Woo, C. A. Orlando, J. F. Camp, and W. H. Akeson. Effects of postmortem storage by freezing on ligament tensile behavior. *Journal of biomechanics*, 19(5):399–404, 1986a.

S. L.-Y. Woo, C. A. Orlando, M. A. Gomez, C. B. Frank, and W. H. Akeson. Tensile properties of the medial collateral ligament as a function of age. *Journal of orthopaedic research*, 4(2):133–141, 1986b.

S. L.-Y. Woo, R. H. Peterson, K. J. Ohland, T. J. Sites, and M. I. Danto. The effects of strain rate on the properties of the medial collateral ligament in skeletally immature and mature rabbits: a biomechanical and histological study. *Journal of Orthopaedic Research*, 8(5): 712–721, 1990.

S. L.-Y. Woo, J. M. Hollis, D. J. Adams, R. M. Lyon, and S. Takai. Tensile properties of the human femur-anterior cruciate ligament-tibia complex: the effects of specimen age and orientation. *The American journal of sports medicine*, 19(3):217–225, 1991.

S. L.-Y. Woo, S. D. Abramowitch, R. Kilger, and R. Liang. Biomechanics of knee ligaments: injury, healing, and repair. *Journal of biomechanics*, 39(1):1–20, 2006.

S.-Y. Woo, P. Lubock, M. Gomez, G. Jemmott, S. Kuei, and W. Akeson. Large deformation nonhomogeneous and directional properties of articular cartilage in uniaxial tension. *Journal of biomechanics*, 12(6):437–446, 1979.

S.-Y. Woo, B. Simon, S. Kuei, and W. Akeson. Quasi-linear viscoelastic properties of normal articular cartilage. *Journal of biomechanical engineering*, 102(2):85–90, 1980.

S.-Y. Woo, M. Gomez, and W. Akeson. The time and history-dependent viscoelastic properties of the canine medial collateral ligament. *Journal of Biomechanical Engineering*, 103(4):293–298, 1981.

A. D. Woolf and B. Pfleger. Burden of major musculoskeletal conditions. *Bulletin of the World Health Organization*, 81(9):646–656, 2003.

B. Wopenka, A. Kent, J. D. Pasteris, Y. Yoon, and S. Thomopoulos. The tendon-to-bone transition of the rotator cuff: a preliminary raman spectroscopic study documenting the gradual mineralization across the insertion in rat tissue samples. *Applied spectroscopy*, 62(12):1285–1294, 2008.

J. O. Wright, N. W. Skelley, R. P. Schur, R. M. Castile, S. P. Lake, and R. H. Brophy. Microstructural and mechanical properties of the posterior cruciate ligament: A comparison of the anterolateral and posteromedial bundles. *JBJS*, 98(19):1656–1664, 2016.

R. W. Wright, E. Preston, B. C. Fleming, A. Amendola, J. T. Andrish, J. A. Bergfeld, W. R. Dunn, C. Kaeding, J. E. Kuhn, R. G. Marx, et al. A systematic review of anterior cruciate ligament reconstruction rehabilitation: part ii: open versus closed kinetic chain

exercises, neuromuscular electrical stimulation, accelerated rehabilitation, and miscellaneous topics. *The Journal of Knee Surgery*, 21(3):225–234, 2008.

J. Wu and W. Herzog. Elastic anisotropy of articular cartilage is associated with the microstructures of collagen fibers and chondrocytes. *Journal of biomechanics*, 35(7):931–942, 2002.

F. Xie, L. Yang, L. Guo, Z.-j. Wang, and G. Dai. A study on construction three-dimensional nonlinear finite element model and stress distribution analysis of anterior cruciate ligament. *Journal of Biomechanical Engineering*, 131(12):121007, 2009.

M. Yagi, E. K. Wong, A. Kanamori, R. E. Debski, F. H. Fu, and S. L. Woo. Biomechanical analysis of an anatomic anterior cruciate ligament reconstruction. *The American Journal of Sports Medicine*, 30(5):660–666, 2002.

L. Yahia and G. Drouin. Study of the hysteresis phenomenon in canine anterior cruciate ligaments. *Journal of biomedical engineering*, 12(1):57–62, 1990.

L.-H. Yahia and G. Drouin. Microscopical investigation of canine anterior cruciate ligament and patellar tendon: collagen fascicle morphology and architecture. *Journal of Orthopaedic Research*, 7(2):243–251, 1989.

K. Yamamoto, S. Hirokawa, and T. Kawada. Strain distribution in the ligament using photoelasticity. a direct application to the human acl. *Medical Engineering & Physics*, 20(3):161–168, 1998.

K. Yasuda, E. Kondo, H. Ichiyama, Y. Tanabe, and H. Tohyama. Clinical evaluation of anatomic double-bundle anterior cruciate ligament reconstruction procedure using hamstring tendon grafts: comparisons among 3 different procedures. *Arthroscopy: The Journal of Arthroscopic & Related Surgery*, 22(3):240–251, 2006.

E. Yelin, L. Murphy, M. G. Cisternas, A. J. Foreman, D. J. Pasta, and C. G. Helmick. Medical care expenditures and earnings losses among persons with arthritis and other rheumatic conditions in 2003, and comparisons with 1997. *Arthritis & Rheumatology*, 56(5):1397–1407, 2007.

A. A. Young, R. C. Appleyard, M. M. Smith, J. Melrose, and C. B. Little. Dynamic biomechanics correlate with histopathology in human tibial cartilage: a preliminary study. *Clinical orthopaedics and related research*, 462:212–220, 2007.

T. Zantop, M. Herbort, M. J. Raschke, F. H. Fu, and W. Petersen. The role of the anteromedial and posterolateral bundles of the anterior cruciate ligament in anterior tibial translation and internal rotation. *The American journal of sports medicine*, 35(2):223–227, 2007a.

T. Zantop, T. Schumacher, N. Diermann, S. Schanz, M. J. Raschke, and W. Petersen. Anterolateral rotational knee instability: role of posterolateral structures. *Archives of orthopaedic and trauma surgery*, 127(9):743–752, 2007b.

W. Zhang, H. Y. Chen, and G. S. Kassab. A rate-insensitive linear viscoelastic model for soft tissues. *Biomaterials*, 28(24):3579–3586, 2007.

X. Zhang, G. Jiang, C. Wu, and S. L. Woo. A subject-specific finite element model of the anterior cruciate ligament. In *Engineering in Medicine and Biology Society, 2008. EMBS 2008. 30th Annual International Conference of the IEEE*, pages 891–894. IEEE, 2008.

L. Zhao, P. V. Lee, D. C. Ackland, N. D. Broom, and A. Thambyah. Microstructure variations in the soft-hard tissue junction of the human anterior cruciate ligament. *The Anatomical Record*, 2017.

B. Zielinska and T. L. H. Donahue. 3d finite element model of meniscectomy: changes in joint contact behavior. *Journal of biomechanical engineering*, 128(1):115–123, 2006.